Investigation of Carbamazepine-Nicotinamide cocrystal solubility and dissolution by a UV imaging system

PhD Thesis

Ning Qiao

This thesis is submitted in partial fulfilment of the requirements of De Montfort University for the award of Doctor of Philosophy

April 2014

Faculty of Health and Life Sciences

De Montfort University

Leicester

CONTENTS

DECLARATION

I declare that the word described in this thesis is original work undertaken by myself for the Doctor of Philosophy degree, at the Pharmacy School, Faculty of Healthy and Life Sciences, De Montfort University, Leicester, United Kingdom.

No part of the material described in this thesis has been submitted for the award of any other degree or qualification in this or any other university or college of advanced education.

Ning Qiao

ABSTRACT

In this study, the ability of pharmaceutical cocrystals on improving solubility and dissolution behaviour of poorly water soluble drug has been studied by a novel technique SDI300 UV imaging surface dissolution system. Pharmaceutical cocrystals of poorly water soluble drug carbamazepine (CBZ) were synthesized, which are 1: 1 carbamazepine - nicotinamide (CBZ-NIC) cocrystal, and 2:1 carbamazepine - succinic acid (CBZ-SUC) cocrystal.

Firstly, dissolution and solution mediated phase transformation behaviour (SMPT) of CBZ-NIC cocrystal was studied by *in situ* techniques of UV imaging and Raman spectroscopy. This study has shown that *in situ* UV imaging and Raman spectroscopy with a complementary technique of SEM can provide an in depth understanding of cocrystal dissolution processes. It has been found that CBZ-NIC cocrystal including other polymorphs of CBZ III and I and mixture are converting to CBZ DH during dissolution.

The influence of surfactants, SLS and Tween 80, on the solubility and dissolution behavior of the CBZ-NIC cocrystal has been studied. Results show that the SMPT of CBZ III and CBZ-NIC cocrystal can be altered by inclusion of a surfactant in dissolution medium. However, CBZ III and CBZ-NIC cocrystal have shown different transformation behavior with different surfactants.

The solubility and dissolution behaviour of CBZ-NIC cocrystal, CBZ-SUC cocrystal in four biomedia (simulated gastric fluid, pH1.2 HCl buffer, simulated intestinal fluid, and pH 6.8 PBS buffer) were studied. Results have shown that equilibrium solubility of CBZ samples varied in different media. The two cocrystals dissolution rates show different trends as that of parent drug CBZ III. This can be explained by that the formation of cocrystal change the dissolution ability of CBZ III.

ACKNOWLEDGEMENTS

First I would like to express my sincere appreciation to my supervisors Dr Mingzhong Li and Dr Walkiria Schlindwein for their continuous support and guidance throughout my PhD studies. Your profound knowledge, creativeness, enthusiasm, patience, encouragement give me great help to do my PhD research.

I am very grateful to all technicians in the faculty of Health and Life Sciences who provide me technical support and equipment support for my experiments.

I would like to thank my PhD colleagues in my lab Huolong Liu, Shi Qiu and Yan Lu, for years of friendship , accompany and productive working environment.

More specifically, I wish to express my sincere gratitude to China Scholarship Council who gives me financial supports to pursue my PhD study.

Finally, I wish to thank my beloved parents, my dearest sister and brother for their endless love, care and encouraging me to fulfil my dream.

PUBLICATIONS

Journal publications

[1] **Ning Qiao**, Mingzhong Li, Walkiria Schlindwein, Nazneen Malek, Angela Davies, Gary Trappitt, Pharmaceutical cocrystals: An overview. International Journal of Pharmaceutics, 2011. 419(1–2): p. 1-11.

[2] **Ning Qiao**, Ke Wang, Walkiria Schlindwein, Angela Davies, Mingzhong Li, *In situ* monitoring of carbamazepine–nicotinamide cocrystal intrinsic dissolution behaviour. European Journal of Pharmaceutics and Biopharmaceutics, 2013. 83 (3): p. 415-426.

[3] Mingzhong Li, **Ning Qiao**, and Ke Wang, Influence of sodium lauryl sulfate and Tween 80 on carbamazepine–nicotinamide cocrystal solubility and dissolution behaviour. Pharmaceutics, 2013. 5(4): p. 508-524.

[4] Investigation of solubility and dissolution behaviour of carbamazepine-nicotinamide cocrystal and carbamazepine-succinic acid cocrystal in biomedia. Publication in preparation.

Conference publications

[1] **Ning Qiao**, Ke Wang, Walkiria Schlindwein, Angela Davies, Mingzhong Li, *In situ* monitoring of carbamazepine–nicotinamide cocrystal intrinsic dissolution behaviour, Proceeding 2012 APS Pharmsci Conference, Nottingham, UK, 12th-14th September 2012

[2] **Ning Qiao** and Mingzhong Li, Investigation of the effects of surfactants on Carbamazepine–Nicotinamide Cocrystal Solubility and Dissolution Behaviour,

Proceeding the 44th annual conference of the British Association for Crystal Growth, Manchester, UK,16th-18th June 2013

[3] **Ning Qiao** and Mingzhong Li, Investigation of the effects of surfactants on Carbamazepine–Nicotinamide Cocrystal Solubility and Dissolution Behaviour, Proceeding 2013 APS Pharmsci Conference, Edinburgh, UK, 2nd- 4th September 2013

Oral Presentation

Ning Qiao, Investigation of the Effects of Surfactants on Carbamazepine-Nicotinamide Cocrystal Solubility and Dissolution Behaviour, APS Biopharmaceutics Applied biopharmaceutics-understanding bioequivalence, biowavers and IVIVCs, The Academy of Pharmaceutical Sciences, MSD innovation centre, Hoddesdon, London, UK, 10th July 2013

LIST OF FIGURES

LIST OF TABLES

ABBREVIATIONS

ATR-FTIR	attenuated total reflectance-Fourier transform infrared spectroscopy
API	active pharmaceutical ingredient
BCS	biopharmaceutics classification system
CBZ	carbamazepine
CBZ III	carbamazepine form III
CBZ I	carbamazepine form I
CBZ DH	carbamazepine dihydrate
CBZ-NIC cocrystal	1: 1 carbamazepine – nicotinamide cocrystal
CBZ-SUC cocrystal	2:1 carbamazepine - succinic acid cocrystal
CMC	critical micelle concentration
CSC	surfactant critical stabilization concentration
CSD	Cambridge structural database
DSC	differential scanner chromatography
FTIR	Fourier transform infrared spectroscopy
GRAS	generally recognized as safe
HPLC	high performance liquid chromatography

IR	infrared spectroscopy
IDR	intrinsic dissolution rate
NIC	nicotinamide
PXRD	powder X-ray Diffraction
RC	reaction cocrystallisation
SUC	succinic acid
SMPT	solution mediated phase transformation
SEM	scanning electron microscope
SSNMR	solid state nuclear magnetic resonance spectroscopy
SXRD	single crystal X-ray Diffraction
SLS	sodium lauryl sulphate
SGF	simulated gastric fluid
SIF	simulated intestinal fluid
TGA	thermal gravimetric analysis
UV/Vis	ultraviolet–visible spectroscopy

Chapter 1 Introduction

1.1 Research background

In the pharmaceutical industry, it is the poor biopharmaceutical properties rather than toxicity or lack of efficacy that are the main reasons why less than 1% of active pharmaceutical compounds eventually get into the marketplace[1-3]. Among these biopharmaceutical properties, solubility remains a key issue, with drugs often discarded during commercial production due to their low solubility. Improving the solubility of drugs is currently one of the main challenges for the pharmaceutical industry. Many approaches have been adopted for improving the aqueous solubility of drugs including micronization [4-6], salt formation [7], solid dispersion [8], emulsification [9, 10], solubilisations using co-solvents [11], and the use of polymer drug vehicles for delivery of poorly soluble drugs [12]. Although these techniques have been shown to be effective at enhancing oral bioavailability, success of these approaches is dependent on the specific physicochemical nature of the molecules being studied [13-16]. Over the last decades, there has been growing interest in the design of pharmaceutical cocrystals, which emerge as a potential method for enhancing the bioavailability of drugs with low aqueous solubility. Apart from offering potential improvements in solubility, dissolution rate, bioavailability and physical stability, pharmaceutical cocrystals frequently enhance other essential properties of the Active Pharmaceutical Ingredient (API) such as hygroscopicity, chemical stability, compressibility and flowability [17].

Researchers have done lots of work to study the solubility and dissolution behavior of cocrystals, which is one of the major aspects of cocrystals research areas. For poorly soluble neutral compounds, cocrystallisation is a very feasible method to improve solubility, and cocrystals can provide higher and lower dissolution rates compared to the APIs. However, pharmaceutical cocrystals dissolution process is still largely underexploited, and many problems remain unsolved, for example, high solubility of

pharmaceutical cocrystals result in a supersaturation of poorly soluble APIs and further crystallization of APIs, which is called solution mediated phase transformation (SMPT). The advantage of pharmaceutical cocrystals on improving APIs dissolution rate could be lost if SMPT happened. So, there is a clear need for better understanding about the dissolution process of cocrystals in the context of pharmaceutical cocrystals development. In this work, a new powerful dissolution test technology, ActiPix SDI 300 UV surface imaging system (Paraytec Ltd., York, UK), has been employed to study the dissolution process of cocrystals. ActiPix SDI 300 UV surface imaging system has been designed to improve our understanding of the kinetics and mechanism of drug substance release into dissolution medium. It can visualise the solution concentration distribution during dissolution in real time. It provides a platform for generating spatial and temporary information of the dissolved solution phase of a solid drug during dissolution when it is combined with a channel flow cell method. Through applying UV surface imaging system into cocrystals dissolution study, several important results have been achieved.

1.2 Research aim and objectives

The aim of this study was to investigate how pharmaceutical cocrystals can improve the solubility and dissolution properties of poorly water soluble drugs under different environments. It was expected that the mechanism of pharmaceutical cocrystals dissolution can be better explained and understood.

The specific objectives of this research are briefly listed as followings:

Objective 1: Review the background, research method, and development results of current cocrystals research areas, and also give a critical and cohesive literature review about pharmaceutical cocrystals;

Objective 2: Synthesize and characterize two pharmaceutical cocrystals of poorly water soluble drug of carbamazepine (CBZ), which are 1:1 carbamazepine-nicotinamide

cocrystal (CBZ-NIC cocrystal) and 2:1 carbamazepine-succinic acid cocrystal (CBZ-SUC cocrystal);

Objective 3: Establish one dissolution testing method using UV surface imaging system, Raman spectroscopy and SEM to *in-situ* monitor the dissolution process of cocrystals forms of sample. Apply this method to investigate the solution mediated phase transformation behaviour of CBZ-NIC cocrystal during its dissolution process;

Objective 4: Study the effects of two different surfactants, sodium lauryl sulphate and Tween 80, on CBZ-NIC cocrystal solubility and dissolution behaviour;

Objective 5: Investigate the solubility and dissolution behaviour of CBZ-NIC cocrystal and CBZ-SUC cocrystal in four biomedia, including pH1.2 HCl buffer, pH 6.8 phosphate buffer, simulated gastric fluid, and simulated intestinal fluid.

1.3 Thesis structure

This thesis is organized into 8 chapters:

Chapter 1 briefly described the background, objectives, and structure of the proposed PhD research.

Chapter 2 presented a brief and systematic overview of pharmaceutical cocrystals. The definitions and basic theories of pharmaceutical cocrystals and recent progresses in pharmaceutical cocrystals were introduced in this chapter.

Chapter 3 introduced all materials and analytical approaches used in this study. The principles and experimental settings of all analytical techniques were given in this chapter. Operations of instrument and methods development were described in details. Preparation of dissolution media and different test samples were also given in this chapter.

Chapter 4 characterised all samples used in this study. The characterisation results of different forms of CBZ samples (CBZ I, CBZ DH) two cocrystals of CBZ, which are CBZ-NIC cocrystal, CBZ-SUC cocrystal were given. The molecular structures of CBZ-NIC cocrystal and CBZ-SUC cocrystal were also presented in this chapter.

Chapter 5 established the method to monitor the dissolution process of a cocrystal through *in situ* UV imaging and Raman spectroscopy in combination with a complementary technique of SEM. In this chapter, evolution of the intrinsic dissolution rate (IDR) of CBZ-NIC cocrystal was monitored by the UV imaging dissolution system. The solid state change that might occur during dissolution of the cocrystal was monitored by *in situ* Raman Spectroscopy.

Chapter 6 investigated the role of surfactants in inhibiting the solution mediated phase transformation (SMPT) of a cocrystal. Two surfactants of sodium lauryl sulphate and Tween 80 were selected to investigate their effects on the solubility and intrinsic dissolution rate of CBZ-NIC cocrystal in this chapter.

Chapter 7 studied the solubility and dissolution behaviour of CBZ, CBZ-NIC cocrystal, CBZ-SUC cocrystal in simulated gastric fluid, pH1.2 HCl buffer, simulated intestinal fluid, and pH 6.8 PBS buffer.

Chapter 8 summarized the presented work and results obtained from this research. Further opportunities in the research area of pharmaceutical cocrystals were also discussed in this chapter.

Chapter 2 Literature Review

2.1 Chapter overview

In this chapter, a brief and systematic review of pharmaceutical cocrystals was presented. To start with, cocrystal background was introduced, which will give the reader a general knowledge about cocrystal research area. The concept of the pharmaceutical cocrystals and several key issues of pharmaceutical cocrystals including cocrystals formation theory, design strategies, formation methods, physicochemical properties studies, characterisation techniques were individually described. Recent progress on pharmaceutical cocrystals, especially theoretical research development on cocrystals dissolution and solubility, were illustrated in this chapter. Finally, pharmaceutical cocrystals research of carbamazepine, a biopharmaceutics classification system (BCS) II drug, was reviewed.

2.2 Cocrystal background review

2.2.1 Cocrystal definition

Cocrystals can be defined in a number of ways [18, 19]. A restrictive definition utilised by Aakeroy and Salmon [20] is that cocrystals are structurally homogeneous crystalline materials containing two or more components present in definite stoichiometric amounts. The cocrystal components are discrete neutral molecular reactants which are solids at ambient temperature. Based on this definition of cocrystals, a pharmaceutical cocrystal means a cocrystal with one of the cocrystal components as an API and the other components are called coformers.

In Schultheiss' review paper, the pharmaceutical cocrystals examples were enriched by including both neutral API and ionic form API [18]. A pictorial description of cocrystals and other possible multicomponent systems along with their respective

hydrates and solvates are displayed and compared in Fig. 2.1. Example 1 is a pharmaceutical cocrystal which formed by a neutral API and coformer through noncovalent interactions. Example 2 is a salt cocrystal formed by ionic API and neutral coformer. A pharmaceutical salt is also introduced in Fig. 2.1, example 3, which is formed by ionic API and acid. The difference between salt and cocrystal is that whether proton transfer has happened: if proton transfer has happened during one compound formation, the compound is salt; if no proton transfer happened, the compound is cocrystal.

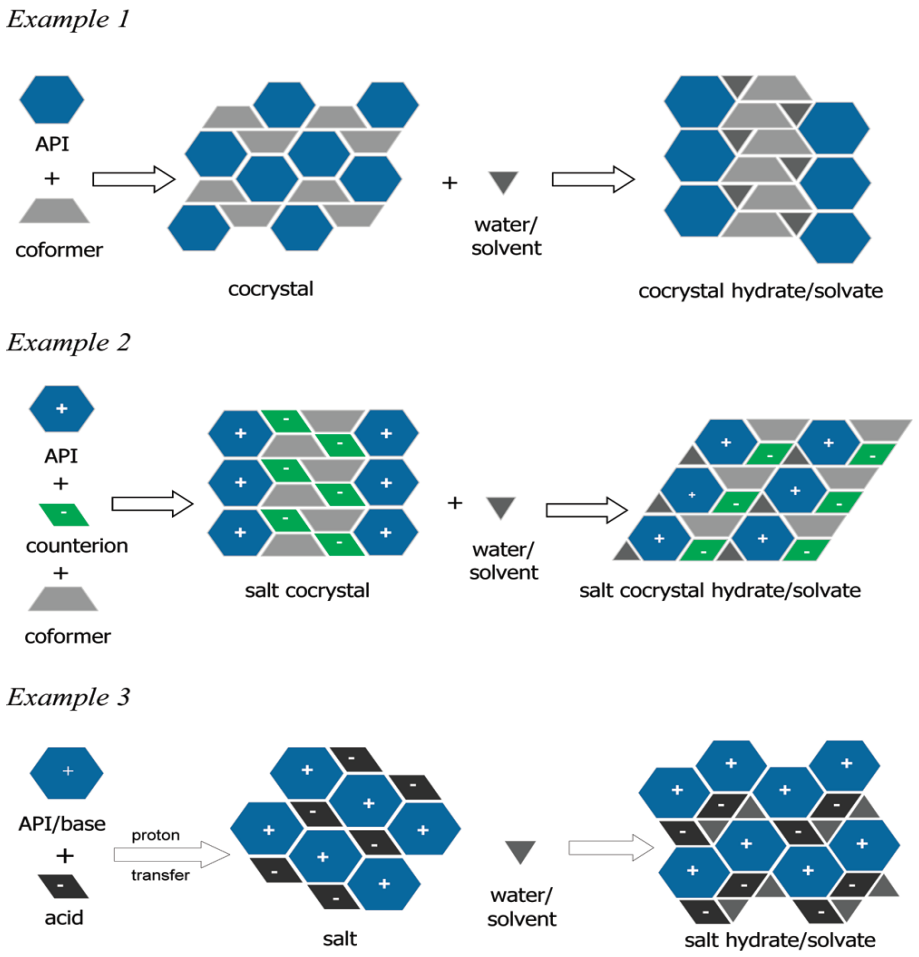

Fig. 2.1 Cocrystals, salt cocrystals, and salts along with their respective solvate/hydrate forms [18]

2.2.2 Crystal engineering

A pharmaceutical cocrystal can be designed by crystal engineering with an intention to improve the solid-state properties of an API without affecting its intrinsic structure. Crystal engineering can be defined as an application of the concepts of supramolecular chemistry to the solid state with particular emphasis upon the idea that crystalline solids are actual manifestations of self-assembly [21-24]. Cocrystals are constructed from intermolecular interactions such as van der Waals contact forces, π···π stacking interactions, and hydrogen bonding [25-28]. The most common hydrogen bonds utilized in crystal engineering utilised in pharmaceutical cocrystals are shown in Fig. 2.2. Crystal engineering involves modification of the crystal packing of a solid material by changing the intermolecular interactions [29].

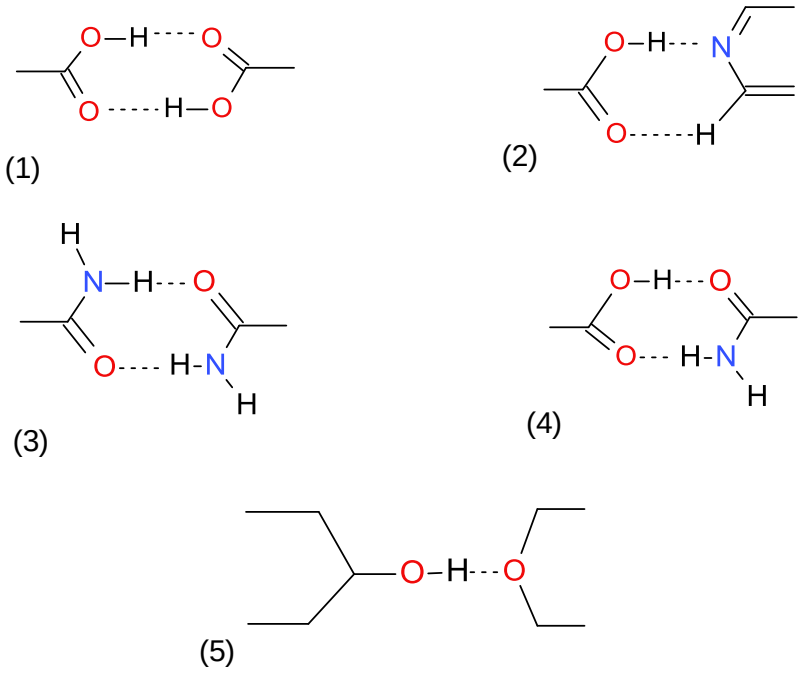

Fig. 2.2 Typical hydrogen bonds utilized in crystal engineering

2.2.3 Pharmaceutical cocrystals design strategies

As pharmaceutical cocrystals have rapidly emerged as a new class of API solids, much work has focused on exploring the crystal engineering and design strategies. Pharmaceutical cocrystals design is a multi-stage process, as schematically illustrated in Fig. 2.3 [29].

In order to get a desirable cocrystal product of an API, the first step is to study the structure of the target API molecule and find out the functional groups which can form intermolecular interaction with suitable coformers.

The next step is to choose a cocrystal coformer. The primary request for a coformer is to be pharmaceutically acceptable, for example, pharmaceutical excipients and compounds classified as generally recognized as safe (GRAS) for use as food additives. Coformer selection is the crucial step for designing a cocrystal.

During the design process, there are lots of worthwhile empirical and theoretical guidance, such as Cambridge Structural Database (CSD), hydrogen bond theories, and many empirical conclusions [13, 26, 30-39] .

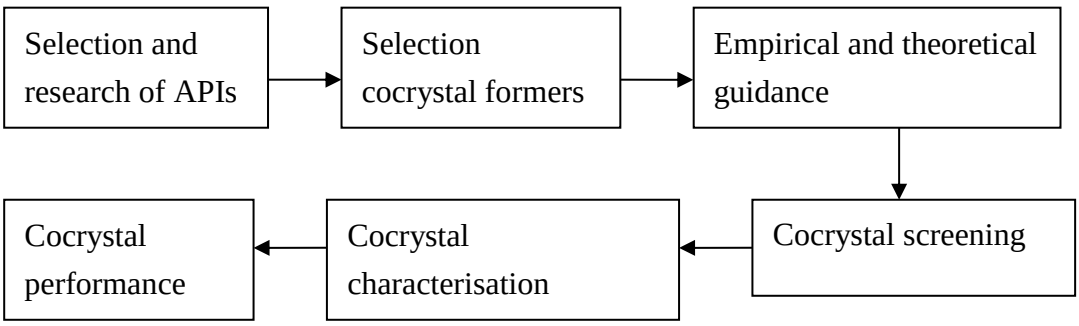

Fig. 2.3 Steps for cocrystal design and preparation

The next step is cocrystal screening, which is an experimental process to determine if a particular coformer candidate is able to cocrystallise with a targeted API. After a small

scale screening exercise, proper coformers could be selected to do scale up experiments. Various screening methods have been developed for cocrystal screening, such as solution method [40], hot-stage thermal microscopy method [41-43], computed crystal energy landscape method [44].

The aim of cocrystal characterization is to investigate the physical, chemical, and crystallographic properties of cocrystals. Usually, characterization includes the chemical structural conformation and crystallographic analysis of the newly formed supramolecularsynthon, its thermal features, stability and solubility. Details of different cocrystal characterisation techniques will be given in section 2.2.5 Cocrystal characterisation techniques.

The final step is the performance tests of newly formed cocrystal, which includes both *in vitro* and *in vivo* tests. *In vitro* tests focus on intrinsic dissolution and dissolution tests, while *in vivo* tests refer to animal bioavailability measurements, the measurement of the rate and extent of an API that reaches systemic circulation [45].

2.2.4 Cocrystal formation methods

To date, many ways of producing cocrystals have been reported. The most common formation methods are based on solution and grinding [27, 28]. The solution method is of great importance due to most of the cocrystals which qualify for single X-ray diffraction (SXRD) testing can only be prepared through this method. Solution methods include evaporation of a heterometric solution method, reaction crystallisation method, and cooling crystallisation. Grinding methods include neat grinding and solvent drop grinding. Apart from solution and grinding methods, there are also many newly emerging methods, such as cocrystallisation using supercritical fluid, hot-stage microscopy, and ultrasound assisted cocrystallisation.

2.2.4.1 Solution methods

In practice, solution cocrystallisation is based on the following two strategies [46]: (1) use of solvents or solvent mixtures where the cocrystal congruently saturates and thus the components have similar solubility, or (2) use of nonequivalent reactant concentrations in order to reach the cocrystal stability region in noncongruently saturating solvents [29, 31, 47].

Strategy one is adopted when the two cocrystal components have similar solubility in solvent and solution cocrystallisation with equimolar components will lead to the formation of the 1:1 cocrystal from solvent evaporation method. To date, many successful cocrystal examples were obtained by this method [26, 37, 48]. Strategy two is applied when cocrystal components have nonequivalent solubility, solution cocrystallisation through evaporation of an equimolar solution may result in the formation of single component crystal or a mixture of individual component and cocrystal. The reaction cocrystallisation (RC) approach has been adopted for this situation. RC experiments are performed by adding the less soluble reactant to a saturated or close to saturated solution of the more soluble reactant and then the solution becomes supersaturated with respect to cocrystal. Examples of cocrystal synthesized by RC method were reported [46, 49, 50].

Another solution method called cooling crystallisation involves varying the temperature of the crystallisation system, which has recently attracted much more attention for potential of a large scale of cocrystal production. First, large amounts of reactants and solvent are mixed in a reactor typically a jacketed vessel, and then the system is heated to a higher temperature to make sure all solutes are totally dissolved in the solvent and is followed by a cooling down step. Cocrystals will precipitate when solution becomes supersaturated with respect to cocrystal as the temperature drops down [42]. Several examples of cocrystals prepared through cooling crystallisation method have been published [51-53].

2.2.4.2 Grinding methods

There are two different techniques for cocrystal formation via grinding [54-56]. The first method is neat grinding, which is also called dry grinding, consisting of mixing the stoichiometric cocrystal components together and grinding them either manually, using a mortar and pestle, or mechanically, using a ball mill or a vibratory mill. To date many pharmaceutical cocrystals have been successfully synthesised by neat grinding [17, 57, 58]. The second technique for cocrystal synthesis via grinding is that of liquid-assisted grinding (also referred to as solvent-drop, wet cogrinding), in which minor amounts of an appropriate solvent is added in. Significant improvements in kinetics of cocrystal formation by grinding can be achieved by the addition of minor amounts of an appropriate solvent [37, 48, 59-61].

2.2.4.3 Other formation methods

Recently several novel methods have appeared in the area of pharmaceutical cocrystallisation. The application of supercritical fluid technology into cocrystal formation has been carried out by Padrela et al. [24, 62]. Ultrasound has been used to prepare cocrystals from solution or suspension/slurry [30, 38, 63]. Ultrasound assisted solution cocrystallisation has been studied using a noncongruently soluble pair of caffeine and maleic acid in methanol [64].

2.2.5 Cocrystal characterisation techniques

Cocrystal characterisation is an important constituent part within cocrystal research. The basic physicochemical properties of cocrystals can usually be characterised by Powder X-ray Diffraction (PXRD), Single Crystal X-ray Diffraction (SXRD), Infrared spectroscopy (IR), Raman spectroscopy, Differential Scanning Calorimetry (DSC), Solid State Nuclear Magnetic Resonance Spectroscopy (SSNMR), Scanning Electron Microscopy (SEM), and Terahertz spectroscopy.

SXRD is a characterisation technique for the determination of solid-state structure of cocrystals at an atomic level. However, the problem is that a single pharmaceutical cocrystal which is qualified for SXRD testing cannot always be produced. Therefore, PXRD are utilised more frequently to verify the formation of cocrystals. While, PXRD cannot distinguish solvates, hydrates or polymorphs from cocrystals, to make things worse, pharmaceutical cocrystals are prone to forming isostructural phases [29].

Raman spectroscopy is a spectroscopic technique used to study vibrational, rotational, and other low-frequency modes in a system, which has been demonstrated to be a powerful tool for distinguishing isostructural phase. There are many applications using Raman spectroscopy to identify characteristic peaks of cocrystal products [17, 42, 46, 64, 65].

IR is a very common spectroscopic technique in determining the chemical conformation of compounds. It can be a very powerful tool in distinguishing cocrystals from salts when a carboxylic acid is involved in hydrogen bond formation [66].

Recently, high-resolution SSNMR has shown to be a versatile and powerful tool for characterisation of pharmaceutical cocrystals [27, 67]. The application of different kinds of NMR methods in pharmaceutical cocrystal characterisation was introduced by Khan et al. [23]

DSC is the most widely used technique for the thermal property testing of cocrystals. DSC is the preferred technique for obtaining comprehensive melting point data and additional thermal data, such as the enthalpy of melting, can also be obtained simultaneously. In addition to being a characterisation technique, DSC has recently been used as a screening tool for rapid cocrystal screening [39, 68].

SEM is a type of electron microscope that images a sample by scanning it with a high-energy beam of electrons in a raster scan pattern. It is applied to determine the cocrystal micrograph and particle size in many examples [48, 62, 69, 70].

Terahertz time-domain-spectroscopy (THz-TDS) has emerged as a versatile spectroscopic technique and an alternative to PXRD in the characterisation of molecular crystals. It has been demonstrated that terahertz spectroscopy has the ability to distinguish between chiral and racemic hydrogen bonded cocrystals that are similar in molecular and supramolecular structure [71].

It is important to stress that no single technique is adequate to completely characterise the properties of cocrystal. Integration of various characterization techniques could help elucidate a better understanding of samples when analyzing cocrystalline materials.

2.2.6 Physicochemical properties of cocrystals

Physical and chemical properties of cocrystals are of great importance to the development of APIs. The overall motivation for investigating pharmaceutical cocrystals as an alternative approach during drug development is the adjustment of the physiochemical properties to improve the overall stability and efficacy of a dosage form [31]. Physicochemical properties, such as crystallinity, melting point, solubility, dissolution, and stability, have been studied extensively by researchers. A systematical review of these properties was given by Schultheiss and Newman [18]. Some key physicochemical properties of pharmaceutical cocrystals are summarised as following.

2.2.6.1 Melting point

Melting point is the temperature at which the solid phase is at equilibrium with the liquid phase. It is a fundamental physical property and an important consideration during solid drug development. There are complex correlations between the melting

point of pharmaceutical product and its processability, solubility and stability. Large amount of research work has been carried out to investigate if the melting point of a cocrystal changes with respect to the individual components and if the melting points can be estimated and modulated within a series of cocrystals [1, 72, 73].

2.2.6.2 Stability

Stability is a very important parameter when evaluating the properties of a pharmaceutical cocrystal. Usually, the stability testing of a newly developed cocrystal includes four aspects: relative humidity stress, thermal stress, chemical stability, and solution stability.

The relative humidity stress test is used to identify the best storage conditions for the product because the amount of water present in the cocrystal can lead to quality deterioration [24, 42, 48, 74, 75]. Thermal stress and chemical stability are relatively less studied areas about cocrystal properties. Very few reports were found [76, 77] and these limited studies showed that thermal stress studies can provide valuable information about physicochemical stability. Solubility stability is defined by Schultheiss and Newman [18] as the ability of the cocrystal components to stay in solution and not readily crystallise. Solution stability is an important parameter during drug development. Stability experiments accompany solubility or dissolution experiments to provide a more complete understanding of the behaviour of cocrystals in release media.

2.2.6.3 Solubility

Solubility is another important parameter for evaluating the properties of a pharmaceutical cocrystal. Traditional methods for improving solubility of poorly water soluble drugs include salt formation [78], solid dispersion (emulsification) [8], and particle size reduction (micronisation) [79], solubilisation of drugs in co-solvents [11]

and micellar solutions [9]. However, there are practical limitations with these techniques [13, 62], the success of these approaches is dependent on the specific physicochemical nature of the molecules being studied. Pharmaceutical cocrystallisation as a novel way to improve the physicochemical properties of a drug such as solubility, which can potentially be applied to a wide range of molecules and has attracted great interest from researchers [1, 5, 13, 29, 42, 80-86]. Many valuable research results have been obtained and these are selectively described as following.

Shiraki et al. [82] tried to improve the solubility of two APIs, exemestane (EX) and megestrol acetate (MA), through preparing two novel cocrystals, exemestane-maleic acid (EX-MAL) and megestrol acetate-saccharin (MA-SA) from organic solutions with different particle sizes. Aakeroy's study showed that cocrystals can not only increase but also decrease the solubility of active ingredient [1]. Researchers hypothesized that if they can incorporate an API with a series of crystalline solids characterized by considerable structural consistency, then may be able to fine-tune aqueous solubility. This hypothesis was demonstrated by systematically modulated aqueous solubility of an anticancer drug (hexamethylenebisacetamide) through cocrystallisation method. In addition to experimental studies, some theoretical research on cocrystal solubility has been carried out. More details on theoretical research about pharmaceutical cocrystals' solubility will be given in section 2.3.

2.2.6.4 Intrinsic Dissolution Rate (IDR)

Intrinsic dissolution measures the rate of dissolution of a pure drug substance from a constant surface area, which is independent of formulation effects and measures the intrinsic properties of the drug as a function of dissolution media, e.g. pH, ionic strength and counter-ions. The sample used in the intrinsic dissolution test is pressed into a disk or pellet, which should be no form change upon pressing and the disk needs to remain intact during the experiment. Most of the APIs studied for cocrystallisation are

classified as BCS II drugs, which have high permeability and low solubility. Thus, IDR is a good indicator for the *in vivo* absorption efficiency of APIs. Although the IDR is an important parameter to be investigated, it may become more complicated with cocrystals. Various factors need to be considered and extra experiments may be needed to obtain and interpret intrinsic dissolution data on cocrystals correctly [18]. Large amount of research has been carried out on cocrystal solubility and intrinsic dissolution behaviour, many instructive results have been obtained and these are selectively described as followings.

In Shiraki et al.'s stduy [82], the IDRs of two newly formed cocrystal EX-MAL and MA-SA have been improved compared to the respective original crystals. LEE studied the dissolution characteristics of an acetaminophen-theophylline (AT) cocrystal compared with its pure components and physical mixtures [87]. In Lee's research, intrinsic dissolution behaviour was conducted using a rotating disk. Results show that the AT cocrystal had a faster dissolution rate than AT physical mixtures, and the dissolution profiles were congruent (1:1 mole ratio) under different pH conditions. Although cocrystallisation method was developed to be an approach to improve the solubility and dissolution behaviour of API, not all the cocrystals exhibit better dissolution behaviour. Christine Grossjohann and coworkers examined the 1:1 cocrystal benzamide-dibenzyl sulfoxide, comprising the poorly water soluble dibenzyl sulfoxide (DBSO) and the more soluble benzamide (BA) [88]. Dissolution was examined through intrinsic dissolution studies. Dissolution studies revealed that dissolution of DBSO from the cocrystal was not enhanced in comparison to the pure compound or a physical mix. In some cases, the higher dissolution rate cannot obtain or maintain for longer time, this is due to a phenomenon 'solution mediated phase transformation' which will be discussed later in section 2.3.3.

2.2.6.5 Bioavailability

Bioavailability expresses the rate and extent of a drug which reaches into the systemic circulation, one of the principal pharmacokinetic properties of drugs. The ultimate goal for cocrystal investigation is to improve the bioavailability of an API. Animal bioavailability is an important parameter to consider when preparing new forms of a compound. There are limited numbers of animal bioavailability studies on cocrystals. The cocrystal of glutaric acid and 2-[4-(4-chloro-2-fluorphenoxy) phenyl] pyrimidine-4-carboxamide was used to demonstrate an improvement in the oral bioavailability of the API in dogs [42]. Single dose dog exposure studies confirmed that the cocrystal increased plasma AUC (area under the plasma concentration time curve) values by three times at two different dose levels. Another pharmacokinetic study on indomethacin-saccharin cocrystal also showed an improved bioavailability of cocrystal over pure API, indomethacin [70].

2.3 Theoretical development on solubility prediction of pharmaceutical cocrystals

2.3.1 Prediction of cocrystal solubility

Pharmaceutical cocrystals, which emerge as a potential approach to improve the solubility and dissolution of poorly water soluble drug, have attracted extensive research. However, true cocrystal solubility is not readily measured for highly soluble cocrystals because they can transform to the most stable drug form in solutions. Large amount of theoretical research on cocrystal solubility has been carried out with the purpose to provide a more appropriate method for cocrystal solubility measurement and explain the mechanism of solubility improvement by cocrystal. Rodr ́guez-Hornedo's research group has done lots contribution on cocrystal solubitliy study. In one of Rodriguez-Hornedo's study, the solubility and thermodynamic stability of pharmaceutical cocrystals has been predicted based on eutectic point information [84, 86].

Definition of cocrystal eutectic point

The cocrystal eutectic point or transition concentration, invariant point, is a key parameter that establishes the regions of thermodynamic stability of cocrystal relative to its components [84-86]. This is an isothermal invariant point where two solid phases coexist in equilibrium with solution. For poorly water soluble drugs and more soluble coformers, we consider the eutectic point for solid drug and cocrystal in equilibrium with solution.

Cocrystal eutectic constants and prediction of solubility behavior

In Rodriguez-Hornedo's publication [86], the cocrystal to drug solubility ratio (α) is shown to determine the excess eutectic coformer concentration and the eutectic constant (K_{eu}), which is the ratio of solution concentrations of cocrystal components at the eutectic point. The solution eutectic composition and cocrystal solubility ratio are a function of component ionization, complexation, solvent, and stoichiometry. These fundamental relationships can be applied to predict the solubility and thermodynamic stability of new cocrystals.

Three equations and equilibrium constants are considered to predict the cocrystal solubility, eutectic composition, and solution complexation from the eutectic of solid drug A and cocrystal A_yB_z where B is coformer

$$A_{solid} \rightleftharpoons A_{soln} \qquad S_{drug} = a_{drug} \qquad \text{(Equ.2-1)}$$

$$A_yB_{z\,solid} \rightleftharpoons yA_{soln} + zB_{soln} \qquad K_{sp} = a_{drug}^{y} a_{coformer}^{z} \qquad \text{(Equ.2-2)}$$

$$A_{soln} + B_{soln} \rightleftharpoons AB_{soln} \qquad K_{11} = \frac{a_{complex}}{a_{drug} a_{coformer}} \qquad \text{(Equ.2-3)}$$

where S_{drug}, K_{sp}, and K_{11} are the intrinsic drug soubility in pure solvent, cocrystal solubility product, and complexation constant, respectively. Combining S_{drug}, K_{sp}, and K_{11} gives the concenteration of complex at the eutectic as

$$[AB]_{soln} = K_{11}\left(K_{sp}S_{drug}^{(z-y)}\right)^{1/z} \qquad \text{(Equ.2-4)}$$

As described in definition of cocrystal eutectic point section, for poorly water soluble drugs and more soluble coformers, we consider the eutectic for solid drug and cocrystal in equilibrium with solution. This eutectic is most relevant for describing cocrystal solubility, stability, and equilibrium behavior relative to the drug. The eutectic constant (K_{eu}) is the concentration ratio of total coformer to total drug that satisfies the equilibrium Equ.2-1 to 3.

$$K_{eu} = \frac{[B]_{eu}}{[A]_{eu}} = \frac{[B]+[AB]}{[A]+[AB]}$$

$$= \left[\frac{\left(K_{sp}/S_{drug}^{y}\right)^{1/z}+K_{11}\left(K_{sp}S_{drug}^{(z-y)}\right)^{1/z}}{S_{drug}+K_{11}\left(K_{sp}S_{drug}^{(z-y)}\right)^{1/z}}\right] \qquad \text{(Equ.2-5)}$$

Considerations of ionization for either component can be added to this equation. For the case of a monoprotic acidic coformer and basic drug Equ.2-5 is rewritten as

$$K_{eu} = \frac{[B]_{eu}}{[A]_{eu}} = \frac{[B]_{unionized}+[B]_{ionized}+[AB]}{[A]_{unionized}+[A]_{ionized}+[AB]}$$

$$= \left[\frac{\left(\frac{K_{sp}}{S_{drug}^{y}}\right)^{1/z}\left(1+\frac{Ka_{coformer}}{[H^+]}\right)+K_{11}\left(K_{sp}S_{drug}^{(z-y)}\right)^{1/z}}{S_{drug}\left(1+\frac{[H^+]}{Ka_{drug}}\right)+K_{11}\left(K_{sp}S_{drug}^{(z-y)}\right)^{1/z}}\right] \qquad \text{(Equ.2-6)}$$

where $[H^+]$ is the hydrogen ion concentration and Ka is the dissociation constant for the acidic conformer or the conjugate acid of the basic drug. Considering the case of

components with multiple Ka values and negligible solution complexation the K_{eu} as a function of pH is

$$K_{eu} = \frac{\left(\frac{K_{sp}}{S_{drug}^{y}}\right)^{1/z}\left(1+\sum_{f=1}^{g}\frac{\prod_{h=1}^{f}Ka_{h}^{acidic}}{[H^{+}]^{f}}+\sum_{i=1}^{j}\frac{[H^{+}]^{i}}{\prod_{k=1}^{i}Ka_{k}^{basic}}\right)_{coformer}}{S_{drug}\left(1+\sum_{l=1}^{m}\frac{\prod_{n=1}^{l}Ka_{n}^{acidic}}{[H^{+}]^{l}}+\sum_{p=1}^{q}\frac{[H^{+}]^{p}}{\prod_{r=1}^{p}Ka_{r}^{basic}}\right)_{drug}} \qquad \text{(Equ.2-7)}$$

where *g* and *m* are the total number of acidic groups for each component and *j* and *q* are the total number of basic groups. In this case, the eutectic constant is a function of the cocrystal solubility product, drug solubility, and ionization. Letting the ionization terms for drug and coformer equal δ_{drug} and $\delta_{coformer}$ Equ.2-7 simplifies to

$$K_{eu} = \left(\frac{K_{sp}\delta_{coformer}^{z}}{S_{drug}^{(y+z)}\delta_{drug}^{z}}\right)^{1/z} \qquad \text{(Equ.2-8)}$$

K_{eu} can also be expressed as a function of the cocrystal to drug solubility ratio (α) in pure solvent using the previously described equation for cocrystal solubility [84]

$$K_{eu} = zy^{y/z}\alpha^{(y+z)/z} \qquad \text{(Equ.2-9)}$$

$$\text{where } \alpha = S_{cocrystal}/(S_{drug}\delta_{drug}) \qquad \text{(Equ.2-10)}$$

$$\text{and } S_{cocrystal} = \sqrt[y+z]{K_{sp}\delta_{coformer}^{z}\delta_{drug}^{y}/(y^{y}z^{z})} \qquad \text{(Equ.2-11)}$$

For a drug with known solubility, Equ.2-9 allows prediction of cocrystal solubility from the eutectic constant or vice versa. For a 1:1 cocrystal (i.e., y=z=1) Equ.2-9 becomes $K_{eu} = \alpha^2$ indicating that K_{eu} is the square of the solubility ratio of cocrystal to drug in pure solvent. Thus, a cocrystal with two times higher solubility has a four times greater K_{eu}. Furthermore, a K_{eu} greater than 1 indicates the 1:1 cocrystal is more soluble than the drug, whereas cocrystals less soluble than the drug have K_{eu} values below 1. The

derived equations apply to any ionization or temperature condition as long as the appropriate equilibrium constants and solubilities are taken into consideration.

Cocrystal transition concentration determination

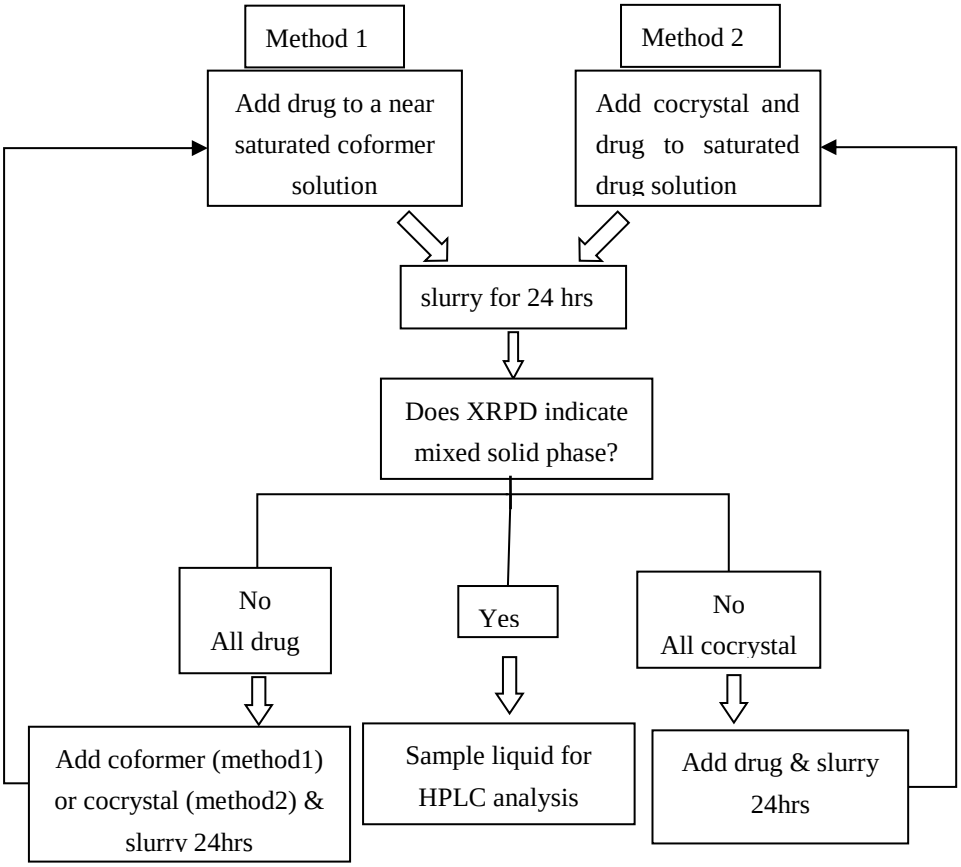

Fig. 2.4 Flowchart of method used to establish the invariant point and determine equilibrium solution transition concentrations of cocrystal components[84]

Methods used for the determination of transition concentrations C_{tr} hve been presented in David J. Good's publication [84]. A flowchart of two methods used to determine cocrystal transition concentrations is given in Fig. 2.4. Method 1: The measurements of cocrystal C_{tr} values were performed by precipitating cocrystal as a result of stirring excess solid drug in a coformer solution wherein cocrystal synthesis occurs through reaction crystallization method. Method 2: C_{tr} values were also obtained by dissolution of cocrystal in saturated drug solutions containing excess solid drug. Each cocrystal C_{tr} was determined from both supersaturated cocrystal conditions by reaction

crystallization method and from undersaturation by cocrystal dissolution. Samples were confirmed to have two solid phases (drug and cocrystal) at equilibrium for at least 24 hours before the solution was isolated from the solids and analysed by HPLC. An aliquot of the solid phase was isolated from solution for X-ray analysis then solid reactant(s) were added as required to reach mixed solid phase equilibrium. This process was repeated in 24 hours iterations until a stable mixed solid phase was achieved. Samples were held at constant temperature for all transition concentration measurements.

2.3.2 Cocrystal dissolution in surfactant solutions

Pharmaceutical cocrystals, as a promising way to improve the bioavailability of poorly soluble drug with higher aqueous solubility, its solubility and dissolution behaviour has been widely studied. The dissolution of cocrystals in surfactant solutions will be discussed in this section.

Cocrystal forms with higher solubility are however characterized by conversion to a less soluble form of the parent drug when exposed to solvent or solution. This phenomenon is called solution mediated phase transformation, which will be discussed in next section. Current approaches aim at delaying the conversion to drug but may require high additive levels to achieve transient stability. Neal Huang and Na ŕ Rodr ǵuez-Hornedo have discovered that micellar additives with different solubilisation capacity for cocrystal components, such as surfactants, impart thermodynamic stability to otherwise unstable cocrystal phases [89-91]. The theoretical foundation for controlling cocrystal solubility and stability is presented by considering the contributions of micellar solubilisation and ionization of cocrystal components [90]. For a 1:1 cocrystal RHA, where R represents a nonionizable drug, HA represents a weakly acidic coformer, and M represents micellar surfactant, the relevant equilibria are listed below,

$$RHA_{solid} \overset{K_{sp}}{\leftrightarrow} R_{aq} + HA_{aq} \quad \text{(Equ.2-12)}$$

$$HA_{aq} \overset{K_a}{\leftrightarrow} A^-_{aq} + H^+_{aq} \quad \text{(Equ.2-13)}$$

$$R_{aq} + M \overset{K_S^R}{\leftrightarrow} R_m \quad \text{(Equ.2-14)}$$

$$HA_{aq} + M \overset{K_S^{HA}}{\longleftrightarrow} HA_m \quad \text{(Equ.2-15)}$$

$$A^-_{aq} + M \overset{K_S^{A^-}}{\longleftrightarrow} A^-_m \quad \text{(Equ.2-16)}$$

The subscript aq denotes species in the aqueous phase. The subscript m refers to species in the micellar phase. K_{sp} is the cocrystal solubility product. K_a is the ionization constant for the coformer HA. K_S^R, K_S^{HA} and $K_S^{A^-}$ are the micellar solubilisation constants for cocrystal components and their ionized forms. Activities are replaced by concentrations as a first approximation applicable to dilute solutions. All the equilibrium constants used in above equations are given below, where the terms in brackets refer to concentrations.

$$K_{sp} = [\mathrm{R}]_{\mathrm{aq}}\mathrm{HA}_{\mathrm{aq}} \quad \text{(Equ.2-17)}$$

$$K_a = \frac{[\mathrm{A}^-]_{aq}[\mathrm{H}^+]_{\mathrm{aq}}}{[\mathrm{HA}]_{\mathrm{aq}}} \quad \text{(Equ.2-18)}$$

$$K_S^R = \frac{[\mathrm{R}]_{\mathrm{m}}}{[\mathrm{R}]_{\mathrm{aq}}[\mathrm{M}]} \quad \text{(Equ.2-19)}$$

$$K_S^{HA} = \frac{[\mathrm{HA}]_{\mathrm{m}}}{[\mathrm{HA}]_{\mathrm{aq}}[\mathrm{M}]} \quad \text{(Equ.2-20)}$$

$$K_S^{A-} = \frac{[A^-]_{\mathrm{m}}}{[A^-]_{\mathrm{aq}}[\mathrm{M}]} \quad \text{(Equ.2-21)}$$

Through derivation, the total solubility of cocrystal RHA, $S_{RHA,T}$, is expressed in terms of experimentally accessible solution properties as,

$$S_{RHA,T} = \sqrt{K_{sp}(1 + K_S^R[M])\left(1 + \frac{K_a}{[H^+]} + K_S^{HA}[M]\right)} \qquad \text{(Equ.2-22)}$$

where the micellar surfactant concentration [M] is the total surfactant concentration minus the critical micellar concentration (CMC).

It is evident from Equ.2-22 that cocrystal solubility is not linearly dependent on micellar concentration. This is in contrast to the linear dependence of the micellar solubilization of a single component solid phase of a nonionizable drug R:

$$S_{R,T} = S_{R,aq}(1 + K_S^R[M]) \qquad \text{(Equ.2-23)}$$

where $S_{R,aq}$ is the solubility of crystal R in the aqueous pseudo phase.

Eq. 2-22 and 2-23 are shown graphically in Fig. 2.5 for the case of a nonionizable, hydrophobic drug and its cocrystal with an ionizable, hydrophilic coformer, where $K_S^{HA} = 0$, and Equ.2-22 can be further simplified as

$$S_{RHA,T} = S_{RHA,aq}\sqrt{1 + K_S^R[M]} \qquad \text{(Equ.2-24)}$$

Fig. 2.5 (a) reveals that cocrystal and drug solubility surfaces intersect along a curve of given surfactant concentration and pH values and identifies stability region for cocrystal or drug by two critical parameters. The first parameter is the surfactant critical stabilization concentration (CSC) or the surfactant concentration where cocrystal and drug solid phases are in equilibrium with the solution. The second parameter is the pH_{max} or the pH value at the CSC. Fig. 2.5 (b) shows the distribution of the drug in micellar and aqueous environments. The cocrystal thermodynamic stability relative to the drug decreases with surfactant concentration. A thermodynamically unstable cocrystal in pure solvent becomes stable at the CSC where all curves intersect.

Cocrystal is more soluble than the drug below CSC, equally soluble to drug at CSC, and less soluble than the drug above CSC.

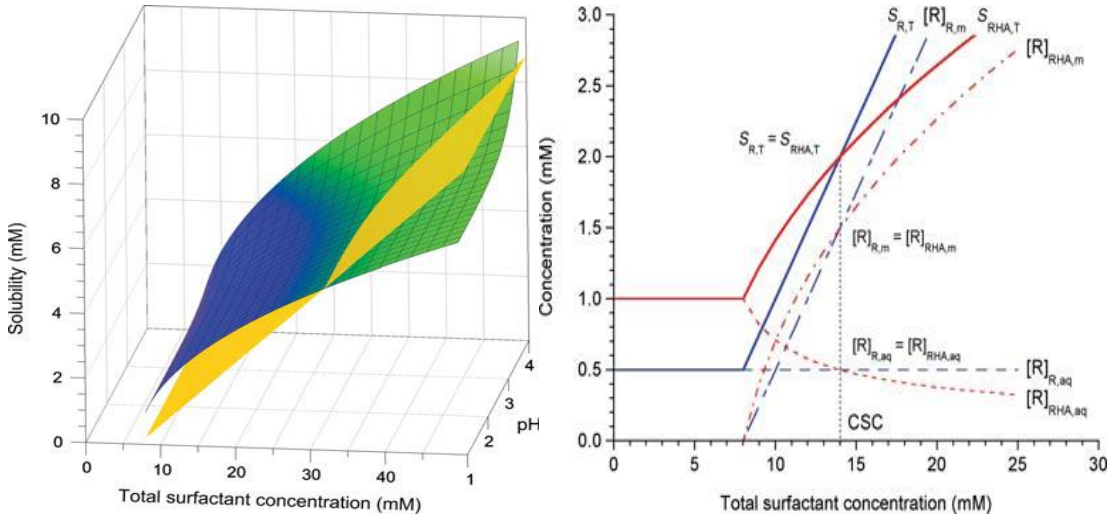

(a) (b)

Fig. 2.5 (a) cocrystal RHA(blue/green) and drug R (yellow) solubility dependence on surfactant concentration and pH (b) distribution of drug between the aqueous and micellar environments in surfactant solutions at equilibrium with cocrystal RHA and crystal R [90].

The existence of CSC and pH_{max} (in the case of ionisable cocrystal component) is a consequence of the lower rate of increase of cocrystal solubility with surfactant concentration as compared with that of drug solubility. It is evident from Equ. 2-24 and Equ. 2-23 that cocrystal solubility depends on $\sqrt{[M]}$ (when $K_s^{HA} = 0$), whereas the drug solubility depends on [M].

The theoretical analysis in this study demonstrates how surfactant additives with different solubilisation capacity for cocrystal components can impart thermodynamic stability to otherwise unstable cocrystal phases.

2.3.3 Solution mediated phase transformation

Solubility improvement of poorly soluble drug compounds is a key aspect to ensuring the successful development of many new drugs. Methods used to improve the solubility

of drug compounds include salt formation, forming an amorphous solid or dispersion and using a metastable polymorph, as well as cocrystal formation [48, 82, 87, 92]. All these solubility enhancement approaches can improve the drug dissolution rate which is one of the key factors affecting the drug absorption. However, these approaches can also result in a phenomenon called 'solution mediated phase transformation' (SMPT) which is crystallization of a stable solid phase during dissolution of a metastable phase caused by supersaturated conditions in solution or at the surface of the dissolving solid. A main concern of the SMPT is that the advantage of the improved drug dissolution rate could be lost if crystallization of a stable phase occurs during dissolution, as the dissolution rate will gradually change to that of the stable crystalline form [93].

SMPT is facilitated through exposure to a liquid. The SMPT can be described as three key stages: (1) dissolution of a metastable phase to create a local supersaturation, (2) nucleation of a stable phase, and (3) growth of the stable phase. Nucleation and growth of the more stable phase often occurs on the surface of the metastable phase, reducing the advantage of the formation of the drug metastable forms. Therefore, transformation to a less soluble solid during dissolution is an important aspect to consider when evaluating approaches to increase the solubility of a poorly soluble drug [93, 94].

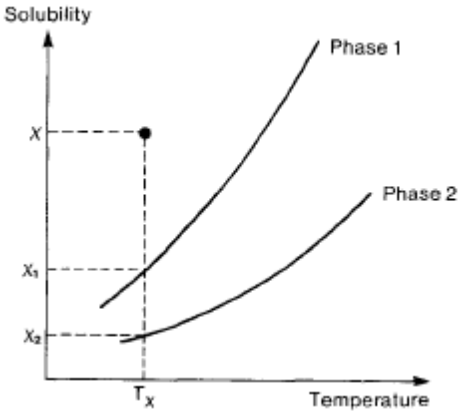

Fig. 2.6 Phase diagram for a monontropic system [94]

A detailed kinetic analysis is available for processes involving SMPT in Davey and Cardew's publication [94, 95]. SMPT can proceed by a mechanism in which crystals of the stable phase grow and those of the metastable phase dissolve. Davey and Cardew discussed the kinetic with a generalised phase diagram for a monotropic system, shown in Fig. 2.6. It is clear that for a solution having composition x and temperature T_x precipitation can yield both the metastable phase 1 and the stable phase 2. The composition x is supsaturated with metastable phase 1, thus metastable phase 1 first precipitation. The starting point for the transformation is slurry of monosized crystals of phase 1 in contact with a saturated solution containing nuclei of phase 2. As these nuclei grow so the solution composition falls below the solubility of phase 1 and the solution becomes undersaturated with respect to this phase. The crystals of phase 1 thus dissolve producing supersaturation for the continued growth of phase 2. This dissolution-growth process continues until all phase 1 has disappeared and the solution composition has fallen to the solubility of phase 2.

SMPT has been extensively studied for the formations of salts, polymorphs and amorphous solids over many years [96-107]. Recently, much work has been carried out to grow hollow needle crystals through the solvent mediated phase transitions [108-110]. However, there are very few reports on studies of the solution mediated phase transformation of cocrystals, among which different dissolution behaviours of cocrystals have been found [48, 80, 90, 92, 111, 112]. Some case studies about this aspect are selectively indicated as followings.

Lee studied the dissolution characteristics of an acetaminophen-theophylline (AT) cocrystal compared with its pure components and physical mixtures [87]. Results show that the AT cocrystal had a faster dissolution rate than AT physical mixtures. Thus, the AT cocrystal exhibited higher transient solubility compared with its two pure components. Equilibrium solubilities of theophylline from the cocrystal were lower than transient values due to SMPT of cocrystal to theophylline hydrate but no precipitation

of free acetaminophen occurred. Childs prepared three cocrystals of fluoxetine hydrochloride (FH) [80], which are 1:1 cocrystal of fluoxetine hydrochloride - benzoic acid (FH-BZ), 2:1 cocrystal of fluoxetine hydrochloride-succinic acid (FH-SC), and fluoxetine hydrochloride - fumaric acid (FH-FM). The results of IDR experiments show that cocrystals FH-BZ and FH-FM dissolve more slowly than FH, and cocrystal FH-SC dissolves more quickly than FH. Powder dissolution experiments demonstrated that the solid present at equilibrium corresponds to the cocrystal for FH-BZ and FH-FM, while FH-SC completely transformed to FH upon prolonged slurry in water. Researchers have found that a compound, AMG 517 formed a 1:1 co crystal with sorbic acid. During powder dissolution test, the concentration of drug dissolving from the cocrystal decrease from 10 times that of the parent drug at 1 hour to the same level of free drug at 2.5 hours due to the SMPT [72]. Another example, the powder dissolution rate of the fluoxetine HCl-succinic acid cocrystal exhibited 1.7 times that of fluoxetine HCl alone, but it decreased to the level of the pure drug in 20 minutes [80]. SMPT of both the indomethacin-saccharin and acetaminophen-theophylline cocrystals was affected by solution pH [48, 111]. The cocrystal of a low solubility compound with glutaric acid was found to have an IDR of the compound alone in water at 37°C and a SMPT started at 90 minutes [92]. It has been found that the mechanisms of dissolution enhancement of two cocrystals of Exemestane-maleic acid (EX-MAL) and Megestrol acetate-saccharin (MA-SA) were different, in which with the cocrystal EX-MAL, fine particle formation resulted in dissolution rate enhancement, whereas with the cocrystal MA-SA, enhancement was due to the maintenance of the cocrystal form and rapid dissolution before transformation to the original crystal [112].

Recently, the theoretical study of effects of surfactant additives on cocrystals dissolution, which described in former section, has shown that surfactants can impart thermodynamic stability to cocrystals that otherwise convert to parent drug solids in an aqueous solution [90]. SMPT also be applied to interpret the solvent-drop grinding

method of preparing cocrystals [37, 59, 61, 113]. In this manner, the solution mediated conversion is advantageous for controlling cocrystallization kinetics and polymorph selection. Although these transformations do not occur during a dissolution process, it is interesting to note this application of SMPT [93].

Characterisation of the solid state transition is important for SMPT phenomenon research. Much work has been done to monitor the solid phase transition during intrinsic dissolution in a channel flow-through dissolution apparatus using *in situ* Raman spectroscopic measurements. Combined with multivariate analysis techniques such as principal component analysis and partial least squares, Raman spectroscopy has demonstrated that it cannot only detect different crystallised solid forms but also quantitatively assess each of solid compositions, offering a deeper understanding of the SMPT phenomena during dissolution [106, 114-118].

2.4 Carbamazepine (CBZ) cocrystals studies

2.4.1 CBZ introduction

CBZ (5H-dibenz (b, f) azepine-5-carboxamide) (other brand name: Tegretol, Equetro, Epitol, et al.) was discovered by chemist Walter Schindler in 1953 [119], and now it is a widely prescribed anticonvulsant and mood-stabilizing drug used primarily in the treatment of epilepsy and bipolar disorder, as well as trigeminal neuralgia. CBZ with the chemical name of 5H-dibenz (b, f) azepine-5-carboxamide is a white or off-white powdered crystal. It has at least four anhydrous polymorphs, a dihydrate as well as other solvates [97, 120-123]. The molecule structure of CBZ is shown in Fig. 2.7. CBZ is classified as a class II drug, with the properties of low water solubility and high permeability, in the BCS. Solubility of CBZ has been studied by many researchers [99, 124-127]. Improving its solubility or dissolution rate can enhance the bioavailability of CBZ. Since CBZ has been discovered, large amount of research has been done on the formation, morphology, transformation, solubility and dissolution behavior of CBZ

aimed to improve the bioavailability of it.

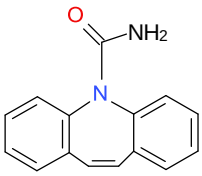

Fig. 2.7 Molecular structure of CBZ

At the beginning of this study, three candidate model drugs were valuated, which are indomethacin, ibuprofen, and CBZ. Indomethacin [1- (4-chlorobenzoyl) -5-methoxy-2-methyl-1H-indole-3-acetic acid] is a BCS class II drug with anti-inflammatory, antipyretic and analgesic properties. Indomethacin exists in polymorphic forms α and γ, and the latter of which is thermodynamically stable at room temperature and is practically insoluble in water. The poor solubility of indomethacin is claimed to be responsible for its low and erratic oral bioavailability. Ibuprofen, (RS) -2- (4-(2-methylpropyl) phenyl) propanoic acid, is a non-steroidal anti-inflammatory drug. It is used for the relief of arthritis, fever, as an analgesic, and additionally it possesses an antiplatelet effect. Ibuprofen is only very slightly soluble in water, less than 1 mg of ibuprofen dissolves in 1 mL water. In fact, indomethacin and ibuprofen has been classic model compounds for demonstrating the ability of cocrystallisation method to improve solubility and dissolution rate. Some research about cocrystallisation of indomethacin and ibuprofen has been reported [7, 22, 41, 48, 70]. So, at the beginning of this study, indomethacin and ibuprofen were also selected as candidate model drugs. But the preliminary UV imaging dissolution test of indomethacin and ibuprofen demonstrate that these two drugs are not suitable for UV imaging dissolution method. Indomethacin has an extraordinary slow dissolution rate which cannot be detected by UV imaging system after hours of dissolution. For ibuprofen, its compressibility is not suitable for UV imaging dissolution system. A firm ibuprofen sample compacts cannot be prepared. Ibuprofen solid sample will flow away under the dissolution flow medium

in few minutes after a sample compacts loading into the dissolution cell. Only CBZ exhibit a proper dissolution rate under the UV imaging dissolution test system. Finally, CBZ was selected as the only model drug for cocrystal preparation and dissolution study.

2.4.2 CBZ cocrystal studies

Recent years, pharmaceutical cocrystal emerges as a potential approach to enhance the solubility of poorly soluble drug, which has been applied to improve the CBZ solubility. About forty coformers have been reported in the literature can form cocrystals with CBZ, which have been summarized in Table 2.1. Quantitative research has been carried out on the formation, properties and bioavailability of CBZ cocrystals. As the result, many useful results have been obtained and these are selectively indicated as followings.

Table 2. 1 Examples of CBZ cocrystals reported in the literature

CBZ cocrystals	referrences
1:1 CBZ-acetone, 1:1 CBZ-DMSO, 2:1CBZ-terephthalaldehyde, 1:1 CBZ-acetic acid , 1:1 CBZ-butyric acid , 2:1CBZ- adamantane-1,3,5,7-tetracarboxylic acid, 1:1 CBZ-formamide	Fleischman[73]
1:1 CBZ-nicotinamide (NIC)	Weyna, Chieng et al. [37, 49, 73, 128-130]
2:1CBZ-benzoquinone	Weyna, Fleischman[37, 73] McMahon[131]
1:1 CBZ-saccharin,	Weyna, Fleischman et al. [37, 73, 132]
1:1 CBZ-trimesic acid, 1:1 CBZ-5-nitroisophthalic acid	Fleischman, McMahon [73, 131]
2:1 CBZ-4,4'-bipyridine, 1:1 CBZ-cinnamic acid, 2:1 CBZ-4-aminobenzoic acid,1:1CBZ-2,6-pyridinedicarboxylic acid	Weyna, McMahon [37, 131]
2:1 CBZ-succinic, 1:1 CBZ-benzoic, 1:1CBZ-ketoglutaric acid, 2:1 CBZ-maleic acid, 2:1 CBZ-glutaric acid, 2:1 CBZ-malonic acid, 2:1 CBZ-oxalic, 2:1 CBZ-adipic acid, 1:1 CBZ-camphoric acid, 1:1 CBZ-4-hydroxybenzoic acid, 1:1 CBZ-salicylic acid, 1:1 CBZ-1-Hydroxy-2-naphthoic, 1:1CBZ-DL-Tartaric, 1:1CBZ-L-Tartaric, CBZ-glycolic, CBZ-fumaric acid, CBZ-DL-malic acid, CBZ-L-malic acid	Childs[46]
1:1 CBZ-2,2,2-Trifluoroethanol	Lohani[133]
2:1 CBZ-furfural	Johnston[134]

1:1 CBZ-aspirin (acetylsalicylic acid)	Vishweshwar, McMahon et al. [37, 131, 135]
2:1 CBZ-terephthalaldehyde,	Weyna[37]
1:1 CBZ-isonicotinamide	Habgood[44]

2.4.2.1 CBZ cocrystals preparation strategies

Researchers have summarized that, generally, there are two strategies have been adopted for CBZ cocrystallisation: one strategy is to employ the peripheral hydrogen bonding capabilities that are not engaged in the pure form of CBZ; the second strategy involves breakage of the CBZ amide-amide dimer and formation of a supramolecular heterosynthon between CBZ and coformer [73]. The two strategies explain the formation of CBZ cocrystals on the molecular level. Both the two CBZ cocrystallisation strategies were employed by McMahon to prepare CBZ cocrystal with properly selected coformers [131], to exploit the hydrogen bonding capabilities of the primary amide moiety found in CBZ.

2.4.2.2 CBZ cocrystals preparation methods and kinetics

So far, lots CBZ cocrystals have been obtained by different preparation methods. In Childs' study [46], four different screening techniques were used to form CBZ cocrystals containing pharmaceutically acceptable carboxylic acids. Tween-seven unique solid phases utilizing eighteen carboxylic acid coformers were generated. This study demonstrated that CBZ cocrystals can be formed in aqueous media and the coformer solution concentration and solubility are important factors for the formation and stability of CBZ cocrystals. The CBZ-NIC cocrystal was chosen as a model system to study the reaction cocrystallization pathways and kinetics in aqueous and organic solvents by Rodr ǵuez-Hornedo[49]. Another example focused on solvent drop grinding as a method for CBZ cocrystallisation [37], and results revealed that eight CBZ cocrystals that were grown from solution can also be prepared by solvent drop grinding method. Recently, Di Profio's research group has prepared CBZ-saccharin cocrystals by using a new membrane-based technology [136]. Some research work has been carried

out to study on the CBZ cocrystal formation kinetics. Seefeldt investigated the cocrystallization pathways and kinetics of carbamazepine and NIC from amorphous equimolar phases [128]. The formation kinetics of CBZ-NIC cocrystal prepared by neat grinding with different initial polymorphic forms of CBZ (form I, III and dihydrate) were studied by Chieng et al.[129].

2.4.2.3 CBZ cocrystals properties studies

The stability of CBZ-NIC cocrystal prepared by neat grinding with different initial polymorphic forms of CBZ (form I, III and dihydrate) were studied by Chieng et al.[129]. CBZ-NIC cocrystals were stored under certain conditions with different temperatures and relative humidity for up to 28 days. Results showed that the CBZ-NIC cocrystal is stable when stored under elevated temperature and humidity conditions. Water molecules appear to have a significant effect on the stability of CBZ-NIC cocrystals: high humidity promotes cocrystal formation and stability during storage.

CBZ cocrystal has been compared with marketed products in Hickey's study [132]. The preparation of 1:1 cocrystal of CBZ-saccharin was achieved on a 30 g scale with a conventional cooling crystallisation process from alcohol solution without seeding. The study illustrates the utility of a cocrystal as a type of material that is suitable for drug development. The benefits of using the CBZ-saccharin cocrystal include (1) relative lack of polymorphism and equivalent chemical stability to the anhydrous polymorph, (2) favourable dissolution properties and suspension stability, and (3) comparable oral absorption profile in dogs compared with the commercial immediate release product.

Efforts have been made by Rodr ́guez-Hornedo's research group on studying the solubility and dissolution of CBZ cocrystals [84-86, 89-91, 137]. One of Rodr ́guez-Hornedo's research estimated the aqueous solubility for seven CBZ cocrystals [84], which was estimated to be 2-152 times greater than the solubility of the stable carbamazepine dihydrate form. Cocrystal solubility is shown to be directly proportional

to the solubility of constituent reactants for CBZ cocrystals. Another work by Rodr ǵuez-Hornedo developed a mathematical model that can be applied to describe the solubility of CBZ-NIC cocrystal in organic solvents [137]. Two CBZ cocrystals, 1:1 CBZ-salicylic acid (CBZ-SLC) cocrystal and 2:1 CBZ-4-aminobenzoic acid monohydrate (CBZ-4ABA-HYD) cocrystal, were prepared and used as model to study how ionization properties of cocrystal components modify the solubility-pH dependence of cocrystals [85]. Rodr ǵuez-Hornedo's research group has also studied how to engineer cocrystal solubility, thermodynamic stability, pH_{max}, and eutectic points by micellar solubilization using CBZ cocrystal sampels [89-91].

Limwikrant et al. characterized the CBZ-malonic acid (MA) cocrystal phases yielded via two different cogrinding methods and investigated the formation mechanism of any new polymorphs identified [138]. Two polymorphs of CBZ-NIC cocrystals and two polymorphs of CBZ-saccharin cocrystals were prepared and characterized by Adam J. Matzger [65]. These results are notable because CBZ-NIC and CBZ-saccharin are among the most widely studied pharmaceutical cocrystals.

2.4.2.4 CBZ cocrystals future research

As a typical BCS II drug, CBZ has been widely studied on cocrystallisation with the purpose to improving CBZ solubility. However, most of these research focused on new cocrystal screening and formation. Not so much research has been done on its dissolution and solubility studies.The final target of phamarceutical cocrystallization is to improve the bioavailbility, which need a throughly and better understanging of the dissolution and solutility properties of formed cocrystals. In this study, a new dissolution testing technique of UV imaging surface dissolution system was adopted to study CBZ cocrystals dissotluion and solubiltiy behaviour. Solution mediated phase transformation on CBZ cocrystals in solvent was studied. Investigation of the effects of surfactants on stablizing CBZ cocrystals has been done. CBZ cocrystals dissoltuion in

biomedia was carried out to study the relation of cocrystla dissoltuion *in vitro* and *in vivo*. All these reserarch has been performed around one purpose: to give a better understanding of pharmaceutical cocrystals dissoltuion and solubiltiy behaviour.

2.5 Introduction of pharmaceutical cocrystal coformers: nicotinamide and succinic acid

At the begging of this study, several coformers were screened to make cocrystal with the model drug of CBZ. Among these coformers, NIC is the most widely study coformer to cocrystallize with CBZ. Large amounts of research has been reported about CBZ-NIC cocrystal. For cocrystal dissoluiton testing by the UV imaging dissolution system method, it has one requirement that the API should have special UV absorbption wavelength, at which the coformer does not have aborption. As CBZ cocrystal coformer, NIC can meet this requirement for UV imaging method. We choose NIC as our first coformer. The second coformer, SUC acid, it represents a group of coformers: dicarboxylic acid coformer group. Dicarboxylic acid has make up the majority of CBZ cocrystal coformers. SUC is one of the dicarboxylic acid coformer which can meet the UV absorption requirement for UV imaging dissolution system method.

NIC (pyridine-3-carboxamide) is the amide of nicotinic acid (vitamin B_3). NIC is a water soluble vitamin and is part of the vitamin B group. It has four known polymorphs, I-IV, with the room temperature stable phase I melting at 129.5 ℃. The molecular stucture for NIC is shown in Fig. 2.8. The amide group in NIC is the most useful function group to form cocrystal through hydrogen bond [29]. NIC has been widely used in cocrystal formation, many NIC cocrystals have been reported, such as 1:1 trans-cinnamic acid-NIC cocrystal [139], 1:1 celecoxib-NIC cocrystal [140], ibuprofen-NIC cocrsytal [141], 1:1 theophylline-NIC cocrystal [17], 1:1 acetazolamide-NIC cocrystal [113]. And NIC has also been used as coformer to cocrystallize with CBZ, the most commonly reported drug to form cocrystal [37, 49, 73, 128-130].

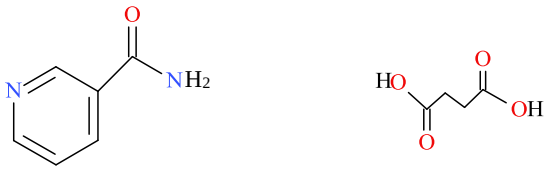

NIC SUC

Fig. 2.8 Molecular structures of NIC and SUC

SUC (butanedioic acid) is a diprotic, dicarboxylic acid with structural formula HOOC-(CH_2)2-COOH, shown in Fig.2.8. It is a white, odorless solid, melting at 184 ℃. Carboxylic acids have been investigated as cocrystal formers most extensively [29], which is attributable to that the carboxylic functional groups can serve as both hydrogen bond donor and acceptor to facilitate cocrystal formation. SUC as a dicarboxylic acid is one of the most common pharmaceutically acceptable cocrystal formers used in pharmaceutical cocrystals. Many SUC cocrystals have been sucessfully prepared, such as 2:1 piroxicam-SUC cocrystal [142], 2:1 meloxicam-SUC cocrystal [57], 2;1 CBZ-SUC cocrystal [46].

2.6 Definitions of basics of pharmaceutical physical chemistry [143]

Solution

A solution can be defined as a mixture of two or more components that form a single phase, which is homogeneous down to the molecular level. The two components are solvent and solute. Solvent determines the phase of the solution and usually constitutes the largest proportion of the system. Solutes are the components dispersed as molecules or ions throughout the solvent. Usually, the solutes are said to be dissolved in the solvent.

Solubility

The extent to which the dissolution proceeds under a given set of experimental conditions is referred to as the solubility of the solute in the solvent. Thus, the solubility of a substance is the amount of solute that passes into solution when equilibrium is established between the solution and excess substance (undissolved solute solid).

Type of solution

Solutions may be classified based on the physical phase of the solutes and solvent. Solutions studied in pharmaceutical research area all have liquid solvents. And, the solutes are predominantly in solid phase. Solutions talked about in this study are made with solid solutes in liquid solvents.

Ideal solutions and real solutions

Ideal solution is a solution with thermodynamic properties analogous to those of a mixture of ideal gases. The vapour pressure of the solution obeys Raoult's law, and the activity coefficient (which measures deviation from ideality) of each component is equal to one. Vapour pressure is referred to the pressure exerted by the vapour at equilibrium between the vaporous and liquid phases. Raoult's law states that the partial vapour pressure exerted by a volatile component in a solution at a given temperature is equal to the vapour pressure of the pure component at the same temperature. The majority of real solutions do not exhibit ideal behaviour, because the forces of interactions between the solute -solute, solute-solvent, and solute-solvent are unequal. These inequalities change the effective concentration of solute and solvent, and consequently, deviations from Raoult's law are exhibited by real solutions.

Ionization of solutes

Solutes have the ability to dissociate into ions when the dielectric constant of solvent is high enough to cause sufficient separation of the attractive force between the oppositely charged ions. The dissociation of water can be represented as,

$$H_2O \rightleftharpoons H^+ + OH^- \quad \text{(Equ. 2-25)}$$

In order to measure the concentration of H^+ in solutions, the concept of pH was introduced. pH is defined as,

$$pH = -\log_{10}[H^+] \quad \text{(Equ. 2-26)}$$

pH has important implications in pharmaceutical science.

Many drugs are weak acids or weak bases. For these drugs, equilibria exist between undissociated drug molecules and their ions in solutions. For a weak acid drug HA the equilibrium may be represented as,

$$HA \rightleftharpoons H^+ + A^- \quad \text{(Equ. 2-27)}$$

For a weak basic drug B, the equilibrium may be represented as,

$$B + H^+ \rightleftharpoons BH^+ \quad \text{(Equ. 2-28)}$$

The ionization constant K_a for weak acid is defined as following equation,

$$K_a = \frac{[H^+][A^-]}{[HA]} \quad \text{(Equ. 2-29)}$$

The symbol pKa is introduced to represent the negative logarithm of the acid dissociation constant Ka and equation 2-29 is rewritten as

$$pK_a = -\log_{10}K_a = -\log_{10}\frac{[H^+][A^-]}{[HA]} = pH + \log_{10}\frac{[HA]}{[A^-]} = pH + \log_{10}\frac{c_u}{c_i} \quad \text{(Equ. 2-30)}$$

c_u and c_i represent the concentrations of the unionized and ionized species respectively. This equation is named as the Henderson-Hasselbalch equation.

For weak base with one ionisable group, the Henderson-Hasselbalch equation can be obtained through the same derivation process, shown below

$$pK_a = pH + \log_{10} \frac{c_i}{c_u} \qquad \text{(Equ. 2-31)}$$

where c_i and c_u represent the concentrations of the protonated and unionized species in the solution. pKa values of drugs are very useful data to reflect the ionization behaviour of drugs, a series of important drugs' pKa values can be found in pharmaceutical handbook.

Kinetics of drug release

The kinetics of drug release have been widely studied. Many mathematical models and theories have been established aimed to give better understanding about the drug release process. Among these theories, diffusion is the principal release mechanism, which has been thoroughly studied. The diffusion controlled mathematical model of drug release is based on Higuchi model. Higuchi published a mathematical model on 1961 which can be used to illustrate drug release from diffusion-controlled systems[144]. He analysed the kinetics of release from an ointment assuming that the drug is homogeneously dispersed in the planar matrix and the medium into which it is released acts as a perfect sink under pseudo steady-state conditions. Higuchi derived following equation for the cumulative amount q(t) of drug released at time t:

$$\frac{q(t)}{q\infty} = K\sqrt{t} \qquad \text{(Equ. 2-32)}$$

where $q\infty$ is the cumulative amount of drug released at infinite time and K is a composite constant.

Noyes-Whitney equation describing the dissolution process

In 1897, Noyes and Whitney published mathematical model which provide a better way to understand the drug dissolution process [145]. The classic Noyes-Whitney equation described that the solid substance dissolution rate would be affected by its solution concentration, the equation is shown below:

$$\frac{dM}{dt} = k(C_s - C_i) \qquad \text{(Equ. 2-33)}$$

where dM/dt is the dissolution rate; dM is the amount of drug dissolved in unit time t;

k is dissolution rate constant; Cs is the solubility of the drug; Ci is the concentration of the dissolved drug.

Basics of drug molecule design[146]

Drug design, or rational drug design, is the inventive process of finding new medications based on the knowledge of biological target. The drug is usually an organic small molecule which activates or inhibits the function of a biomolecule such as a protein, which in turn results in therapeutic benefit to patients. The aims of drug design are to improve drug pharmacokinetic properties, to optimise chemical and metabolic stability, to optimise hydrophilic-hydrophobic balance. Drugs must have both hydrophilic and hydrophobic (lipophilic) characteristics. The hydrophilic characteristic of drug make it soluble in aqueous conditions, the hydrophobic characteristic facilitate the drug to permeate cross cell membranes. Usually, the larger alkyl group in drugs increase its hydrophobicity; the polar group increase its hydrophilic property. The hydrophilic and hydrophobic properties of drugs can be adjusted by removing or involving target function groups. A proper hydrophilic-hydrophobic balance help drug reach the desired therapeutic efficacy.

Biopharmaceutics classification system

The biopharmaceutics classification system (BCS) is a system to differentiate drugs on the basis of their solubility and permeability. According to the BCS, drug substances are classified into four classes based on their aqueous solubility and permeability membrane properties, shown in Fig. 2.9.

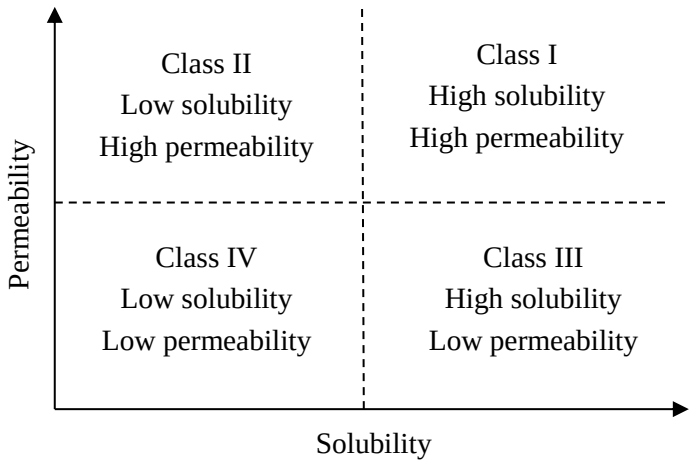

Fig. 2. 9 Biopharmaceutics classification system (BCS)

For BCS II and BCS IV drugs, the solubility enhancement can improve its oral bioavailability. Especially for BCS II drugs, which have low solubility and high permeability, solubility enhancement is an important strategy to improve the oral bioavailability. The model drug studied in this work, carbamazepine (CBZ), is a BCS II drug.

Therapeutic range profile

Therapeutic range refers to either the dosage range or blood plasma or serum concentration which can treat disease effectively while staying within the safety range. Fig. 2.10 shows a normal therapeutic range profile. From the figure, it can be seen clearly that when the drug concentration within the therapeutic range, it gives a relative

higher efficacy and very lower toxicity or adverse effects. Therapeutic range is an important parameter for medicine dosage development.

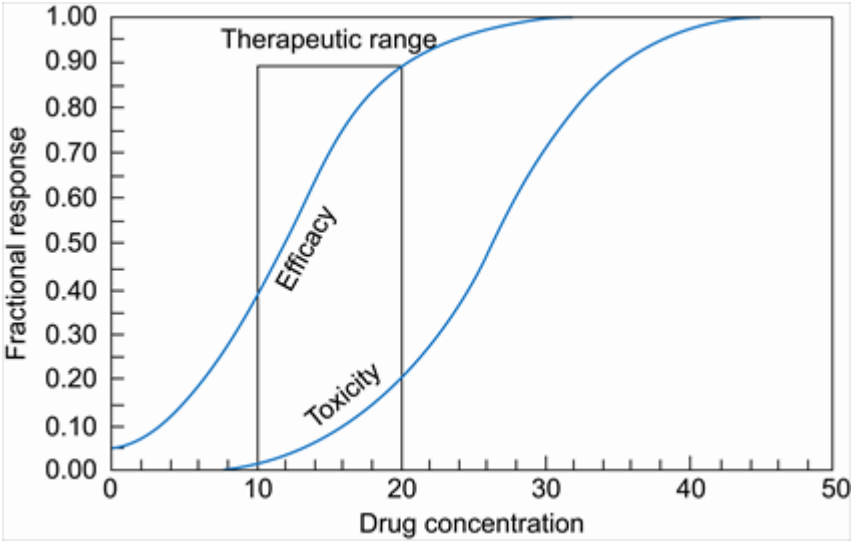

Fig.2. 10 Therapeutic range profile [147]

Polymorphism and transformation

In material sciences, polymorphism is a solid crystalline phenomenon of a given compound resulting from the ability of at least two different crystal structures of the molecules of that compound in the solid state. There are two types of polymorphism, monotropic and enantiotropic system. For a monotropic system, any transition between different polymorph is irreversible. For an enantiotropic system, it may be possible to convert reversibly between the two polymorphs on heating and cooling or through physical contact with a lower energy polymorph. For the model drug in this study CBZ, four polymorphs have been reported, CBZ form I to IV [148]. Among these polymorphs, CBZ form III is most stable form at room temperature and used in the marketed tablets products. CBZ III can transform to CBZ I through heating.

Polymorphism is very important in drug and commercial product development in the pharmaceutical industry due to the properties of formulated pharmaceutical products such as bioavailability and stability are often directly related with the physicochemical

and mechanical properties of the existing polymorphs in the formulation. In pharmaceutical industry, many drugs are under the regulatory approval for only a single crystal form or polymorph.

Phase diagram

Phase diagram is a chart used to show conditions at which thermodynamically distinct phases can occur at equilibrium. Lines in a phase diagram represents equilibrium or phase boundaries, which refer to lines that mark conditions under which multiple phases can coexist at equilibrium. Phase transition occurs along line of equilibrium.

Cocrystal system can be described by an isothermal ternary phase diagram. Typical phase diagrams for a 1:1 cocrystal are shown in Fig. 2.11. These phase diagrams contain the following information: three chemical constituents, which are two cocrystal components A and B, and the solvent; four phases, which are liquid, crystalline drug, coformer and cocrystal. The phases exsit in each region are: 1: solution; 2: A and solvent; 3: A and cocrystal; 4: B and solvent; 5: B and cocrystal; 6: cocrystal. The intersection points M and N are so called ‘‘invariants’’ or ‘‘eutectic’’. This is an isothermal invariant point where two solid phases (component A/B and cocrystal) coexist in equilibrium with solution.

In Fig. 2.11(1), A and B have similar solubilities in solvent and solution cocrystallisation with equimolar components will lead to the formation of the 1:1 cocrystal from solvent evaporation. Cocrystal components A and B have non-equivalent solubilities shown in Fig. 2.11(2) and solution cocrystallisation through evaporation of an equimolar solution may result in the formation of single component crystal. The reaction cocrystallisation approach has been adopted for this situation, which are performed by adding reactant B to a saturated or close to saturated solution of reactant A and then the solution becomes supersaturated with respect to cocrystal AB, where cocrystallisation proceeds along the route R as shown in Fig. 2.11(2). From descriptions

above, cocrystal ternary phase diagram can give instructions on cocrystallisation method selection.

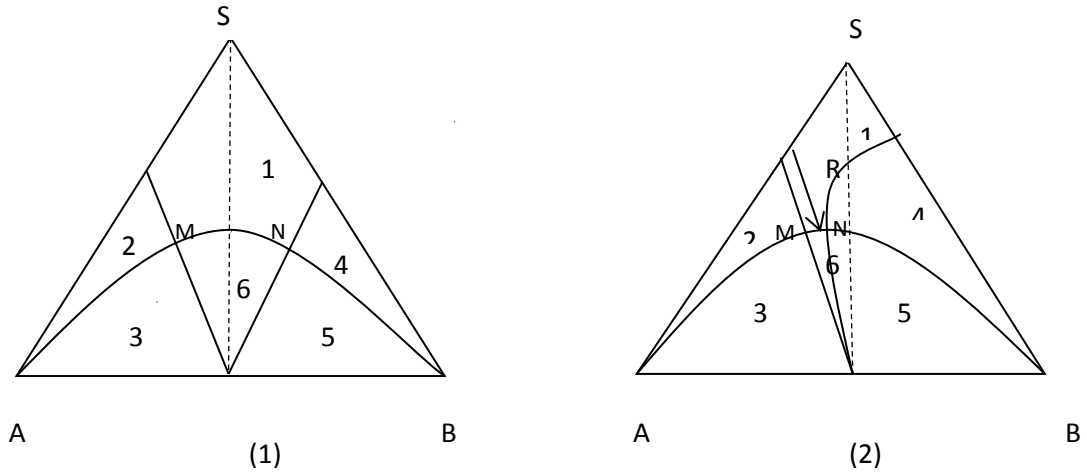

Fig.2. 11 Typical cocrystal isothermal ternary phase diagram

In vitro vs in vivo

In vitro dissolution studies of drugs means test the dissolution behaviour of drugs in test-tubes, flasks, or petri dishes etc. rather than in human or animal bodies. *In vivo* dissolution studies are testing drug dissolution behavior using a living organism. *In vivo* testing is often performed over *in vitro* because it is better suited for observing the overall effects of an experiment on a living subject. But *in vitro* dissolution studies are more widely employed at the beginning of drug development. The *in vitro* studies results can give some instruction for *in vivo* dissolution studies. The relationships between *in vitro* dissolution and *in vivo* input rate have been categorized into different levels. For novel drug delivery systems and modified release products, the establishment of *in vitro* dissolution and *in vivo* correlations helps in establishing dissolution specifications and allows the waiver for *in vivo* bioequivalence study[149].

2.7 Chapter conclusions

Pharmaceutical cocrystals, which emerge as a potential method for enhancing the bioavailability of drugs with low aqueous solubility, have attracted lots researchers' interest. In this chapter, a brief and systematic overview of pharmaceutical cocrystals was presented.

Firstly, concept and several key issues of pharmaceutical cocrystals including cocrystals formation theory, design strategies, formation methods, physicochemical properties studies, characterisation techniques were individually described. The fundament theory about cocrystal design was explained by crystal engineering. The pharmaceutical design strategy was illustrated by six steps in the design flowchart. Two main methods were introduced for pharmaceutical cocrystals formation, solution method and grinding method. Some analytical techniques, IR, Raman spectroscopy, and DSC et al. were introduced for physicochemical properties characterisation of cocrystals.

After the background review about pharmaceutical cocrystals, theoretical development on cocrystal solubility study was illustrated in this chapter. Cocrystal solubility and thermodynamic stability behaviour can be predicted by eutectic constant. The effects of surfactant on stabilizing cocrystal were studied to maintain the solubility advantage of pharmaceutical cocrystals. The phenomenon of SMPT happened during cocrystal dissolution process was introduced in this part.

Finally, pharmaceutical cocrystals research on CBZ, a BCS II drug, was reviewed. Two strategies for CBZ cocrystal preparation were given. Many reported CBZ cocrystals examples were introduced, including its formation strategies, preparation methods and kinetics, polymorph studies, properties compared with marketed products, et al. Opportunities for further development of CBZ pharmaceutical cocrystals were discussed at last.

Chapter 3 Materials and Methods

3.1 Chapter overview

In this chapter, materials and analytical methods used in this study were introduced. Firstly, all materials were given in details, including the name, formula, purity, and manufacturer.

Then, several analytical methods were introduced including IR, DSC, TGA, HPLC, light microscopy, UV-Vis spectroscopy, surface tension meter, SEM, UV imaging dissolution system, and Raman spectroscopy. These analytical approaches have been applied in order to identify the formation of cocrystal and characterise its physicochemical properties. FTIR and ATR-FTIR were used to perform qualitative analysis of cocrystal structure by providing IR spectrum. Raman spectrometer was employed to qualitative characterise cocrystal and quantitative analysis of phase transition of samples during dissolution process. DSC and TGA were utilised to do thermal analysis of tested samples. Leica microscope and SEM were used to do morphology characterisation of solid compacts in dissolution test. HPLC was used to measure the solubility. UV-Vis spectrometry was utilised to get the UV absorbance spectra of drugs and based on this information to select proper research samples for dissolution tests. CAM 200 surface tension meter was used to identify the critical micelle concentration of surfactant solutions through measure its surface tension. Specially, ActiPix D100 UV imaging dissolution system was utilised in this research to study dissolution behaviour. In this chapter, the analytical methods were introduced from the aspects of principle of these methods, instrumental models, experimental settings and operational procedures. Methods for measurement of cocrystal eutectic points and solubilities were also described in this chapter.

Finally, all sample preparation works in this thesis were presented. The preparations of five dissolution media (pH4.5 acetate buffer (0.06M), pH 1.2 HCl buffer, simulated gastric fluid (SGF), pH 6.8 phosphate buffer solution (PBS) and simulated intestinal fluid pH 6.8 (SIF)) were given. Different forms of CBZ, CBZ dihydrate (CBZ DH), and CBZ form I (CBZ I), were prepared. Two CBZ cocrystals were prepared, which are 1: 1 carbamazepine - nicotinamide (CBZ-NIC) cocrystal, and 2:1 carbamazepine - succinic acid (CBZ-SUC) cocrystal.

3.2 Materials

All materials were used as received, no further process on it.

Table 3.1 Raw materials for experiment

Materials	Formula	Purity/grade	Manufacturer
carbamazepine form III	$C_{15}H_{12}N_2O$	≥99.0%	Sigma-Aldrich Company Ltd., Dorset, UK
nicotinamide	$C_6H_6N_2O$	≥99.5%	Sigma-Aldrich Company Ltd., Dorset, UK
succinic acid	$C_4H_6O_4$	≥99.0%	Sigma-Aldrich Company Ltd., Dorset, UK
ethyl acetate	$C_4H_8O_2$	>99%	Fisher Scientific, Loughborough, UK
ethanol	CH_3CH_2OH	>99%	Fisher Scientific, Loughborough, UK
sodium acetate	$C_2H_3NaO_2$	99%	Sigma-Aldrich Company Ltd., Dorset, UK
acetic acid	$C_2H_4O_2$	≥99.7%	Sigma-Aldrich Company Ltd., Dorset, UK
potassium bromide	KBr	≥99% purity, for spectroscopy IR grade	Fisher Scientific, Loughborough, UK
double distilled water	H_2O	double distilled	Lab made by Bi-Distiller (WSC044.MH3.7, Fistreem International Limited, Loughborough, UK)
Tween 80	$C_{64}H_{124}O_{26}$	≥99.0%	Fisher Scientific, Loughborough, UK
sodium lauryl sulfate	$NaC_{12}H_{25}SO_4$	>99%	Fisher Scientific, Loughborough, UK
methanol	CH_3OH	HPLC grade	Fisher Scientific, Loughborough, UK
sodium chloride	NaCl	≥99.5%	Sigma-Aldrich Company Ltd., Dorset, UK

potassium phosphate monobasic	KH_2PO_4	≥99.0%	Sigma-Aldrich Company Ltd., Dorset, UK
sodium hydroxide	NaOH	0.2M	Fisher Scientific, Loughborough, UK
hydrochloric acid	HCl	0.2M	Fisher Scientific, Loughborough, UK
hydrochloric acid	HCl	1M	Fisher Scientific, Loughborough, UK
pepsin powder	-	general purpose grade	Fisher Scientific, Loughborough, UK
pancreatin powder	-	for biochemistry	Fisher Scientific, Loughborough, UK
0.45 µm nylon syringe filter	-	-	Thermo Scientific Nalgene, Rochester, NY, USA

3.3 Methods

3.3.1 ActiPix SDI 300 UV imaging dissolution system

3.3.1.1 Introduction to UV imaging dissolution system

Traditional dissolution testing determines drug release to the bulk, but does not enable an understanding of the events happening close to the surface of a solid or a tablet. UV imaging is a new imaging approach that can be used to study the dissolution behavior of chemical compounds. UV imaging instrumentation offers recording of absorbance maps with a high spatial and temporal resolution which facilitates the abundant collection of information regarding the evolving solution concentrations [150]. A lot of researches have been carried out to develop the utility of SDI 300UV imaging dissolutions system, many accomplishments have been obtained [151-153].

An ActiPix SDI 300 UV surface imaging system (Paraytec Ltd., York, UK) was used to study the dissolution behaviour in this work. The system is shown in the photograph in Fig. 3.1. ActiPix SDI 300 UV surface imaging system is a new technology that has been designed to improve our understanding of the kinetics and mechanism of drug substance release into dissolution medium. It has the ability to offer a better handle on oral dosage drug product development by looking directly at the solid-liquid interface during the

dissolution process. The fundamental theory for the design and development of UV imaging dissolution system relies on the fact that most pharmaceutical drug substances contain a UV chromophore, and that UV absorbance is a sensitive and robust measurement approach. The use of an imaging detector of UV surface imaging system can record a 2D UV movie of the dissolution process at the surface of a drug. With spatially resolved absorbance and thus concentration data, UV imaging system can give information on the concentration gradient and how it changes with experimental conditions.

Fig. 3.1 Photo of ActiPix SDI 300 UV surface imaging dissolution system

The ActiPix SDI 300 UV surface imaging system comprises a sample flow cell, syringe pump, temperature control unit, UV lamp and detector, and control and data analysis system [150, 152-155]. The schematic of ActiPix SDI 300 UV imaging system is shown in Fig. 3.2. The syringe pump is used for infusion of the dissolution medium which passes through the temperature control unit to the channel flow cell in which the dissolution process occurs. The main parts of flow cell cartridge are a Quartz cell (63mm×4mm×7mm (L×W×H)) and a plastic sample holder. Before a dissolution test starts, the sample compact is loaded on the sample holder and then inserted into the Quartz cell. The UV light source of SDI 300 UV imager is a pulsed Xenon lamp with a

replaceable wavelength filter. The detection area is a 9 mm×7 mm (1280×1024 pixels) complementary metal oxide semiconductor (CMOS) image sensor for recording light transmission through the flow cell.

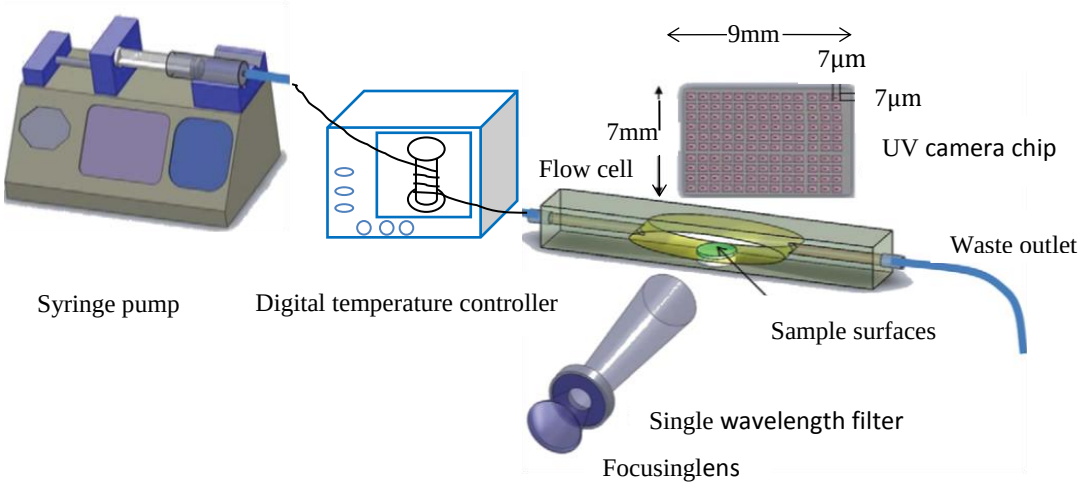

Fig. 3.2 Schematic of ActiPix SDI 300 dissolution system showing temperature controller, sample holder, dissolution flow cell, and UV imaging detector array

Real time UV image of absorbance map of tested sample during dissolution in flow cell can provided by UV imaging dissolution system, one UV image sample is shown in Fig. 3.3. In this image, the area in blue colour shows the background (pure buffer) absorbance and tense light colour indicates high absorbance at the lower right corner. The test sample was located at the bottom centre of image and the contours depict lines with the same absorbance. The absorbance map indicates the spatial concentration distribution of the dissolved sample in the flow cell at the recording time, which was affected by the flow rate and diffusion coefficient of target compound. In order to determine the rate of dissolution from the UV dissolution images recorded, an IDR of each image is calculated from the flow rate, absorbance intensities in the measurement zone, surface area of the compact and molecular weight and extinction coefficient of the drug.

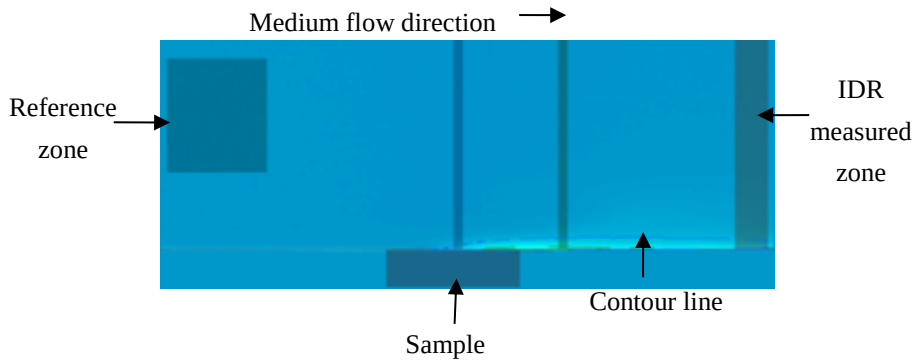

Fig. 3.3 UV image by SDI 300 UV imaging dissolution system

The build in software of UV imaging dissolution system can calculate and provide results of intrinsic dissolution rate (IDR) of tested samples based on following equations

$$IDR = \frac{\sum_{z=0}^{H/2} v_z M c_z W \Delta z}{S} \qquad \text{(Equ.3-1)}$$

$$v_z = \frac{3Q}{2HW}\left(1 - \frac{(2z-H)^2}{H^2}\right) \qquad \text{(Equ.3-2)}$$

where v_z = velocity at z; M = molecular weight; c_z = concentration at z; W = width of flow cell, see Fig. 3.4; Δz = effective pixel height; S = surface area of sample; H = height of low cell in observation region; Q = volume flow rate. Equ.3-1 and 3-2 are the equations used to combine molecular absorbance with the profile of fluid velocity. In summary, taken what is known about the molecule (molecular weight, extinction coefficient) and applied to absorbance data to arrive at a mass. This is the mass that passes through a measurement slit (Δz) at a given velocity (v_z), which is orthogonal to the solid surface. An integration of all the measurement slits divided by the exposed surface area returns the total mass removed from the solid surface.

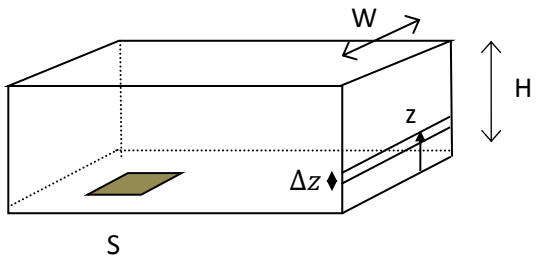

Fig. 3.4 Flow cell used in UV imaging system

3.3.1.2 Operation of UV imaging dissolution system

Filter selection for UV imaging system

Before dissolution testing, one proper UV filter should be selected for UV imaging dissolution system. The requirement for filter is that our target compound (CBZ) has obviously absorbance under the wavenumber of selected UV filter, while other components are not sensitive to this wavenumber. UV absorbance spectra of CBZ, NIC, and SUC were obtained and used for selection of an appropriate filter for UV imaging dissolution tests.

The UV spectra of CBZ, NIC, and SUC are shown in Fig. 3.5. CBZ has significant absorbance at 300 nm, while the SUC and NIC have no absorbance at this wavelength. This means the amount of CBZ in the mixture of CBZ and NIC or SUC can be quantitative analyzed by UV imaging dissolution system equipped with a 300 nm UV filter without disturbance of NIC or SUC. So, a UV filter with wavelength of 300 nm was selected for this study.

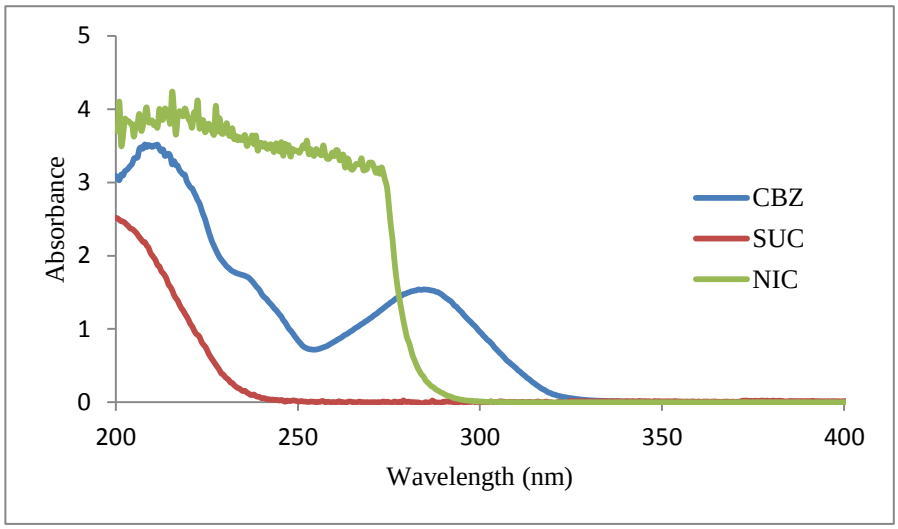

Fig. 3.5 UV spectra of CBZ, NIC, and SUC

UV imaging calibration

UV imaging calibration was performed by imaging a series of CBZ standard solutions in the test buffers with a series of different concentrations. The standard solutions were infused one by one from lower to higher concentrations, each of which was infused for several minutes at a flow rate of 1 mL/min. Buffer was infused before and after the series of standard solutions for several minutes in order to detect a baseline drift. The absorbance for each standard solution in each image was calculated by the average of a fixed absorbance area (width: from 2.1-7.0 mm; height: 1.0-2.5 mm) located in the centre of the viewing area. Experiments were repeated three times for construction of a UV calibration curve. Six calibrations were carried out in this study for CBZ tested by UV imaging in different buffers.

(1) Calibration in acetate buffer

UV imaging calibration was performed by imaging a series of CBZ standard solutions in the pH4.5 acetate buffer with concentrations of 4.23×10^{-3} mM, 2.12×10^{-2} mM, 4.23×10^{-2} mM, 1.27×10^{-1} mM, 2.12×10^{-1} mM, 3.17×10^{-1} mM, and 4.23×10^{-1} mM, at 37 °C. A calibration curve was obtained. The absorbance - concentration profile is obtained

by averaging time dependent absorbance profiles over the three calibration experiments. Because the absorption for 3.17×10^{-1} mM and 4.23×10^{-1} mM solutions have deviation from linearity, the five lowest concentrations were used to construct a CBZ calibration curve shown in Fig. 3.6. Calibration equation and molecular absorbance coefficient were shown in Table 3.2. The calibration curve was validated with a series of standard solutions with known concentrations, validation result was also shown in Table 3.2.

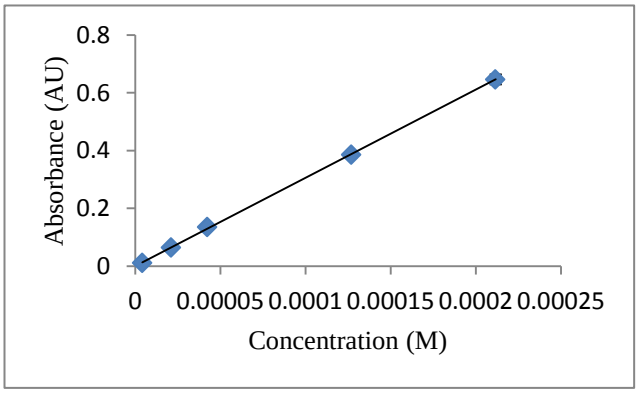

Fig. 3.6 UV imaging calibration curve: CBZ in pH 4.5 acetate buffer at 37 °C

(2) Calibration in water

UV imaging calibration was performed at 25 °C by imaging a series of CBZ standard solutions in pure water with concentrations of 4.23×10^{-3} mM, 2.12×10^{-2} mM, 4.23×10^{-2} mM, 8.46×10^{-2} mM, 1.69×10^{-1} mM, and 2.54×10^{-1} mM. Calibration curve is shown in Fig. 3.7.

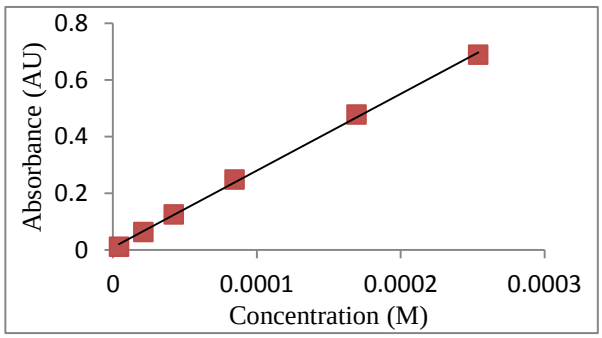

Fig. 3.7 UV imaging calibration curve: CBZ in H_2O at 25 °C

Calibration equation and molecular absorbance coefficient were shown in Table 3.2. The calibration curve was validated by a series of CBZ standard solutions in different surfactant concentration solutions, validation results shown in Table 3.2. The results show that SLS and Tween 80 did not affect the accuracy of the model and the calibration curve was applicable for the dissolution test with surfactant solutions.

(3) Calibration in four biomedia

UV imaging calibration was performed by imaging a series of CBZ standard solutions in four biomedia, including SGF, pH 1.2 buffer, pH 6.8 buffer and simulated intestinal SIF, at 37 °C. Prepare series of CBZ standard solutions with different concentration of 8.47×10^{-3} mM, 4.23×10^{-2} mM, 8.46×10^{-2} mM, 1.69×10^{-1} mM, 2.54×10^{-1} mM, and 3.39×10^{-1} mM. Calibration curves were constructed by plotting absorbance of each solution against its concentration, which were shown in Fig. 3.8.

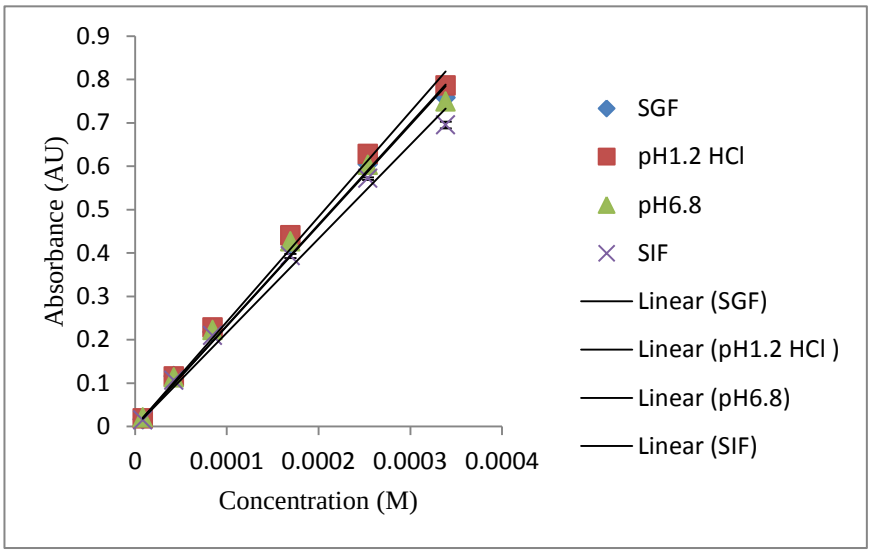

Fig. 3.8 UV imaging calibration curve: CBZ in SGF, pH 1.2 HCL buffer, pH6.8 PBS, and SIF (37°C)

Calibration equations and molecular absorbance coefficients of CBZ in different medium were listed in Table 3.2. The calibration curves were validated with standard solutions with known concentration in each of biomedium. Four solutions were tested

by UV imaging and the concentrations were calculated based on corresponding calibration curve, results shown in Table 3.2.

Table 3.2 UV imaging calibration curves for CBZ in different media, and validation results

media	calib equations (C[a] in unit of M)	ε[b] (m^2*mol^{-1})	validation		
			C_r [c] (mM)	C_m [d] (mM)	$\lvert C_m - C_r \rvert / C_r$%
acetate buffer	Y=(3053.5±20.4)×C, R^2=0.9999	763.4±5.1	8.5×10^{-2}	8.1×10^{-2}	4.7
H_2O	Y=(2762.3±17.7)×C, R^2=0.9999	690.6±4.4	1.7×10^{-1}[e]	1.8×10^{-1}	4.8
			2.5×10^{-1}[f]	2.5×10^{-1}	1.6
SGF	Y=(2327.1±2.3)C, R^2=0.9995	581.8±0.57	2.1×10^{-1}	2.2×10^{-1}	4.4
pH1.2 HCl	Y= (2418.2±30.0)C, R^2=0.9956	604.6±7.5	2.1×10^{-1}	2.2×10^{-1}	5.3
pH6.8 PBS	Y=(2317.1±29.0)C, R^2=0.9914	579.3±7.3	2.1×10^{-1}	2.3×10^{-1}	6.3
SIF	Y= (2165.1±17.6)C, R^2=0.9905	541.3±4.4	2.1×10^{-1}	2.0×10^{-1}	5.9

a: CBZ concentration

b: molecular absorbance coefficient

c: real concentration of validation standard solutions

d: measured concentration of validation standard solutions

e: add10.403 mM SLS in H_2O

f: add 7.634 mM Tween80 in H_2O

Sample compacts preparation

Before the UV imaging dissolution testing, test sample compacts need to be prepared, which was made by filling sample into sample cup (stainless steel cylinder, inner diameter: 2mm) and compressed with a set of press tools (shown in Fig. 3.9) which including: Quickset MINOR torque screw driver (Torqueleader, M.H.H. engineering Co. Ltd., England), pozi screw driver and three press plates. The details for sample compact preparation are: Tighten the middle plate to the base plate using pozi screw driver; insert one sample cup into the middle plate; insert the sample powder (around 5mg); insert the compression rod into the top plate; load the top plate into the middle plate through the location holes (the sample will stick to the compression rod); lightly tighten the top plate screws; set the scale on the torque wrench (40cNm used in this study); compress the sample with setted torque wrench, turn the wrench handle until it 'click', leave at compressed for 1 min then release the handle; take the sample cup out with pliers.

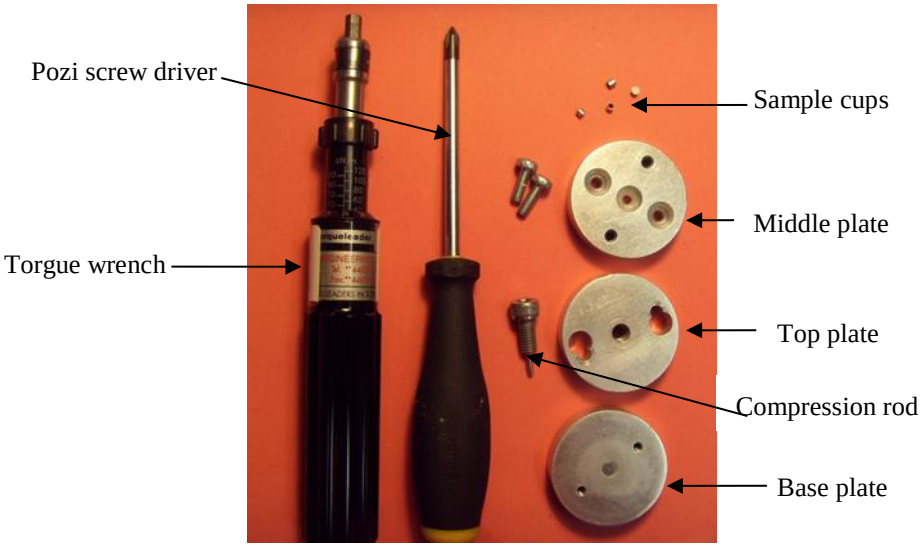

Fig. 3.9 UV imaging sample press tools

Dissolution testing procedures

When sample compact is ready, dissolution test can start. A dissolution test was performed as following: set up the equipment and fill the system with buffer; program the UV imaging test method; drive bubbles out of the cartridge to get a clear imaging area; start the test program; after recording a dark image and reference image, pause recording and insert a sample compact; fill the Quartz dissolution cell with buffer (1 mL/min) and make sure no bubbles in the cell or pipe, then start the pump programme and resume the UV image recording. Each sample has been tested in triplicate. When finish experiment, IDR can be calculated by the build in software through input some basic information about the testing, such as the molecular weight of sample, flow rate, and the molecular absorbance coefficient obtained through calibration.

3.3.2 Enspectr R532 Raman spectrometry

3.3.2.1 Introduction to Enspectr R532 Raman spectrometry

Raman spectroscopy is a spectroscopic technique used to observe vibrational, rotational, and other low-frequency modes in a system [156, 157]. It relies on Raman scattering, of monochromatic light, usually from a laser in the visible, near infrared, or near ultraviolet range. The Raman effect occurs when light impinges upon a molecule and interacts with the electron cloud and the bonds of that molecule. For the spontaneous Raman effect, which is a form of light scattering, a photon excites the molecule from the ground state to a virtual energy state, shown in Fig. 3.10 When the molecule relaxes it emits a photon and it returns to a different rotational or vibrational state. The difference in energy between the original state and this new state leads to a shift in the emitted photon's frequency away from the excitation wavelength. If the final vibrational state of the molecule is more energetic than the initial state, the emitted photon will be shifted to a lower frequency for the total energy of the system to remain balanced. This shift in frequency is designated as a Stokes shift. If the final vibrational state is less energetic than the initial state, then the emitted photon will be shifted to a higher frequency, and this is designated as an anti-Stokes shift. Raman scattering is an example of inelastic scattering because of the energy transfer between the photons and the molecules during their interaction. The shift in energy gives information about the vibrational modes in the system. Raman spectroscopy is commonly used in chemistry, since vibrational information is specific to the chemical bonds and symmetry of molecules. Therefore, it provides a fingerprint by which the molecule can be identified. A common laboratory instrument that uses this technique is a Raman spectrometer, which is used to get the Raman spectrum of test samples. Sample is illuminated with a laser beam. Light from the illuminated spot is collected with a lens and sent through a monochromator. Wavelengths close to the laser line due to elastic Rayleigh scattering are filtered out while the rest of the collected light is dispersed onto a detector.

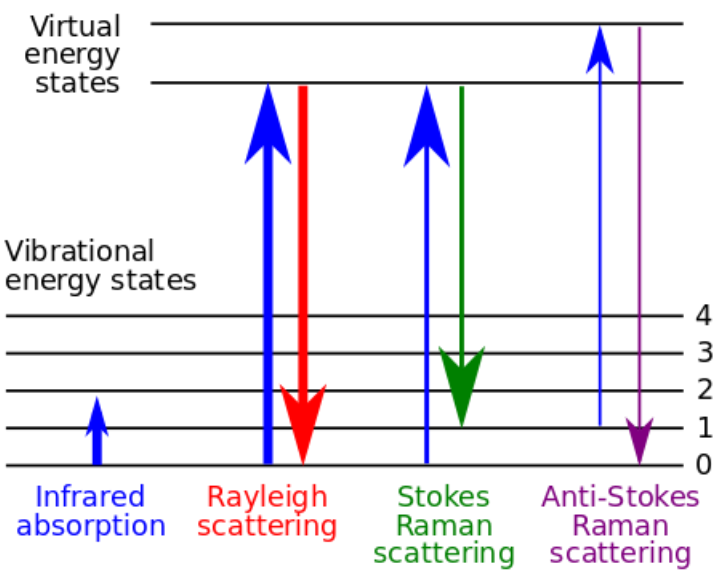

Fig. 3. 10 Energy-level diagram showing the states involved in Raman [157]

EnSpectr R532® Raman spectrometer (Enhanced Spectrometry, Inc., Torrance, USA), shown in Fig. 3.11, is used for measuring Raman spectra of liquids, solids, powders, and gels. The equipment set consists of a 20-30 mW output power laser source with a wavelength of 532 nm, Czerny-Turner spectrometer, scattered light collection and analysis system. The instrument is equipped with a low-noise multichannel detector for measurement of intensity and spectral parameters of scattered light. A built-in USB controller provides the PC connection. The equipment set consists of a single grating spectrometer without moving parts connected to a firmly fixed laser assembly. The spectral range of the equipment (140-6000 cm^{-1}) covers the vibration regions of organic and inorganic molecules as well as photoluminescence visible range. It takes one second to measure a spectrum of an unknown substance, determine positions and relative intensities of Raman and luminescence lines-the fingerprints of a substance under study, search and find the matching spectra in the reference database. In this study, EnSpectr R532® Raman spectrometer was used to measure Raman spectra and characterize samples.

Fig. 3.11 EnSpectr R532® Raman spectrometer

3.3.2.2 Operation of Enspectr R532 Raman spectrometry

Raman spectroscopy qualitative characterisation

Raman spectra were obtained using an EnSpectr R532® Raman spectrometer. The measurements were carried out at room temperature. The integration time was 200 milliseconds and each spectrum was obtained based on an average of 50 or 100 scans.

In situ Raman spectroscopy method

In situ monitoring of solution mediated phase transformations was carried out by the same Raman spectrometer as used in Raman spectra characterization, with a special sample stage connect to the spectrometer. The experiment set up is shown in Fig. 3.12. A test compact was immersed in a small cup with 5mL dissolution medium on an adjustable stage at room temperature. The spectrometer was fixed on the top of the stage vertically. The cup position can be controlled accurately at both vertical and horizontal directions to achieve a higher quality spectrum. The Raman spectra during *in situ* monitoring were automatically collected every 5 minutes for 3 hours controlled by a LabVIEW programme. The same integration time and scans were set for each spectrum

as those of the off-line measurements. Experiments of *in situ* Raman monitoring for each test sample were performed in triplicate.

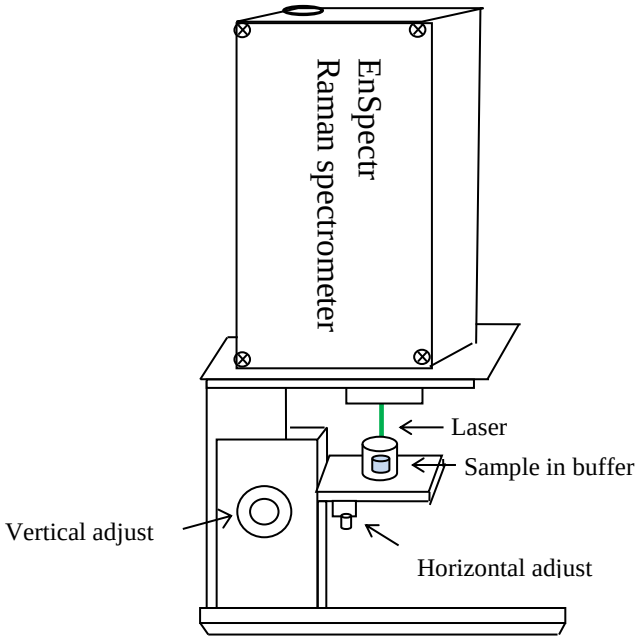

Fig. 3.12 Schematic diagram of in situ monitoring of dissolution by EnSpectr R532[@] Raman spectrometer

Raman spectroscopy quantitative characterisation

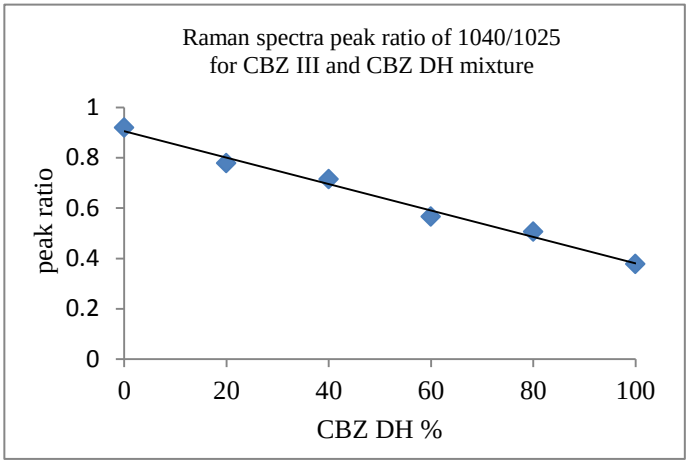

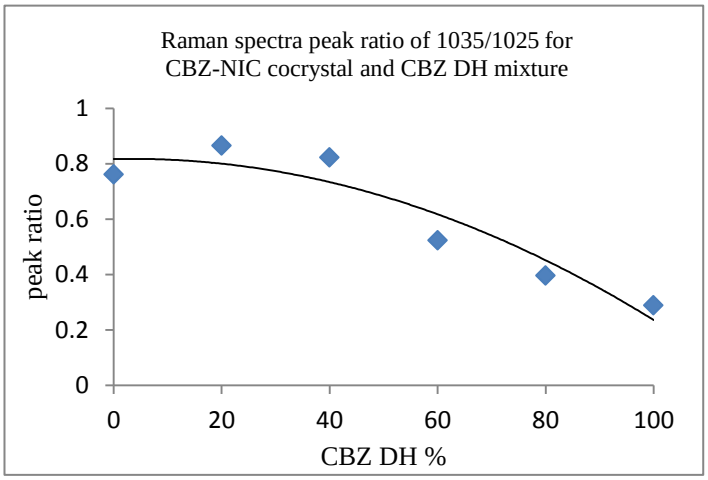

Fig. 3.13 Raman calibration curve for (a) mixture of CBZ III and CBZ DH; (b) mixture of CBZ-NIC cocrystal and CBZ DH

In order to quantify the percentage of CBZ DH crystallised during the dissolution of CBZ III and CBZ-NIC cocrystal, Raman calibration work has been done in the following steps. CBZ III and CBZ-NIC cocrystal were blended separately with CBZ DH to form binary physical mixtures at 20% (w/w) intervals from 0 to 100% of CBZ DH in the test samples. Each sample was prepared in triplicate and measured by Raman spectroscopy. Ratios of the characteristic peak intensities were used to construct the calibration models (details about characteristic peak were described in Chapter 4). For CBZ III and CBZ DH mixture, the ratio of peak intensity at 1040 to 1025 cm^{-1} were used to make calibration curve; for CBZ-NIC cocrystal and CBZ DH mixture, the ratio of peak intensity at 1035 to 1025 cm^{-1} were used to make calibration curve. Calibration curves for CBZ III and CBZ DH mixture, CBZ-NIC cocrystal and CBZ DH mixture were obtained and shown in Fig. 3.13. Equations fitted for the calibration cuves were shown in Table 3.3. The calibration equations were validated by mixtures with known proportions, and the results for validation were shown in Table 3.3.

Table 3.3 Raman calibration equations and validations

mixture	calib equations	validation		
		P_{DH}^{r}	P_{DH}^{m}	$\lvert P_{DH}^{m} - P_{DH}^{r} \rvert / P_{DH}^{r}\%$

CBZ III and CBZ DH	$y = -0.0053x + 0.9057$ $R^2 = 0.9894$	70	73	4
CBZ-NIC cocrystal and CBZ DH	$y = -6E\text{-}05x^2 + 0.0004x + 0.8171$ $R^2 = 0.896$	70	82	17

y: characteristic peak ratio of 1040/1025 for CBZ III and CBZ DH mixture, and 1035/1025 for CBZ-NIC cocrystal and CBZ DH mixture

x: percentage of CBZ DH in the mixture

P_{DH}^{r}: real DH percentage

P_{DH}^{m}: measured DH percentage

3.3.3 Infrared (IR) Spectroscopy

3.3.3.1 Introduction to IR Spectroscopy[158]

IR spectroscopy is the spectroscopy of the infrared region of the electromagnetic spectrum. Infrared light has a longer wavelength and lower frequency than the visible light. The IR spectroscopy technique can be used to identify and qualitative study chemical molecules.

The fundamental theory underpinning IR spectroscopy is that molecules absorb specific frequencies which are characteristic of their structures. The frequencies of the absorbed radiations match the transition energy of the bonds or groups that vibrates. The energies are determined by the structure of the molecular potential energy surfaces, the associated vibronic coupling, and the masses of the atoms. The infrared spectra of samples can be recorded through passing a beam of infrared light through the samples. When the frequency of the IR is the same as the vibrational frequency of a bond, the absorption occurs. Determination of the transmitted light gives the quantitative information about absorbed energy for each frequency. Alternatively, the whole wavelength range is scanned at once using a Fourier transform instrument. Fourier transform infrared (FTIR) spectroscopy is a characterisation technique that capable to record infrared spectra. Infrared light is passing through an interferometer and then through the sample (or the sample first then interferometer). The distribution of infrared light that passes through the interferometer is changed by a moving mirror inside the

FTIR equipment. The signal directly recorded, named "interferogram", represents light output as a function of mirror position. Fourier transform data-processing technique transforms the raw data into the desired result (the sample's spectrum): Light output as a function of infrared wavelength (or wavenumber).

3.3.3.2 Operation of IR Spectroscopy

Two FTIR spectrometer techniques were used in this study, which are Shimadzu FTIR-8300 (Shimadzu Europa, Milton Keynes, UK) and ALPHA A4 sized Benchtop Attenuated total reflectance-fourier transform infrared spectroscopy (ATR-FTIR) (Bruker UK Limited).

Measurement settings for Shimadzu FTIR-8300are: resolution 4 cm^{-1}, data range 4000-400 cm^{-1}, and number of runs per spectrum 5, sample was prepared using the KBr pellet technique. Sample was prepared according to next procedures: 1) small amount of test sample was mixed thoroughly with relative more KBr (three spatulas of sample mixed with seven spatulas of KBr) in a mortar while grinding with the pestle; 2) appropriate amount of mixed sample and KBr powder was added to cover bottom in IR sample pellet die; 3) Place the die in press and press at 5000-10000 psi; 4) carefully remove the pressed sample from die and place in the FTIR sample holder and the sample was ready for testing. Before testing sample, a reference sample was tested by the FTIR as background.

ALPHA A4 sized Benchtop ATR-FTIR spectrometer was used in later part of this study for IR spectra measurement. ATR is the abbreviation of Attenuated total reflectance. It is a sampling technique used in conjunction with infrared spectroscopy which enables samples to be examined directly in the solid or liquid state without further preparation. Measurement settings for ALPHA ATR-FTIR are: resolution 2cm^{-1}, data range 4000-400 cm^{-1}. The ALPHA ATR-FTIR spectrometer has a smaller size which occupies the footprint of an A4 sheet of paper. ALPHA ATR-FTIR spectrometer equipped with a

single-reflection diamond ATR sampling module, which make the sample handling greatly simplified. Sample can be tested directly without pre-processing.

3.3.4 Ultraviolet–visible spectrometry (UV-Vis)

UV-Vis is the absorption spectroscopy in the ultraviolet-visible electromagnetic spectral region. In the UV-Vis electromagnetic spectrum region, chemical molecules undergo electronic transitions. Molecules which contain π-electrons or non-bonding electrons can absorb the energy in the form of ultraviolet or visible light to excite these electrons from the ground state to higher anti-bonding molecular orbitals.

The apparatus used in ultraviolet-visible spectroscopy technique is called UV-Vis spectrophotometer. A UV-Vis spectrophotometer is composed with the following basic parts: a light source, a sample holder, a diffraction grating in a monochromator or a prism used for separating the different wavelengths of light, and a detector. UV spectrophotometer can be employed to measure UV absorbance map of samples through scan the sample solutions in a UV wavelength range. And UV-Vis spectrophotometer can also be used to do quantitative analysis based on Beer-Lambert Law. The Beer-Lambert law states that the UV absorbance of a sample solution is directly proportional to the concentration of the absorbing species and the path length. Thus, for a fixed path length, UV-Vis spectroscopy can be used to measure the concentration of the absorbing species in a solution.

UV-Vis spectrophotometer measures the intensity of light passing through a sample solution, and compares it to the intensity of light before it passes through the sample. The Beer-Lambert law, shown as following Equ.3-1,

$$A = \log_{10}\left(\frac{I_0}{I}\right) = \epsilon \cdot C \cdot L \qquad \text{(Equ. 3-1)}$$

where A is the measured absorbance, I is the transmitted intensity at a given wavelength, I_0 is the intensity of the incident light, L is the path length through the sample solution, and C is the concentration of the absorber. For each species and wavelength, ϵ is a constant named as the molar absorptivity or molecular extinction coefficient. The value for ϵ can be obtained through calibration curve. For calibration, a series of test sample solutions with known concentration are tested by UV-Vis spectrophotometer from lower concentration to higher concentration. Calibration curve is obtained by plotting the absorbance of each solution versus its concentration. The molecular extinction coefficient ϵ can be calculated from the gradient of the linear calibration curve.

In this study, UV spectra of CBZ, NIC and SUC were obtained using a Helios γ UV–Vis spectrophotometer (Thermo Electron Corporation, Cambridge, UK). Measurement settings for UV–Vis spectrophotometer are: resolution 2 cm^{-1}, data range 200 - 400 nm. The results were used for filter selection in UV imaging dissolution experiments.

3.3.5 Differential scanner calorimetry (DSC)

3.3.5.1 Introduction to DSC[159]

DSC is a thermoanalytical technique in which the thermal effects of tested samples, such as the melting point and enthalpies of phase transitions, can be measured. The fundamental theory for the DSC technique is that when the sample undergoes a physical transformation such as phase transitions, the amount of heat flow to the sample will change compared with the reference which tries to maintain both at the same temperature. Whether less or more heat the sample needed depends on whether the physical transformation process is exothermic or endothermic. When a sample undergoes the endothermic phase transition, like a solid sample melts to a liquid, it will require more heat flowing to the sample to increase its temperature at the same rate as the reference. On the other hand, when sample undergoes exothermic processes (such as

crystallization) less heat is needed to increase its temperature. Through observing the difference in heat flow between the sample and reference, DSC equipment is capable to measure the amount of heat absorbed or released during such physical phase transitions.

3.3.5.2 Operation of DSC

In this study, DSC measurements were conducted for all test samples using a Perkin Elmer Jade DSC (PerkinElmer Ltd, Beaconsfield, UK). The Jade DSC was controlled by Pyris Software. The temperature and heat flow of the instrument were calibrated using an indium and zinc standards. Test samples (8-10 mg) were analysed in crimped aluminium pans with pin-hole pierced lids. Measurements were carried out at a heating rate of 20°C/min under a nitrogen flow rate of 20 mL/min.

3.3.6 Thermal gravimetric analysis (TGA)

3.3.6.1 Introduction to TGA[160]

TGA is a method of thermal analysis in which changes in physical and chemical properties of materials are measured as a function of increasing temperature, or as a function of time. TGA is commonly used to determine selected characteristics of materials that exhibit either mass loss or gain due to decomposition, oxidation, or loss of volatiles (such as moisture).

The basic principle underlying TGA technique is a high degree of precision in three measurements: mass change, temperature, and temperature change. Thus, the basic parts of TGA apparatus are a precision balance with a pan loaded with the sample, and a programmable furnace. The furnace can be programmed in two ways: heating at a constant heating rate, or heating to acquire a constant mass loss with time. For a thermal gravimetric analysis by TGA apparatus, sample is continuously weighs as it is heated. As the temperature increasing, components of the sample are decomposed resulting in

the weight percentage of each mass change can be measured and recorded. TGA testing results are plotted with mass loss on the Y-axis versus temperature on the X-axis.

3.3.6.2 Operation of TGA

In this study, TGA for CBZ DH was run in a Perkin Elmer Pyris 1 TGA (PerkinElmer Ltd, Beaconsfield, UK). Weight calibration was performed using standard references of alumel and nickel. Samples (8-10 mg) in crucible baskets were used for TGA runs from 25-190°C with a constant heating rate of 20°C /min under a nitrogen purge flow rate of 20 mL/min. The water content of CBZ DH was obtained through TGA testing.

3.3.7 High performance liquid chromatography (HPLC)

3.3.7.1 Introduction to HPLC

HPLC is a chromatographic technique used to separate a mixture of compounds in analytical chemistry and biochemistry with the purpose of identifying, quantifying or purifying the individual components of the mixture. In HPLC, small volume of analyte is injected through a loop in a continuously flowing solution (mobile phase) that passes through a column packed with porous stationary phase (usually various surface-modified versions of silica). While passing through the column these analytes in solution are capable of interacting with end groups on the surface of the column. Given that different compounds have different affinity to the column content results in separation of compounds in the course of chromatography. The separated analytes then flow through a detector (usually UV-Vis) and the detector's readings are treated by instruments software and presented as a chromatogram showing the peaks which correspond to individual compounds eluted from the column. The time point that corresponds to the peak maximum is referred to the retention time, the area under the peak, width, and height of the peak of individual compound in the analyte are used for the quantitative analysis. In this study, HPLC technique is one of most important

techniques which has been used in lots quantitative analysis work for cocrystal solubility measurement.

3.3.7.2 Operation of HPLC

In this study, sample concentrations were analysed by Perkin Elmer series 200 HPLC system. A HAISLL 100 C18 column (5μm, 250×4.6mm) (Higgins Analytical, Inc. Mountain View, USA) at ambient temperature was used. The mobile phase composed of 70% methanol and 30% water, and the flow rate was 1mL/min using an isocratic method. Concentration of CBZ, NIC, and SUC has been measured under the wavelength of 285, 250, and 210 nm respectively. HPLC calibration has been done for the three chemicals; the standard curves were shown in Fig. 3.14. Calibration equations were listed in Table 3.4.

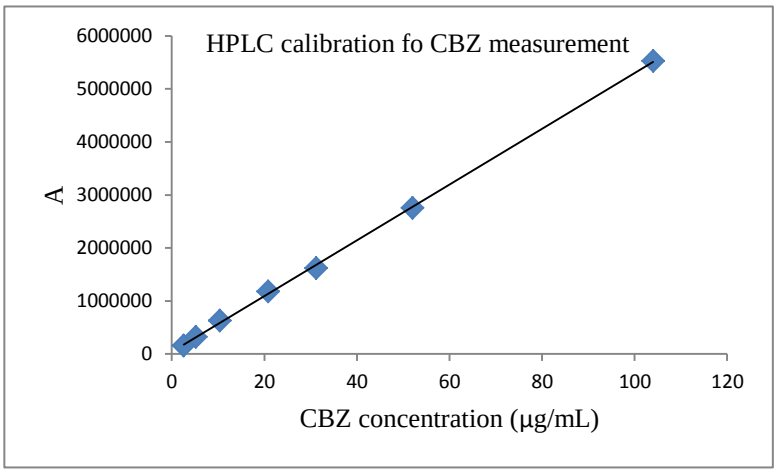

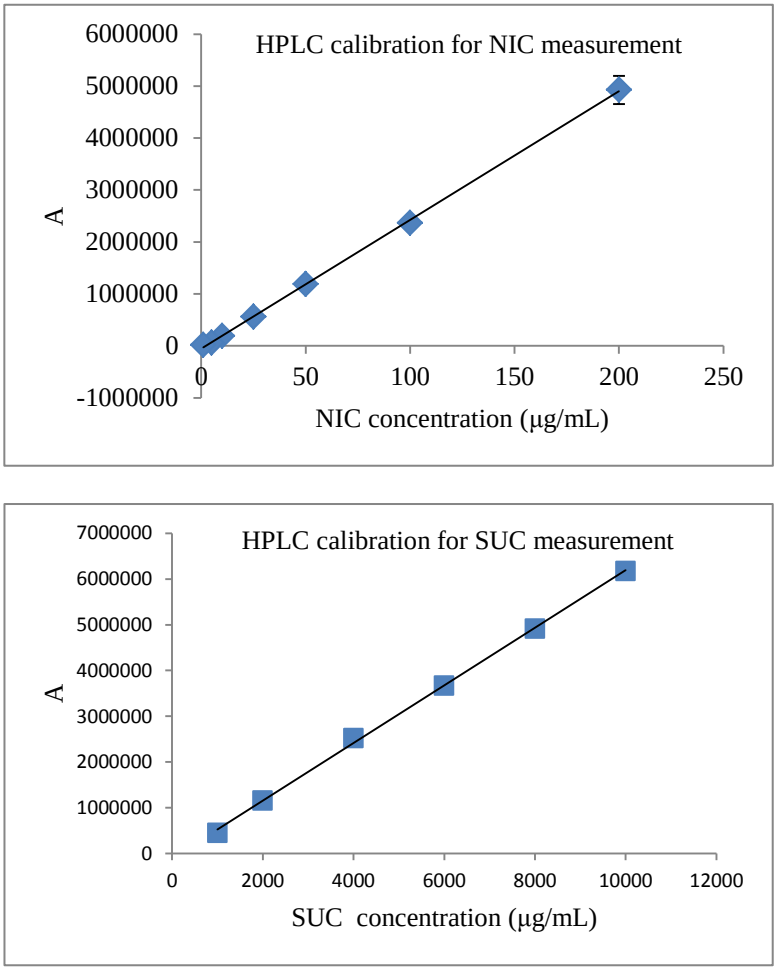

Fig. 3.14 HPLC calibration curve for measurement of (a) CBZ (b) NIC (c) SUC

HPLC calibration curves were validated by standard solutions of CBZ, NIC and SUC with known concentration, run the standard solutions and calculate its concentration using calibration curves respectively. The calculated concentrations were compared with real concentration, results shown in Table 3.4.

Table 3.4 HPLC calibration and validation

test sample	calib equations	validation		
		C_r	C_m	$\lvert C_m - C_r \rvert / C_r\%$
CBZ	y = 52569x+40920, R ²= 0.9996	50	51	2
NIC	y = 24761x-53758, R ²= 0.9997	100	97	3
SUC	y= 630.2x-105798, R ²= 0.9993	5000	5310	6

x: in unit of μg/mL

C_r: validation solution real concentration, μg/mL

C_m: validation solution measured concentration, μg/mL

3.3.8 Leica microscope

Microscope is an apparatus which can be used to observe samples that are too small for the naked eye. There are many types of microscopes. The most common type of microscope is the optical microscope which uses light to photo the sample. An optical microscope equipped with one or more lenses producing an enlarged image of sample. Optical microscopes contains refractive glass and occasionally of plastic or quartz, to focus light into the eyes or another light detector. The microscope used in this study is an optical microscope, LEICA DM 750 microscope.

LEICA DM 750 microscope equipped a lens of ten-time magnification, infinity 2-1C camera and Studio Capture Video microscopy software (version 4; Studio86 Designs, Lutterworth, UK) was used in this work to study the morphology of solid samples. All sample compacts were analysed prior to and after a UV imaging dissolution test using a LEICA DM 750 microscope.

3.3.9 Scanning electron microscope (SEM)[161]

SEM is an electron microscope that provides images of a sample through scanning the sample with a focused beam of electrons. Various signals produce as the resulting of interaction between electrons emitted by SEM and with atoms at or near the surface of the sample. These signals can be detected and provide information about the sample's surface topography and composition. The resolution of SEM can be better than one nanometer. Sample can be observed under different conditions: in high vacuum, low vacuum and in wet conditions.

The types of signals by a SEM mentioned in above paragraph include secondary electrons, characteristic X-rays, back-scattered electrons, light (cathodoluminescence), specimen current and transmitted electrons. In secondary electron imaging, the SEM can provide very high-resolution images of a sample surface, resolution less than 1

nanometer in size. Back-scattered electrons are beam electrons which are reflected from the sample by elastic scattering. Images produced by back-scattered electrons can provide information about the distribution of different elements in the sample. Characteristic X-rays are occurred as the result of the electron beam removes an inner shell electron from the sample, causing a higher-energy electron to fill the shell and release energy. The composition and the abundance of elements in samples can be determined by characteristic X-rays.

In this study, SEM micrographs were photographed by a ZEISS EVO HD 15 scanning electron microscope (Carl Zeiss NTS Ltd, Cambridge, UK). The test sample was mounted with Agar Scientific G3347N carbon adhesive tab on Agar Scientific G301 "0.5 aluminium specimen stub (Agar Scientific Ltd, Stansted, UK) and photographed at a voltage of 10.00KV.

3.3.10 CAM 200 surface tension meter

Surface tension is a contractive tendency of the surface of a liquid that allows it to resist an external force. Surface tension has the dimension of force per unit length or of energy per unit area. In this study, a KSV CAM 200 surface tension meter is used to measure the surface tension of surfactant solutions. KSV CAM 200 is a computer controlled and user programmable video based instrument designed for the measurement of: Surface and Interfacial tension, Static Contact Angles, Dynamic Contact Angles, and Surface Free Energy of Solids. The light source of CAM 200 is LED based. The LEDs are housed in a reflective sphere which integrates their light and directs it towards the sample. The light is strobed and monochromatic. These features help to assure a sharp image. CAM 200 uses a Jai CV-M50 monochrome video camera module using a CCD solid stage image sensor. The objective lens provided with the camera is telecentric with a 55 mm focus length. The result was analyzed by CAM200 software.

The critical micelle concentration (CMC) is defined as the concentration of surfactants above which micelles form and all additional surfactants added to the system go to micelles. CMC is an important characteristic of a surfactant, which can be determined from the break in the curve of surface tension versus log of surfactant concentration. In this study, the CMCs of two surfactants, SLS and Tween 80, were determined in aqueous solutions in the presence of saturated CBZ as following. A series of above surfactant solutions were prepared and the surface tensions of these solutions were tested by KSV CAM200 surface tension meter at room temperature. Figure has been drawn by plotting surface tensions vs. concentrations. As the concentration of surfactant increases, surface tension decreases and finally levels at the minimum value. The point where surface tension curve reach its minimum value is described as CMC, shown in Fig. 3.15.

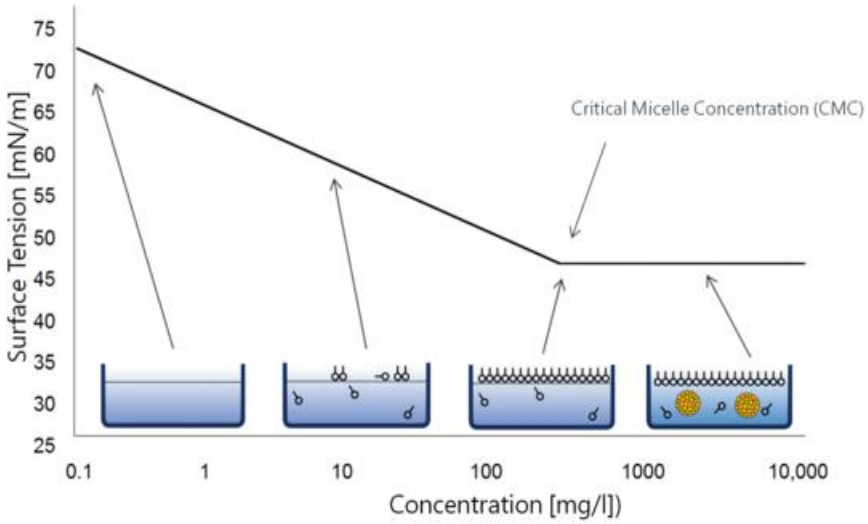

Fig. 3.15 Surface tension of a surfactant solution with increasing concentration, formation of micelles[162]

3.3.11 Solubility test methods

3.3.11.1 Equilibrium solubility test

In this study, all solubility tests were determined using an air-shaking bath method. Excess amount of samples were added into a small vial containing certain volume of media and vortexes for 20 seconds. The vials were placed in a horizontal air-shaking bath at certain temperature at 100 rpm for certain hours. Aliquots were filtered through 0.45μm filters (Thermo Scientific Nalgene, Rochester, NY, USA) and diluted properly for determination of the concentrations of targeted components by HPLC. Solid residues were retrieved from the solubility tests and air dried for 30 minutes. All of dried solids were characterized by FTIR, Raman and DSC. All solubility tests were carried out in triplicate.

3.3.11.2 Cocrystal eutectic points measurement test

The solubility of CBZ was measured as a function of the coformers' concentration in order to determine the eutectic point of cocrystal. To measure solubility of CBZ as function of coformers' concentration, known amounts of coformer of increasing concentration (initial coformer concentration) were dissolved in 5mL of buffer in screw capped vials. Then excess amount of solid CBZ DH was added to each vial. Air-shaking bath method was used to measure the solubilities of two components after certain time of equilibrium. Solid phases at equilibrium were confirmed by IR, Raman and DSC. All tests were carried out in triplicate.

Through the measurement of CBZ solubility as function of NIC in water at 25℃ [84, 86] using above method, eutectic point of CBZ-NIC cocrystal in water was determined. Then, CBZ-NIC cocrystal eutectic points were measured as a function of SLS or Tween 80 concentration in water at 25℃, by adding excess CBZ DH in a solution of mixture of surfactant and near saturated NIC for 72 hours equilibrium.

The solubility of CBZ as function of two coformers (NIC and SUC) in four media (pH 1.2 HCl buffer, pH 6.8 PBS, SGF, and SIF) was determined respectively using the same method above mentioned. The experiments were performed at 37°C for 24hours equilibrium.

3.4 Preparations

3.4.1 Dissolution media preparation

Five dissolution media were prepared in this work, which are pH4.5 acetate buffer (0.06M), pH 1.2 hydrochloric acid buffer (pH 1.2 HCl buffer), simulated gastric fluid (SGF), pH 6.8 phosphate buffer solution (PBS) and simulated intestinal fluid pH 6.8 (SIF). The preparation details for each medium are listed as following

pH4.5 acetate buffer (0.06M): Dissolve 2.99 g sodium acetate in water, add 14 mL of 2 M acetic acid (make up 60.05 g glacial acetic acid up to 500 mL with water), and dilute to 1000 mL with water [163].

pH 1.2 HCl buffer: Mix 250.0 mL of 0.2 M sodium chloride (Dissolve 11.69 g of sodium chloride in water and dilute to 1000.0 mL) and 425 mL of 0.2 M hydrochloric acid, and dilute to 1000.0 mL with water [164].

SGF: Dissolve 2.0 g of sodium chloride and 3.2 g of pepsin powder in water, add 80 mL of 1 M hydrochloric acid and dilute to 1000.0 mL with water [164].

pH 6.8 PBS: Mix 250.0 mL of 0.2 M potassium dihydrogen phosphate (KH_2PO4) and 112 mL of 0.2 M sodium hydroxide, and dilute to 1000.0 mL with water [164].

SIF: Mix 77.0 mL of 0.2 M sodium hydroxide (NaOH), 250.0 mL of a solution containing 6.8 g of potassium dihydrogen phosphate (KH_2PO4), and 500 mL of water.

Add 10.0 g of pancreas powder, mix and adjust the pH if necessary. Dilute to 1000.0 mL with water [164].

3.4.2 Test samples preparation

Preparation of Carbamazepine dihydrate (CBZ DH)

Excess amount of anhydrous CBZ III was added into double distilled water and stirred for 48 hours at constant temperature 37°C. The suspension was filtered and dried for 30 minutes on the filter. TGA was used to determine the water content in the isolated solid and confirm complete conversion to the hydrate.

Preparation of Carbamazepine form I (CBZ I)

CBZ I was prepared by heating CBZ III at 170°C in an oven for 2 hours [165]. Raman spectroscopy and DSC were used to confirm conversion of CBZ III to CBZ I.

Preparation of physical mixture of CBZ III and NIC (CBZ-NIC mixture)

1:1 molar ratio mixture of CBZ III and NIC was prepared by mixing 0.4 mmol CBZ III (94.5 mg) and 0.4 mmol NIC (48.8 mg) thoroughly.

Preparation of CBZ-NIC cocrystal

CBZ-NIC cocrystal was prepared through an evaporation method. A 1:1 molar ratio mixture of CBZ III (94.5 mg, 0.4 mmol) and NIC (48.8 mg, 0.4 mmol) was completely dissolved in 20 mL of ethyl acetate in a 50 mL conical flask with aid of stirring and slightly heating. The solution was allowed to evaporate in a controlled fume hood (room temperature, air flow 0.50-1.0 m/s). When all the solvent evaporated, solid product was obtained on the bottom of the flask. The approximate yield was 127.9 mg (89.3%).

Preparation of physical mixture of CBZ III and SUC (CBZ-SUC mixture)

2:1 molar ratio mixture of CBZ III and SUC was prepared by mixing 8 mmol CBZ III (1.8962 g) and 4 mmol SUC (0.4722 g) thoroughly.

Preparation of CBZ-SUC cocrystal

CBZ-SUC cocrystal was prepared according to the method described in Child's publication [46]. CBZ (8 mmol, 1.8962 g) and SUC (4 mmol, 0.4722 g) were dissolved in a mixture of 60 mL ethanol and 30 mL ethyl acetate with 30 minutes of sonication, followed by heating to 54 ℃ for approximately 45 minutes. The resulting clear solution was filtered through a 0.2 μm nylon filter into a clean glass jar and the jar was capped. White precipitate was observed after several minutes. The solution was allowed to evaporate slowly overnight (in fume hood without air flow), followed by fast evaporation for 2 days (in fume hood at air flow 0.50-1.0 m/s). The resulting dried solids were composed of blades and plates. The approximate yield was 2.2 g (93%).

3.5 Chapter conclusions

This chapter introduced all materials, methods, and sample preparation in this study. Firstly, all materials used in this study were presented in details，which including the name, formula, purity, and producer. Then, research methods including analytical techniques and experiments were introduced. A number of different analytical approaches have been applied to identify the formation of test samples and characterise its physicochemical properties, such as FTIR, ART-FTIR, Raman spectrometry, DSC, TGA, SEM et al. ActiPix SDI 300 UV imaging dissolution system, which used in the solubility and dissolution behaviour study of cocrystal, have been fully introduced in this chapter. Solubility test methods: air-shaking bath method for equilibrium solubility test; method for measurement of cocrystal eutectic points and critical micelle concentration were given in this chapter. Finally, test samples and dissolution media preparation were presented. Five dissolution media were used in this study, which are pH4.5 acetate buffer (0.06M), pH 1.2 HCl buffer, SGF, pH 6.8 PBS and SIF. The

preparation methods for different CBZ samples (CBZ I, CBZ DH, CBZ-NIC, CBZ-SUC cocrystals and mixtures) were introduced.

Chapter 4 Sample Characterisations

4.1 Chapter overview

In this chapter, test samples prepared in this study were characterized, and the characterisation results were discussed. Different forms of CBZ samples, CBZ DH, and CBZ I, and two CBZ cocrystals, CBZ-NIC cocrystal, and CBZ-SUC cocrystal, were characterised. Different characterisation techniques, such as TGA, Raman spectroscopy, IR spectroscopy, and DSC were used to characterise these newly formed products. Characterisation results were given and discussed. All characterisation results have demonstrated the successfully formation of CBZ I, CBZ DH and the two CBZ cocrystals. The molecule structures of CBZ-NIC cocrystal, and CBZ-SUC cocrystal were also presented in this chapter.

4.2 Materials and methods

4.2.1 Materials

Anhydrous CBZ III, NIC, and SUC, ethyl acetate, ethanol and potassium bromide were used in this chapter; details of this material can be found in chapter 3 materials and methods.

4.2.2 Methods

FTIR, ATR, Raman spectroscopy, DSC, TGA have been applied to do the characterisation. FTIR spectra of CBZ III, NIC, CBZ-NIC cocrystal and mixture were obtained by a Shimadzu FTIR-8300 spectrometer. IR spectrum of CBZ-SUC cocrystal was obtained by an ALPHA A4 sized Benchtop ATR-FTIR spectrometer. Details about these techniques can be found in chapter 3 materials and methods.

4.3 Results

4.3.1 TGA analysis of CBZ DH

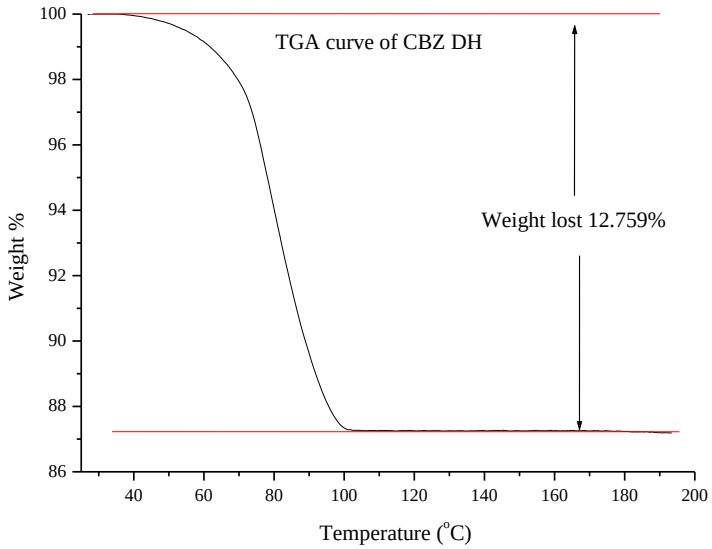

Fig. 4.1 TGA thermograph of CBZ DH

TGA thermograph of CBZ DH is shown in Fig. 4.1. According to the three TGA results, the average of the water content of CBZ DH is 12.759±0.007% (means, n=3). This value is slightly lower than the theoretical stoichiometric water content of 13.2% w/w, which may be due to a small portion of water loss inside the TGA equipment at the initial temperature under the nitrogen flow. The TGA result demonstrates the formation of CBZ DH.

4.3.2 DSC analysis of test samples

DSC results of different CBZ forms

The DSC traces and thermal data for CBZ DH, CBZ I, and CBZ III are presented in Fig. 4.2, (DSC data shown in Table 4.1). CBZ I had a single melting transition with a peak around 195°C and CBZ III first melt around 175°C, then recrystallized and formed a

more stable form, CBZ I, in agreement with reported thermal behaviour [98]. The dehydration process of CBZ DH happened during 80-120°C. After dehydration process under DSC heating conditions, CBZ DH converted back to CBZ III which melted around 175°C and then recrystallized and formed a more stable form CBZ I, which melted around 195°C [166].

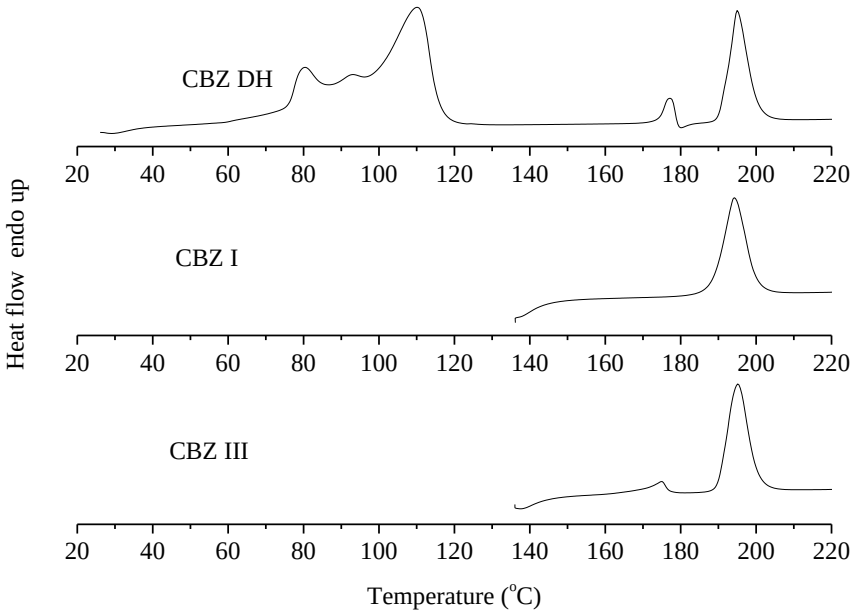

Fig. 4.2 DSC thermograph of: CBZ DH, CBZ I and CBZ III

Table 4.1 DSC thermal data for test samples

Sample	Onset (°C)	Peak(°C)	ΔH(J/g)
CBZ III	169.45	174.81	10.8492
	190.09	195.12	115.7066
CBZ I	188.36	194.19	111.127
CBZ DH	174.11	177.36	10.9556
	190.81	194.96	78.1268
NIC	120.34	133.07	171.5889
CBZ-NIC mixture	121.64	127.97	49.4972
	158.08	162.29	97.6472
CBZ-NIC cocrystal	158.80	163.84	115.6588
SUC	188.84	196.03	195.0547
CBZ- SUC mixture	177.46	182.00	16.0541
	184.02	188.66	107.7684
CBZ- SUC cocrystal	190.54	195.38	134.0538

DSC results of CBZ-NIC Cocrystal

DSC curve patterns of CBZ III, NIC, CBZ-NIC mixture, and CBZ-NIC cocrystal are shown in Fig. 4.3**,** (DSC data shown in Table 4.1). A DSC curve of pure NIC has shown an endothermic peak attributed to melting around 129-133°C. CBZ-NIC physical mixture shows a complex thermal behaviour. An endothermic event around 130°C was due to melting of NIC, and a major endothermic peak was around 162°C resulting from the melting of newly formed CBZ-NIC cocrystal under DSC heating. The DSC thermal graph for CBZ-NIC cocrystal has shown a single endothermic transition attributed to the melting transition with a peak round 163°C, which is in the range of between the melting points of two individual pure compounds. The thermal behaviour of the CBZ-NIC cocrystal is distinct with a different melting transition from that of either of the individual compounds, suggesting the formation of a new compound, in agreement with the reported thermal behaviour of CBZ-NIC cocrystal [73].

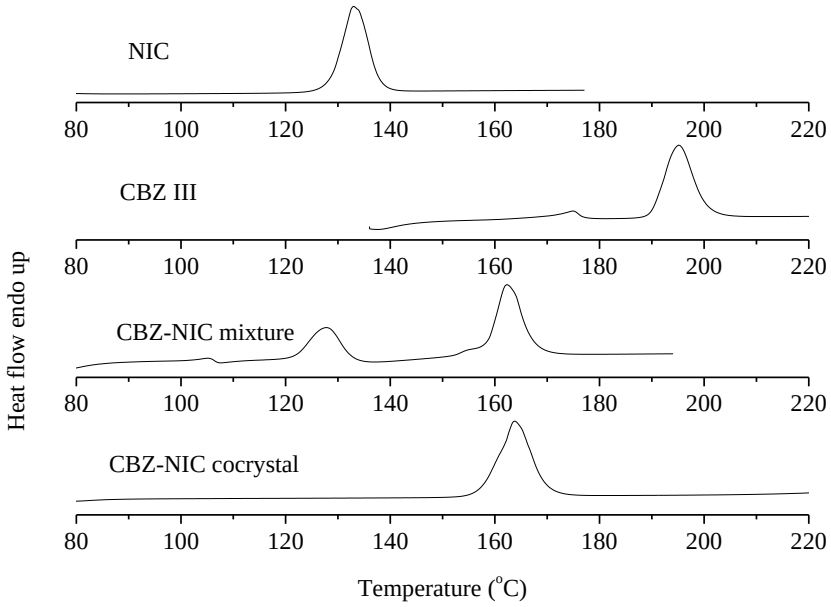

Fig. 4.3 DSC thermograph of CBZ-NIC cocrystal

DSC results of CBZ-SUC cocrystal

The DSC thermal graphs of CBZ III, SUC, CBZ-SUC mixture, and CBZ-SUC cocrystal are shown in Fig. 4.4 (DSC data shown in Table 4.1). DSC curve of pure SUC has shown an endothermic peak attributed to melting around 196 °C. CBZ-SUC physical mixture has more than one melting peak around 182-188 °C due to the coexistence of two components. CBZ-SUC cocrystal has a single endothermic peak around 195 °C attributed to the melting of cocrystal shown in DSC figure. The single melting point demonstrates that CBZ-SUC cocrystal is a new prepared pure compound rather than a physical mixture of CBZ and SUC.

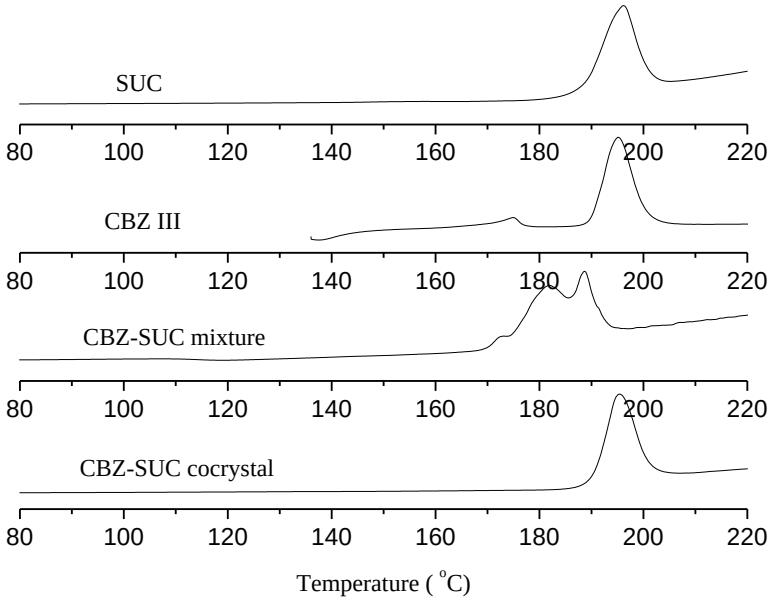

Fig. 4.4 DSC thermograph of CBZ-SUC cocrystal

4.3.3 IR spectroscopy analysis of CBZ-NIC cocrystal and CBZ-SUC cocrystal

The IR spectra for CBZ III, NIC and CBZ-NIC cocrystal are presented in Fig. 4.5. Characteristic peaks are in agreement with spectra reported in the literatures [167, 168].

The IR spectrum for CBZ III has peaks at 3465 and 1677 cm-1, corresponding to carboxamide N-H and C=O stretch, respectively. The spectrum of NIC has a peak

corresponding to carboxamide N-H stretch at 3364 cm^{-1}, double peaks at 1695 and 1680 cm^{-1} for C=O stretch. The IR spectrum of CBZ-NIC mixture shows both CBZ and

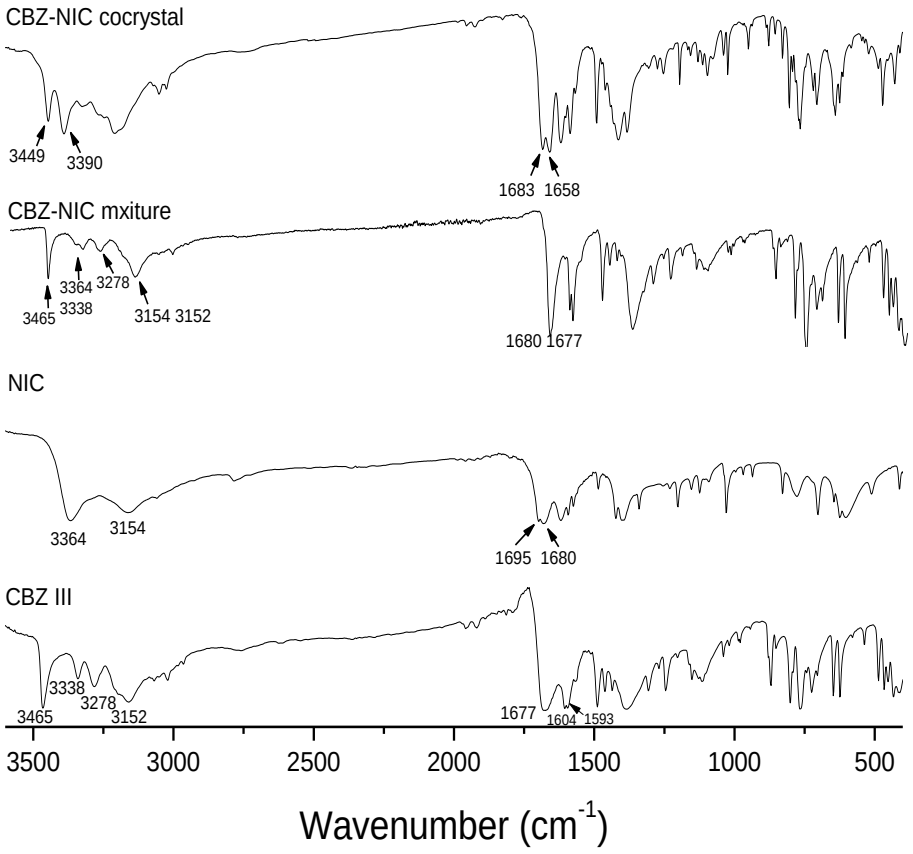

Fig. 4.5 IR spectrum of CBZ III, NIC, CBZ-NIC mixture and cocrystal

NIC, and mixture, which suggesting that both molecules are present in a new phase. The carboxamide N-H and C=O stretching frequencies of CBZ were shifted to 3449 and 1658 cm^{-1} respectively. This suggests that the carboxamide group of CBZ has formed a strong hydrogen bond. While, the N-H stretching frequency of NIC shifted to higher position at 3390 cm^{-1}, C=O stretching peak frequency moved to 1683 cm^{-1}. Summary of IR peak identities of CBZ, NIC and CBZ-NIC cocrystal is shown in Table 4.2.

Table 4.2 IR peaks summary of CBZ, NIC and CBZ-NIC cocrystal

Compound	Peak position (cm^{-1})	Assignment
CBZ III	3465,3338, 3278, 3152	$-NH_2$
	1677	-(C=O)-
NIC	3364	$-NH_2$
	1695, 1680	-(C=O)-
CBZ-NIC Cocrystal	3449	$-NH_2$ of CBZ
	3390	$-NH_2$ of NIC
	1683	-(C=O)- of NIC
	1658	-(C=O)- of CBZ

The ATR-FTIR spectra for CBZ III, SUC, CBZ-SUC mixture and CBZ-SUC cocrystal are presented in Fig. 4.6. SUC has following characteristic peaks: two peaks at around 1651 and 1198 cm^{-1} corresponding to the stretching vibration of carbonyl group; a characteristic peak at 1406 cm^{-1} for the hydroxyl bending, and some weak peak around

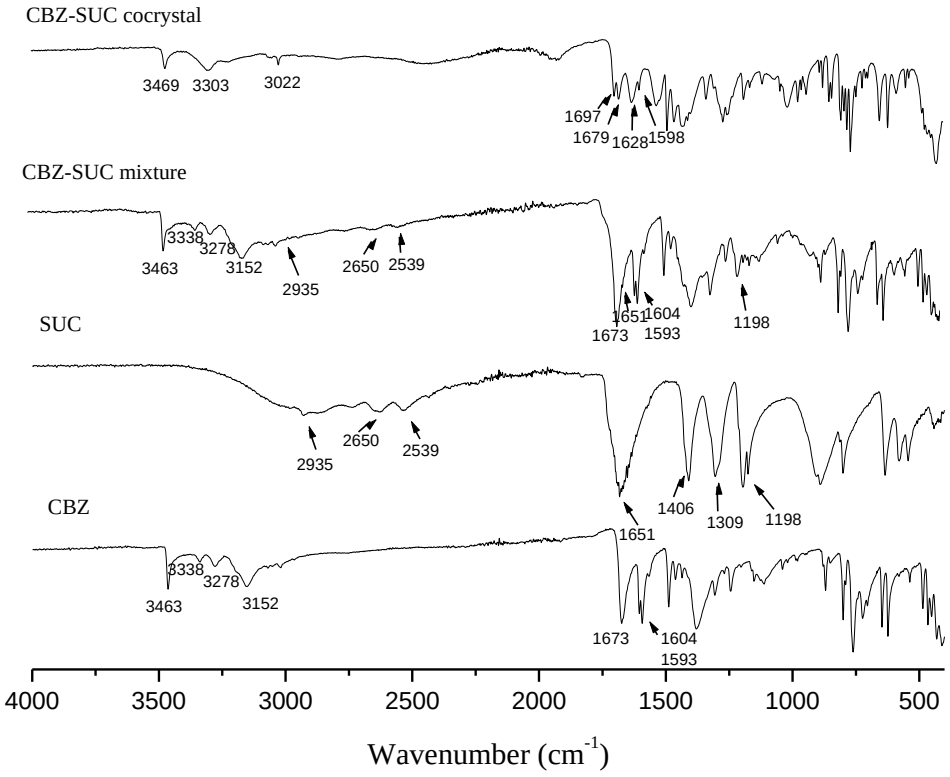

Fig. 4.6 IR spectrum of CBZ, SUC, CBZ-SUC mixture and CBZ-SUC cocrystal

2500 to 3000 cm^{-1} for hydroxyl stretching; a characteristic peak at 1309 cm^{-1} for the symmetric stretching vibration of carboxylic group. The IR spectrum of CBZ-SUC mixture shows both CBZ and SUC characteristic peaks. Spectrum of CBZ-SUC cocrystal has different pattern from mixture which demonstrates the formation of cocrystal. The carboxamide N-H and carbonyl stretching frequencies of CBZ were shifted to 3469 and 1697 cm^{-1} respectively. The hydroxyl and carbonyl stretching of SUC shifted to higher position at 3022 and 1679 cm^{-1} respectively. IR peaks are summarized in Table 4.3.

Table 4.3 IR peaks summary of CBZ, SUC and CBZ-SUC cocrystal

Compound	Peak position (cm^{-1})	Assignment
CBZ	3463, 3338, 3278, 3152	$-NH_2$
	1673	-(C=O)-
SUC	2935,2650,2539	OH
	1651,1198	-(C=O)-
	1406	OH
	1309	-COOH
CBZ- SUC cocrystal	3469	$-NH_2$ of CBZ
	1697	-(C=O)- of CBZ
	3022	-OH of SUC
	1679	-COOH of SUC

4.3.4 Raman spectroscopy analysis of CBZ-NIC cocrystal and CBZ-SUC cocrystal

Raman analysis for CBZ-NIC system

Raman spectra of CBZ DH, CBZ I, CBZ III, NIC, CBZ-NIC mixture and CBZ-NIC cocrystal are shown in Fig. 4.7 (spectra data shown in Table 4.4), in agreement with existing data reported in the literatures [116, 167, 169, 170].

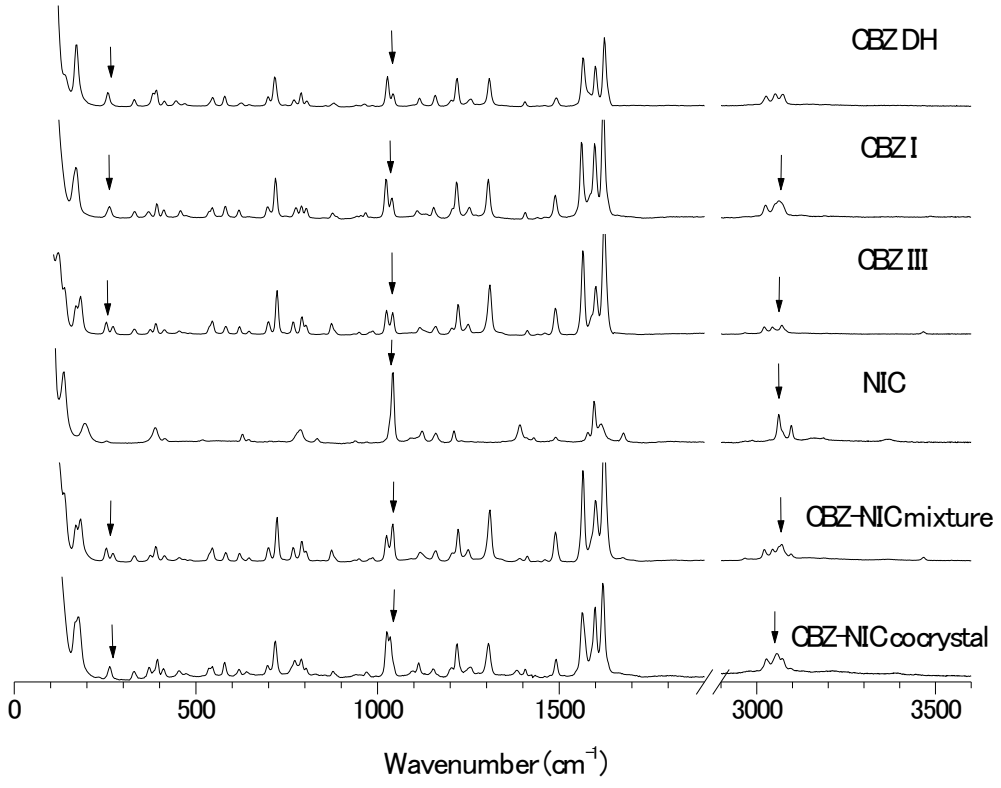

(a)Raman spectrum for the range of 0-3600cm^{-1}

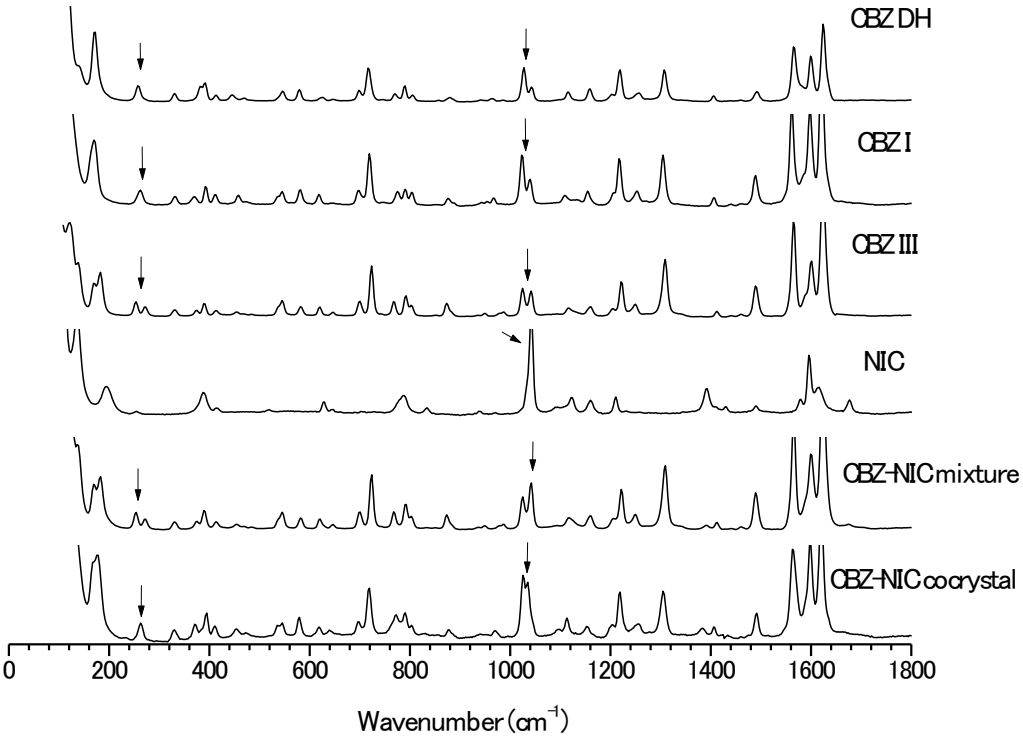

(b) Enlarged Raman spectrum for the range of 0-1800 cm^{-1}

Fig. 4.7 Raman spectrum of CBZ DH, CBZ I, CBZ III, CBZ-NIC mixture and CBZ-NIC cocrystal

There are several characteristic peaks available to compare and identify different CBZ samples. CBZ III has a double peak at 272 cm^{-1} and 253 cm^{-1} due to lattice vibration, while CBZ I and CBZ DH only have a single peak at 253 cm^{-1} and the peak at 272 cm^{-1} disappear. There are two C-H bending peaks at 1040 cm^{-1} and 1025 cm^{-1} from the ortho-substitued benzene ring of CBZ molecule and the relative intensities of these two peaks decreases from 0.97 of CBZ III to 0.38 of CBZ DH [167]. Therefore the change in the relative intensities of these two C-H bending modes can also be used to indicate the solid transition from CBZ III to CBZ DH during dissolution.

CBZ III and CBZ DH show triple peaks in the rage of wavenumbers 3070-3020 cm^{-1}, including one non-aromatic C-H stretch peak at 3020 cm^{-1}, one aromatic C-H stretch peak at 3043 cm^{-1} and one aromatic asymmetric stretch peak around 3071 cm^{-1}. CBZ I has double peaks at this area, a sharp peak at 3025 cm^{-1} due to non-aromatic C-H stretch and a broad peak at 3060 cm^{-1} due to aromatic C-H stretch. The relative intensities of Raman spectra at 3060 and 3025 cm^{-1} positions for CBZ I and CBZ DH are 1.29 and 0.66 respectively. The change of this ratio was used to indicate the transition of CBZ I to CBZ DH during *in situ* Raman experiments.

Two most significant peaks for NIC are pyridine ring stretching peak at 1042cm^{-1} and C-H stretching peak at 3060 cm^{-1}. Raman spectrum for CBZ-NIC mixture shows both characteristic peaks from CBZ III and NIC. It has double peaks at 272 and 253 cm^{-1} resulting from CBZ III. The peak intensity at 1040 cm^{-1} becomes higher than peak intensity at 1025 cm^{-1} due to the strong ring stretch peak at 1042 cm^{-1} from NIC and the same phenomenon can be observed that the peak intensity increases at 3060 cm^{-1}. The ratio of the spectral intensities at 1040 to 1025 cm^{-1} was monitored during *in situ* Raman experiments for CBZ-NIC mixture to indicate the solid transition from mixture to CBZ DH.

For CBZ-NIC cocrystal, its Raman spectrum shows a single peak at 264 cm^{-1} and the pattern of spectrum in the ranges of 1020-1040 cm^{-1} and 2950- 3500 cm^{-1} are different from those of the physical mixture. Differences among the Raman spectra of CBZ-NIC cocrystal, CBZ III, NIC and CBZ-NIC mixture have demonstrated that CBZ-NIC cocrystal is not just a physical mixture of the two components and that a new structure has been generated. A ratio of the spectral intensities at 1035 to 1025 cm^{-1} was monitored during *in situ* Raman experiments for CBZ-NIC cocrystal to indicate the solid transition from cocrystal to CBZ DH

Raman analysis for CBZ-SUC system

Raman spectra of CBZ III, SUC, CBZ-SUC cocrystal and CBZ-SUC mixture are shown in Fig. 4.8, which is in agreement with data reported in the literatures [46].

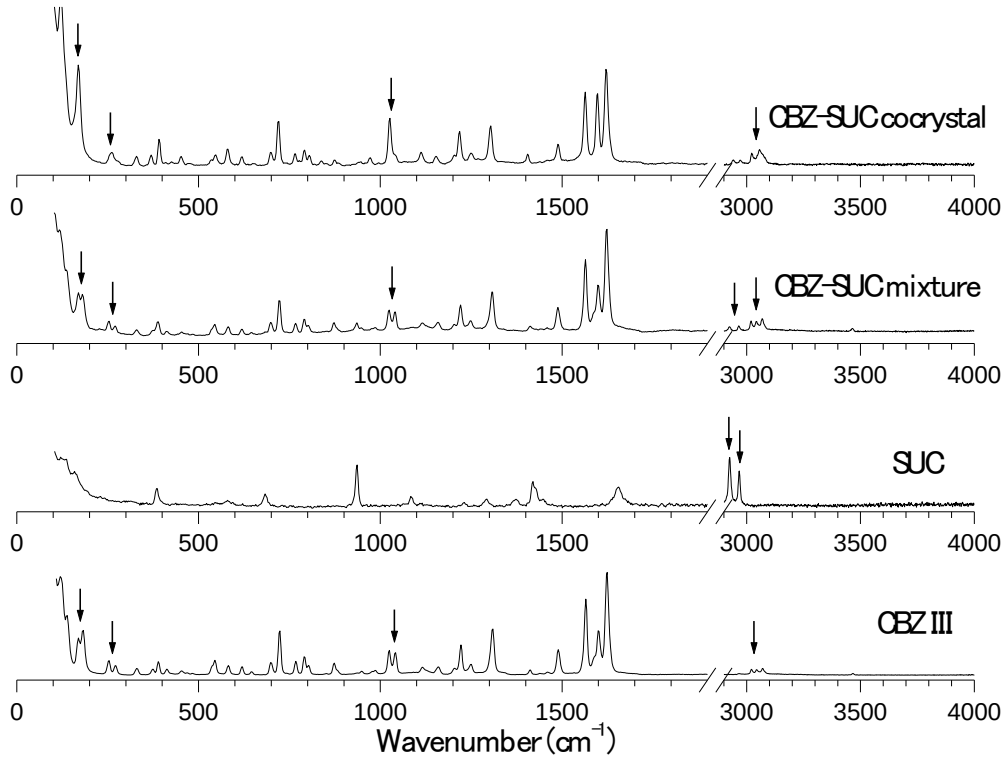

(a)Raman spectrum for the range of 0-4000cm^{-1}

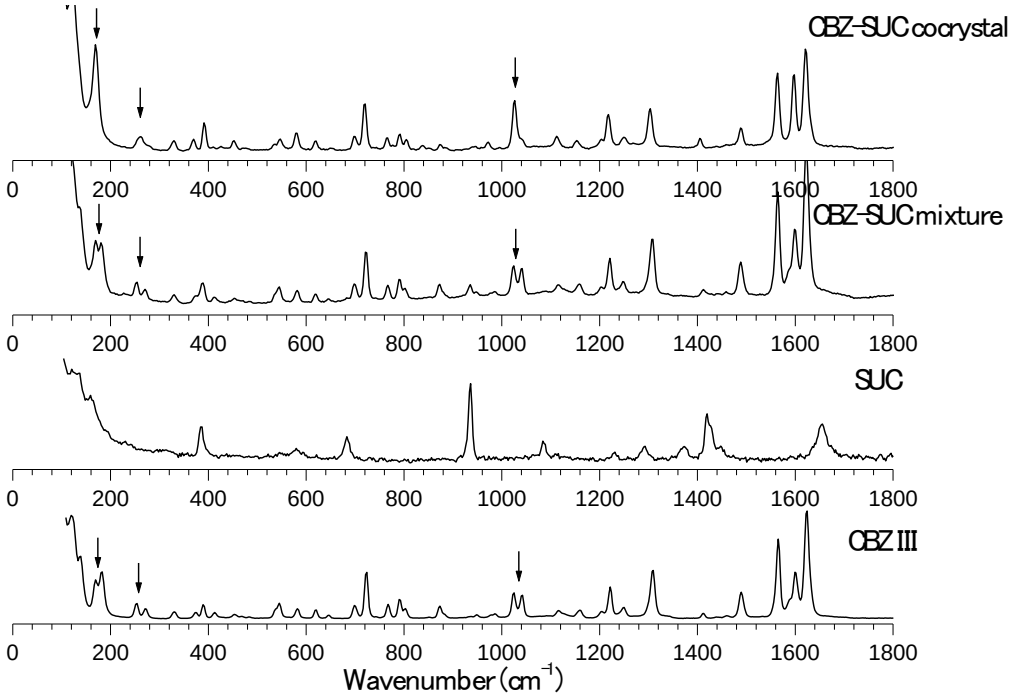

(b) Enlarged Raman spectrum for the range of 0-1800 cm^{-1}

Fig. 4.8 Raman spectrum of CBZ, SUC, CBZ-SUC mixture and CBZ-SUC cocrystal

CBZ III has exhibited all the characteristic peaks as described in the former part of 'Raman analysis of CBZ-NIC system'. SUC shows two characteristic peak around 2930 and 2970 cm^{-1} corresponding to the O-H stretching of carboxylic group. Raman spectrum of CBZ-SUC mixture shows both CBZ and SUC characteristic peaks. The Raman spectrum of CBZ-SUC cocrystal shows a distinctive pattern compared with CBZ-SUC mixture. Single peak has been found around 170 and 260 cm^{-1} for cocrystal. The intensity of peak at 1040 cm^{-1} in mixture spectrum is comparable to that of peak at 1020 cm^{-1}, while in cocrystal's spectrum the peak at 1040 cm^{-1} almost disappear. The triple peaks in the range of 3020 to 3070 cm^{-1} in spectra of CBZ and mixture became double peaks in cocrystal spectrum.

Table 4.4 Raman peaks for CBZ III, CBZ I, CBZ DH, NIC, SUC, CBZ-NIC cocrystal, and CBZ-SUC cocrystal

Compound	Peak position (cm^{-1})	Assignment
CBZ III	double peak at 272, 253	lattice vibration

	1040, 1025, peak intensity ratio 0.97	C-H bending
	triple peaks at 3020, 3043, and3071	non-aromatic C-H stretch aromatic C-H stretch aromatic asymmetric stretch
CBZ I	single peak at 253	lattice vibration
	double peaks at 3025, 3060	non-aromatic C-H stretch aromatic C-H stretch
CBZ DH	single peak at 253	lattice vibration
	1040, 1025, peak intensity ratio 0.38	C-H bending
	triple peaks at3020, 3043, and3071	non-aromatic C-H stretch aromatic C-H stretch aromatic asymmetric stretch
NIC	1042	pyridine ring stretch
	3060	C-H stretch
SUC	2930	OH stretch
	2970	OH stretch
CBZ-NIC cocrystal	single peak at 264	lattice vibration
	distinctive peaks at 1020-1040	C-H bending
	distinctive peaks at 2950-3500	C-H stretch
CBZ-SUC cocrystal	single peak at 260	lattice vibration
	single peak at 1040	C-H bending
	double peak at 3020, 3060	O-H stretch-H stretch

4.3.5 Molecular structures of CBZ-NIC cocrystal and CBZ-SUC cocrystal

IR, Raman, and DSC characterization results have demonstrated the formation of the cocrystals: CBZ-NIC cocrystal, and CBZ-SUC cocrystal. The molecular structures of CBZ-NIC cocrystal and CBZ-SUC cocrystal were presented in this section [41, 84].

The molecular structure of CBZ-NIC cocrystal and CBZ-SUC cocrystal are shown in Fig. 4.9. 1:1 CBZ-NIC cocrystal has an amide-to-amide structure. CBZ-NIC cocrystal is formed through hydrogen bonds in which the carboxamide groups from both CBZ and NIC provide hydrogen bonding donors and acceptors. For 2:1 CBZ-SUC cocrystal, the two carboxylic groups of SUC form hydrogen bonds with the carboxamide groups from

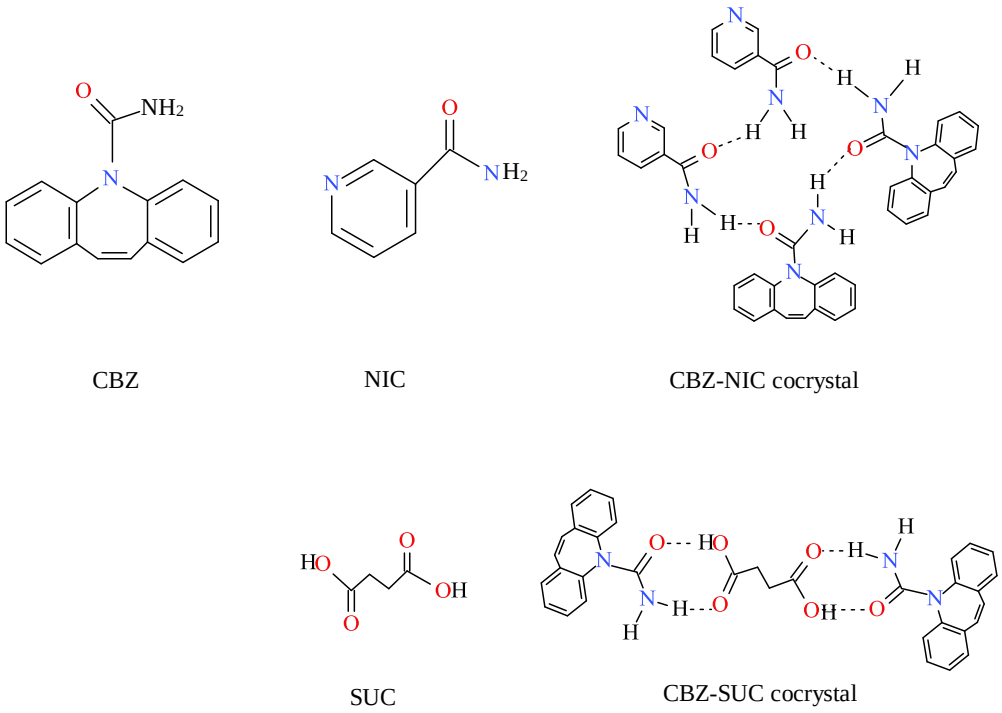

Fig. 4.9 Molecular structures of CBZ, NIC, SUC, CBZ-NIC cocrystal, and CBZ-SUC cocrystal

CBZ result in a cocrystal with 2:1 component molecular ratio. The hydroxyl from carboxylic group of SUC serve as hydrogen bonding donor which form hydrogen bond with the carbonyl of CBZ carboxamide. The carbonyl of carboxylic group from SUC serve as hydrogen bonding acceptor which form hydrogen bonding with amino of CBZ.

4.4 Chapter conclusions

In this chapter, different CBZ samples were characterised, which are CBZ DH, CBZ I, 1:1 CBZ-NIC cocrystal, and 2:1 CBZ-SUC cocrystal. All characterisation results have demonstrated the successfully formation of CBZ I, CBZ DH and the two CBZ cocrystals. Raman spectroscopy analysis provide characteristic peak intensities ratio which can be used in monitoring the solid transition between different CBZ forms during dissolution. The molecule structures of CBZ-NIC cocrystal, and CBZ-SUC cocrystal were also presented in this chapter, which give readers a better understanding of the cocrystal structure formation.

Chapter 5 *In Situ* Monitoring of Carbamazepine-Nicotinamide Cocrystal Intrinsic Dissolution Behaviour

5.1 Chapter overview

In this chapter the phase transition behaviour of cocrystals was studied by *in situ* monitoring of dissolution processes using state of arts techniques of a UV imaging dissolution system and Raman spectroscopy. Evolution of the intrinsic dissolution rate (IDR) of CBZ-NIC cocrystal was monitored by ActiPix SDI 300 UV imaging dissolution system during dissolution. The solid state change that might occur during dissolution of the cocrystal was monitored by *in situ* Raman Spectroscopy. Intrinsic dissolution behaviour of CBZ polymorphs (CBZ form III, CBZ DH, CBZ form I) and physical mixture of CBZ form III and NIC were studied and compared.

5.2 Materials and methods

5.2.1 Materials

Anhydrous CBZ III, sodium acetate, acetic acid, and NIC, ethyl acetate, potassium bromide and double distilled water were used in this chapter. The dissolution medium used in this study was pH4.5 acetate buffer (0.06M). Details about the materials and dissolution medium preparation can be found in chapter 3 materials and methods, section 3.1 materials.

CBZ DH, CBZ I, CBZ-NIC cocrystal, and physical mixture of CBZ III and NIC were prepared and used in this chapter. Preparation and characterisation of these samples can be found in chapter 3, section 3.4 preparations and chapter 4 sample characterisations.

5.2.2 Methods

UV imaging dissolution experiment

An ActiPix SDI 300 UV surface imaging system (Paraytec Ltd., York, UK) was used to study the dissolution behaviour of CBZ-NIC cocrystal, CBZ III, CBZ I, CBZ DH and CBZ-NIC mixture. Details of a description of this dissolution testing system can be found in section 3.3.1.1 Introduction to UV imaging dissolution system.

UV imaging dissolution experiments were carried out at 37°C at a single wavelength filter of 300 nm. Dissolution experiments were performed with a standard acetate buffer (pH4.5), flow rate at 0.2 mL/min. Each sample has been tested for 3 hours in triplicate. The sample compacts used for UV imaging dissolution tests were analysed prior to and after a UV imaging dissolution test using a LEICA DM 750 microscope and an EnSpectr R532® Raman spectrometer. Details about the UV imaging test and calibration procedures can be found in section 3.3.1.2 Operation of UV imaging dissolution system.

In situ monitoring of solution mediated phase transformations

In situ monitoring of solution mediated phase transformations of CBZ-NIC cocrystal, CBZ III, CBZ I, and CBZ-NIC mixture to CBZ DH was carried out using EnSpectr R532® Raman spectrometer. The experiment set up and operation procedures can be found in section 3.3.2 Enspectr R532 Raman spectrometry. Experiments of *in situ* Raman monitoring for each test sample were performed in triplicate.

In addition to Raman spectroscopy, the solid state transformations on the surfaces of the drug compacts were investigated by SEM. The compacts were withdrawn from the cups at various time points (5, 30, 90 and 180 minutes) and SEM micrographs of the compacts were photographed by a ZEISS EVO HD 15 scanning electron microscope

(Carl Zeiss NTS Ltd, Cambridge, UK). Details about SEM technique can be found in section 3.3.9 Scanning electron microscope.

5.3 Results

5.3.1 UV imaging dissolution tests

In situ UV imaging dissolution tests

Dissolution behaviours of five samples CBZ DH, CBZ I, CBZ III, CBZ-NIC cocrystal and mixture were monitored by the ActiPix SDI 300 UV imaging dissolution system at a constant flow rate of 0.2 mL/min for 3 hours. The UV images of absorbance maps of a released sample at different selected time points were shown in Fig. 5.1. The absorbance map in each image indicates the spatial concentration distribution of the dissolved CBZ in the flow cell at the recording time, which was affected by the flow rate and diffusion coefficient of CBZ. The effect of the density gradients of the solution on the local solution concentration distribution was not significant because there is a clear upward diffusion of the dissolved CBZ into the bulk buffer solution as the downstream distance increases to form a stable plume. The pattern of the dissolved CBZ is in agreement with expectations from the convective-diffusion theory, which describes transport-controlled dissolution involving two fundamental processes of molecular diffusion and forced convection as a result of fluid flow [171].

From these recorded images, it is clearly shown that different samples have different absorbance profiles which are changing as a function of the dissolution time. Generally the highest absorbance profile for each sample was obtained around 5 minutes after a dissolution test started and then it gradually declined to a steady state around 30 minutes. CBZ DH generated the thinnest plume of the dissolution layer which became stable around 5 minutes after the dissolution test started, indicating that CBZ DH has the smallest and most stable dissolution rate among the five samples. Compared with CBZ

Fig. 5.1 UV images of drug release at different selected times (at 0, 5, 10, 20 and 30 min)

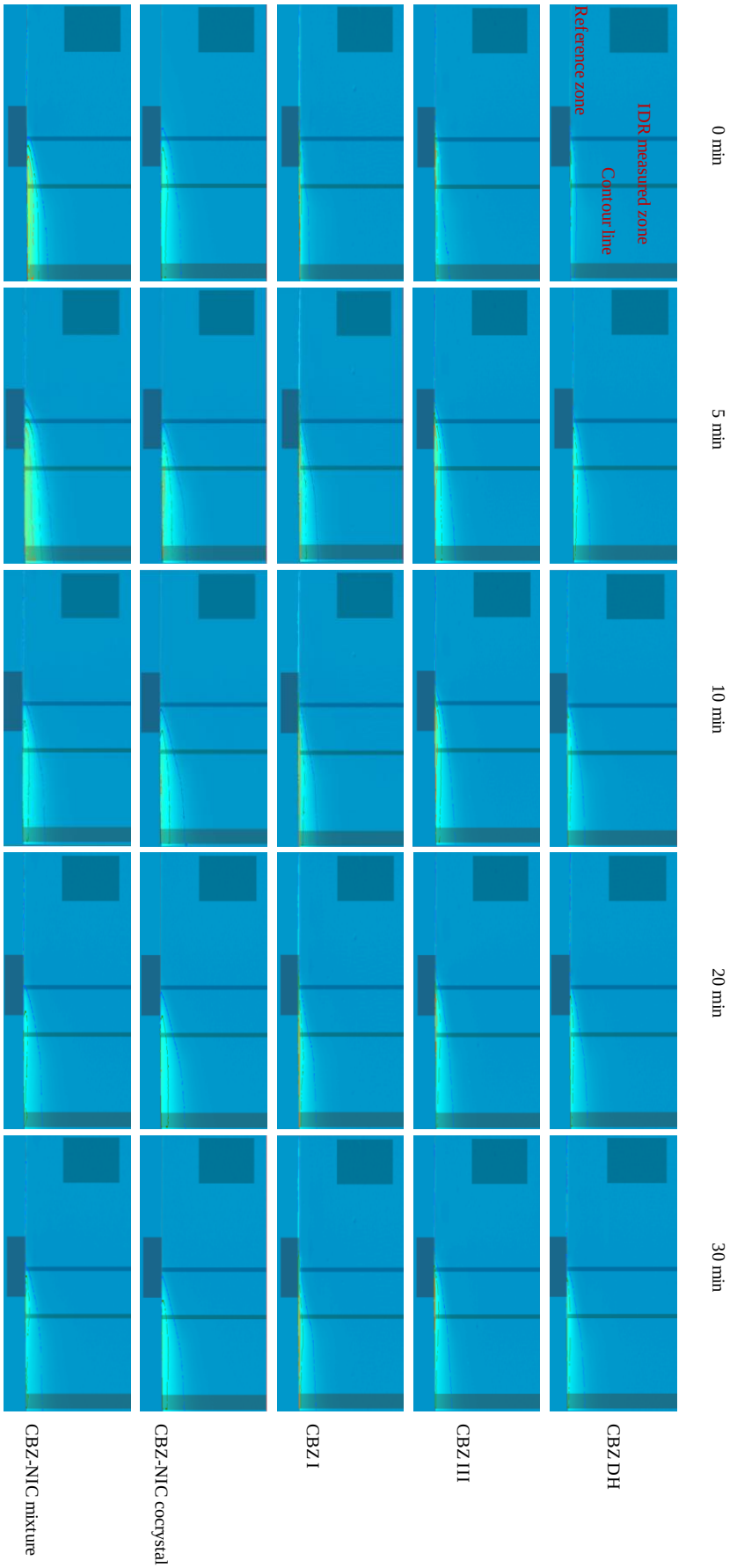

DH, the other four samples show relative thicker plumes of the absorbance area of CBZ when the samples were loaded in the flow cell, in particular for CBZ-NIC cocrystal and mixture. It is revealed that both of CBZ-NIC cocrystal and mixture have higher dissolution rates. Similar to those of CBZ DH, the absorbance pattern of dissolution images of CBZ-NIC cocrystal was stable, indicating a constant dissolution rate and stable form of the cocrystals. However, for CBZ-NIC mixture, although a thicker plume of dissolution layer was obtained at the beginning of the test, the size of dissolution layer quickly decreased to the level of CBZ DH due to quickly dissolved NIC. For CBZ III and CBZ I, there was a significant decrease in the size of absorbance area for the first 20 minutes of the dissolution tests and became stable after that. This can be explained by the precipitation of a more stable form CBZ DH on the surfaces of the compacts to reduce the dissolution rate of the test samples in the buffer.

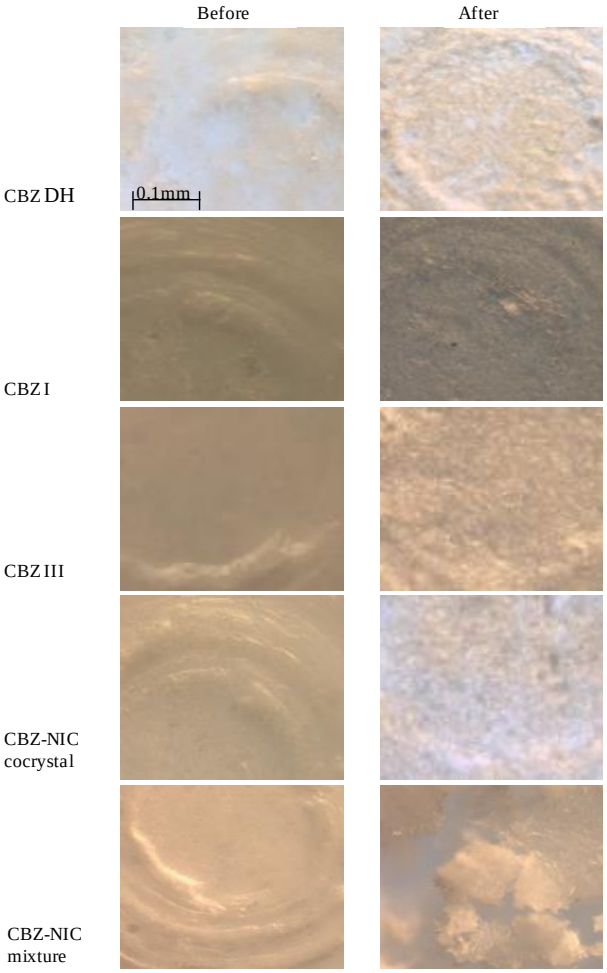

Fig. 5.2 Light microscopy photographs of the sample compacts

Change in the dissolution rate and crystallization of a stable form of CBZ DH were confirmed with images of sample compacts by light microscopy in Fig. 5.2. Prior to the dissolution tests, all of the compact surfaces were very smooth. After dissolution tests, the microscope images show that small needle shaped crystals have appeared on the compact surfaces for CBZ DH, CBZ I, CBZ III and CBZ-NIC cocrystal, indicating that the solid state changes due to crystallization of CBZ DH from the supersaturated solutions on the compact surfaces. However, it is shown that there is a significantly different surface morphology of the CBZ-NIC mixture compact after a dissolution test. There were a lot of holes that appeared on the surface due to dissolved NIC, which can explain the reasons of the significant changes of dissolution images recorded.

Comparison of the Raman spectra of test samples prior to and immediately after a UV imaging dissolution test are shown in Fig. 5.3.

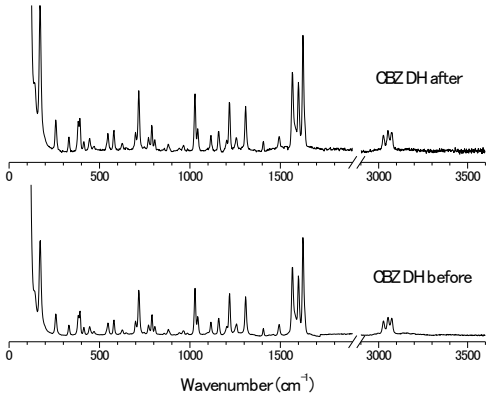

(a1) CBZ DH Raman spectrum from 0-3600cm^{-1}

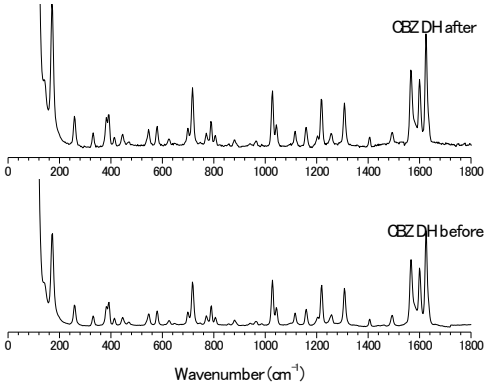

(a2) CBZ DH Raman spectrum from 0-1800cm^{-1}

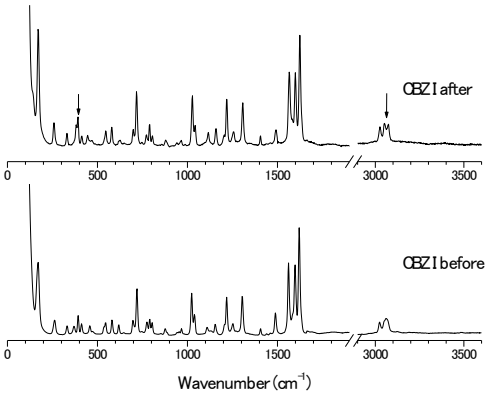

(b1) CBZ I Raman spectrum from 0-3600cm^{-1}

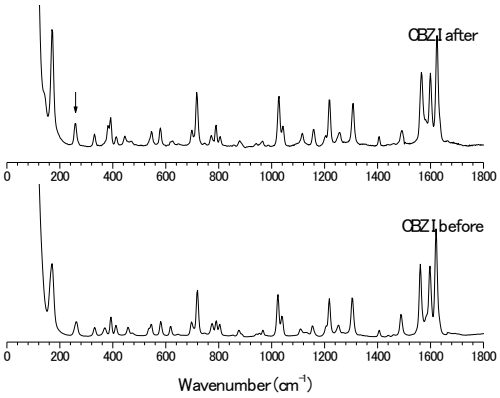

(b2) CBZ I Raman spectrum from 0-1800cm^{-1}

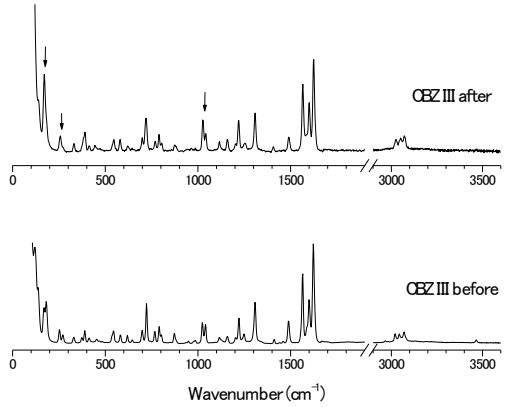

(c1) CBZ III Raman spectrum from 0-3600cm^{-1}

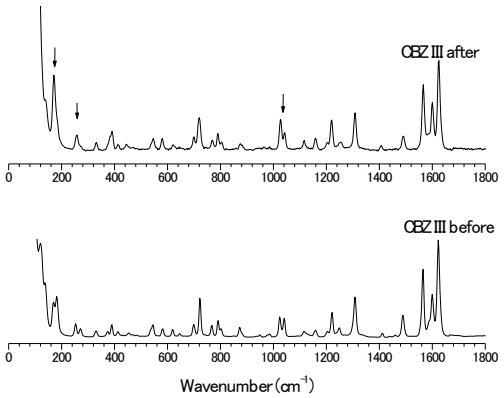

(c2) CBZ III Raman spectrum from 0-1800cm^{-1}

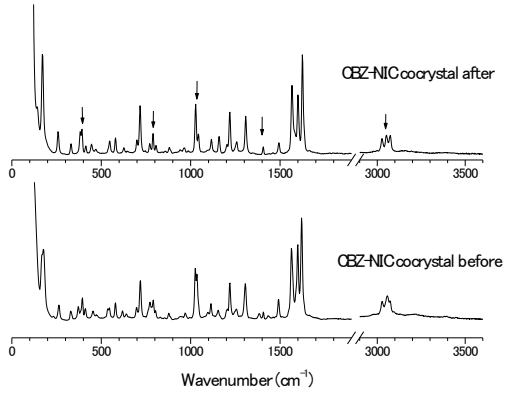

(d1) CBZ-NIC cocrystal Raman from 0-3600cm^{-1}

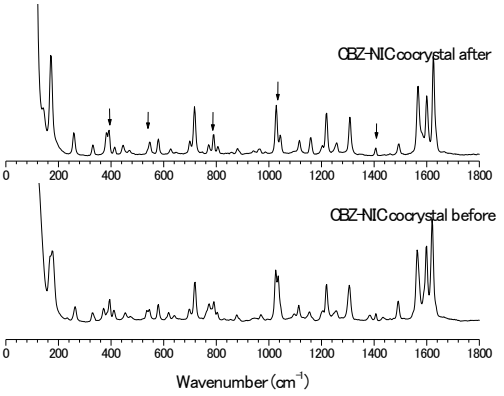

(d2) CBZ-NIC cocrystal Raman from 0-1800cm^{-1}

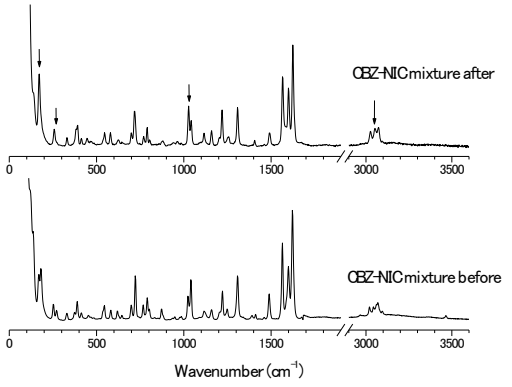

(e1) CBZ-NIC mixture Raman from 0-3600cm^{-1}

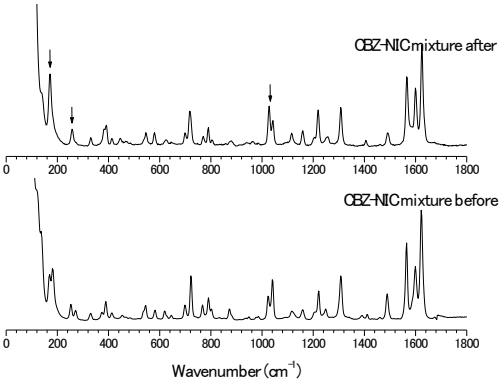

(e2) CBZ-NIC mixture Raman from 0-1800cm^{-1}

Fig. 5.3 Raman spectra of the compacts before and after 3-hours UV imaging dissolution tests

There is no change of CBZ DH Raman spectra during a 3 hours test. All Raman spectra of the other samples show some differences between before and after the dissolution tests in Fig. 5.3 (b)-(e). For CBZ I, the most obviously change happened around 3060 cm^{-1} area: double peaks become triple peaks, shown in Fig. 5.3(b). The main changes of

Raman spectrum for CBZ III have been pointed out by arrows in Fig. 5.3(c), including two characteristic changes: the ratio of relative intensities of peak at 1040 cm^{-1} to peak at 1025 cm^{-1} decreases, and double peaks disappear around 250 cm^{-1}. For CBZ-NIC cocrystals, it has been shown that the ratio of the relative intensities of 3060 cm^{-1} to 3025 cm^{-1} and 1035 cm^{-1} to 1025 cm^{-1} decrease shown in Fig. 5.3(d). The main changes of Raman spectrum of CBZ-NIC mixture are the same as those of CBZ III in Fig. 5.3(e). All these changes show the tendency of solid state conversion to CBZ DH, indicating precipitation of CBZ DH on the compact surfaces.

Evolution of the IDRs of CBZ DH, CBZ I, CBZ III, CBZ-NIC cocrystal and mixture during dissolution is shown in Fig. 5.4. Within the first 3 minutes, all IDRs of the test samples reached its maximum values, summarised in Table 5.1. During the course of 3 hours dissolution test, the IDR of CBZ DH is almost constant at 0.0065 mg/min/cm^2, indicating amount of CBZ DH precipitated from solution is not significant. The IDR profiles of CBZ I and CBZ III are similar, in which the maximum IDRs were obtained

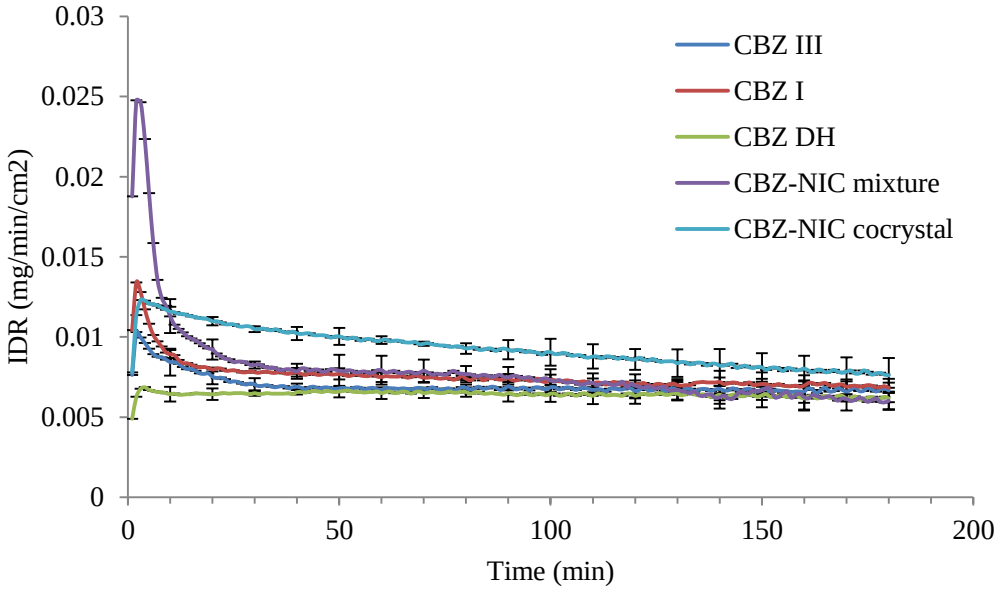

Fig. 5.4 Intrinsic dissolution rates as a function of dissolution time obtained by UV imaging at a flow rate of 0.2 mL/min (n=3)

in 2 minutes and then decreased quickly to relative stable values. However, the transition times are different for two samples. CBZ I has the IDR_{max} of 0.0134 mg/min/cm^2 which declined to 0.080 mg/min/cm^2 within 15 minutes and then it

decreased gradually to the CBZ DH level within 2 hours. Transition time of CBZ III is much faster than that of CBZ I, which took about 30 minutes to decline the IDR_{max} of 0.0103 mg/min/cm^2 to that of CBZ DH. The biggest variability of the IDR of CBZ-NIC mixture has been displayed in Fig. 5.4 and its IDR_{max} is the biggest among the five test samples due to effect of a very high concentration of NIC in the solution. Evolution of the IDR profile of CBZ-NIC mixture is similar to that of CBZ III within 35 minutes but with a higher value of 0.0080 mg/min/cm^2, which was affected by continuously dissolved NIC from the compact. When most of NIC in the mixture had dissolved, the IDR declined to a lower value of 0.0063 than that of CBZ DH due to reduction of the compact surface area for dissolution. Compared with CBZ I, CBZ III and CBZ-NIC mixture, the IDR of CBZ-NIC cocrystal is constant over time. It reached the maximum value of 0.0123 mg/min/cm^2 and declined slowly during dissolution and it became the highest IDR since the 8th minute among all the five samples.

Table 5.1 Comparison of IDRs and calculated apparent and equilibrium solubility for test samples (n=3)

	IDR_{max} (mg/min/cm^2)	Time to IDR_{max} (min)	IDR_{stable}	Time to stable	Apparent solubility (mg/mL)	Equilibrium solubility (mg/mL)
CBZ DH	0.0069 ±0.0011	4	0.0065 ±0.0005	5	0.2100 ±0.0050*	0.1978 ±0.0161**
CBZ III	0.0103 ±0.0031	2	0.0070 ±0.0004	30	0.3135 ±0.0949**	0.2141 ±0.0123**
CBZ I	0.0134 ±0.0023	2	0.0080 ±0.0002	15	0.4078 ±0.0688**	0.2425 ±0.0063**
CBZ-NIC cocrystal	0.0123 ±0.0004	3	decreasing	-----	0.3746 ±0.0111**	-----
CBZ-NIC mixture	0.0248 ±0.0055	2	0.0080 ±0.0003	35	-----	-----

*: measured solubility; **: calculated solubility

5.3.2 *In situ* monitoring of solid state transformation during dissolution using Raman spectroscopy

In situ monitoring of the solution mediated phase transformations of CBZ III, CBZ I, CBZ-NIC cocrystal, and CBZ-NIC mixture to CBZ DH was carried out using the Enspectr R532 Raman spectroscopy, described in the previous section 3.3.2. In total, 36 spectra were recorded for each sample during 3 hours dissolution. The Raman spectra at different selected time points were shown in Fig. 5.5. Similar to the previous result, there was no change of CBZ DH Raman spectra during the 3 hours dissolution test in Fig. 5.5 (a). The dynamic evolutions of Raman spectra of the other four samples are

clearly shown in Fig. 5.5 (b)-(e) and details of progression to CBZ DH have been revealed.

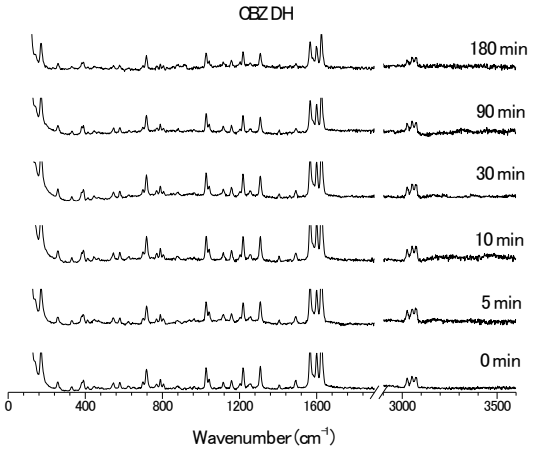

(a1) CBZ DH Raman 0-3600 cm^{-1}

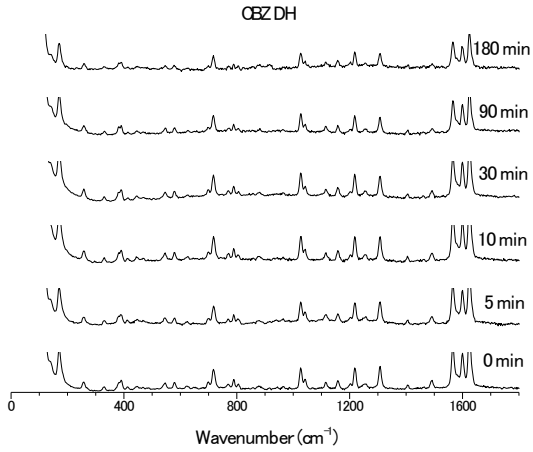

(a2) CBZ DH Raman 0-1800 cm^{-1}

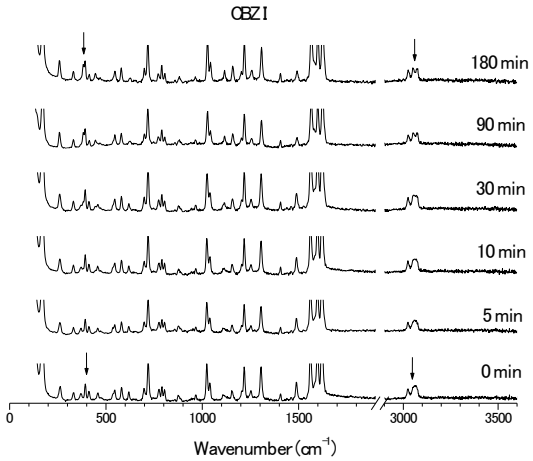

(b1) CBZ I Raman 0-3600 cm^{-1}

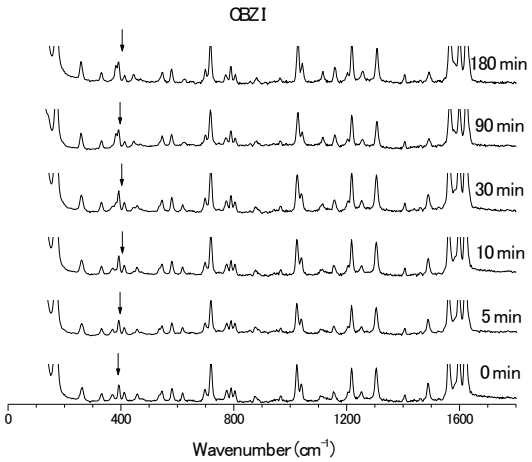

(b2) CBZ I Raman 0-1800 cm^{-1}

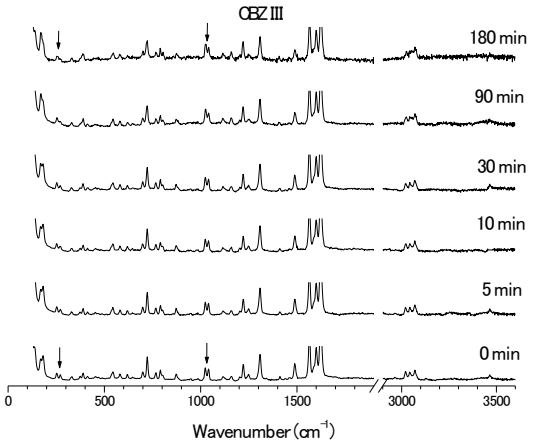

(c1) CBZ III Raman 0-3600 cm^{-1}

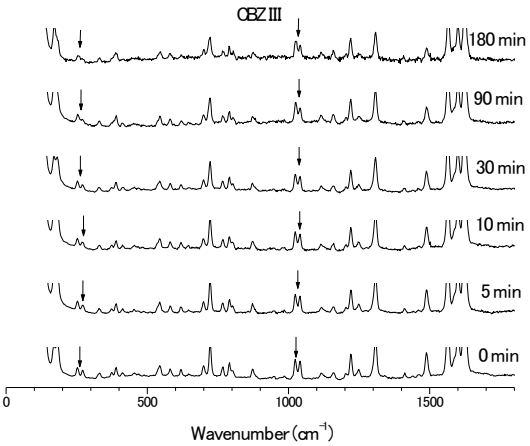

(c2) CBZ III Raman 0-1800 cm^{-1}

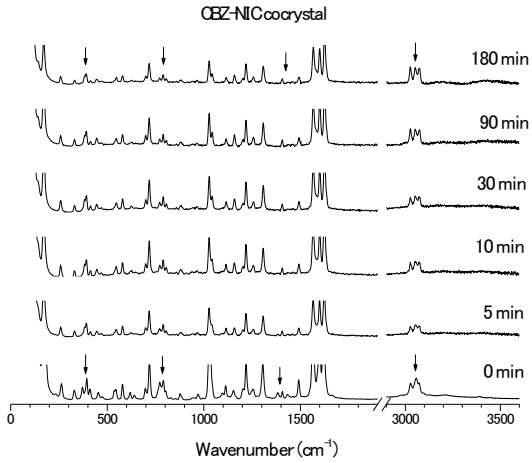

(d1) CBZ-NIC cocrystal Raman 0-3600 cm^{-1}

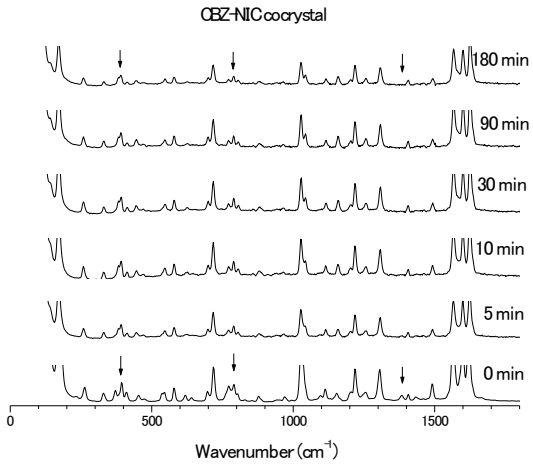

(d2) CBZ-NIC cocrystal Raman 0-1800 cm^{-1}

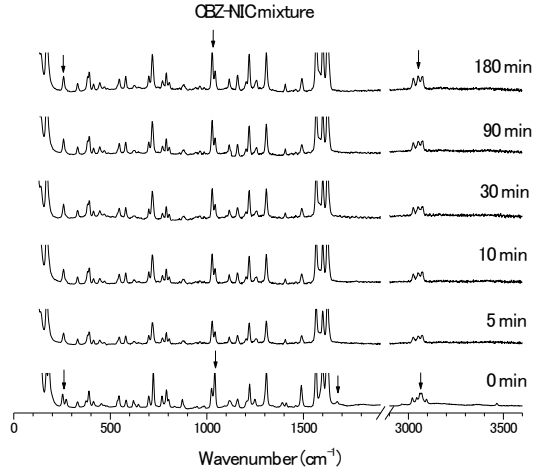

(e1) CBZ-NIC mixture Raman 0-3600 cm^{-1}

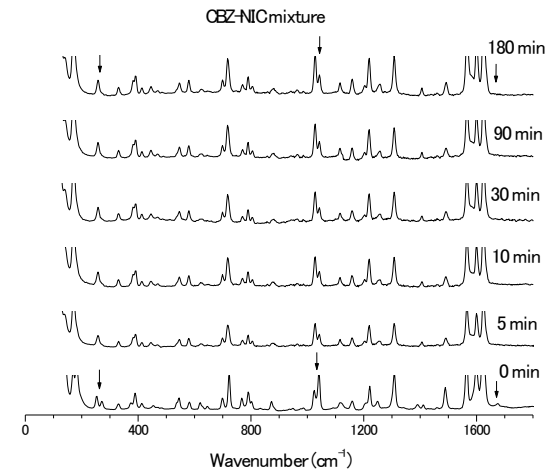

(e2) CBZ-NIC mixture Raman 0-1800 cm^{-1}

Fig. 5.5 Raman spectra of compact surfaces at different selected times (at 0, 2, 15, 30, 60, 180 min): (a) CBZ DH; (b) CBZ I; (c) CBZ III; (d) CBZ-NIC cocrystal; (e) CBZ-NIC mixture

In order to quantify the solid state change during dissolution, ratios of characteristic spectral intensities for each sample are used as indicators for a phase change during dissolution are summarized in Table 5.2, in which the ratios of start and end of the experiments are presented. Details about the selection of characteristic peak for each of samples have been described in section 4.3.4.

Table 5.2 Indicators used in situ Raman spectrometer monitoring (n=3)

Ratio of intensities	1035/1025		1040/1025		3060/3025	
	begin	finish	begin	finish	begin	finish
CBZ DH	0.24 ±0.04		0.38 ±0.01		0.66 ±0.02	
CBZ III	–	–	0.97 ±0.10	0.73 ±0.02	–	–
CBZ I	–	–	–	–	1.29 ±0.06	0.76 ±0.02
CBZ-NIC cocrystal	0.65 ±0.08	0.25 ±0.04	–	–	–	–
CBZ-NIC mixture	–	–	1.2 ±0.18	0.49 ±0.04	–	–

Evolution of the selected peak ratios during dissolution are shown in Fig. 5.6. For CBZ DH, all of three ratios selected were constant during dissolution as the same of those before a test, indicating they are the characteristic peaks which keep constant during dissolution. For CBZ III, the peak intensity ratio of 1040 to 1025 cm^{-1} decreased from 0.97 to 0.73 while CBZ DH value is 0.38, indicating a fraction of CBZ DH formed on the surface of the compact. For CBZ I, the ratio of 3060 to 3025 cm^{-1} dropped from 1.29 to 0.76, while CBZ DH has a ratio of 0.66. Obviously, neither CBZ III nor CBZ I has completed the hydrate conversion. For CBZ-NIC cocrystal, the peak ratio of 1035 to 1025 cm^{-1} decreased from 0.65 to 0.25, very close to DH of 0.24. For CBZ-NIC mixture, the peak ratio of 1040 to 1025 cm^{-1} decreased from 1.2 to 0.49, indicating more CBZ III in the mixture was converted into CBZ DH. This may be due to removal of NIC, leading more dissolution medium to get into the compact to facilitate the hydrate transition of CBZ III.

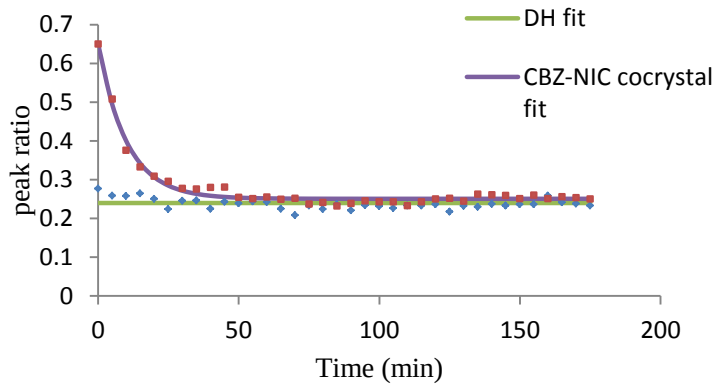

(a)

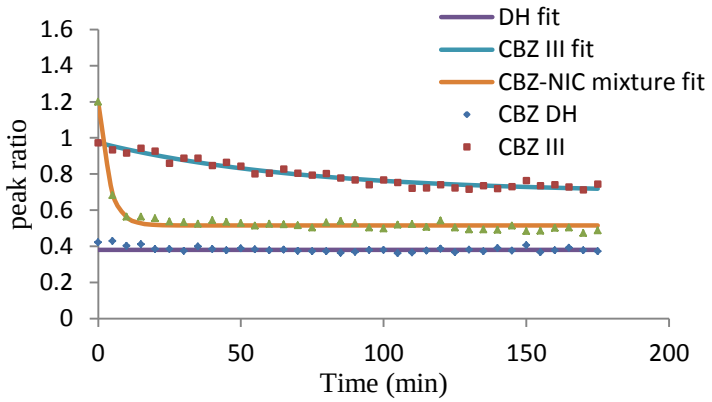

(b)

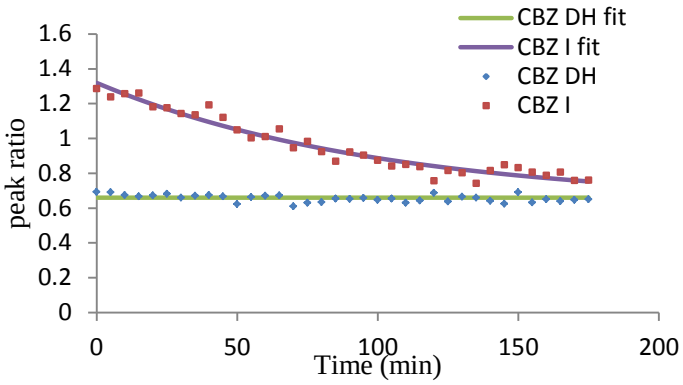

(c)

Fig. 5.6 Evolution of ratios of characteristic peaks: (a) 1035/1025 for CBZ DH and CBZ-NIC cocrystal; (b) 1040/1025 for CBZ DH, CBZ III and CBZ-NIC mixture; (c) 3060/3025 for CBZ DH and CBZ I

5.3.3 SEM

SEM characterisation of the surfaces of sample compacts has been carried out. Five sample compacts were placed into the medium buffer for 3 hours separately. During the 3 hours dissolution, SEM micrographs of each sample compact were taken at five time points: 0, 5, 30, 90, and 180 minutes, shown in Fig. 5.7.

SEM photos in the first column were taken before dissolution testing, all sample compacts have smooth surfaces and no particular shaped crystal was observed for each of samples. Significant change happened to all samples only after 5 minutes when contacting with the medium buffer solution.

SEM photos in the second column were taken after 5 minutes dissolution in medium, it can be seen that the smooth surfaces have disappeared and some needle-shaped CBZ DH crystals were observed on the surfaces of all sample compacts. And these newly formed CBZ DH crystals have the similar shape as those of CBZ DH uncompressed sample, shown in Fig. 5.8. Among five samples, the smallest amount of needle-shaped crystals was observed on the surface of CBZ DH compact. There are several crystal clusters scattered on CBZ DH compact surface while the other four sample compact surfaces are covered with needled crystals completely. Long needle-shaped crystals were formed on the surfaces of both CBZ III and CBZ I compacts due to recrystallization of CBZ DH from the solutions. Smaller sizes of CBZ DH crystals were

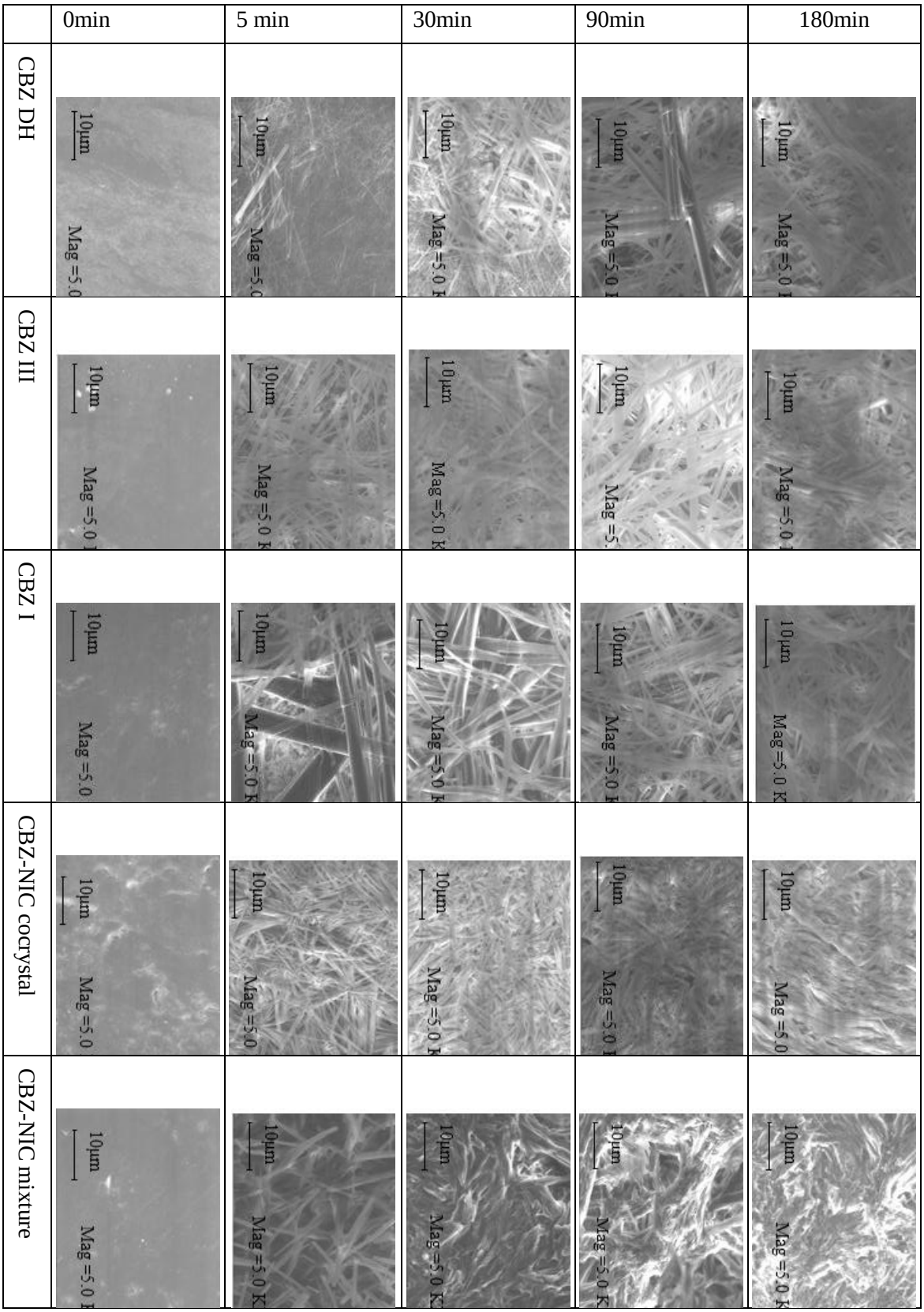

Fig. 5.7 SEM photos taken off-line of the compact surfaces during dissolution at different time points (0, 5, 30, 90, and 180min)

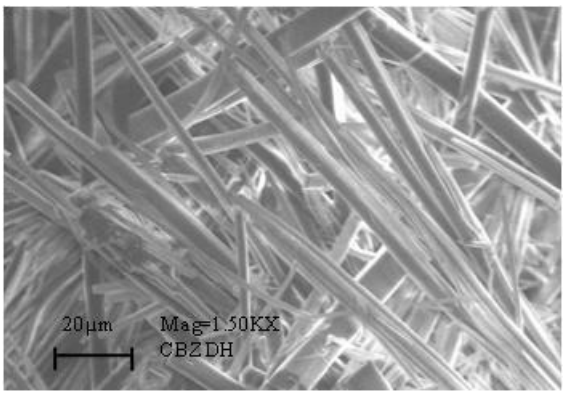

Fig. 5.8 SEM photo for CBZ DH uncompressed sample

evenly formed on the surface of CBZ III compact compared with those of CBZ I, which may be due to a lower supersaturated solution of CBZ generated. It was not a surprise that similar CBZ DH crystals were found on the surface of CBZ-NIC mixture as those of CBZ III, but there were many holes appeared on the compact surface due to the quick dissolve of NIC, which can be seen clearly by visual inspection. On the surface of CBZ-NIC cocrystal compact, smaller sizes of CBZ DH were found compared with CBZ III, I and mixture. It could explain the reason that CBZ-NIC cocrystal has the highest IDR due to slower growth of CBZ DH crystals from the solution.

SEM photos in the last three columns were taken after 30 minutes, 90 minutes and 180 minutes dissolution respectively. As dissolution time longer, surface of sample compacts exhibited some changes. SEM photos for CBZ DH show that the crystal size increases slightly, but the amount of crystals is constant. After 30 minutes, there were no significant change of CBZ DH crystals on the surfaces of CBZ III and CBZ I compacts, indicating the equilibrium state could have established with the solution. For CBZ-NIC mixture, the compact surface appears many caves due to dissolved NIC after 30 minutes. For CBZ-NIC cocrystal, it appears that more CBZ DH crystals are precipitated but there was no evidence of growth of crystals.

5.4 Discussion

From the UV imaging dissolution tests, it is clearly shown that all of test samples of CBZ III, CBZ I and CBZ-NIC cocrystal and mixture have undergone solution mediated phase transformations by precipitating a lower free energy state of CBZ DH. However,

the kinetics of these phase transformations is different. Based on the IDR profiles obtained from UV images recorded for CBZ III and CBZ I, it was suggested that the transformation process happened rapidly once a supersaturated free CBZ concentration was generated during dissolution, which cannot be maintained in solution. It followed the three stages of the transformation: creating a local supersaturation; nucleation of a stable phase; growth of the stable phase, which was confirmed by the UV images in Fig. 5.1 and SEM micrographs in Fig. 5.7. However, for CBZ-NIC cocrystal, the growth of crystallised CBZ DH was very slow. The transformation mechanism of CBZ-NIC cocrystal can be considered as the following two main stages:

First, CBZ-NIC cocrystal dissolved congruently and exhibited higher transient solubility compared with its pure component CBZ III. The maximum transient solubility can be considered as the apparent solubility. From the IDR curves in Fig. 5.4, apparent solubility of CBZ III, CBZ I and CBZ-NIC cocrystal can be predicted based on the measured solubility of CBZ DH because an IDR is directly proportional to its solubility, summarised in Table 5.1. The apparent solubility of CBZ-NIC cocrystal is 0.3746 mg/mL compared with its pure component CBZ III of 0.3135 mg/mL and is less than that of CBZ I apparent solubility of 0.4078 mg/mL. Apparent solubility of CBZ III and I is in good agreement with the reported data [99]. The apparent solubility is in order of CBZ I > CBZ-NIC cocrystal > CBZ III > CBZ DH.

Second, during CBZ-NIC cocrystal dissolution, a supersaturated free CBZ concentration was generated and can be maintained due to the complexity. When the cocrystal dissolved into the dissolution medium as the CBZ-NIC 1:1 complex, dissociation rate from CBZ-NIC complex to individual compounds decides the rate of solution medicated phase transformation. If the dissociation rate from CBZ-NIC complex in solution to individuals is slow, the crystallization of CBZ DH can be delayed, which can be indicated from the IDR-time profiles generated from the dissolution tests. CBZ-NIC mixture shows a significantly larger IDR at the beginning and this was caused by the effect of dissolved NIC on the UV absorbance. From the 10^{th} minute, the IDR of the mixture became smaller than that of the cocrystals and this may be due to the reduced NIC effect. Loss of NIC during dissolution can generate several holes on the compact surface, leading to a lower IDR, shown in Fig. 5.2.

Eventually the IDR of the CBZ-NIC mixture is smaller than that of CBZ DH due to the reduced surface area for dissolution. Although free CBZ and NIC coexisted in the solution for a while, there was no evidence of formation of a complex. CBZ-NIC cocrystal has revealed significant advantages than the two anhydrous samples CBZ III and CBZ I with the highest IDR and slowest phase conversion rate. The change rate of IDR of CBZ-NIC cocrystal is the slowest among the test samples. IDR of CBZ-NIC cocrystal has been declined by 81% over 3 hours, compared with 74% decrease for CBZ I in 15 minutes and 87% for CBZ III in 30 minutes. The enhancement of solubility and dissolution rate is significant about 1.8 times of that CBZ DH at the beginning and declined to 1.2 times after a 3-hour dissolution test. The stable IDRs in Table 5.1 is in order of CBZ-NIC cocrystal > CBZ I ≈ CBZ III ≈ CBZ DH>CBZ-NIC mixture.

In situ Raman monitoring results with SEM measurements for CBZ-NIC cocrystal, physical mixture, CBZ III and CBZ I have shown that CBZ DH crystals have crystallised on the surface of the compacts. Evolution of a ratio of characteristic peaks in Fig. 5.6 can be used to study the conversion kinetics of the samples. There is no conversion for CBZ DH so that the ratios of characteristic peaks should keep constant as the same as those before a test, which have been confirmed by the results in Fig. 5.6. A first-order kinetics model [116] was used to study the rate of conversation and the unconverted portion in a compact during dissolution as

$$Y=B+Ae^{-kt} \qquad \text{(Equ.5-1)}$$

where k represents the rate of conversion, B and A are constants. The unconverted portion on a compact surface can be calculated as

$$\text{Percentage of unconverted portion} = (B-B_{DH})/(B_0-B_{DH}) \qquad \text{(Equ.5-2)}$$

where B_0 is the ratio of characteristic peaks for the pure form of a sample and B_{DH} is the ratio of characteristic peaks for the pure CBZ DH shown in Table 5.2.

The fitted curves for each of the samples are shown in Fig. 5.6 and the calculated conversion rate constants and unconverted portions after 3-hour dissolution are in Table 5.3. The results of CBZ III and CBZ I are very close to the published data [116].

The rate of conversion represents the speed of phase conversion. CBZ III has a faster conversion rate from the starting material (CBZ III) to CBZ DH compared with that of CBZ I, which is consist with the UV imaging results. The UV imaging results show that the IDR value transition time of CBZ III is much faster than that of CBZ I. After the IDR data decreasing in the first 15 minutes of dissolution for both CBZ III and CBZ I, CBZ III kept decreasing to a much lower IDR level than CBZ I in the followed 30 minutes. While CBZ I took about 2 hours to decrease to the similar level as CBZ III, and kept it for the last hour. At the end of 3-hours dissolution, CBZ III has a slightly lower IDR than that of CBZ I, however the Raman analysis has shown that CBZ III has a higher unconverted portion than that of CBZ I. A higher unconverted portion of CBZ III means that a smaller percent of CBZ DH was found on the surface of CBZ III sample compact. Although less CBZ DH on CBZ III sample compact, it has a lower dissolution rate due to the lower apparent solubility of CBZ III (0.3135mg/mL) compared with that of CBZ I (0.4078mg/mL). Although a higher unconverted portion was found on the compact surface of CBZ III, the overall dissolution rate is lower than that of CBZ I. For CBZ-NIC mixture, it is not surprised that that it has a faster conversion rate and lower portion of unconverted CBZ III compared with those of CBZ III alone, which are consistent with those of UV imaging results. For CBZ-NIC cocrystal, it has a lower unconverted portion than those of CBZ form III and form I. The finding can be confirmed from the SEM micrographs in Fig. 5.7, in which more CBZ DH crystals are precipitated on the surface of CBZ-NIC cocrystal compact. However, the CBZ-NIC has a higher conversion rate than those of CBZ III and I, which is contradictory to that of the UV imaging results, in which the equilibrium solubility and dissolution rate of CBZ-NIC cocrystal are much higher than those of CBZ III and I. Therefore study of solid stage conversion alone during dissolution will not be enough to understand the dissolved drug in the solution.

Table 5.3 First-order rate constants and unconverted portions after 3-hours dissolution for test samples (n=3)

	CBZ-NIC cocrystal	CBZ-NIC physical mixture	CBZ III	CBZ I
Rate constant (min^{-1})	0.0975±0.0161	0.2275±0.2166	0.0126±0.0062	0.0101±0.0050
Unconverted portion (%)	7.83±1.19	13.72±6.05	62.32±8.29	15.92±2.33

5.5 Chapter conclusions

In this chapter, phase transition behaviour of CBZ-NIC cocrystal during dissolution and improvement of dissolution rate have been studied.

Cocrystals have shown huge potential to improve the dissolution rate and absorption of a poorly water soluble drug. However, solution mediated phase transformation of cocrystals could greatly reduce the enhancement of its apparent solubility and dissolution rate. On the other hand, the time scale of solution mediated phase transformation of cocrystals is an important consideration for potentially improved bioavailability. Therefore evolution of the drug concentration in the solution during dissolution of cocrystal needs to be understood and evaluated. Relationship between dissociation rate of the cocrystal complex in the solution and dissolution rate of cocrystal solid is important, which will influence the crystallization of the component with low solubility of drug compound and the dissolution profile of the cocrystal.

Dissolution and transformation behaviour of CBZ-NIC cocrystal was studied by different *in situ* techniques of UV imaging and Raman spectroscopy. It has been found that CBZ-NIC cocrystal including other polymorphs of CBZ III and I and mixture are converting to CBZ DH during dissolution. Compared with CBZ III and I, the rate of IDR of CBZ-NIC cocrystal decreases slowly, indicating the rate of crystallization of CBZ DH from the solution is slow. *In situ* solid-state characterisation during dissolution has shown the evolution of conversion of CBZ-NIC cocrystal and polymorphs to its dihydrate form, which cannot completely be understood by merely measuring the dissolved drug concentration. This study has shown that *in situ* UV imaging and Raman spectroscopy with a complementary technique of SEM can provide an in depth understanding during dissolution. The information from the experiments on transformation behaviour of CBZ-NIC cocrystal is valuable for understanding the mechanisms of cocrystal dissolution.

Chapter 6 Investigation of the Effects of Surfactants on Carbamazepine-Nicotinamide Cocrystal Solubility and Dissolution Behaviour

6.1 Chapter overview

In order to critically evaluate and understand the role of surfactants in inhibiting the solution mediated phase transformation (SMPT) of a cocrystal, two surfactants of sodium lauryl sulphate (SLS, or Sodium dodecyl sulfate SDS) and Tween 80 (Polysorbate 80) were selected to investigate their effects on the solubility and intrinsic dissolution rate (IDR) of CBZ-NIC cocrystal in this chapter. SLS is an anionic surfactant and Tween 80 is a nonionic surfactant, both of which have been widely used in various drug dosage forms to control wetting, stability, and solubilisation of hydrophobic drugs. The chemical structures of SLS and Tween 80 are shown in Fig. 6.1.

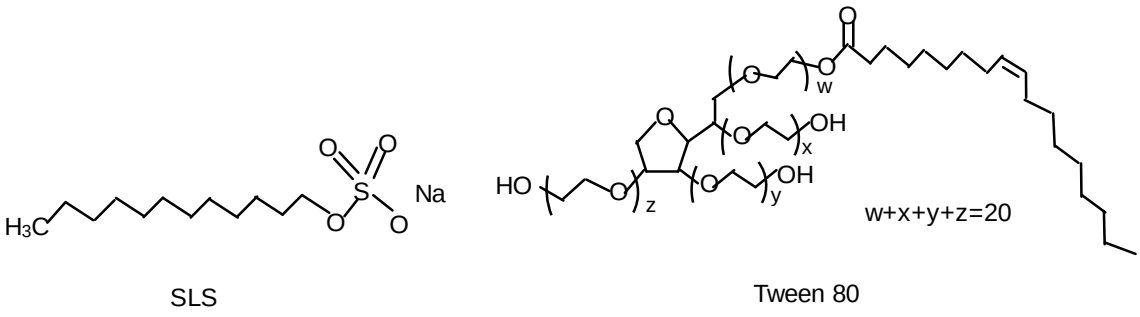

Fig. 6.1 Molecular structure of SLS and Tween80

The solubility of CBZ-NIC cocrystal at different concentrations of surfactant solutions was predicted from measurement of eutectic points or transition concentrations where solid cocrystal and drug are in equilibrium with solution [84-86]. Evolution of the IDR of CBZ-NIC cocrystal at different concentrations of surfactant solutions was monitored by the UV imaging dissolution system during dissolution. The solid-state changes of CBZ-NIC cocrystal after dissolution were quantified by Raman spectroscopy. Comparison of solubility and intrinsic dissolution behaviour of CBZ polymorphs (form III and DH) and physical mixture of CBZ form III and NIC were also given in this chapter.

6.2 Materials and methods

6.2.1 Materials

Anhydrous CBZ III, NIC, ethyl acetate, Tween 80, SLS, methanol (HPLC grade), and double distilled water were used in this chapter, details about this material are listed in chapter 3 Materials and methods. CBZ DH, 1:1 CBZ-NIC cocrystal and equimolar physical mixture of CBZ III and NIC were prepared as described in section 3.4.2 Test samples preparation.

6.2.2 Methods

6.2.2.1 Equilibrium solubility

The solubility of CBZ DH, CBZ-NIC cocrystal, and physical mixture in both water and surfactant solutions were determined using an air-shaking bath method. Details about this method were described in section 3.3.11.1 Equilibrium solubility test. The tests have been done at 25°C for 72 hours. CBZ and NIC concentrations were determined by Perkin Elmer series 200 HPLC. Surfactant solutions used in this study are at the following concentrations: 0.35, 1.7, 3.5, 6.9, 10.4, 17.3, 34.7 mM SLS; and 0.076, 0.76, 1.5, 2.3, 3.8, 7.6, 17.3, 34.7 mM Tween80. All solubility tests were carried out in triplicate.

6.2.2.2 Cocrystal eutectic points

Cocrystal eutectic points or transition concentrations were measured as a function of SLS or Tween 80 concentration in water at 25 ℃ [151, 172]. Details of the measurement can be found in section 3.3.11.2. Cocrystal eutectic points measurement test.

For 1:1 AB cocrystal without consideration of ionization for either component, its aqueous solubility was determined from eutectic concentration measurements by following equation [84],

$$S_{AB} = \sqrt{K_{sp}} = \sqrt{[A]_{eu}[B]_{eu}} \qquad \text{(Equ.6-1)}$$

where K_{sp} is the cocrystal solubility product and $[A]_{eu}$ and $[B]_{eu}$ are the eutectic concentrations of drug and coformer at equilibrium.

6.2.2.3 Critical micelle concentration and solubilisation capacity

The critical micellar concentrations (CMCs) of SLS and Tween 80 were determined in aqueous solutions in the presence of saturated CBZ from the surface tension dependence on surfactant concentration by a KSV CAM200 surface tension meter at room temperature.

The molar solubilisation capacities of SLS and Tween 80 for CBZ can be obtained according to the following equation:

$$S_{CBZ,T} = S_{CBZ,aq}(1 + K_s^{CBZ}[M]) \qquad \text{(Equ.6-2)}$$

where $S_{CBZ,T}$ is the solubility of CBZ in micellar solution; $S_{CBZ,aq}$ is the solubility of CBZ in water; $[M] = C - CMC$ is the surfactant micellar concentration; and C is the surfactant concentration.

6.2.2.4 Intrinsic dissolution study by UV imaging system

The dissolution behaviour of CBZ III, the CBZ-NIC cocrystal, and the physical mixture of CBZ III and NIC in both pure water and at different concentrations of surfactant solutions was studied by an ActiPix SDI 300 UV surface imaging system (Paraytec Ltd., York, UK). Details of description of the system can be found in section 3.3.1 ActiPix SDI 300 UV imaging dissolution system. All dissolution tests were performed at 25°C in triplicate. The concentrations of each surfactant used in the study were: 0.35 and 10.4 mM of SLS solutions, 0.076 and 7.6 mM of Tween 80 solutions.

The sample compacts used in UV imaging dissolution tests were analysed prior to and immediately after dissolution tests using a LEICA DM 750 microscope and EnSpectr R532® Raman spectrometer. The percentage of CBZ DH crystallised during dissolution were quantitative analysed by Raman spectroscopy.

6.3 Results

6.3.1 Results of solubilisation by surfactants

The equilibrium solubility of CBZ DH (CBZ III), CBZ-NIC cocrystal and physical mixture of CBZ III and NIC in water, and at different concentrations of SLS and Tween 80 after 72 hours are shown in Fig. 6.2 and details of data are in Table 6.1. Generally, there was no significant difference in the solubility between the parent drug (CBZ), cocrystal and the physical mixture. FTIR, and Raman spectra (shown in Appendix, A1.1.1-2) of solid residue indicated that CBZ-NIC cocrystal had totally converted to CBZ DH, therefore the same solubility of cocrystal and CBZ DH was found.

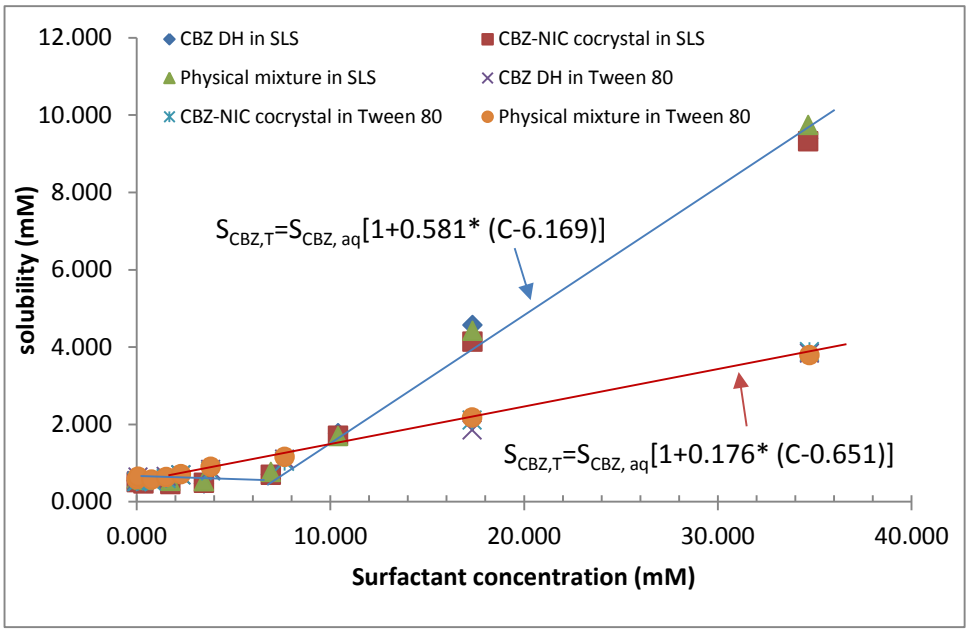

Fig. 6.2 Solubility of CBZ as function of surfactant concentration

Table 6.1 Equilibrium solubility of CBZ DH, CBZ-NIC cocrystal and physical mixture at 25°C as function of surfactant concentration after 72 hours

	concentration	CBZ DH (CBZIII) (mM)	cocrystal		physical mixture	
	mM	CBZ	CBZ (mM)	NIC (mM)	CBZ (mM)	NIC (mM)
	0.000 (water)	0.538±0.038	0.502±0.028	2.613±0.140	0.575±0.036	2.569±0.164
	0.347	0.476±0.020	0.473±0.030	2.482±0.162	0.550±0.024	2.776±0.042
	1.734	0.457±0.015	0.450±0.041	2.382±0.230	0.525±0.020	2.672±0.103
SLS	3.468	0.461±0.011	0.487±0.019	2.449±0.109	0.516±0.021	2.565±0.104
	6.935	0.695±0.004	0.694±0.015	2.469±0.039	0.763±0.015	2.648±0.121

	10.403	1.762±0.202	1.704±0.088	2.475±0.140	1.684±0.062	2.546±0.081
	17.339	4.557±0.859	4.139±0.173	16.066±4.084	4.412±0.234	15.337±1.066
	34.677	9.385±0.191	9.324±0.212	14.148±0.607	9.732±0.481	17.010±1.081
Tween 80	0.000 (water)	0.538±0.038	0.502±0.028	2.613±0.140	0.575±0.036	2.569±0.164
	0.076	0.623±0.034	0.520±0.023	2.581±0.077	0.646±0.033	2.574±0.102
	0.763	0.574±0.039	0.531±0.026	2.442±0.055	0.573±0.041	2.534±0.148
	1.527	0.643±0.054	0.588±0.032	2.453±0.062	0.636±0.005	2.636±0.009
	2.290	0.683±0.052	0.683±0.025	2.576±0.073	0.714±0.024	2.625±0.060
	3.817	0.828±0.021	0.783±0.048	2.578±0.045	0.902±0.114	2.785±0.279
	7.634	1.092±0.083	1.035±0.048	2.440±0.023	1.154±0.120	2.647±0.124
	17.328	1.841±0.149	2.097±0.225	15.755±0.253	2.177±0.206	17.535±4.597
	34.733	3.830±0.095	3.871±0.407	15.182±0.410	3.789±0.126	16.418±1.112

Based on the measured solubility data of CBZ, the molar solubilisation capacities and CMCs of SLS and Tween 80 can be estimated, as summarized in Table 6.2. It is shown that the estimated CMCs of SLS and Tween 80 are in good agreement with those measured by the surface tension technique. The change of surface tension at different surfactant concentrations of aqueous solutions in the presence of saturated CBZ is shown in Fig. 6.3. Tween 80 has a higher solubilisation capacity at a low concentration due to its lower CMC. However, the anionic surfactant SLS showed a dramatic solubilizing ability with CBZ when its concentration was higher than its CMC. When the concentration of SLS is higher than a critical value of 8.567 mM, SLS has a higher solubilisation capacity for CBZ than Tween 80, which can be seen from the solubility data of CBZ in Fig.6.2.

Table 6.2 Estimated molar solubilisation capacity and CMC

surfactant	Solubilisation capacity (mM^{-1})	CMC estimated (mM)	CMC measured (mM)
SLS	0.581	6.196	5.5
Tween 80	0.176	0.651	0.012 – 1.05

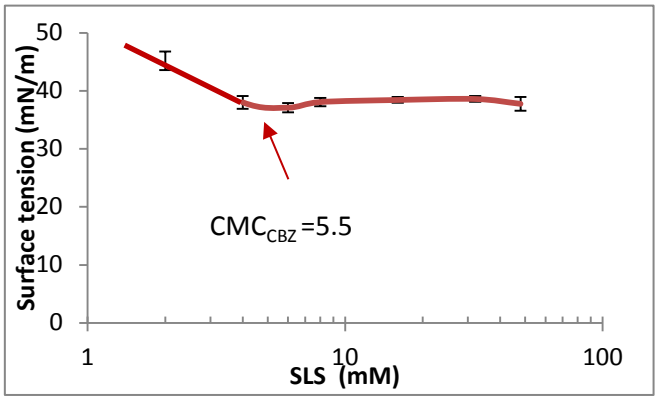

(a) SLS

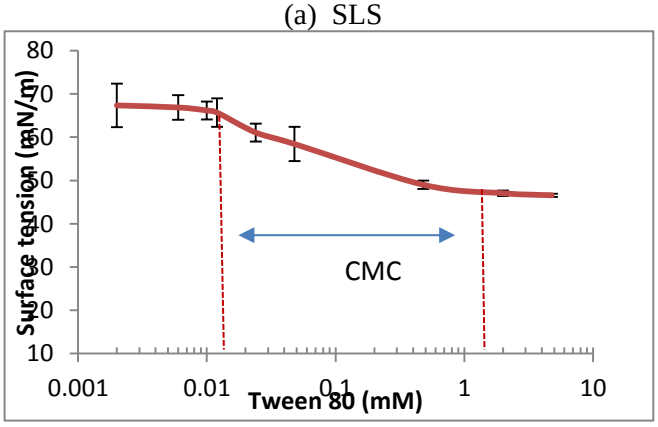

(b) Tween 80

Fig. 6.3 Surface tension versus surfactant concentration: (a) SLS; (b) Tween80

The apparent solubility of CBZ was measured as a function of the coformer NIC concentration in order to determine CBZ-NIC cocrystal eutectic point (shown in Fig.6.4), in which four regions can be identified:

Region I: from 0 to 1000 mM initial NIC concentrations, the solubility of CBZ increases rapidly with increasing concentration of NIC, indicating the 1:1 complex formation of CBZ and NIC. The solubility of CBZ can increase up to 10 times in comparison to CBZ solubility in water. In this region, the solubility limit of the complex formed is not exceeded and the solid residue should be CBZ DH only, which was confirmed by DSC, FTIR and Raman analyses (figures shown in Appendix, A1.2.1-3; data shown in Table 6.3). In this region, the measured concentration of NIC was the same as that of the initial NIC.

Region II: from 1000 to 2400 mM initial NIC concentrations, the solubility of CBZ increases at a higher rate. When the solubility limit of the 1:1 complex formed was

exceeded in this region, CBZ-NIC cocrystal precipitated. In the meantime, higher order complexes of CBZ and NIC were generated, resulting in a further 18 times increase in the CBZ equilibrium solubility in water. The solid residue indicated the presence of two phases of CBZ-NIC cocrystal and CBZ DH confirmed by DSC, FTIR and Raman analyses **(**figures shown in Appendix, A1.2.1-3; data shown in Table 6.3). According to the definition, any point in the region II should be a eutectic point of CBZ-NIC cocrystal. In this study, we set the highest total CBZ concentration point as its eutectic point shown in Fig.6.4 as $[CBZ]_{eu} = 15.1mM$ and $[NIC]_{eu} = 1956.8\,mM$.

Region III: from 2400 to 3000 mM initial NIC concentrations, the concentration of CBZ decreases with increasing NIC concentration in solution. In this region, all of the solid CBZ DH was consumed to form the complex to generate the supersaturated solution of the complex, resulting in precipitation of large amount of CBZ-NIC cocrystal and reduction of CBZ concentration in solution. For this reason, the overall CBZ concentration decreased in solution shown in Fig. 6.4. It has been shown that CBZ-NIC cocrystal and NIC are coexisting in solid residues, shown in DSC, FTIR and Raman analyses **(**figures shown in Appendix, A1.2.1-3; data shown in Table 6.3).

Region IV: Above 3000 mM initial NIC concentration, the concentrations of CBZ and NIC in the solution are constant. The solid residues indicated the presence of two phases of CBZ-NIC cocrystal and NIC, confirmed by DSC, FTIR and Raman analyses **(**figures shown in Appendix, A1.2.1-3; data shown in Table 6.3).

Table 6.3 Characteristic peaks for solid forms identification

	DSC	FTIR	Raman
Region I	DH dehydration peak 80-120°C; CBZ I melting point 195°C	DH characteristic peak at 3429, 3360, 3280, 3182cm^{-1}	DH single peak at 253 cm^{-1}; DH ratio of peaks at 1040 to 1025 cm^{-1}
Region II	DH dehydration peak 80-120°C; cocrystal melting point around 163°C	DH characteristic peak at 3429cm^{-1}; cocrystal show weak characteristic peaks at 3449, 3390cm^{-1};	show DH characteristic peaks; cocrystal characteristic peaks were overlayed by DH peaks

Region III	NIC melting point around 130°C; cocrystal melting point around 163°C	NIC peak at 1680cm^{-1}; cocrystal characteristic peak at 3449cm^{-1}; the mixture of NIC peak 3154 and cocrystal peak 3183cm^{-1}	NIC peak at 1042, 3060 cm^{-1}; cocrystal single peak at 264 cm^{-1}, peak ratio around 1000 show cocrystal characteristics
Region IV	relative larger NIC melting point around 130°C, indicate more NIC; cocrystal melting point around 163°C	NIC peak at 1680cm^{-1}; cocrystal characteristic peak at 3449cm^{-1}; the mixture of NIC peak 3154 and cocrystal peak 3183cm^{-1}	NIC peak at 1042, 3060 cm^{-1}; cocrystal single peak at 264 cm^{-1}, peak ratio around 1000 show cocrystal characteristics

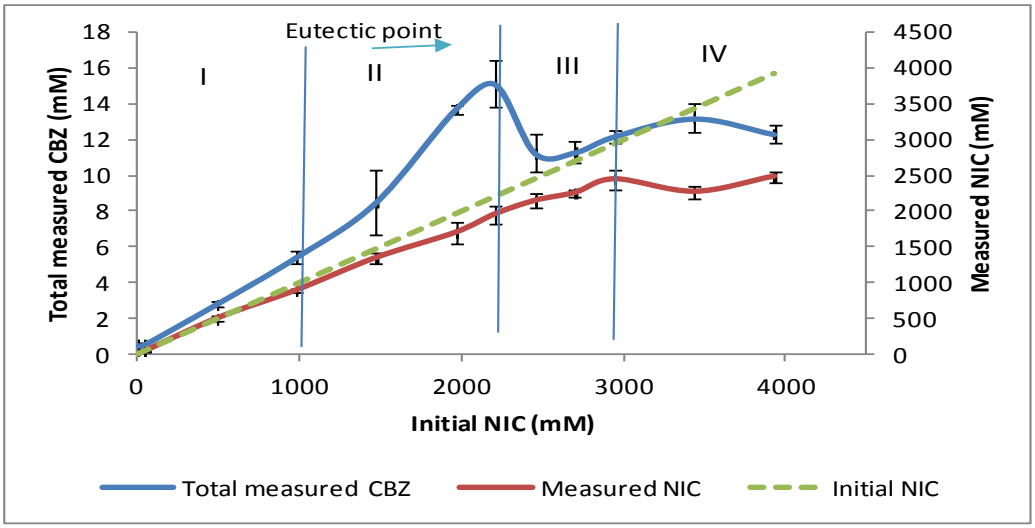

Fig. 6.4 CBZ solubility profile as a function of NIC concentration after 72 hours

Table 6.3 shows the total concentrations of CBZ and NIC at the eutectic points of different concentrations of SLS and Tween 80. Compared with the eutectic point in water, the solubility of CBZ increased slightly with an increase in SLS concentration while the concentration of NIC was constant with SLS concentration (which was slightly smaller than that in pure water). According to the solubility definition of a 1:1 cocrystal shown in Equ. 6-1, the solubility of CBZ-NIC cocrystal at different concentrations of SLS is shown in Table 6.3. The solubility of CBZ-NIC cocrystal was nearly constant and same as that in water when SLS concentration was below its CMC and it increased slightly when the SLS concentration was above its CMC.

Compared with the eutectic point in water, the solubility of CBZ was almost constant with an increase in Tween 80 concentration, while concentration of NIC decreased at

higher concentration of Tween 80 solutions. The solubility of the CBZ-NIC cocrystal was nearly same as that in water at a lower concentration of Tween 80 solution and then decreased slightly when Tween 80 concentration increased (see Table 6.4).

Table 6.4 CBZ-NIC cocrystal eutectic point, cocrystal solubility and solubility ratio

Solvent	concentration (mM)	$[CBZ]_{eu}$ (mM)	$[NIC]_{eu}$ (mM)	Cocrystal solubility S_{cc} (mM)	Solubility ratio $S_{cc}/S_{CBZ,aq}$
Water		15.10±1.32	1956.8+126.8	171.9	319
	0.35	15.9±1.8	1665.2±62.6	162.8	302
	1.7	16.3±0.76	1807.9±90.3	171.5	319
	3.5	17.6±0.63	1818.9±57.0	178.7	332
SLS	6.7	17.5±0.65	1914.0±136.3	183.2	340
	10.4	17.7±0.42	1811.1±65.7	179.2	333
	17.3	18.1±0.70	1934.6±51.8	187.3	348
	34.7	16.1±2.77	1839.5±255.9	171.8	319
	0.076	15.5±0.68	1847.3±15.6	169.5	315
	0.76	15.9±0.37	1852.3±56.9	171.7	319
	1.5	16.0±0.70	2024.3±50.9	180.2	335
Tween80	2.3	17.4±1.65	1853.3±109.9	179.5	334
	3.8	16.75±2.78	1624.5±69.1	164.9	306
	7.6	14.98±0.45	1691.1±87.4	159.2	296
	17.3	15.33±0.89	1638.9±79.8	158.5	294

6.3.2 Results of intrinsic dissolution rate

The IDR profiles from compacts of the pure CBZ III, CBZ-NIC cocrystal, and physical mixtures of CBZ III and NIC at different dissolution media are shown in Fig. 6.5.

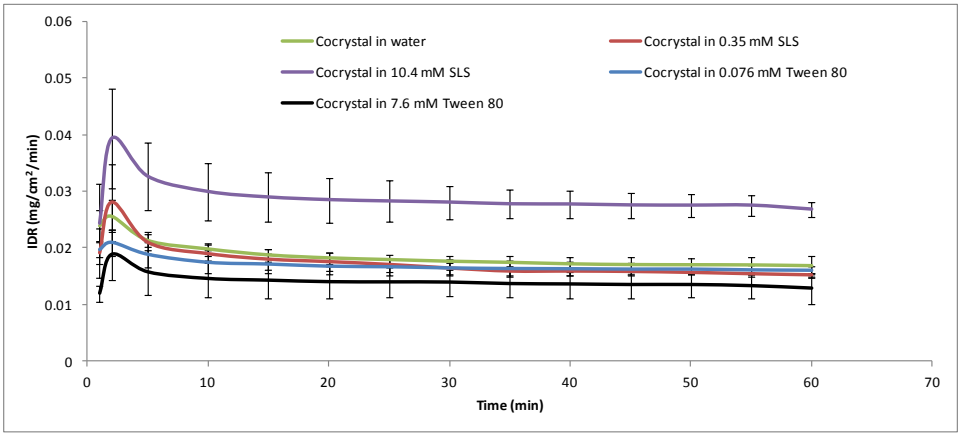

(a)

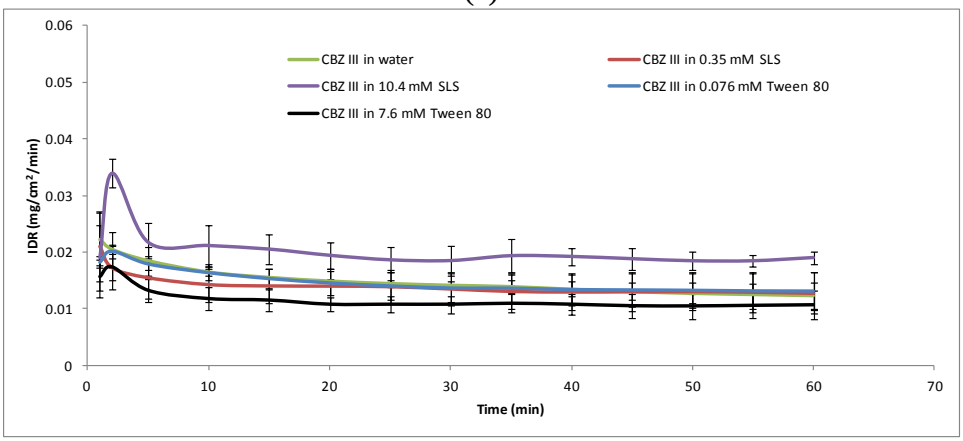

(b)

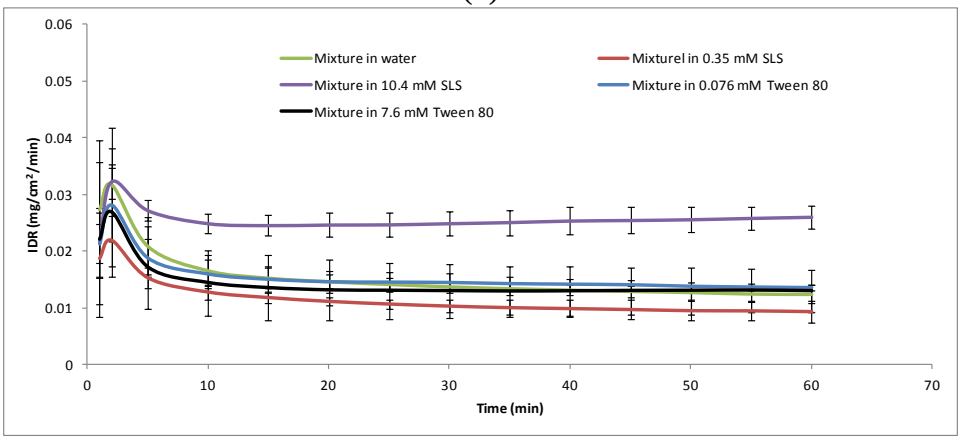

(c)

Fig. 6.5 Dissolution profiles of test samples at different dissolution media: (a) CBZ-NIC cocrystal; (b) CBZ III; (c) equimolar physical mixture of CBZ III and NIC

Table 6.5 Light microscopy photographs of the sample compacts before and after dissolution tests in 10.4 mM SLS and 7.7 mM Tween 80 dissolution media

Sample	Surfactant	Before	After

CBZ-NIC cocrystal	10.4 mM SLS		
	7.6 mM Tween 80		
CBZ III	10.4 mM SLS	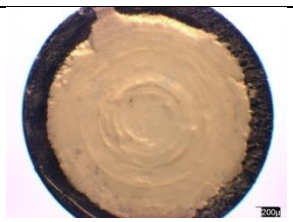	
	7.6 mM Tween 80		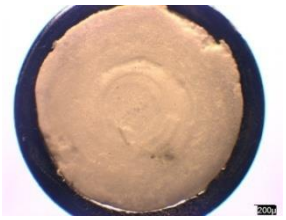
Physical mixture of CBZ III and NIC	10.4 mM SLS		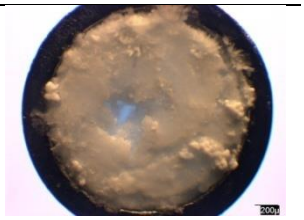
	7.6 mM Tween 80		

All IDR profiles show the same trend: (1) within the first 2 minutes IDR of a test sample reached its maximum value and then decreased quickly within 10 minutes; (2) after 20 minutes of dissolution, all IDRs of test samples reached static values. The IDR of each sample during dissolution in each dissolution medium was decreasing, indicated by the growth of solid material on the surface of sample compact that can be visualized by light microscopy (see Table 6.5). Prior to dissolution tests, all of the compact

surfaces were smooth. After dissolution tests, the microscope images show that small needle-shaped crystals have appeared on the compact surfaces, indicating that solid state changes due to crystallisation of CBZ DH from the supersaturated solutions on compact surfaces.

The IDRs of CBZ-NIC cocrystal are shown in Fig. 6.5 (a). It was found that IDR profile of CBZ in the 0.35 mM SLS dissolution medium was almost identical to that in water. In 0.076 mM Tween 80 dissolution medium, its dissolution profile was slightly lower than that in pure water. In 10.4 mM SLS dissolution medium, IDR profile of CBZ-NIC cocrystal increased significantly in comparison with that in water, indicating that SLS can increase cocrystal dissolution rate when its concentration was higher than its CMC. To our surprise, in the 7.6 mM Tween 80 dissolution medium, the CBZ dissolution profile was much lower than that in water.

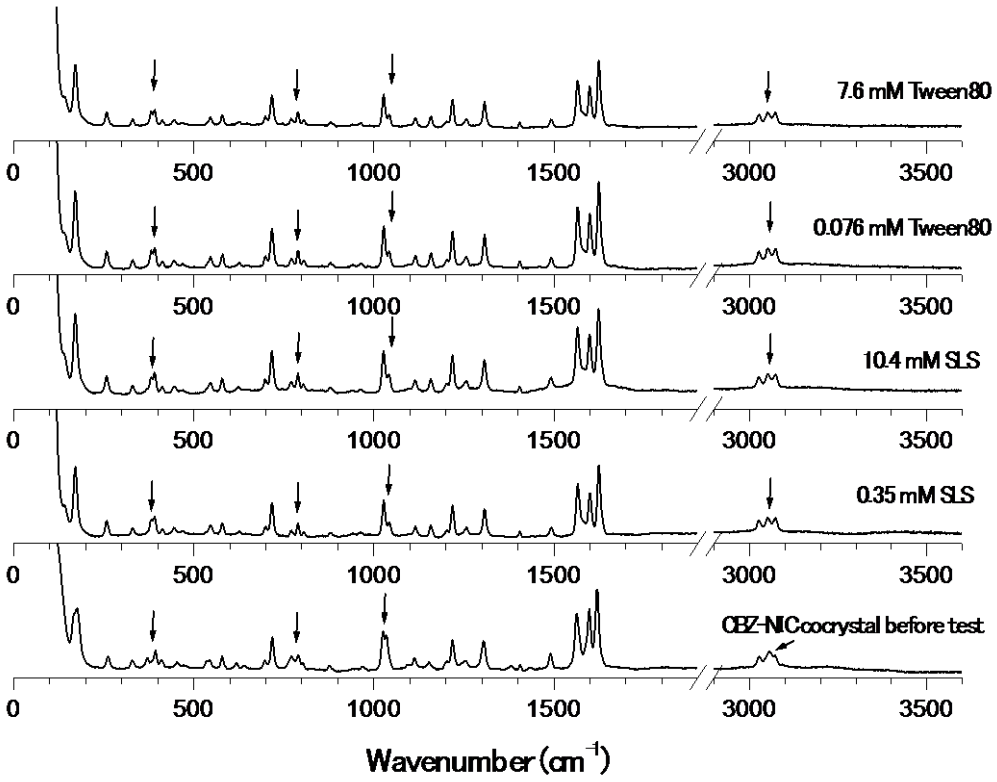

(a1) CBZ –NIC cocrystal Raman spectrum 0-3600cm^{-1}

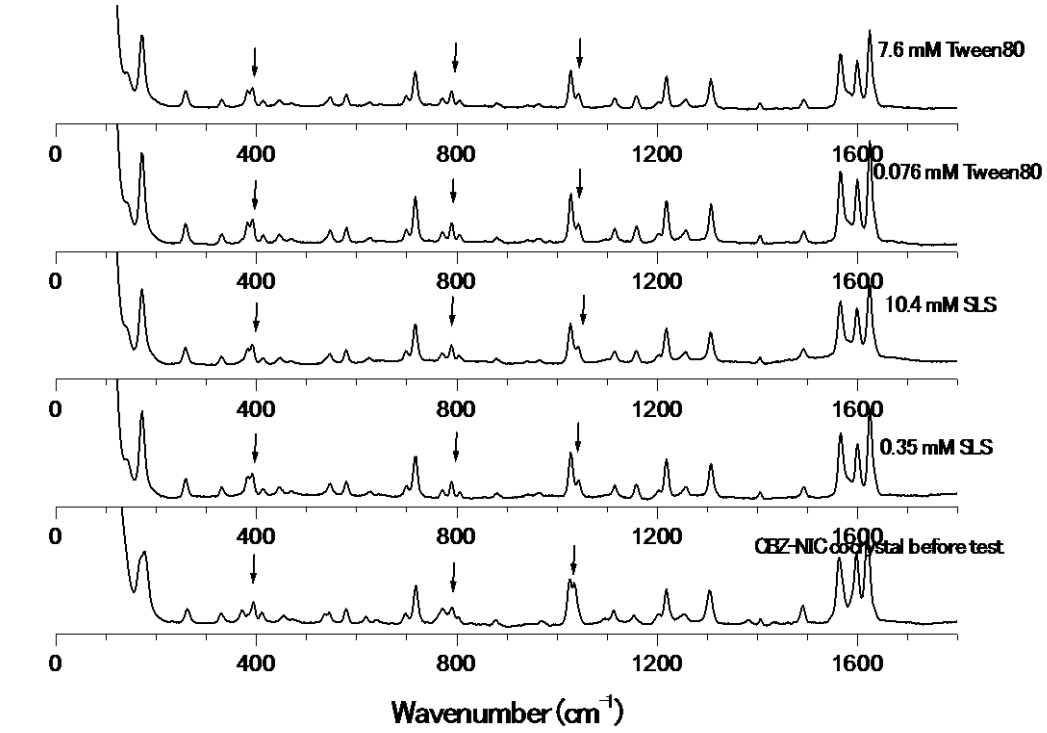

(a2) CBZ –NIC cocrystal Raman spectrum 0-1800cm^{-1}

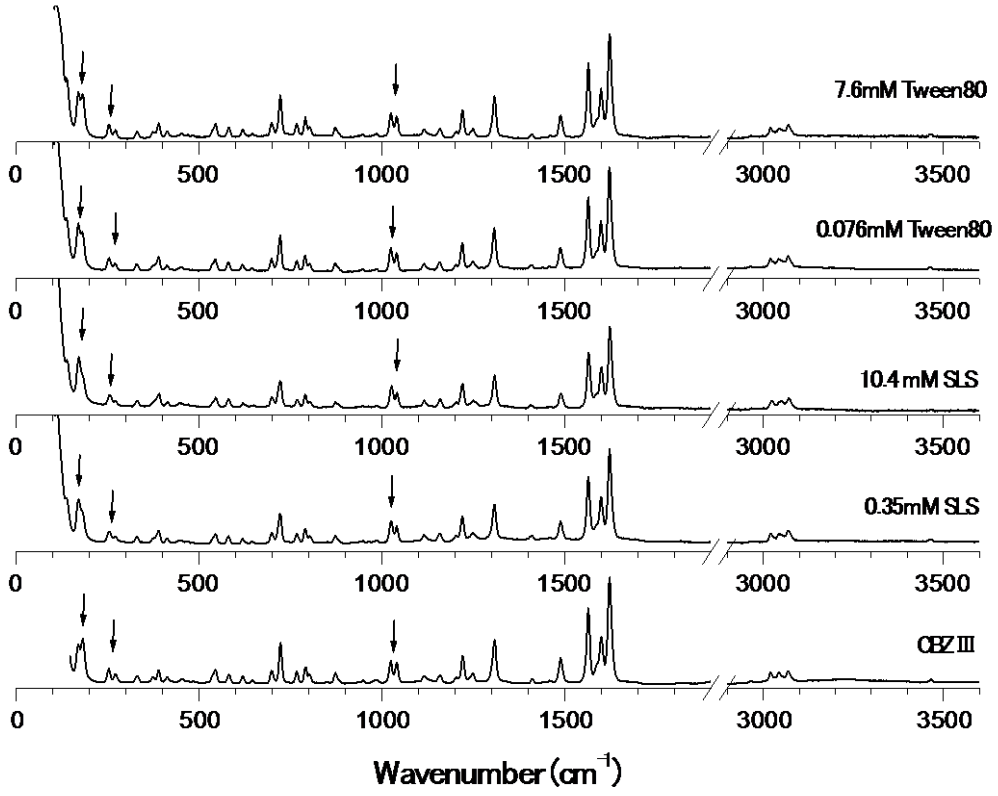

(b1) CBZ III Raman spectrum 0-3600cm^{-1}

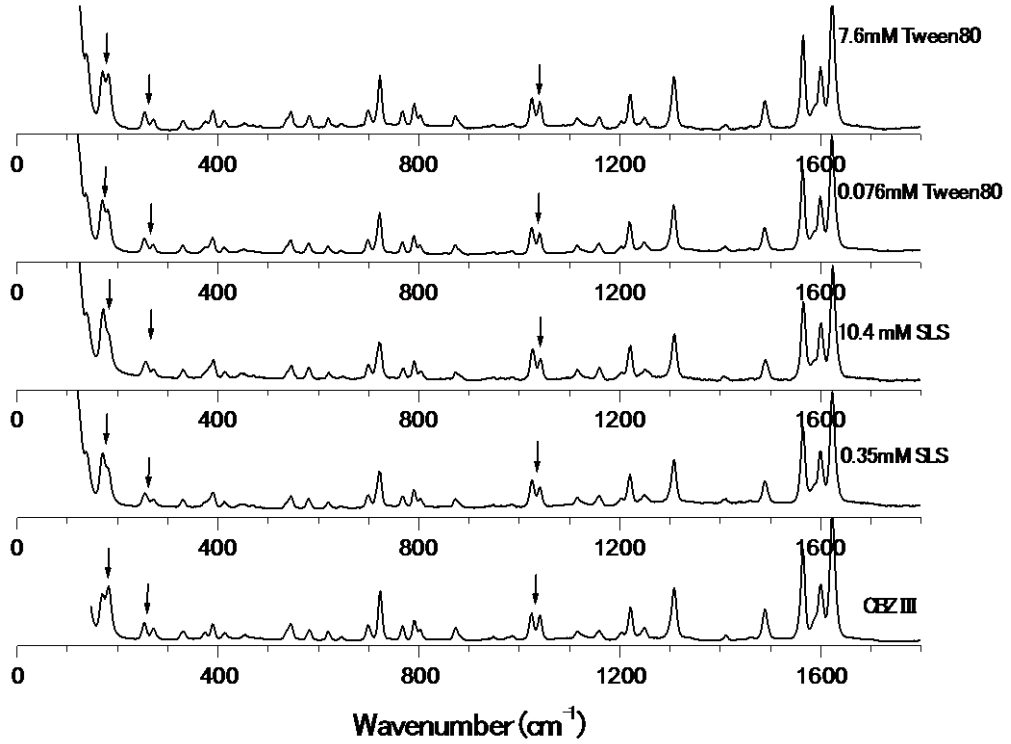

(b2) CBZ III Raman spectrum 0-1800cm^{-1}

Fig. 6.6 Raman spectra of the compacts before and after UV imaging dissolution at different dissolution media: (a) CBZ-NIC cocrystal; (b) CBZ III

Raman spectroscopy was used before and after UV imaging to characterize solid state (see Fig. 6.6), and showed some characteristic peaks of starting material has changed after the dissolution tests, which are in good agreement with previous findings [151]. The ratios of peak intensity at 1035 to 1025 cm^{-1}, 1040 to 1025 cm^{-1} have changed for CBZ-NIC cocrystal and CBZ III due to the transformation to CBZ DH. In order to quantify solid-state change during dissolution, calibration models were built to quantify the percentage of CBZ DH on the surface of a sample compacts after dissolution test, details about calibration model were shown in section 3.3.2.

The percentage of CBZ DH covering on the surface of CBZ-NIC cocrystal sample compact for each dissolution test is shown in Fig. 6.7(a). Interestingly the percentages of CBZ DH crystals on the surfaces of CBZ-NIC cocrystal compacts in 0.35 mM SLS and 10.4 mM SLS dissolution media are nearly constant (i.e. 81% in 0.35 mM SLS solution and 78% in 10.4 mM SLS dissolution solution), which nearly equal to that (i.e. 77%) of CBZ-NIC cocrystal in water. By contrast, the percentages of CBZ DH covering the surfaces of CBZ-NIC cocrystal compacts in both 0.076 mM Tween 80 and 7.6 mM

Tween 80 (i.e. 94% in both Tween 80 solutions) are much higher than that of CBZ-NIC cocrystal in water.

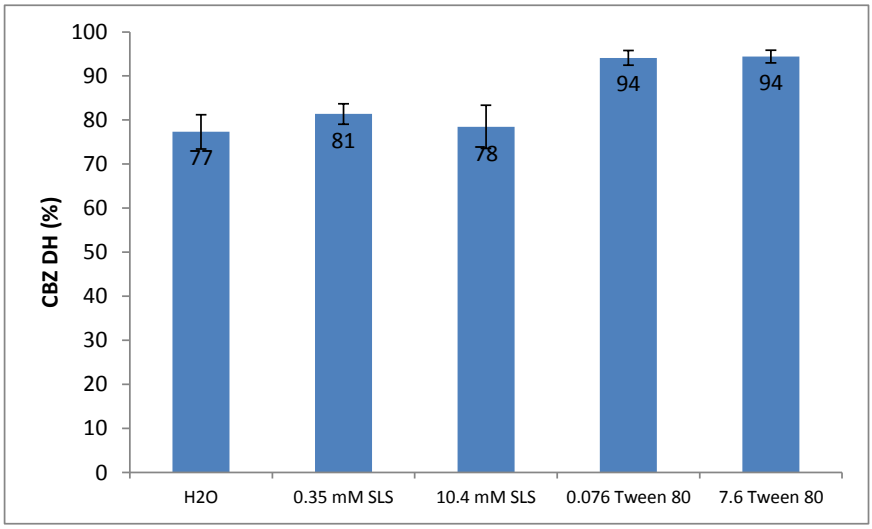

(a)

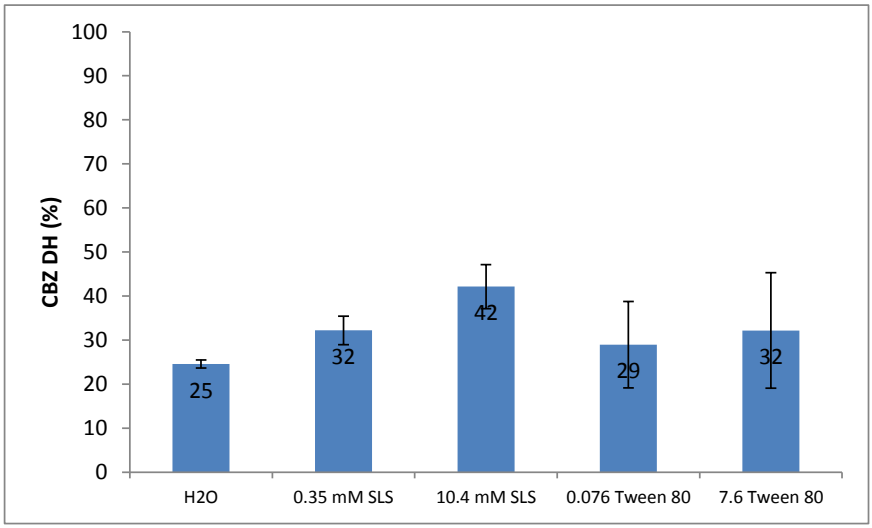

(b)

Fig. 6.7 Comparison of percentages of CBZ DH on the surfaces of sample compacts after dissolution test: (a) CBZ-NIC cocrystal; (b) CBZ III

CBZ III is an anhydrous form of CBZ and has similar dissolution behavior to that of CBZ-NIC cocrystal in different surfactant solutions. If a surfactant concentration was lower than its CMC, the IDR profile of CBZ III in the 0.35 mM SLS dissolution or 0.076 mM Tween 80 was similar to that in water, as shown in Fig. 6.5(b). When compared with the dissolution behavior of CBZ III in water, the IDR profile of CBZ III increased significantly in 10.4 mM SLS dissolution medium and decreased in 7.6 mM

Tween 80 dissolution medium. The percentage of CBZ DH covering on the surface of CBZ III sample compact for each dissolution test based on Raman spectra is shown in Fig. 6.7(b). The percentages of CBZ DH crystals on the surfaces of CBZ III compacts increased significantly with SLS concentration in comparison with that in pure water. A similar trend was found in a Tween 80 dissolution medium: the percentages of CBZ DH covering the surfaces of CBZ III compacts in both 0.076 mM Tween 80 and 7.6 mM Tween 80 dissolution media increased, but to a lesser extent than those in the SLS dissolution media.

Evolution of the IDRs of the equimolar physical mixture of CBZ III and NIC at different dissolution media is shown in Fig. 6.5(c). The biggest variability of the IDRs of the physical mixture is shown, which is consistent with that of dissolving polyphase mixtures in which the more soluble component dissolves more rapidly from the surface of compact, leaving behind a porous layer of the less soluble component [88, 172]. Light microscopy showed that holes appeared on the compact surface due to dissolved NIC (see Table.6.5), resulting in a significant change of the dissolution rate. Similar trends of effects of dissolution media on IDR of physical mixture was found with the 10.4 mM SLS dissolution medium, the IDR profile increased significantly compared with that of pure water in Fig.6.5(c).

6.4 Discussion

6.4.1 Discussion of solubility enhancement by surfactants

From this study, it has been shown that CBZ-NIC cocrystal has the same equilibrium solubility of CBZ DH (CBZ III) because of dissociation of individual components of CBZ-NIC cocrystal, which in turn is due to weak hydrogen bonds in molecular assembly of the two components of CBZ and NIC. There was no significant effect of the cocrystal coformer NIC on the solubility of CBZ because of a low concentration of NIC in solution. Based on the CBZ solubility profile as a function of NIC concentration, it has been shown in Fig. 6.4 that at a low NIC concentration (up to 40 mM) solubility of CBZ was constant.

The phase solubility diagram of CBZ in the presence of NIC has shown that CBZ solubility has been enhanced significantly and in a nonlinear fashion as a function of NIC concentration (Fig. 6.4). The experimental observations can be explained by stacking complexation mechanism of NIC with CBZ [173], in which linear increases in the solubility of CBZ may be attributed to the formation of 1:1 complexes in Region I and nonlinear increases in Region II, indicating that higher order complexes were formed due to self-association of NIC. Due to the strong interaction of CBZ and NIC in solution, the eutectic point of the CBZ-NIC cocrystal was not a single point, but covered the whole range of Region II from 1000 mM to 2400 mM of NIC concentrations. In this study, the highest total measured CBZ concentration was selected as eutectic point of CBZ-NIC cocrystal (Fig. 6.4), showing that the solubility ratio of Scc /$S_{CBZ,aq}$ was 319. If the lowest total measured CBZ concentration in region II was selected as eutectic point of CBZ-NIC cocrystal, and the solubility ratio of Scc /$S_{CBZ,aq}$ was 130. The reported value of solubility ratio of Scc /$S_{CBZ,aq}$ was 152, which was in the region II of phase solubility diagrams [84].

SLS and Tween 80 have little effects on enhancing the solubility of CBZ-NIC cocrystal in Table 6.4, in which the solubility of the CBZ-NIC cocrystal increased slightly with SLS concentration and decreased with Tween 80 concentration, however, significant solubility enhancement for CBZ DH by SLS was observed above its CMC.

6.4.2 Discussion of effects of surfactants on SMPT of CBZ III and CBZ-NIC cocrystal

Comparing IDRs of CBZ III, CBZ-NIC cocrystal and physical mixture of CBZ III and NIC in the same dissolution medium, it has been shown that CBZ-NIC cocrystal has the highest IDR in Fig. 6.5, indicting the advantages of CBZ-NIC cocrystal in enhancing the dissolution rate [151].

From this study, it has also shown that SMPT of CBZ III and CBZ-NIC cocrystal can be altered by inclusion of a surfactant in dissolution medium. However, CBZ III and CBZ-NIC cocrystal have shown different transformation behaviour affected by different surfactants.

It is well known that surfactants can enhance dissolution of poorly water soluble drugs in two ways, i.e. either by lowering the surface tension at solid drug surface to increase surface area available for dissolution or by increasing drug solubility [174]. The ability of surfactants of SLS and Tween 80 to manipulate the SMPT of CBZ-NIC cocrystals and CBZ III affects the nucleation and/or growth of new crystalline phase of CBZ DH.

Dissolution experiments with CBZ III have shown the increased percentages of CBZ DH precipitated on the surfaces of sample compacts with increasing surfactant concentrations of SLS and Tween 80 (see Fig. 6.7(b)), indicating that both SLS and Tween 80 facilitated surface mediated nucleation of CBZ DH on the dissolving CBZ III. These results are in line with classic nucleation theory which predicts that crystal nucleation increases with decreasing interfacial tension by inclusion of surfactants in dissolution medium [175]. Comparing the two surfactants, anionic surfactant SLS has shown more significant effects on nucleation of CBZ DH during dissolution of CBZ III than Tween 80, indicted by higher percentages of CBZ DH covering on the surface of dissolution compact.

Dissolution experiments of CBZ-NIC cocrystal with and without SLS show the same percentage of CBZ DH precipitated on the surface of each sample compact (Fig. 6.7(a)), indicating that SLS does not facilitate surface mediated nucleation of CBZ DH on the dissolving CBZ-NIC cocrystal. The rate of CBZ DH nucleation for CBZ-NIC cocrystal dissolution was influenced mainly by the coformer NIC, rather than as a consequence of decreasing the interfacial tension by SLS. Dissolution experiments of CBZ-NIC cocrystal with 0.076 and 7.6 mM concentrations of Tween 80 have shown that significant higher of CBZ DH was precipitated as a covering on sample compact surfaces, (94% compared with 77% of CBZ DH crystallised on the surface in pure water), indicating that the rate of CBZ DH nucleation during CBZ-NIC cocrystal dissolution was affected by both the coformer NIC and by Tween 80.

Dissolution rate is the net result of solubilisation rates of original solid phase and formation rates of a less soluble solid phase. SLS has a flexible alkyl chain that exhibits axial polarity (hydrophilic head group and hydrophobic tail) and a well-defined CMC. The transformation process of CBZ-NIC cocrystal and CBZ III to CBZ DH is sensitive

to the SLS concentration in a dissolution medium. The solubility of CBZ for solid of CBZ III has not increased in 0.35 mM SLS dissolution medium below its CMC. Due to increasing in rate of CBZ DH nucleation, the IDR profile of CBZ III in the 0.35 mM SLS dissolution medium was lower than its corresponding profile in water (Fig. 6.5(b)). Because SLS does not influence CBZ DH nucleation for the dissolving CBZ-NIC cocrystal, the IDR profile of the CBZ-NIC cocrystal in the 0.35 mM SLS dissolution medium was almost same as its corresponding profile in water (Fig. 6.5(a)). The solubility of CBZ for solids of CBZ III and CBZ-NIC cocrystal have increased significantly when concentration of SLS is higher than its CMC due to the inclusion of CBZ molecules into the surfactant micelles, resulting in a lack of growth material of CBZ in solution which retards crystallization and inhibits growth of stable crystal form CBZ DH on compact surface. IDR of CBZ III in the 10.4 mM SLS solution was increased 1.3 times relative to that in pure water whilst the IDR of CBZ-NIC cocrystal in the same solution was increased to 1.6 times of its corresponding value in pure water.

Tween 80 is a nonionic surfactant and has a wide range of CMC values because of progressive association and heterogeneous distribution of aggregates. Although Tween 80 can increase the solubility of CBZ in solution, its solubilisation capacity was limited - the large molecule sizes of Tween 80 and its aggregates in solution mean it can form an interfacial barrier to prevent CBZ molecules getting into the bulk solution, resulting in accelerated nucleation and growth of stable crystal form CBZ DH on the sample compact surface. Therefore, experimental results in this work indicated that Tween 80 had opposite effect on IDRs of CBZ III and CBZ-NIC cocrystal as those of SLS, i.e. the inclusion of Tween 80 in dissolution medium reduced the IDRs of CBZ III and CBZ-NIC cocrystal (Fig. 6.5).

6.5 Chapter conclusions

The influence of two surfactants (SLS and Tween 80) on the solubility and dissolution behavior of the CBZ-NIC cocrystal, CBZ III and the physical mixture of CBZ III and NIC has been studied in this chapter. The results show that CBZ DH (CBZ III), CBZ-NIC cocrystal and physical mixture of CBZ III and NIC have the same equilibrium solubility. SLS and Tween 80 have little effect on the solubility of the CBZ-NIC

cocrystal in comparison with the significant solubility enhancement for CBZ DH by SLS above its CMC.

The SMPT of CBZ III and CBZ-NIC cocrystal can be altered by inclusion of a surfactant in dissolution medium. However, CBZ III and CBZ-NIC cocrystal have shown different transformation behavior with different surfactants. IDRs profile of CBZ III and CBZ-NIC cocrystal increased significantly when the concentration of SLS was higher than its CMC in a dissolution medium. The inclusion of Tween 80 in dissolution medium reduced IDRs of CBZ III and CBZ-NIC cocrystal due to its large molecule size which can form an interfacial barrier to prevent CBZ molecules getting into the bulk solution, resulting in accelerated nucleation and growth of stable crystal form CBZ DH on sample compact surface.

Chapter 7 Solubility and Dissolution Behaviour of CBZ-NIC, CBZ-SUC Cocrystals in Biomedia

7.1 Chapter overview

Since complex-heterogeneous gastric intestinal environment has a greater impact on drug dissolution, in recent years there has been considerable interest in exploring how *in vitro* dissolution testing can be used more effectively in the product development phase[176, 177]. An example of this is to using more biorelevant dissolution media, such as simulated gastric fluid, with the aim of improving the connection between the product behaviour observed *in vitro* and that *in vivo*[132].

In this chapter, the solubility and dissolution behaviour of CBZ, CBZ-NIC cocrystal, CBZ-SUC cocrystal in simulated gastric fluid (SGF), pH1.2 hydrochloride acid buffer (pH1.2 HCl buffer), simulated intestinal fluid (SIF), pH 6.8 phosphate buffer (pH 6.8 PBS buffer) have been investigated. First of all, equilibrium solubility of CBZ and two cocrystals in four buffers were determined respectively. Then for the two cocrystals above, the complexation behaviour of cocrystal components was studied through measuring the solubility of CBZ as function of coformers' concentration in four buffers. Finally, the evolution of intrinsic dissolution rate of CBZ III and two cocrystals in four buffers were monitored by ActiPix SDI 300 UV surface imaging dissolution system.

7.2 Materials and methods

7.2.1 Materials

Anhydrous CBZ III, nicotinamide, succinic acid, sodium chloride, potassium phosphate monobasic, ethyl acetate, 0.2 M sodium hydroxide, 0.2 M hydrochloric acid, 1M hydrochloric acid, ethanol, pepsin powder, and pancreatin powder, 0.45 μm nylon syringe filter were used in this chapter. Details about these materials can be found in chapter 3 materials and methods.

The dissolution media used in this chapter were pH 1.2 HCl buffer, SGF, pH 6.8 PBS buffer and SIF, which were prepared according to British Pharmacopeia 2013. CBZ DH,

CBZ-NIC cocrystal, and CBZ-SUC cocrystal were prepared. The preparation details for each buffer and CBZ samples were introduced in section 3.4 Preparations. Details about CBZ samples characterisation have been shown in chapter 4 Sample characterisations.

7.2.2 Methods

7.2.2.1 Equilibrium solubility

The solubility of CBZ DH, the CBZ-NIC, CBZ-SUC cocrystal and its physical mixture in pH 1.2 HCl buffer, pH 6.8 PBS, SGF, and SIF were determined using air-shaking bath method. Experimental procedures were described in details in section 3.3.11.1 Equilibrium solubility test. The experiment has been performed at 37°C at 100 rpm for 24 hours. CBZ, NIC and SUC concentrations were calculated by Perkin Elmer series 200 HPLC system. Solid residues were retrieved from the solubility tests and air dried for 30 minutes. All of dried solids were characterized by FTIR, Raman and DSC. All solubility tests were carried out in triplicate.

7.2.2.2 Solubility of CBZ as function of coformers

The solubility of CBZ as function of NIC, and SUC in pH 1.2 HCl buffer, pH 6.8 PBS, SGF, and SIF was determined respectively at 37°C. Experimental procedures were described in details in section 3.3.11.2 Cocrystal eutectic points measurement test.

7.2.2.3 UV imaging dissolution experiment

The dissolution behavior of CBZ III, CBZ DH, CBZ-NIC cocrystal, and CBZ-SUC cocrystal in four biomedia, pH 1.2 HCl buffer, pH 6.8 PBS, SGF, and SIF, were studied by ActiPix SDI 300 UV surface imaging system (Paraytec Ltd., York, UK). Details about the operation can be found in section 3.3.1 ActiPix SDI300 UV imaging dissolution system. All dissolution tests were performed at 37 °C in triplicate.

7.3 Results

7.3.1 Equilibrium solubility

The equilibrium solubility of CBZ DH (CBZ III), 1:1 CBZ-NIC, 2:1 CBZ-SUC cocrystal and physical mixture in SGF, pH1.2 buffer, pH6.8 PBS, SIF after 24 hours are shown in Fig. 7.1 and details of data are shown in Table 7.1.

Comparing the solubility of one sample in different buffer, for CBZ DH, the highest solubility was found in SGF, which was 0.95 mM. And the solubility of CBZ DH in four mediums was decreasing gradually in the order of SGF, pH1.2, pH6.8 and SIF. The lowest CBZ DH solubility was 0.64 mM in SIF. For the two cocrystals, the highest solubilities were also found in SGF buffer. Generally, the solubilities of cocrystals in four buffers are decreasing in the order of SGF, pH1.2, SIF and pH6.8.

Comparing the solubility between different samples, all cocrystal has higher solubility than CBZ DH in same buffer. CBZ-SUC cocrystal has the highest solubility in all buffers among all tested samples. Most notably, the solubility of CBZ-SUC cocrystal in SGF buffer was the highest of all and which was increased to more than twice level than that of other samples.

There was no big difference between the solubility of CBZ of mixtures in four buffers. Generally, the highest solubility of mixtures was found in pH 1.2 buffer, followed by SIF. The solubility of mixtures in SGF and pH 6.8 buffer were relative lower. Compare the solubility of different mixture, there was no extremely high solubility obtained, all sample have similar solubility.

Table 7.1 CBZ solubility of CBZ DH, CBZ-NIC cocrystal and mixture, CBZ-SUC cocrystal and mixture in SGF, pH1.2 HCl buffer, pH6.8 PBS buffer, SIF (mM)

mM	CBZ DH	CBZ-NIC		CBZ-SUC	
		cocrystal	mixture	cocrystal	mixture
SGF	0.95±0.17	1.05±0.22	0.97±0.13	2.37±0.18	0.89±0.13
pH1.2	0.86±0.14	1.00±0.15	1.04±0.17	1.19±0.25	0.96±0.19
pH6.8	0.79±0.13	0.84±0.13	0.94±0.22	0.96±0.25	0.85±0.18
SIF	0.64±0.14	0.89±0.18	0.99±0.07	1.12±0.18	0.89±0.17

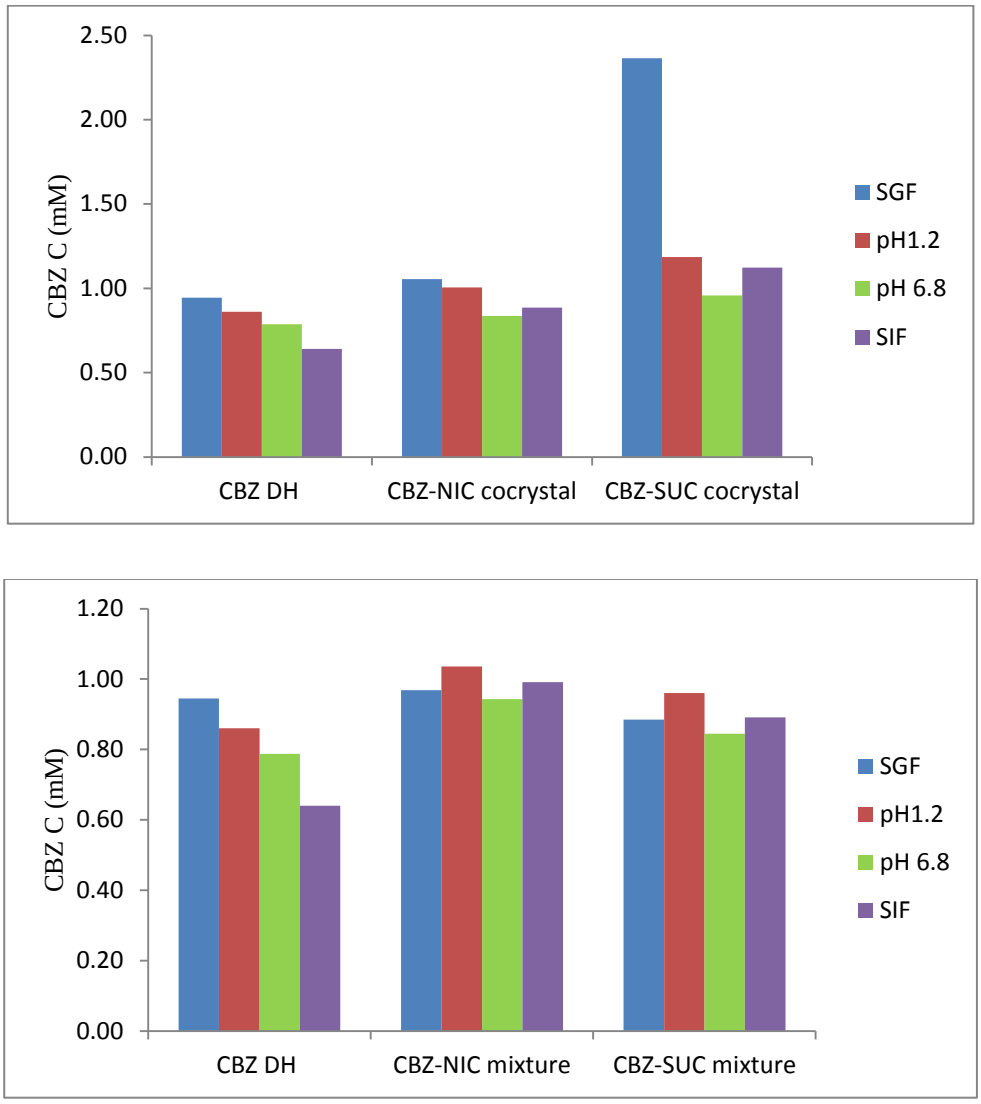

Fig. 7.1 Equilibrium solubility of CBZ DH, cocrystal and mixture in SGF, pH1.2 HCl buffer, pH6.8 PBS buffer, and SIF

The pH value of solutions in each vial was measured by JENWAY 350 pH meter after 24 hours equilibrium and the results were shown in Table 7.2. After 24 hours dissolution, all solutions' pH value has some variations from its original value. For CBZ DH, after 24 hours dissolution in SGF and pH1.2, the pH of solution was increased from 1.2 to 1.46 and 1.43 respectively. Different from CBZ DH, pH of all cocrystal and mixture solutions in SGF medium were decreased slightly (except the pH of CBZ-NIC cocrystal in SGF increased to 1.3). For pH 6.8 buffer, CBZ DH and CBZ-NIC mixture increased its pH value to 7.03 and 6.99 respectively after 24 hours dissolution in it, the other samples caused a decrease in the pH value in this buffer. For SIF, all sample

dissolution in SIF caused a decrease in the solution pH value. And the biggest decrease was found with CBZ-NIC cocrystal which decreased the pH value from 6.8 to 4.95.

Table 7.2 pH of CBZ DH, CBZ-NIC cocrystal and mixture, CBZ-SUC cocrystal and mixture in SGF, pH 1.2 HCl buffer, pH 6.8 PBS buffer, SIF

mM	CBZ DH	CBZ-NIC		CBZ-SUC	
		cocrystal	mixture	cocrystal	mixture
SGF	1.46±0.01	1.30±0.01	1.14±0.01	1.19±0.01	1.16+0.01
pH1.2	1.43±0.01	1.19±0.01	1.07±0.04	1.16±0.01	1.14±0.01
pH 6.8	7.03±0.01	6.79±0.02	6.99±0.01	6.60±0.01	6.50±0.02
SIF	5.02±0.03	4.95±0.07	5.61±0.42	5.18±0.02	5.16±0.02

IR, Raman, and DSC characterization results of the solid residue after equilibrium tests were shown in appendix A.2.1.1-3. Characterization results show that solid residue of cocrystal and mixture samples in all media have transformed to DH, except the CBZ-SUC cocrystal in SGF buffer. DSC, IR, and Raman characterization results of solid residue after equilibrium solubility test in four biomedia for CBZ-SUC cocrystal shown in Fig. 7.2 demonstrate that after equilibrium solubility test in SGF CBZ-SUC cocrystal still keep cocrystal structure. In Fig. 7.2.(a), DSC results of CBZ-SUC cocrystal after equilibrium solubility test in SGF has a single endothermic peak around 195°C corresponding to the melting of CBZ-SUC cocrystal; while the DSC results of solid residue from other three media show dehydration peaks around 80 to 120°C due to CBZ DH. In Fig. 7.2.(b), the IR spectrum of solid from equilibrium solubility test in SGF show characteristic peaks of CBZ-SUC cocrystal around 3400-3000 cm^{-1} range, while the other three spectra show the CBZ DH IR patterns. In Fig. 7.2.(c), Raman spectrum of solid residue from SGF biomedium shows characteristic peak of CBZ-SUC cocrystal around 400, 100 and 2900 cm^{-1}. The above three characteristic technique can demonstrate that CBZ-SUC cocrystal after equilibrium solubility test in SGF still keep its cocrystal structure.

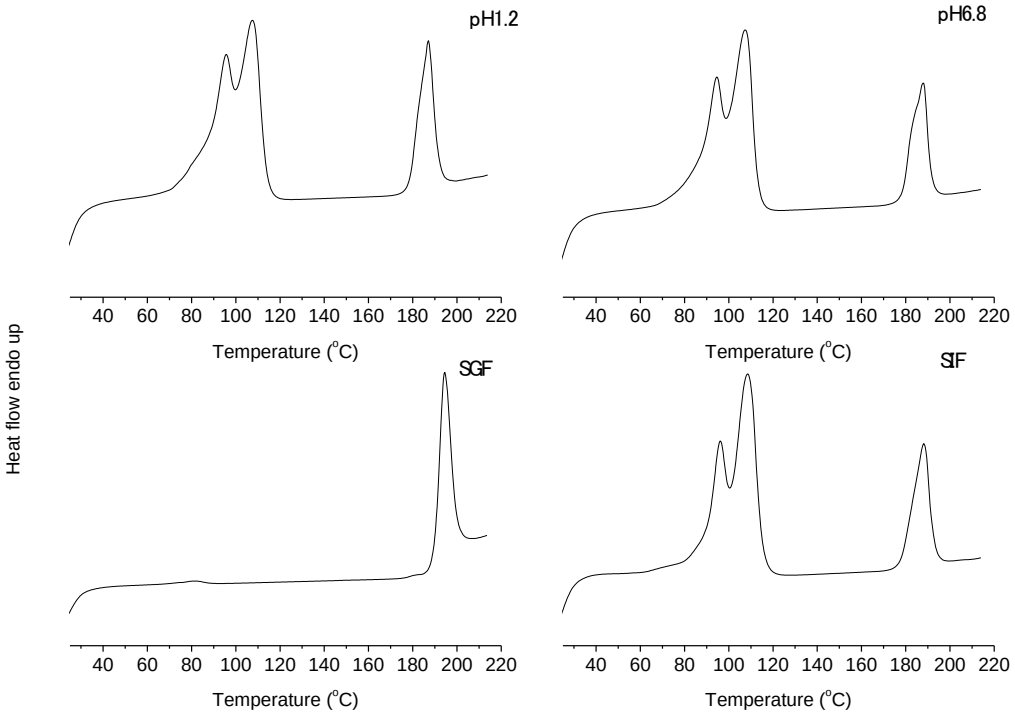
pH1.2
pH6.8
SGF
SIF
Heat flow endo up
40 60 80 100 120 140 160 180 200 220
Temperature (°C)

(a) DSC

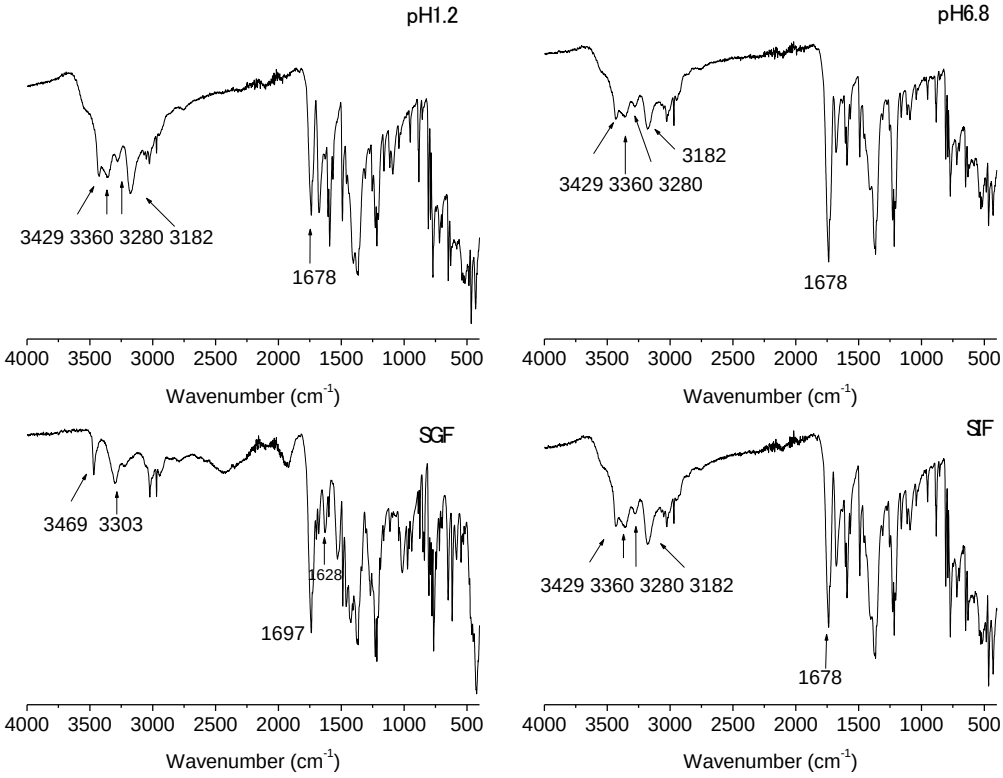
pH1.2
3429 3360 3280 3182
1678
pH6.8
3182
3429 3360 3280
1678
SGF
3469 3303
1628
1697
SIF
3429 3360 3280 3182
1678
4000 3500 3000 2500 2000 1500 1000 500
Wavenumber (cm-1)

(b) IR

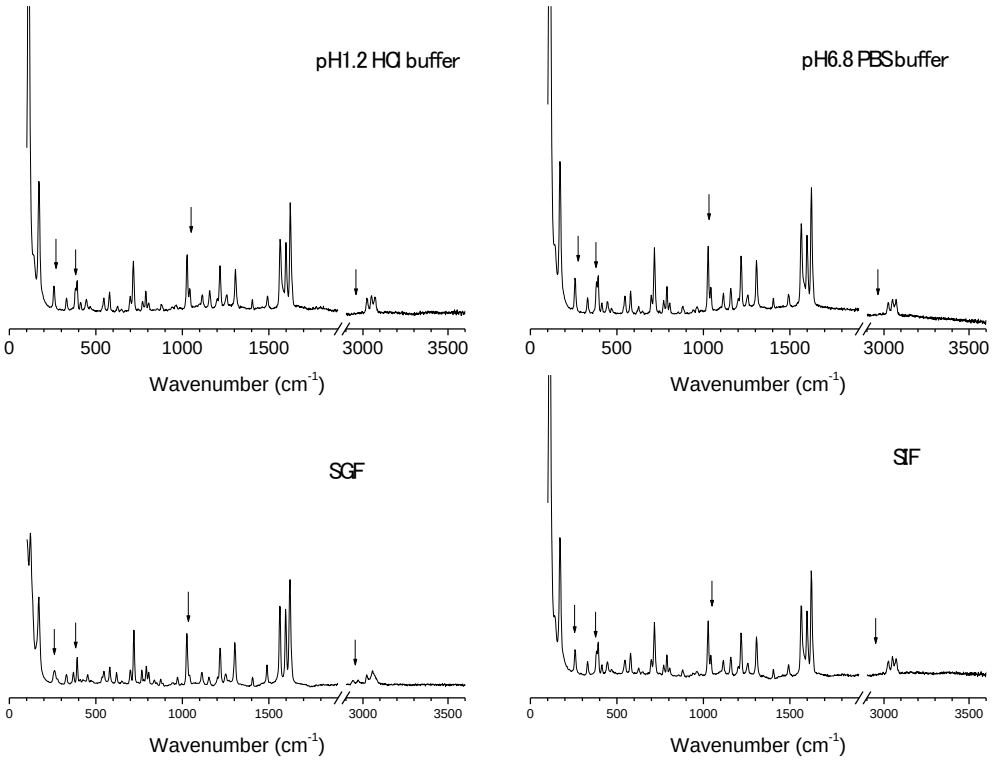

(c) Raman

Fig. 7. 2 DSC, IR, Raman characterisation of solid residue from equilibrium solubility test of CBZ-SUC cocrystal in four biomedia: pH1.2, pH6.8, SGF, SIF

7.3.2 Solubility of CBZ as function of coformers

Before measuring the solubility of CBZ as function of coformers in biomedia at 37 °C, coformers solubility in biomedia at 37°C were measured, and the results were shown in Table 7.3.

Table 7.3 NIC and SUC solubility in SGF, pH1.2 HCl buffer, pH6.8 PBS buffer, SIF at 37°C (mM)

mM	SGF	pH1.2	pH6.8	SIF
NIC	4771.17±259.30	5815.65±302.96	5626.71±272.23	5124.06±391.99
SUC	933.00±148.11	943.75±74.57	1094.11±49.76	1079.67±28.05

7.3.2.1 CBZ solubility as function of NIC in biomedia

Based on NIC solubility, the maximum NIC concentration in each medium was set at a value near to its solubility. The equilibrium solubility of CBZ was measured as a

function of the NIC concentration, results were shown in Fig. 7.3, 7.4 and data were shown in Table 7.4.

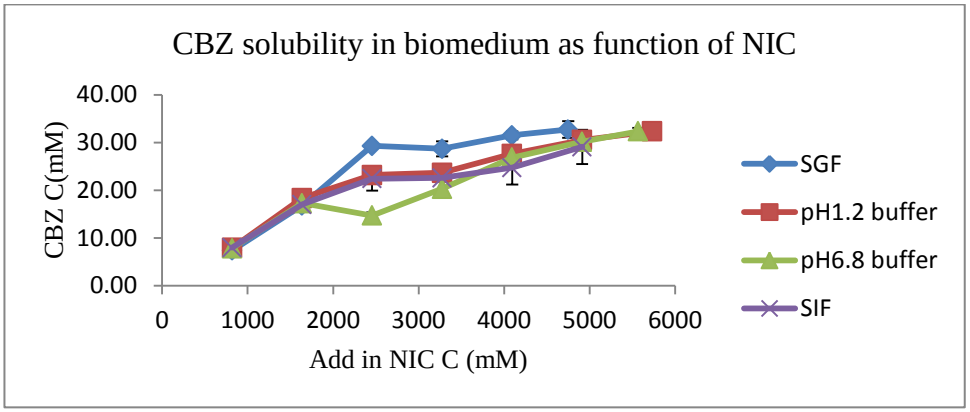

Fig. 7.3 CBZ solubility as function of NIC in four media

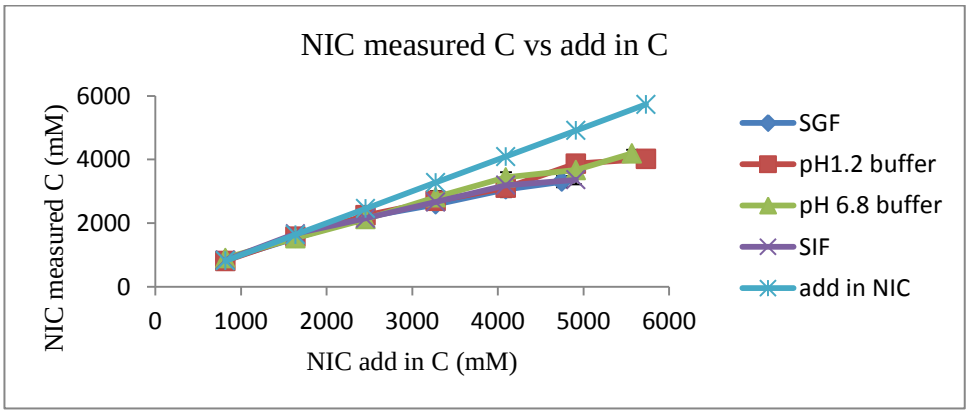

Fig. 7.4 Measured NIC concentration vs. add in NIC concentration

Table 7.4 CBZ solubility as function of NIC in four biomedia, and measured NIC concentration (mM)

pH1.2			pH6.8		
initial NIC C	Measured CBZ C	measured NIC C	initial NIC C	measured CBZ C	Measured NIC C
818.87	7.95±0.52	812.67±77.99	818.87	7.84±0.72	905.24±6.42
1637.73	18.36±0.75	1573.03±131.35	1637.73	17.28±0.30	1529.38±105.83
2456.60	23.20±0.27	2247.71±23.45	2456.60	14.71±0.67	2127.73±158.46
3275.47	23.67±1.33	2700.76±151.22	3275.47	20.31±1.50	2814.17±195.92
4094.33	27.62±0.17	3109.98±291.29	4094.33	26.84±0.53	3436.38±168.10
4913.20	30.53±1.09	3869.27±112.06	4913.20	30.16±0.82	3668.90±106.98
5732.07	32.36±0.72	4016.41±266.80	5568.29	32.35±0.69	4191.49±118.36
SGF			SIF		
initial NIC C	Measured CBZ C	measured NIC C	initial NIC C	measured CBZ C	Measured NIC C
818.87	7.40±0.52	857.97±15.84	818.87	7.96±0.62	840.70±23.20
1637.73	16.81±0.99	1531.16±32.20	1637.73	17.01±0.96	1665.99±48.93
2456.60	29.30±0.24	2190.66±64.59	2456.60	22.41±2.5	2148.70±151.48

3275.47	28.68±1.56	2586.20±105.19	3275.47	22.59±0.69	2665.32±96.41
4094.33	31.51±0.84	3059.37±123.67	4094.33	24.74±3.57	3190.93±230.88
4749.43	32.70±1.75	3303.63±173.67	4913.20	29.09±3.58	3363.02±147.27

The solubility of CBZ increased rapidly as NIC adding in at the beginning of solubility curves indicating the 1:1 complex formation of CBZ and NIC. The rapid increasing in SGF, pH1.2, and SIF buffer is corresponding to initial concentration of NIC from 818.87 to 2456.6 mM. The rapid increasing in pH6.8 buffer is corresponding to initial concentration of NIC from 818.87 to 1637.73 mM. The highest CBZ solubility was found in SGF with initial NIC concentration 2456.6 mM. At the beginning of this rapid increasing stage, the solubility limit of the complex formed was not exceeded and the solid residue should be CBZ DH only (IR, DSC, and Raman characterisation shown in appendix, A2.2.1-3), the measured concentration of NIC was the same as that of the initial NIC, shown in Table 7.4. In the later part of this stage, the solubility limit of the 1:1 complex formed was gradually obtained and exceeded, CBZ-NIC cocrystal start to precipitate (IR, DSC, and Raman characterisation shown in appendix, A2.2.1-3). The highest CBZ concentration point in this stage was set as eutectic point of CBZ-NIC cocrystal. The total concentrations of CBZ and NIC at the eutectic points, and cocrystal solubility calculated based on solubility definition of a 1:1 cocrystal in Equ.6-1, are shown in Table 7.5. CBZ-NIC cocrystal solubility was found higher in acidic buffer than in alkalic buffers. For the two acidic buffers, cocrystal has a higher solubility in SGF than in pH1.2 HCl buffer; for the two alkalic buffers, cocrystal in SIF was also higher than that in the simple pH 6.8 buffer. Cocrystal has a better solubility in simulated buffer.

Table 7.5 CBZ-NIC cocrystal eutectic point, cocrystal solubility and solubility ratio in SGF, pH1.2 buffer, pH6.8 buffer, SIF

Solvent	$[CBZ]_{eu}$ (mM)	$[NIC]_{eu}$ (mM)	Cocrystal solubility S_{cc} (mM)	Solubility ratio $S_{cc} / S_{CBZ, buffer}$
SGF	29.30±0.24	2190.66±64.59	253.34±3.85	268.08
pH1.2	23.20±0.27	2247.71±23.45	227.13±31.48	263.97
pH6.8	17.28±0.30	1529.38±105.83	162.53±6.91	206.32
SIF	22.41±2.5	2148.70±151.48	219.39±19.91	342.66

As solubility limit of the 1:1 complex formed was gradually obtained and exceeded, the concentration of CBZ stop rapid increasing as NIC initial concentration. For SGF, pH1.2, and SIF, CBZ solubility level around eutectic point as NIC initial concentration increase from 2456.6 to 3275.47 mM. CBZ solubility in pH6.8 buffer has slightly decreased as NIC initial concentration increase from1637.73 mM to 2456.6 mM. All of the solid CBZ DH was consumed to form the complex to generate the supersaturated solution of the complex, resulting in precipitation of large amount of CBZ-NIC cocrystal and reduction of CBZ concentration in solution. It has been shown that the CBZ-NIC cocrystal and NIC were coexisting in the solid residues, shown in DSC, FTIR and Raman analysis (A2.2.1-3). NIC measured concentration was lower than that of the initial NIC in this region. As NIC initial concentrations continue increasing, the concentrations of CBZ increase, resulting from higher order complexes of CBZ and NIC were generated. The solid residues were CBZ-NIC cocrystal and NIC, confirmed by DSC, FTIR and Raman, shown in appendix (A2.2.1-3).

Table 7.6 pH of dissolution medium of SGF, pH 1.2 buffer, pH6.8 buffer, and SIF after 24 hours dissolution of CBZ as function of NIC

SGF		pH1.2		pH6.8		SIF	
Original NIC C	pH	Original NIC C	pH	Original NIC C	pH	Original NIC C	pH
818.87	3.88±0.02	818.87	3.95±0.01	818.87	7.18±0.01	818.87	6.89±0.01
1637.73	4.16±0.01	1637.73	4.21±0.01	1637.73	7.26±0.00	1637.73	6.98±0.01
2456.60	4.29±0.01	2456.60	4.35±0.01	2456.60	7.34±0.01	2456.60	7.06±0.01
3275.47	4.41±0.00	3275.47	4.42±0.01	3275.47	7.40±0.01	3275.47	7.15±0.01
4094.33	4.49±0.01	4094.33	4.51±0.01	4094.33	7.48±0.01	4094.33	7.23±0.00
4749.43	4.54±0.01	4913.20	4.58±0.01	4913.20	7.55±0.01	4913.20	7.32±0.01
		5732.07	4.64±0.01	5568.29	7.60±0.01		

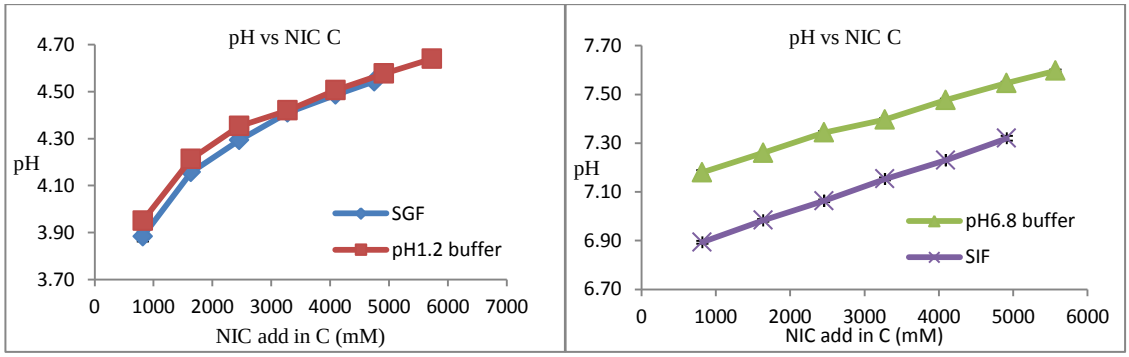

Fig. 7.5 pH vs. initial NIC concentration in four dissolution mediums after 24hours dissolution of CBZ

The pH value of each buffer after 24 hours dissolution was shown in Table 7.6, and Fig. 7.5. The pH value increased to the range of 3.9-4.6 from the original level of 1.2 as NIC original concentration increasing in SGF and pH 1.2 HCl buffer. There is no big difference in pH value between the two buffers with same NIC initial concentration. For pH 6.8 PBS buffer and SIF, the pH value was also increased after 24 hours CBZ dissolution in it. The pH value was increased to the range of 7.18 to 7.6 in pH 6.8 PBS buffer as initial NIC concentration increasing. In SIF buffer, the pH value was slightly lower than that in PBS buffer with same initial NIC concentration.

7.3.2.2 CBZ solubility as function of SUC in biomedia

Based on SUC solubility in four media, the maximum SUC concentration in each medium was set at a value near to its solubility. The equilibrium solubility of CBZ was measured as a function of SUC concentration; results were shown in Fig. 7.6, 7.7 and Table 7.7.

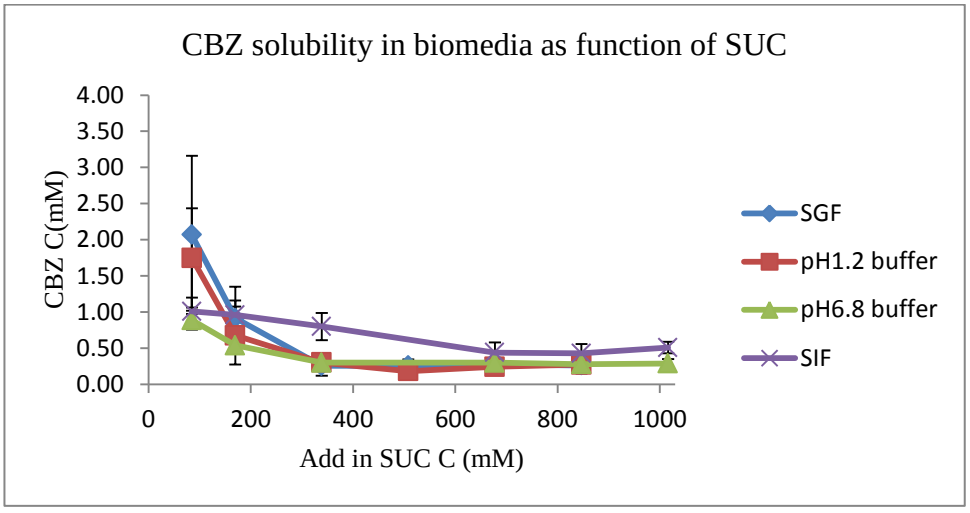

Fig. 7.6 CBZ solubility as function of SUC in four buffers

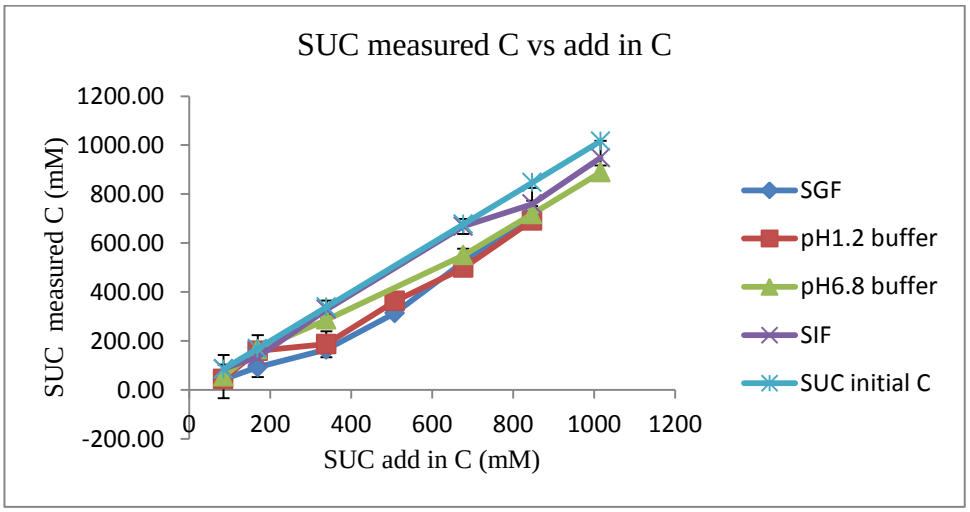

Fig. 7.7 Measured SUC concentration vs. add in SUC concentration

Table 7.7 CBZ solubility as function of SUC in pH1.2 buffer, SGF, pH6.8 buffer, and SIF (mM)

	pH1.2		SGF	
initial SUC C	Measured CBZ C	measured SUC C	Measured CBZ C	measured SUC C
84.68	1.75±0.69	44.68±12.82	2.07±1.09	43.09±7.57
169.36	0.68±0.40	159.86±63.75	0.92±0.24	93.06±40.44
338.72	0.30±0.08	187.15±53.20	0.26±0.14	164.71±8.81
508.09	0.18±0.06	362.87±28.92	0.26±0.09	314.15±11.21
677.45	0.24±0.02	498.61±32.82	0.28±0.09	522.78±18.03
846.81	0.27±0.09	691.85±37.16	0.26±0.04	705.68±45.24
	pH6.8		SIF	
initial SUC C	measured CBZ C	Measured SUC C	measured CBZ C	Measured SUC C
84.68	0.89±0.13	54.79±38.10	1.01±0.19	86.71±17.36
169.36	0.54±0.10	165.58±13.55	0.96±0.39	135.41±28.11
338.72	0.30±0.02	286.86±23.93	0.80±0.19	328.96±36.44
677.45	0.30±0.05	549.97±27.85	0.44±0.14	668.35±30.70
846.81	0.28±0.13	717.99±55.46	0.43±0.13	758.98±66.79
1016.17	0.29±0.06	888.69±28.86	0.51±0.08	947.88±70.33

Figure of CBZ solubility as function of SUC concentration showed a different trend as that as function of NIC concentration. At beginning, CBZ solubility in four biomedia with lowest initial concentration of SUC (84.68 mM) has been increased slightly. As initial SUC concentration increase, CBZ solubility was gradually decreased to very low level, which is lower than CBZ solubility in pure buffers.

The pH value of each buffer after 24 hours dissolution of CBZ as function of SUC was shown in Fig. 7.8 and Table 7.8. pH value of pH 1.2 HCl buffer and SGF decreased slightly, level around 1.0 to 1.1. The pH value of pH 6.8 PBS buffer and SIF decreased

from 6.8 to 3.83 and 3.57 at lowest SUC initial concentration, and pH in the two buffers continue to decrease to around 2.6 at the highest SUC initial concentration.

Table 7.8 pH of dissolution medium of SGF, pH1.2 buffer, pH6.8buffer, and SIF after 24 hours dissolution of CBZ as function of SUC concentration

SGF		pH1.2		pH6.8		SIF	
Original SUC C	pH	Original SUC C	pH	Original SUC C	pH	Original SUC C	pH
84.68	1.12±0.02	84.68	1.07±0.01	84.68	3.83±0.01	84.68	3.57±0.01
169.36	1.14±0.01	169.36	1.05±0.01	169.36	3.45±0.01	169.36	3.32±0.01
338.72	1.11±0.01	338.72	1.03±0.01	338.72	3.10±0.01	338.72	3.01±0.00
508.09	1.08±0.01	508.09	1.02±0.01	677.45	2.79±0.00	677.45	2.72±0.01
677.45	1.07±0.00	677.45	1.00±0.01	846.81	2.75±0.01	846.81	2.63±0.01
846.81	1.07±0.01	846.81	0.99±0.01	1016.17	2.73±0.01	1016.17	2.56±0.01

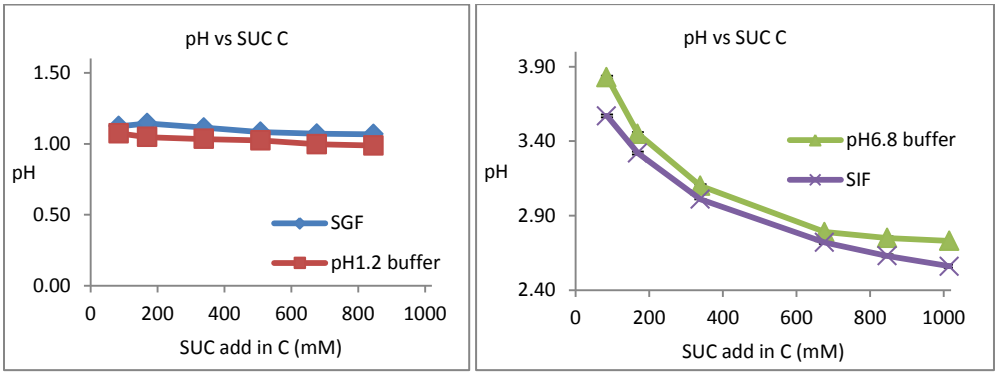

Fig. 7.8 pH vs. initial SUC concentration in four dissolution media after 24hours dissolution of CBZ

7.3.3 Intrinsic dissolution rate

The dissolution behavior of CBZ III, CBZ-NIC cocrystal, and CBZ-SUC cocrystal in pH 1.2 HCl buffer, pH 6.8 PBS, SGF, and SIF, were studied by ActiPix SDI 300 UV surface imaging system. The IDR profiles of CBZ III, CBZ-NIC cocrystal, and CBZ-SUC cocrystal in four biomedia are shown in Fig. 7.9. The IDR profiles of all samples in different biomedia have some properties in common: in first 10 minutes, IDR increased to maximum value and then decreased quickly; in the following 50 minutes, IDR kept decreasing at very slow rate and approach a static rate. To compare the IDRs of samples in four buffers after the first 10 minutes quick change, generally, the IDR of CBZ III in SGF was the largest, followed by SIF and pH 1.2 buffer, the lowest IDR figure was found in pH6.8 PBS buffer (Fig. 7.9.a). IDR of CBZ-NIC cocrystal in biomedium decreases in the order of pH6.8 buffer, pH1.2 buffer, SGF, and SIF (Fig.

7.9.b). For CBZ-SUC cocrystal, its IDR in SGF is much higher than that in the other three buffers (Fig. 7.9.c).

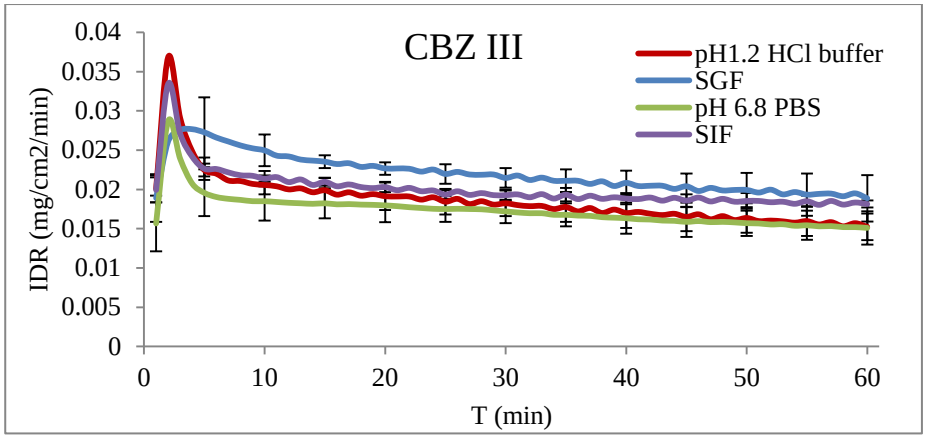

(a)

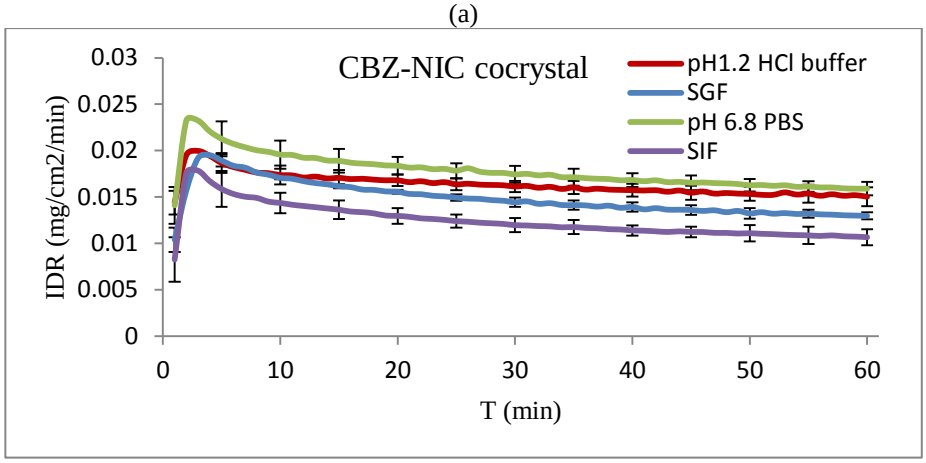

(b)

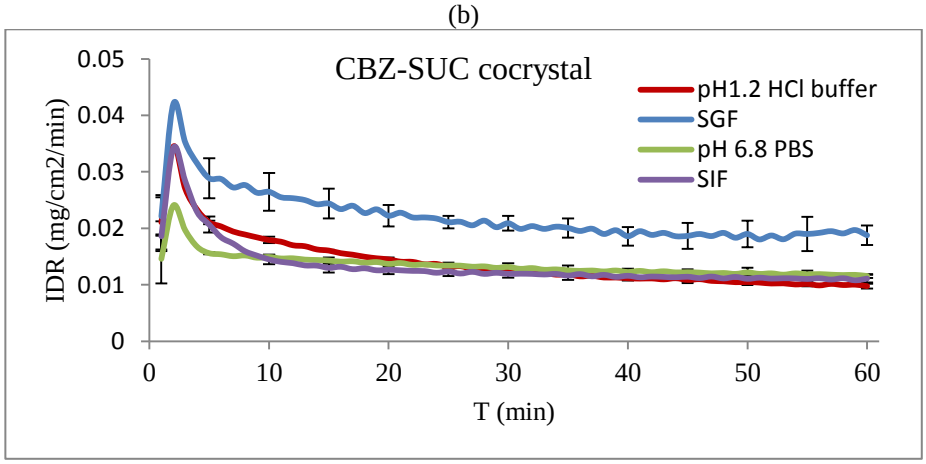

(c)

Fig. 7.9 Dissolution profiles of CBZ DH and cocrystals in biomedia: (a) CBZ DH; (b) CBZ-NIC cocrystal; (c) CBZ-SUC cocrystal

Photos of sample compacts before and after UV imaging dissolution test were taken by light microscope, photos were shown in Fig. 7.10. After one hour dissolution, sample

compact surfaces became rough, and small needle-shaped crystals appeared on the compact surfaces, indicating that the solid state changes due to crystallisation of CBZ DH from the supersaturated solutions on the compact surfaces.

CBZ III	Before	After
SGF		
pH 1.2		
pH 6.8		
SIF		
CBZ-NIC cocrystal	Before	After
SGF		
pH 1.2		
pH 6.8		

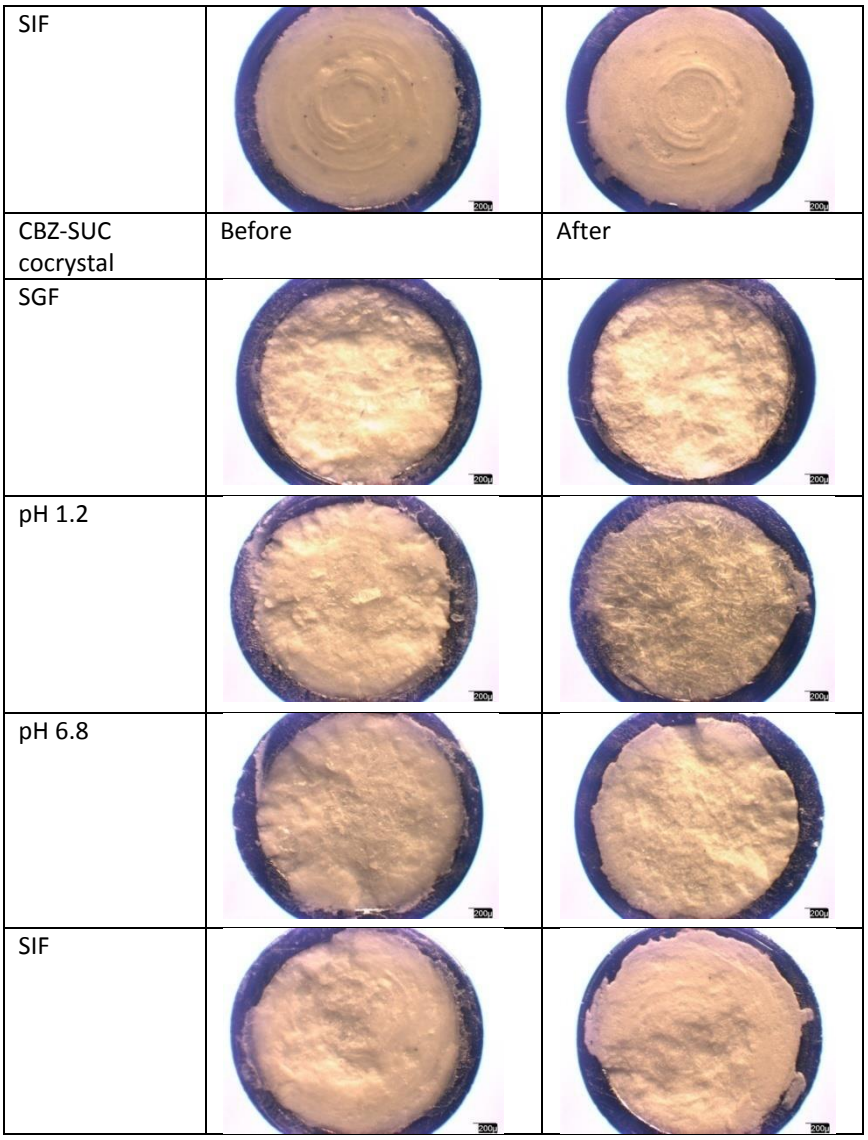

Fig. 7.10 Light microscopy photographs of the sample compacts before and after dissolution tests

Raman spectra of sample before and after dissolution test in different biomedia were shown in Fig. 7.11. After one hour dissolution, Raman spectra of sample compacts showed some change from the original material indicating solid state transformation. Spectra of CBZ III, CBZ-NIC cocrystal, after one hour dissolution in all medium showed the tendency to become CBZ DH. Raman spectra of CBZ-SUC cocrystal after dissolution in SIF, pH6.8 buffer and pH1.2 buffer, showed some change around 400 and 3050 cm^{-1} to become CBZ DH, and the change is more obviously in SIF, pH6.8 buffer than in pH1.2 buffer. But the Raman spectrum of CBZ-SUC cocrystal in SGF did not show the any change.

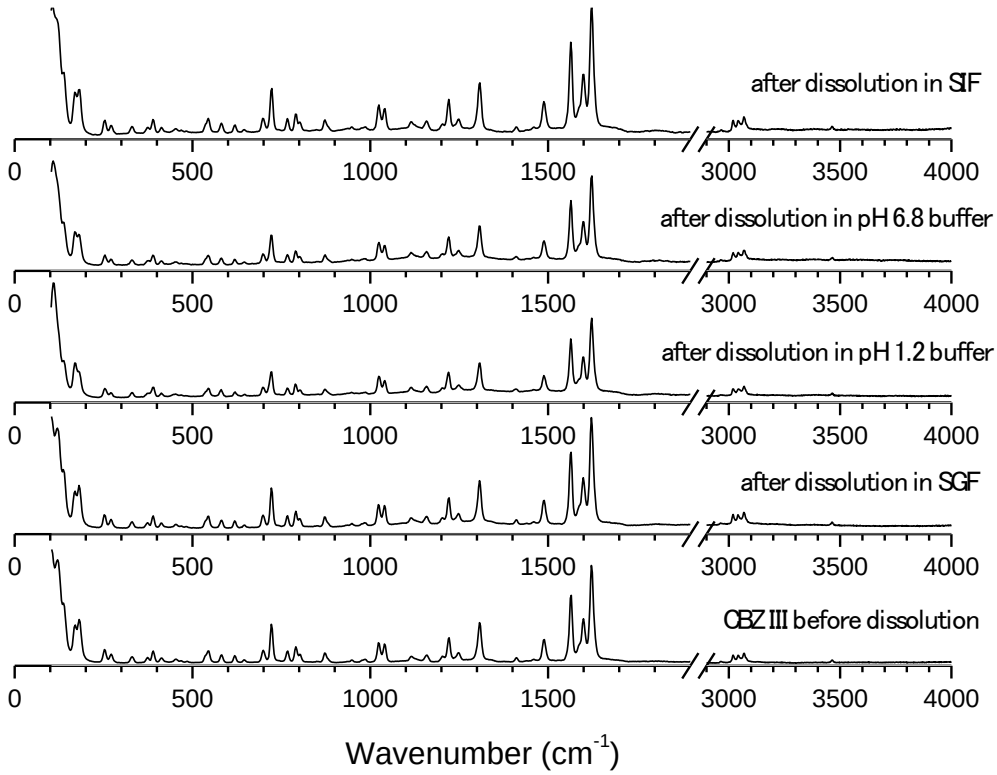

(a1) CBZ III Raman spectrum 0-4000 cm^{-1}

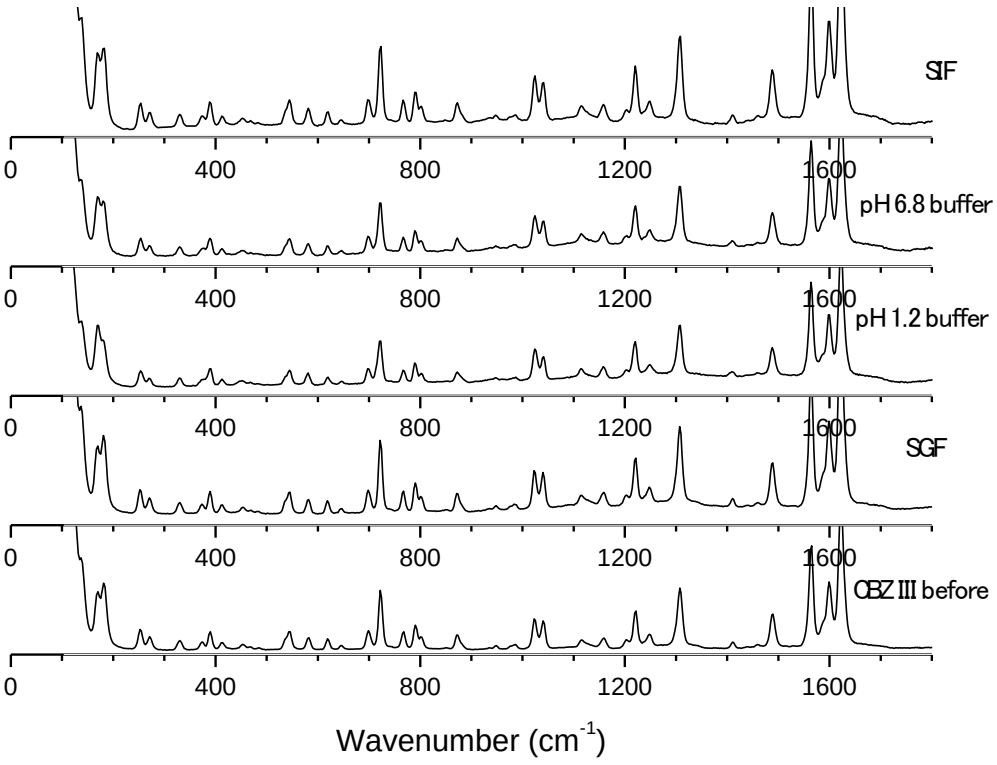

(a2) Englarged CBZ III Raman spectrum 0-1800cm^{-1}

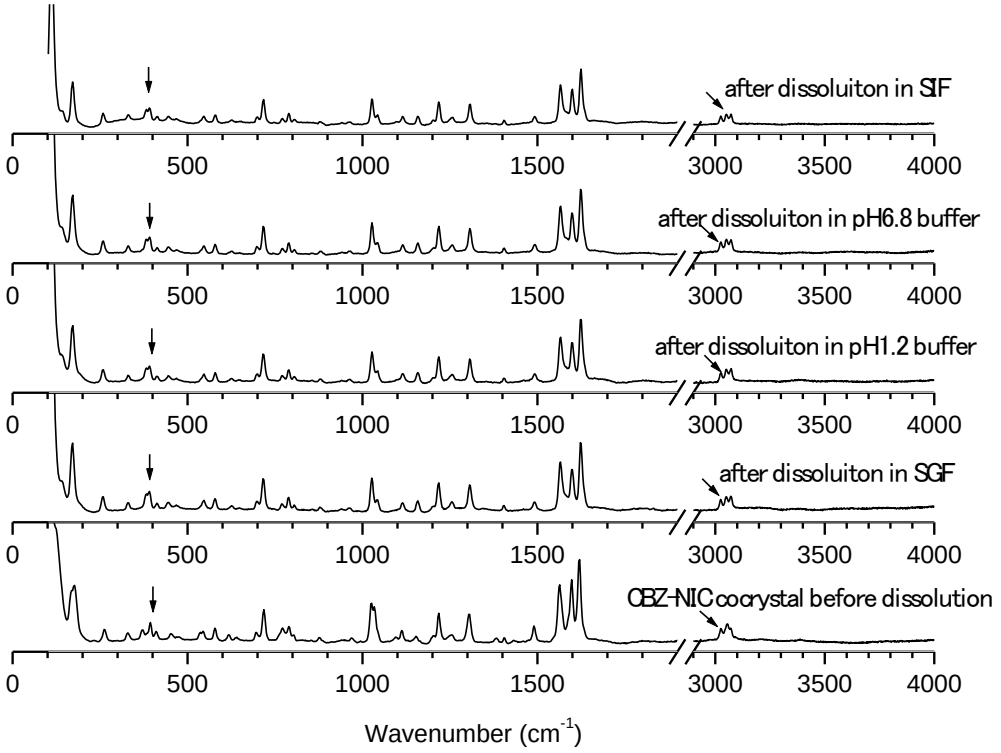

(b1) CBZ-NIC cocrystal Raman spectrum 0-4000 cm^{-1}

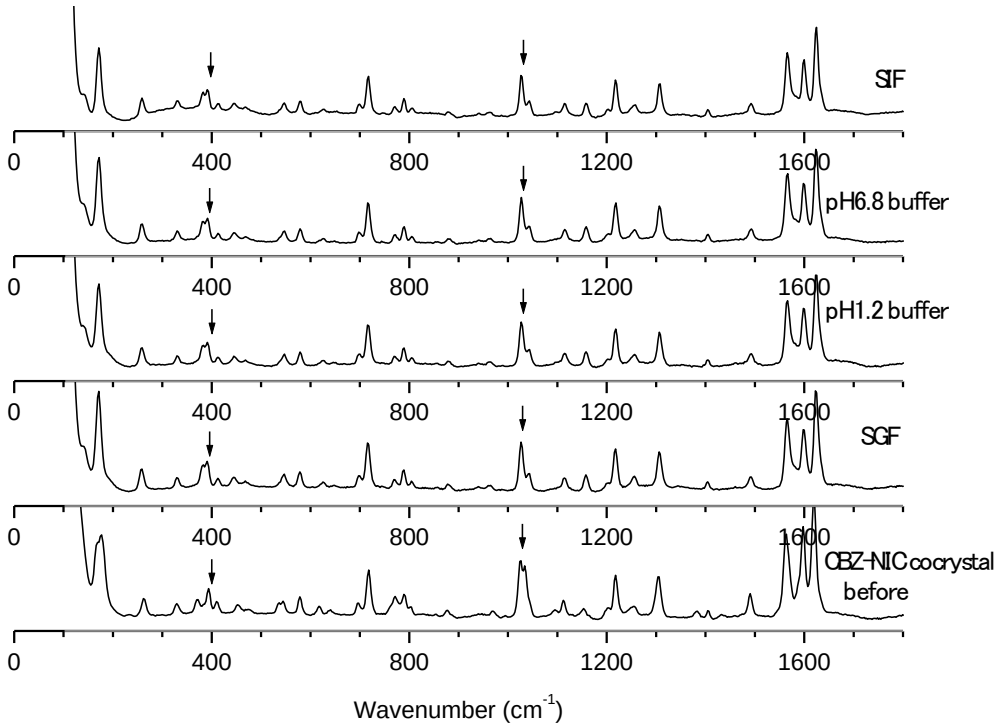

(b2) Englarged CBZ-NIC cocrystal Raman spectrum 0-1800cm^{-1}

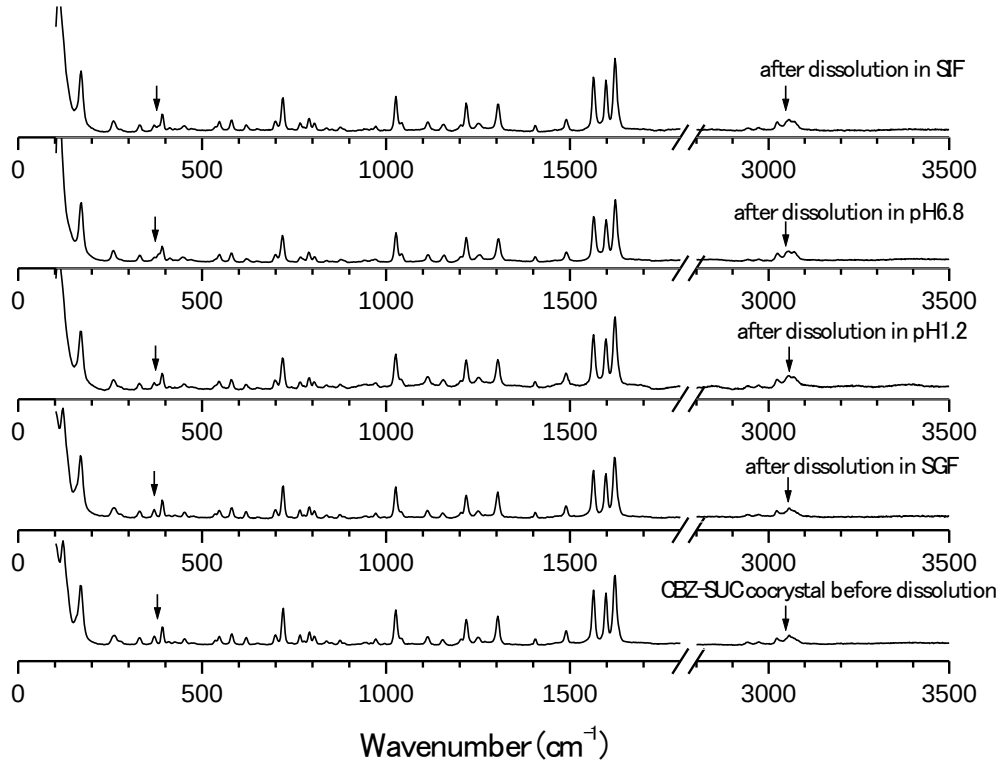

(c1) CBZ-SUC cocrystal Raman spectrum 0-4000 cm^{-1}

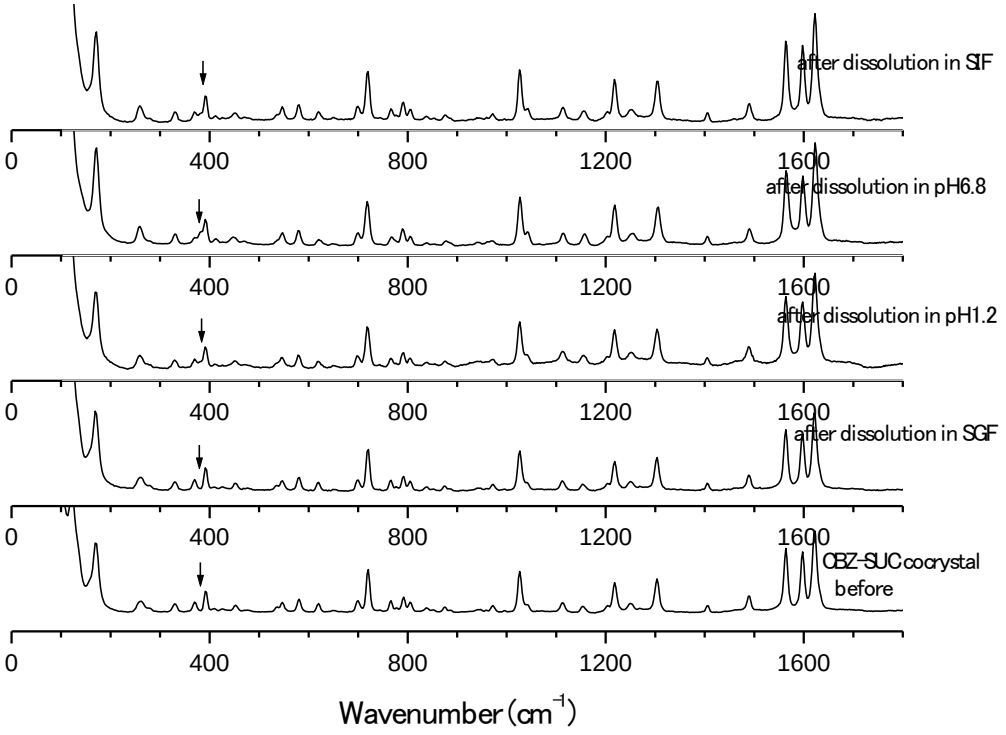

(c2) Englarged CBZ-SUC cocrystal Raman spectrum 0-1800cm^{-1}

Fig. 7.11 Raman spectra of the compacts before and after UV imaging dissolution: (a) CBZ III; (b) CBZ-NIC cocrystal; (c) CBZ-SUC cocrystal

7.4 Discussion

7.4.1 Discussion of solubility in biomedia

7.4.1.1 Equilibrium solubility

Equilibrium solubilities of CBZ DH, CBZ-NIC CBZ-SUC cocrystals and mixtures have been tested in this chapter. Because the transformation from original forms to CBZ DH, the solubilities of most tested samples did not show significant difference. Compared with lots of published CBZ solubilities measured under different experimental settings [178-183], the results in this thesis are at the same level as published data.

Generally, the solubility of CBZ from CBZ DH and two cocrystals has a relative higher solubility in SGF and pH 1.2 buffer than that in SIF and pH 6.8 buffer. This is due to the alkali properties of CBZ which has a higher solubility in acidic buffer. The higher solubility in lower pH buffer are in good agreement with published data[179]. However, the solubility of CBZ from mixture in acidic buffers is not always higher. Probably, the coformer changes the dissolution medium. After 24 hours dissolution, all solutions' pH value has some variations from its original value.

The most distinguish founding from equilibrium solubility test results is that CBZ solubility from CBZ-SUC cocrystal in SGF is more than double as others, which means that CBZ-SUC cocrystal has a more stable structure in SGF buffer. The more stable structure of CBZ-SUC cocrystal in SGF enables part of the cocrystal still keep the original state to reach a higher solubility level after 24 hours dissolution process. Except CBZ-SUC cocrystal in SGF, generally, all cocrystal has a little bit higher solubility than CBZ DH, while these CBZ solubility data does not show big difference. This can be explained by the dissociation of the individual components of cocrystals after long time equilibrium, which in turn is due to the weak hydrogen bonds in the molecular assembly of the two components of cocrystal.

7.4.1.2 CBZ solubility as function of coformer's concentration

The solubility of CBZ in the presence of NIC in four media has increased as NIC initial concentration increasing due to the complexation of NIC and CBZ. CBZ-NIC cocrystal

solubility calculated based on CBZ and NIC concentration at eutectic point show that CBZ-NIC cocrystal solubility was higher in acidic buffer than in alkalic buffers. For the two acidic buffers, cocrystal has a higher solubility in SGF than in pH1.2 HCl buffer; for the two alkalic buffers, cocrystal in SIF was also higher than that in the simple pH 6.8 buffer. Cocrystal has a better solubility in simulated buffer than inorganic buffer.

The solubility of CBZ in the presence of SUC shows different trend as in presence of NIC, which does not show significant increasing as coformer initial concentration increasing. The solubility of CBZ in the presence of SUC has been increased slightly when SUC at relative lower initial concentration. As SUC initial concentration increasing, CBZ solubility decreased and level around 0.4 mM.

7.4.2 Discussion of intrinsic dissolution rates

The dissolution behaviour of CBZ III, CBZ-NIC cocrystal, and CBZ-SUC cocrystal in SGF, pH1.2 buffer, SIF, pH 6.8 buffer was monitored by UV imaging dissolution system. The results show that four biomedia researched in this study have different effect on the IDR of CBZ III and two cocrystals. For parent drug, CBZ III, its IDR in SGF and pH1.2 are higher than that in SIF and pH6.8 buffer respectively. This is because CBZ III is more soluble in lower pH buffer. IDR of CBZ III in SGF and SIF buffer, simulated buffer with organic material (protein), are higher than that in the buffer prepared with only inorganic material at similar pH value. This could be explained by that CBZ III has a special binding reaction with the protein in simulated biomedia, and the binding reaction result in a higher dissolution rate. In sum, pH value and protein binding reaction affect the IDR of CBZ III. The two cocrystals dissolution rate in SGF, pH1.2 buffer, SIF, and pH 6.8 buffer show different trend as that of parent drug CBZ III. This can be explained by that the formation of cocrystal change the ability of CBZ III to bind with organic material in buffer, and also change its pH property. Although cocrystal partly transformed to CBZ DH later, cocrystal still occupied large area of the compact surface.

7.5 Chapter Conclusions

The solubility and dissolution behaviour of CBZ, CBZ-NIC cocrystal, CBZ-SUC cocrystal in SGF, pH1.2 buffer, SIF, pH 6.8 buffer were studied in this chapter. From the study, it has shown that CBZ solubility from CBZ-SUC cocrystal in SGF is more than double as others. Except CBZ-SUC cocrystal in SGF, generally, all cocrystal has a little bit higher solubility than CBZ DH, while these CBZ solubility data does not show big difference. Due to the alkali properties of CBZ which has a higher solubility in acidic buffer, the equilibrium solubility of CBZ from CBZ DH and two cocrystals has a relative higher solubility in SGF and pH 1.2 buffer than that in SIF and pH 6.8 buffer.

The solubility of CBZ in the presence of NIC has increased as NIC initial concentration increasing due to the complexation of NIC and CBZ. CBZ-NIC cocrystal has a higher solubility in acidic buffer than in alkalic buffers and a better solubility in simulated buffer than inorganic buffer. The solubility of CBZ in the presence of SUC shows different trend as in presence of NIC, which does not show significant increasing as coformer initial concentration increasing.

The dissolution behaviour study results show that pH value and protein binding reaction affect the IDR of CBZ III. IDRs of CBZ III in four buffers are decreasing in the order of SGF, SIF, pH 1.2 buffer, and pH6.8 buffer. The two cocrystals dissolution rate show different trend as that of parent drug CBZ III. This can be explained by that the formation of cocrystal change the ability of CBZ III to bind with organic material in buffer, and also change its pH property.

Chapter 8 Conclusions and Future Work

In this chapter, a summary of the presented work and main findings are presented. Limitations of the research are briefly discussed along with potential areas for further research.

8.1 Summary of the presented work

This research mainly investigated solubility and dissolution behaviour of pharmaceutical cocrystal with novel technique of UV surface imaging dissolution system which is expected to provide more contribution on pharmaceutical cocrystal research area.

The research commenced with a critical review about pharmaceutical cocrystal from the basic theory to design strategies, formation and characterisation method and recent progress. The review work helps understand the current status of pharmaceutical cocrystal progress, develop the potential research topics to further improve the performance and our understanding about pharmaceutical cocrystals. Depending upon above review results, the primary aim of this work was established, which is to synthesize pharmaceutical cocrystals, and investigate the solubility and dissolution behavior of cocrystals under different environments using UV surface imaging dissolution system.

Based on cocrystal screening theory and the feasibility of testing dissolution behaviour by UV imaging system, CBZ was selected to be the model drug in this research, and two cocrystals of CBZ, which are 1: 1 CBZ-NIC cocrystal, 2:1 CBZ-SUC cocrystal were prepared and characterised.

This research subsequently studied dissolution and transformation behaviour of CBZ-NIC cocrystal, physical mixture and different forms of CBZ: CBZ I, CBZ III and CBZ DH, by *in situ* techniques of UV imaging and Raman spectroscopy. Solution mediated phase transformation of cocrystals, which could greatly reduce the enhancement of its apparent solubility and dissolution rate, was discussed in this part of research.

This research further investigated the role of surfactants on inhibiting the SMPT of cocrystal. Two surfactants of sodium lauryl sulfate and Tween 80 were chosen to investigate their effects on the solubility and intrinsic dissolution rate of CBZ-NIC cocrystal.

This research finally studied the solubility and dissolution behaviour of CBZ, CBZ-NIC cocrystal, CBZ-SUC cocrystal in simulated gastric fluid, pH1.2 HCl buffer, simulated intestinal fluid, and pH 6.8 PBS buffer.

8.2 Conclusions

This thesis established a method to monitor the dissolution process of cocrystal through *in situ* UV imaging and Raman spectroscopy combined with a complementary technique of SEM, which can provide an in depth understanding of the dissolution process of cocrystals through studying the kinetics and mechanism of drug substance release into dissolution medium.

Dissolution and transformation behavior of CBZ-NIC cocrystal was studied by different *in situ* techniques of UV imaging and Raman spectroscopy. It has been found that CBZ-NIC cocrystal including other polymorphs of CBZ III and I and mixture are converting to CBZ DH during dissolution. Compared with CBZ III and I, the rate of IDR of CBZ-NIC cocrystal decreases slowly, indicating the rate of crystallization of CBZ DH from the solution is slow. *In situ* solid-state characterization during dissolution has shown the evolution of conversion of CBZ-NIC cocrystal and polymorphs to its dihydrate form, which cannot completely be understood by merely measuring the dissolved drug concentration. The information from the experiments on transformation behavior of CBZ-NIC cocrystal is valuable for understanding the mechanisms of cocrystal dissolution, which helps to develop a correlation between *in vitro-in vivo* absorption for formulation development.

The investigation results about surfactants effects show that CBZ DH (CBZ III), CBZ-NIC cocrystal and physical mixture of CBZ III and NIC have the same equilibrium solubility. SLS and Tween 80 have little effect on the solubility of the CBZ-NIC cocrystal in comparison with the significant solubility enhancement for CBZ DH by

SLS above its CMC. The SMPT of CBZ III and CBZ-NIC cocrystal can be altered by inclusion of a surfactant in dissolution medium. However, CBZ III and CBZ-NIC cocrystal have shown different transformation behavior with different surfactants. IDRs profile of CBZ III and CBZ-NIC cocrystal increased significantly when the concentration of SLS was higher than its CMC in a dissolution medium. The inclusion of Tween 80 in dissolution medium reduced IDRs of CBZ III and CBZ-NIC cocrystal due to its large molecule size which can form an interfacial barrier to prevent CBZ molecules getting into the bulk solution, resulting in accelerated nucleation and growth of stable crystal form CBZ DH on sample compact surface.

Research of cocrystal solubility and dissolution in biomedium has shown that CBZ solubility from CBZ-SUC cocrystal in SGF is more than double as others. Except CBZ-SUC cocrystal in SGF, generally, all cocrystal has a little bit higher solubility than CBZ DH, while these CBZ solubility data does not show big difference. Due to the alkali properties of CBZ which has a higher solubility in acidic buffer, the equilibrium solubility of CBZ from CBZ DH and two cocrystals has a relative higher solubility in SGF and pH 1.2 buffer than that in SIF and pH 6.8 buffer. However, the solubility of CBZ from mixture in acidic buffers is not always higher. The solubility of CBZ in the presence of NIC has increased as NIC initial concentration increasing due to the complexation of NIC and CBZ. CBZ-NIC cocrystal has a higher solubility in acidic buffer than in alkalic buffers and a better solubility in simulated buffer than inorganic buffer. The solubility of CBZ in the presence of SUC shows different trend as in presence of NIC, which does not show significant increasing as coformer initial concentration increasing. The dissolution behavior study results show that pH value and protein binding reaction affect the IDR of CBZ III. IDRs of CBZ III in four buffers are decreasing in the order of SGF, SIF, pH 1.2 buffer, and pH6.8 buffer. The two cocrystals dissolution rate show different trend as that of parent drug CBZ III. This can be explained by that the formation of cocrystal change the ability of CBZ III to bind with organic material in buffer, and also change its pH property.

8.3 Future work

The future research about pharmaceutical cocrystal in our lab will be focused on

following aspects,

Cocrystal crystallography structure, preparation scale up, stability test, formulation, commercial products

Cocrystals can provide higher and lower dissolution rates compared to the API, while the concepts of cocrystal and crystal engineering remain largely underexploited, and there are many basic questions about pharmaceutical cocrystal that remain unanswered. It is necessary to get a thoroughly understanding about the relations between the structure and dissolution behaviour. Effort should be made to study the structure of cocrystal from the crystallography aspect.

To date, no cocrystal drug products appear to be on the market, there is still a long time to waiting before this pharmaceutical cocrystal research in lab becomes a product in market. Further research is desirable to test the physicochemical stability of cocrystal, formulation development and implement manufacturing of final dosage forms on commercial scale. To achieve all the above targets, the first thing we need to do is to scale up cocrystal preparation. Because the amount of cocrystal needed in the following research is greatly increased, which cannot easily provided by slow evaporation method. Processes to produce cocrystals on a large scale will likely require different approaches.

UV imaging system improvement

The ActiPix SDI 300 UV surface imaging system, as a new technology that has been designed to improve our understanding of the kinetics and mechanism of drug substance release into dissolution medium, can provide two-dimensional images of the dissolution process. The employ of UV imaging system in this research has obtained good results; however, there are still some obvious limitations about this method. First of all, the target drug should be the only one among all components in drug sample which can be quantitative measured under the present used UV filter. This limitation poses a difficulty on selected research objects for researchers, due to cocrystal always have more than one component, and what is more, the API and coformers have overplayed UV absorption area most time. Efforts should be made on enlargement of application of UV imaging dissolution system. Secondly, lots of practice is needed to operate this

testing system proficiently. In order to make the system more easy control, it is highly necessary to do some modification to optimize the operation, such as decrease the probability of bubbles emerging during dissolution testing, simplify the loading process of sample compact, automatically provide visualisation information as soon as the contact of drug component and medium. Last, in some cases the effluent should be collected and tested to validate the IDRs calculated by the software based on the images. This can be done manually or can be done automatically through connecting the UV imaging system with quantitative analysing equipment.

REFERRENCES

1. Aakeröy, C.B., S. Forbes, and J. Desper, *Using Cocrystals To Systematically Modulate Aqueous Solubility and Melting Behavior of an Anticancer Drug.* J. Am. Chem. Soc., 2009. **131**(47): p. 17048-17049.
2. PhRMA, *Pharmaceutical Industry Profile 2006*, 2006, PhRMA: Washington, DC.
3. Ramanathan, T., Ed, *Mass Spectrometry in Drug Metabolism and Pharmacokinetics*, 2009, John Wiley & Sons, Inc: Hoboken, NJ. p. 1-4.
4. Rasenack, N., H. Hartenhauer, and B.W. Müller, *Microcrystals for dissolution rate enhancement of poorly water-soluble drugs.* Int. J. Pharm., 2003. **254**(2): p. 137-145.
5. Cho, E., et al., *Enhanced dissolution of megestrol acetate microcrystals prepared by antisolvent precipitation process using hydrophilic additives.* Int. J. Pharm. , 2010. **396**(1-2): p. 91-98.
6. Li, N., et al., *Increased dissolution and physical stability of micronized nifedipine particles encapsulated with a biocompatible polymer and surfactants in a wet ball milling process.* Pharmazie, 2006. **61**(7): p. 595-603.
7. Umeda, Y., et al., *Characterization of multicomponent crystal formed between indomethacin and lidocaine.* Drug Dev. Ind. Pharm., 2009. **35**(7): p. 843-851.
8. Serajuddin, A.T.M., *Solid dispersion of poorly water-soluble drugs: Early promises, subsequent problems, and recent breakthroughs.* J. Pharm. Sci., 1999. **88**(10): p. 1058-1066.
9. Torchilin, V., *Micellar Nanocarriers: Pharmaceutical Perspectives.* Pharm. Res., 2007. **24**(1): p. 1-16.
10. Hong, J.-Y., et al., *A new self-emulsifying formulation of itraconazole with improved dissolution and oral absorption.* J. Control. Release, 2006. **110**(2): p. 332-338.
11. Amin, K., et al., *Lyophilization of polyethylene glycol mixtures.* J. Pharm. Sci., 2004. **93**(9): p. 2244-2249.
12. Yue, X., et al., *Amphiphilic Methoxy Poly(ethylene glycol)-b-poly(ϵ-caprolactone)-b-poly(2-dimethylaminoethyl methacrylate) Cationic Copolymer Nanoparticles as a Vector for Gene and Drug Delivery.* Biomacromolecules, 2010. **11**(9): p. 2306-2312.
13. Blagden, N., et al., *Crystal engineering of active pharmaceutical ingredients to improve solubility and dissolution rates.* Adv. Drug Delivery Rev. , 2007. **59**: p. 617-630.
14. Vishweshwar, P., et al., *Pharmaceutical co-crystals.* J. Pharm. Sci., 2006. **95**(3): p. 499-516.
15. ter Horst, J.H., M.A. Deij, and P.W. Cains, *Discovering New Co-Crystals.* Cryst. Growth Des. , 2009. **9**(3): p. 1531-1537.
16. Huang, L.F. and W.Q. Tong, *Impact of solid state properties on developability assessment of drug candidates.* Adv. Drug Delivery Rev., 2004. **56**(3): p. 321-334.
17. Lu, J. and S. Rohani, *Preparation and Characterization of Theophylline-Nicotinamide Cocrystal.* Org. Process Res. Dev., 2009. **13**(6): p. 1269-1275.
18. Schultheiss, N. and A. Newman, *Pharmaceutical Cocrystals and Their Physicochemical Properties.* Cryst. Growth Des. , 2009. **9**(6): p. 2950-2967.
19. Shan, N. and M.J. Zaworotko, *The role of cocrystals in pharmaceutical science.* Drug Discov. Today, 2008. **13**(9-10): p. 440-446.
20. Aakeröy, C.B. and D.J. Salmon, *Building co-crystals with molecular sense and supramolecular sensibility.* Cryst. Eng. Comm., 2005. **7**: p. 439-448.

21. Almarsson, O. and M.J. Zaworotko, *Crystal engineering of the composition of pharmaceutical phases. Do pharmaceutical co-crystals represent a new path to improved medicines?* Chem. Commun., 2004(17): p. 1889-1896.
22. Walsh, R.D.B., et al., *Crystal engineering of the composition of pharmaceutical phases.* Chem. Commun. , 2003(2): p. 186-187.
23. Khan, M., V. Enkelmann, and G. Brunklaus, *Crystal Engineering of Pharmaceutical Co-crystals: Application of Methyl Paraben as Molecular Hook.* J. Am. Chem. Soc, 2010. **132**(14): p. 5254-5263.
24. Padrela, L., et al., *Screening for pharmaceutical cocrystals using the supercritical fluid enhanced atomization process.* J. Supercrit. Fluids 2010. **53**(1-3): p. 156-164.
25. Steiner, T., *Competition of hydrogen-bond acceptors for the strong carboxyl donor.* Acta Crystallogr. Sect. B, 2001. **57**(1): p. 103-106.
26. Bis, J.A., et al., *Hierarchy of Supramolecular Synthons: Persistent Hydroxyl···Pyridine Hydrogen Bonds in Cocrystals That Contain a Cyano Acceptor.* Mol. Pharm., 2007. **4**(3): p. 401-416.
27. He, G.W., et al., *Screening for cocrystallization tendency: The role of intermolecular interactions.* J. Phys. Chem. B, 2008. **112**(32): p. 9890-9895.
28. Orpen, A., *Applications of the Cambridge Structural Database to molecular inorganic chemistry.* Acta Crystallogr. Sect. B, 2002. **58**(3 Part 1): p. 398-406.
29. Miroshnyk, I., S. Mirza, and N. Sandler, *Pharmaceutical co-crystals-an opportunity for drug product enhancement.* Expert Opin. Drug Deliv., 2009. **6**(4): p. 333-41.
30. Dhumal, R.S., et al., *Ultrasound Assisted Engineering of Lactose Crystals.* Pharm. Res., 2008. **25**(12): p. 2835-2844.
31. Blagden, N., et al., *Current directions in co-crystal growth.* New J. Chem., 2008. **32**(10): p. 1659-1672.
32. Desiraju, G.R., *Supramolecular Synthons in Crystal Engineering—A New Organic Synthesis.* Angew. Chem. Int. Ed. Engl., 1995. **34**(21): p. 2311-2327.
33. Etter, M.C., *Hydrogen bonds as design elements in organic chemistry.* J. Phys. Chem., 1991. **95**(12): p. 4601-4610.
34. Etter, M.C. and S.M. Reutzel, *Hydrogen bond directed cocrystallization and molecular recognition properties of acyclic imides.* J. Am. Chem. Soc, 1991. **113**(7): p. 2586-2598.
35. Etter, M.C., J.C. MacDonald, and J. Bernstein, *Graph-set analysis of hydrogen-bond patterns in organic crystals.* Acta Crystallogr., Sect. B, 1990. **46**(2): p. 256-262.
36. Dale, S.H., et al., *The co-crystallisation of pyridine with benzenepolycarboxylic acids: The interplay of strong and weak hydrogen bonding motifs.* Cryst. Eng. Comm., 2004. **6**: p. 207-214.
37. Weyna, D.R., et al., *Synthesis and Structural Characterization of Cocrystals and Pharmaceutical Cocrystals: Mechanochemistry vs Slow Evaporation from Solution.* Cryst. Growth Des. , 2009. **9**(2): p. 1106-1123.
38. Dhumal, R.S., et al., *Preparation of amorphous cefuroxime axetil nanoparticles by sonoprecipitation for enhancement of bioavailability.* Eur. J. Pharm. Biopharm., 2008. **70**(1): p. 109-115.
39. Mohammad, M.A., A. Alhalaweh, and S.P. Velaga, *Hansen solubility parameter as a tool to predict cocrystal formation.* Int. J. Pharm. , 2011. **407**(1-2): p. 63-71.
40. Zhang, G.G.Z., et al., *Efficient co-crystal screening using solution-mediated phase transformation.* J. Pharm. Sci., 2007. **96**(5): p. 990-995.
41. Berry, D.J., et al., *Applying Hot-Stage Microscopy to Co-Crystal Screening: A Study of Nicotinamide with Seven Active Pharmaceutical Ingredients.* Cryst. Growth Des. , 2008. **8**(5): p. 1697-1712.

42. McNamara, D.P., et al., *Use of a glutaric acid cocrystal to improve oral bioavailability of a low solubility API.* Pharm. Res., 2006. **23**(8): p. 1888-1897.
43. Lee, T. and P.Y. Wang, *Screening, Manufacturing, Photoluminescence, and Molecular Recognition of Co-Crystals: Cytosine with Dicarboxylic Acids.* Cryst. Growth Des. , 2010. **10**(3): p. 1419-1434.
44. Habgood, M., et al., *Carbamazepine Co-crystallization with Pyridine Carboxamides: Rationalization by Complementary Phase Diagrams and Crystal Energy Landscapes.* Cryst. Growth Des. , 2009. **10**(2): p. 903-912.
45. Bermejo, M. and I. Gonzalez-Alvarez, *How and Where Are Drugs Absorbed?*, in *Preclinical Development Handbook: ADME and Biopharmaceutical Properties*, S.C. Gad, Editor 2007, John Wiley & Sons, Inc.: Hoboken. p. 249-280.
46. Childs, S.L., et al., *Screening strategies based on solubility and solution composition generate pharmaceutically acceptable cocrystals of carbamazepine.* Cryst. Eng. Comm., 2008. **10**(7): p. 856-864.
47. Ainouz, A., et al., *Modeling and prediction of cocrystal phase diagrams.* Int. J. Pharm., 2009. **374**(1-2): p. 82-89.
48. Basavoju, S., D. Boström, and S. Velaga, *Indomethacin–Saccharin Cocrystal: Design, Synthesis and Preliminary Pharmaceutical Characterization.* Pharm. Res., 2008. **25**(3): p. 530-541.
49. Rodríguez-Hornedo, N., et al., *Reaction Crystallization of Pharmaceutical Molecular Complexes.* Mol. Pharm., 2006. **3**(3): p. 362-367.
50. Jayasankar, A., et al., *Role of Cocrystal and Solution Chemistry on the Formation and Stability of Cocrystals with Different Stoichiometry.* Cryst. Growth Des., 2009. **9**(2): p. 889-897.
51. Gagniere, E., et al., *Formation of co-crystals: Kinetic and thermodynamic aspects.* J. Cryst. Growth 2009. **311**(9): p. 2689-2695.
52. Gagniere, E., et al., *Cocrystal Formation in Solution: In Situ Solute Concentration Monitoring of the Two Components and Kinetic Pathways.* Cryst. Growth Des., 2009. **9**(8): p. 3376-3383.
53. He, G., P.S. Chow, and R.B.H. Tan, *Investigating the Intermolecular Interactions in Concentration-Dependent Solution Cocrystallization of Caffeine and p-Hydroxybenzoic Acid.* Cryst. Growth Des. , 2010. **10**(8): p. 3763-3769.
54. Braga, D. and F. Grepioni, *Reactions Between or Within Molecular Crystals.* Angew. Chem. Int. Ed., 2004. **43**(31): p. 4002-4011.
55. Braga, D., et al., *Mechanochemical preparation of molecular and supramolecular organometallic materials and coordination networks.* Dalton Trans., 2006(10): p. 1249-1263.
56. Friščić, T. and W. Jones, *Recent Advances in Understanding the Mechanism of Cocrystal Formation via Grinding.* Cryst. Growth Des., 2009. **9**(3): p. 1621-1637.
57. Myz, S.A., et al., *Synthesis of co-crystals of meloxicam with carboxylic acids by grinding.* Mendeleev Commun., 2009. **19**(5): p. 272-274.
58. Jayasankar, A., et al., *Cocrystal formation during cogrinding and storage is mediated by amorphous phase.* Pharm. Res., 2006. **23**(10): p. 2381-2392.
59. Trask, A.V., W.D.S. Motherwell, and W. Jones, *Solvent-drop grinding: green polymorph control of cocrystallisation.* Chem. Commun., 2004(7): p. 890-891.
60. Braga, D. and F. Grepioni, *Making crystals from crystals: a green route to crystal engineering and polymorphism.* Chem. Commun., 2005(29): p. 3635-3645.
61. Shan, N., F. Toda, and W. Jones, *Mechanochemistry and co-crystal formation: effect of solvent on reaction kinetics.* Chem. Commun., 2002(20): p. 2372-2373.

62. Padrela, L., et al., *Formation of indomethacin-saccharin cocrystals using supercritical fluid technology.* Eur. J. Pharm. Sci., 2009. **38**(1): p. 9-17.
63. Dhumal, R.S., et al., *Particle engineering using sonocrystallization: Salbutamol sulphate for pulmonary delivery.* Int. J. Pharm., 2009. **368**(1-2): p. 129-137.
64. Aher, S., et al., *Ultrasound assisted cocrystallization from solution (USSC) containing a non-congruently soluble cocrystal component pair: Caffeine/maleic acid.* Eur. J. Pharm. Sci., 2010. **41**(5): p. 597-602.
65. Porter Iii, W.W., S.C. Elie, and A.J. Matzger, *Polymorphism in Carbamazepine Cocrystals.* Cryst. Growth Des., 2008. **8**(1): p. 14-16.
66. Aakeröy, C.B., et al., *Cyanophenyloximes: Reliable and Versatile Tools for Hydrogen-Bond Directed Supramolecular Synthesis of Cocrystals.* Cryst. Growth Des., 2006. **6**(4): p. 1033-1042.
67. Li, Z.J., et al., *Solid-State Acid-Base Interactions in Complexes of Heterocyclic Bases with Dicarboxylic Acids: Crystallography, Hydrogen Bond Analysis, and ^{15}N NMR Spectroscopy.* J. Am. Chem. Soc, 2006. **128**(25): p. 8199-8210.
68. Lu, E., N. Rodriguez-Hornedo, and R. Suryanarayanan, *A rapid thermal method for cocrystal screening.* Cryst. Eng. Comm., 2008. **10**(6): p. 665-668.
69. Johnson, S.L. and K.A. Rumon, *Infrared Spectra of Solid 1:1 Pyridine-Benzoic Acid Complexes; the Nature of the Hydrogen Bond as a Function of the Acid-Base Levels in the Complex1.* J. Phys. Chem., 1965. **69**(1): p. 74-86.
70. Jung, M.-S., et al., *Bioavailability of indomethacin-saccharin cocrystals.* J. Pharm. Pharmacol., 2010. **62**(11): p. 1560-1568.
71. Parrott, E.P.J., et al., *Testing the sensitivity of terahertz spectroscopy to changes in molecular and supramolecular structure: A study of structurally similar cocrystal.* Cryst. Growth Des., 2009. **9**(3): p. 1452-1460.
72. Bak, A., et al., *The co-crystal approach to improve the exposure of a water-insoluble compound: AMG 517 sorbic acid co-crystal characterization and pharmacokinetics.* J. Pharm. Sci. , 2008. **97**(9): p. 3942-3956.
73. Fleischman, S.G., et al., *Crystal Engineering of the Composition of Pharmaceutical Phases: Multiple-Component Crystalline Solids Involving Carbamazepine.* Cryst. Growth Des., 2003. **3**(6): p. 909-919.
74. Trask, A.V., W.D.S. Motherwell, and W. Jones, *Physical stability enhancement of theophylline via cocrystallization.* Int. J. Pharm., 2006. **320**(1-2): p. 114-123.
75. Reutzel-Edens, S.M. and A.W. Newman, *Physical Characterization of Hygroscopicity in Pharmaceutical Solids*, in *Polymorphism: in the Pharmaceutical Industry*, R. Hilfiker, Editor 2006, Wiley-VCH Verlag GmbH & Co. KGaA: Weinheim. p. 235-258.
76. Oswald, I.D.H., et al., *The formation of paracetamol (acetaminophen) adducts with hydrogen-bond acceptors.* Acta Crystallogr. Sect. B, 2002. **58**(6): p. 1057-1066.
77. Variankaval, N., et al., *Preparation and Solid-State Characterization of Nonstoichiometric Cocrystals of a Phosphodiesterase-IV Inhibitor and l-Tartaric Acid.* Cryst. Growth Des., 2006. **6**(3): p. 690-700.
78. Agharkar, S., S. Lindenbaum, and T. Higuchi, *Enhancement of solubility of drug salts by hydrophilic counterions: Properties of organic salts of an antimalarial drug.* J. Pharm. Sci., 1976. **65**(5): p. 747-749.
79. Chaumeil, J.C., *Micronization: a method of improving the bioavailability of poorly soluble drugs.* Methods Find. Exp. Clin. Pharmacol., 1998. **20**(3): p. 211-215.
80. Childs, S.L., et al., *Crystal Engineering Approach To Forming Cocrystals of Amine Hydrochlorides with Organic Acids. Molecular Complexes of Fluoxetine Hydrochloride*

with Benzoic, Succinic, and Fumaric Acids. J. Am. Chem. Soc., 2004. **126**(41): p. 13335-13342.

81. Remenar, J.F., et al., *Crystal Engineering of Novel Cocrystals of a Triazole Drug with 1,4-Dicarboxylic Acids.* J. Am. Chem. Soc., 2003. **125**(28): p. 8456-8457.
82. Shiraki, K., et al., *Dissolution improvement and the mechanism of the improvement from cocrystallization of poorly water-soluble compounds.* Pharm. Res., 2008. **25**(11): p. 2581-2592.
83. Reddy, L.S., et al., *Cocrystals and Salts of Gabapentin: pH Dependent Cocrystal Stability and Solubility.* Cryst. Growth Des., 2008. **9**(1): p. 378-385.
84. Good, D.J. and N.r. Rodríguez-Hornedo, *Solubility Advantage of Pharmaceutical Cocrystals.* Cryst. Growth Des., 2009. **9**(5): p. 2252-2264.
85. Bethune, S.J., et al., *Understanding and Predicting the Effect of Cocrystal Components and pH on Cocrystal Solubility.* Cryst. Growth Des., 2009. **9**(9): p. 3976-3988.
86. Good, D.J. and N. Rodriguez-Hornedo, *Cocrystal Eutectic Constants and Prediction of Solubility Behavior.* Cryst. Growth Des., 2010. **10**(3): p. 1028-1032.
87. Lee, H.-G., G.G.Z. Zhang, and D.R. Flanagan, *Cocrystal intrinsic dissolution behavior using a rotating disk.* J. Pharm. Sci., 2010. **100**(5): p. 1736-1744.
88. Grossjohann, C., et al., *Characterisation, solubility and intrinsic dissolution behaviour of benzamide: dibenzyl sulfoxide cocrystal.* Int. J. Pharm., 2012. **422**(1–2): p. 24-32.
89. Huang, N. and N.r. Rodríguez-Hornedo, *Effect of Micellar Solubilization on Cocrystal Solubility and Stability.* Cryst. Growth Des., 2010. **10**(5): p. 2050-2053.
90. Huang, N. and N. Rodríguez-Hornedo, *Engineering cocrystal solubility, stability, and pHmax by micellar solubilization.* J. Pharm. Sci., 2011. **100**(12): p. 5219-5234.
91. Huang, N. and N. Rodriguez-Hornedo, *Engineering cocrystal thermodynamic stability and eutectic points by micellar solubilization and ionization.* Cryst. Eng. Comm., 2011. **13**(17): p. 5409-5422.
92. McNamara, D., et al., *Use of a Glutaric Acid Cocrystal to Improve Oral Bioavailability of a Low Solubility API.* Pharm. Res. , 2006. **23**(8): p. 1888-1897.
93. Greco, K. and R. Bogner, *Solution-mediated phase transformation: Significance during dissolution and implications for bioavailability.* J. Pharm. Sci., 2012. **101**(9): p. 2996-3018.
94. Davey, R.J., et al., *Rate controlling processes in solvent-mediated phase transformations.* J. Cryst. Growth, 1986. **79**(1–3, Part 2): p. 648-653.
95. Cardew, P.T. and R.J. Davey, *The Kinetics of Solvent-Mediated Phase Transformations.* Proceedings of the Royal Society of London. A. Mathematical and Physical Sciences, 1985. **398**(1815): p. 415-428.
96. Greco, K., D.P. McNamara, and R. Bogner, *Solution-mediated phase transformation of salts during dissolution: Investigation using haloperidol as a model drug.* J. Pharm. Sci. , 2011. **100**(7): p. 2755-2768.
97. Kobayashi, Y., et al., *Physicochemical properties and bioavailability of carbamazepine polymorphs and dihydrate.* Int. J. Pharm., 2000. **193**(2): p. 137-146.
98. Rustichelli, C., et al., *Solid-state study of polymorphic drugs: carbamazepine.* J. Pharm. Biomed. Anal. , 2000. **23**(1): p. 41-54.
99. Sehic, S., et al., *Investigation of intrinsic dissolution behavior of different carbamazepine samples.* Int. J. Pharm., 2010. **386**(1-2): p. 77-90.
100. Ono, M., et al., *Effects of dehydration temperature on water vapor adsorption and dissolution behavior of carbamazepine.* Int. J. Pharm., 2002. **239**(1&2): p. 1-12.
101. Tian, F., et al., *Influence of polymorphic form, morphology, and excipient interactions on the dissolution of carbamazepine compacts.* J. Pharm. Sci. , 2007. **96**(3): p. 584-594.

102. Laine, E., et al., *Formation of dihydrate from carbamazepine anhydrate in aqueous conditions.* Int. J. Pharm., 1984. **20**(3): p. 307-314.
103. Kahela, P., et al., *Pharmacokinetics and dissolution of two crystalline forms of carbamazepine.* Int. J. Pharm., 1983. **14**(1): p. 103-112.
104. Rodríguez-Hornedo, N. and D. Murphy, *Surfactant-facilitated crystallization of dihydrate carbamazepine during dissolution of anhydrous polymorph.* J. Pharm. Sci. , 2004. **93**(2): p. 449-460.
105. Konno, H., et al., *Effect of polymer type on the dissolution profile of amorphous solid dispersions containing felodipine.* Eur. J. Pharm. Biopharm. , 2008. **70**(2): p. 493-499.
106. Alonzo, D., et al., *Understanding the Behavior of Amorphous Pharmaceutical Systems during Dissolution.* Pharm. Res. , 2010. **27**(4): p. 608-618.
107. Murphy, D., et al., *Solution-mediated phase transformation of anhydrous to dihydrate carbamazepine and the effect of lattice disorder.* Int. J. Pharm., 2002. **246**(1&2): p. 121-134.
108. Ulrich, J., A. Schuster, and T. Stelzer, *Crystalline coats or hollow crystals as tools for product design in pharmaceutical industry.* J. Cryst. Growth (2011). **doi:10.1016/j.jcrysgro.2011.10.060**.
109. Dette, S.S., et al., *Fascinating control of crystalline microstructures.* Chem. Eng. Res. Des. **88**(9): p. 1158-1162.
110. Martins, D., et al., *Formation of Crystalline Hollow Whiskers as Relics of Organic Dissipative Structures.* Cryst. Growth Des., 2011. **11**(7): p. 3020-3026.
111. Lee, H.G., G.G.Z. Zhang, and D.R. Flanagan, *Cocrystal intrinsic dissolution behavior using a rotating disk.* J. Pharm. Sci. , 2011. **100**(5): p. 1736-1744.
112. Shiraki, K., et al., *Dissolution Improvement and the Mechanism of the Improvement from Cocrystallization of Poorly Water-soluble Compounds.* Pharm. Res. , 2008. **25**(11): p. 2581-2592.
113. Arenas-Garcia, J.I., et al., *Co-Crystals of Active Pharmaceutical Ingredients - Acetazolamide.* Cryst. Growth Des. , 2010. **10**(8): p. 3732-3742.
114. Lehto, P., et al., *Simultaneous measurement of liquid-phase and solid-phase transformation kinetics in rotating disc and channel flow cell dissolution devices.* Int. J. Pharm., 2008. **363**(1&2): p. 66-72.
115. Savolainen, M., et al., *Better understanding of dissolution behaviour of amorphous drugs by in situ solid-state analysis using Raman spectroscopy.* Eur. J. Pharm. Biopharm. , 2009. **71**(1): p. 71-79.
116. Tian, F., et al., *Characterizing the conversion kinetics of carbamazepine polymorphs to the dihydrate in aqueous suspension using Raman spectroscopy.* J. Pharm. Biomed. Anal. , 2006. **40**(2): p. 271-280.
117. Lehto, P., et al., *Solvent-mediated solid phase transformations of carbamazepine: Effects of simulated intestinal fluid and fasted state simulated intestinal fluid.* J. Pharm. Sci. , 2009. **98**(3): p. 985-996.
118. Aaltonen, J., et al., *In situ measurement of solvent-mediated phase transformations during dissolution testing.* J. Pharm. Sci. , 2006. **95**(12): p. 2730-2737.
119. Schindler, W. and F. Häfliger, *Über Derivate des Iminodibenzyls.* Helv. Chim. Acta, 1954. **37**(2): p. 472-483.
120. Kaneniwa, N., et al., *Dissolution behaviour of carbamazepine polymorphs.* Yakugaku Zasshi, 1987. **107**(10): p. 808-13.
121. Meyer, M.C., et al., *The relative bioavailability and in vivo in vitro correlations for four marketed carbamazepine tablets.* Pharm. Res. , 1998. **15**(11): p. 1787-1791.

122. Etter, M.C., *Encoding and decoding hydrogen-bond patterns of organic compounds.* Acc. Chem. Res. , 1990. **23**(4): p. 120-126.
123. McMahon, J.A., et al., *Crystal engineering of the composition of pharmaceutical phases. 3. Primary amide supramolecular heterosynthons and their role in the design of pharmaceutical co-crystals.* Zeitschrift für Kristallographie, 2005. **220**(4-2005): p. 340-350.
124. Liu, W., et al., *Solubility of Carbamazepine (Form III) in Different Solvents from (275 to 343) K.* J. Chem. Eng. Data, 2008. **53**(9): p. 2204-2206.
125. Park, K., J.M.B. Evans, and A.S. Myerson, *Determination of Solubility of Polymorphs Using Differential Scanning Calorimetry.* Cryst. Growth Des., 2003. **3**(6): p. 991-995.
126. Bettini, R., et al., *Solubility and conversion of carbamazepine polymorphs in supercritical carbon dioxide.* Eur. J. Pharm. Sci., 2001. **13**(3): p. 281-286.
127. Qu, H., M. Louhi-Kultanen, and J. Kallas, *Solubility and stability of anhydrate/hydrate in solvent mixtures.* Int. J. Pharm., 2006. **321**(1-2): p. 101-107.
128. Seefeldt, K., et al., *Crystallization pathways and kinetics of carbamazepine–nicotinamide cocrystals from the amorphous state by in situ thermomicroscopy, spectroscopy, and calorimetry studies.* J. Pharm. Sci., 2007. **96**(5): p. 1147-1158.
129. Chieng, N., et al., *Formation Kinetics and Stability of Carbamazepine-Nicotinamide Cocrystals Prepared by Mechanical Activation.* Cryst. Growth Des. , 2009. **9**(5): p. 2377-2386.
130. Jayasankar, A., D.J. Good, and N. Rodríguez-Hornedo, *Mechanisms by Which Moisture Generates Cocrystals.* Mol. Pharm., 2007. **4**(3): p. 360-372.
131. McMahon, J.A., *Crystal engineering of novel pharmaceutical forms.* University of South Florida Scholar Commons, 2006(Graduate School Theses and Dissertations).
132. Hickey, M.B., et al., *Performance comparison of a co-crystal of carbamazepine with marketed product.* Eur. J. Pharm. Biopharm., 2007. **67**(1): p. 112-119.
133. Lohani, S., et al., *Carbamazepine-2,2,2-trifluoroethanol (1/1).* Acta Crystallogr. Sect. E, 2005. **61**(5): p. 1310-1312.
134. Johnston, A., A.J. Florence, and A.R. Kennedy, *Carbamazepine furfural hemisolvate.* Acta Crystallogr. Sect. E, 2005. **61**(6): p. 1777-1779.
135. Vishweshwar, P., et al., *The Predictably Elusive Form II of Aspirin.* J. Am. Chem. Soc., 2005. **127**(48): p. 16802-16803.
136. Di Profio, G., et al., *Direct production of carbamazepine-saccharin cocrystals from water/ethanol solvent mixtures by membrane-based crystallization technology.* Cryst. Eng. Comm., 2011. **13**(19): p. 5670-5673.
137. Nehm, S.J., B. Rodríguez-Spong, and N. Rodríguez-Hornedo, *Phase Solubility Diagrams of Cocrystals Are Explained by Solubility Product and Solution Complexation.* Cryst. Growth Des., 2005. **6**(2): p. 592-600.
138. Limwikrant, W., et al., *Formation mechanism of a new carbamazepine/malonic acid cocrystal polymorph.* Int. J. Pharm., 2012. **431**(1-2): p. 237-240.
139. Chiarella, R.A., R.J. Davey, and M.L. Peterson, *Making Co-CrystalsThe Utility of Ternary Phase Diagrams.* Cryst. Growth Des., 2007. **7**(7): p. 1223-1226.
140. Remenar, J.F., et al., *Celecoxib:Nicotinamide Dissociation: Using Excipients To Capture the Cocrystal's Potential.* Mol. Pharm., 2007. **4**(3): p. 386-400.
141. Oberoi, L.M., K.S. Alexander, and A.T. Riga, *Study of interaction between ibuprofen and nicotinamide using differential scanning calorimetry, spectroscopy, and microscopy and formulation of a fast-acting and possibly better ibuprofen suspension for osteoarthritis patients.* J. Pharm. Sci. , 2005. **94**(1): p. 93-101.

142. Childs, S.L. and K.I. Hardcastle, *Cocrystals of Piroxicam with Carboxylic Acids.* Cryst. Growth Des., 2007. **7**(7): p. 1291-1304.
143. E.Aulton, M., *Pharmaceutics: The science of dosage form design*1988, Leicester: Churchill Livingstone.
144. Higuchi, T., *Rate of release of medicaments from ointment bases containing drugs in suspension.* Journal of Pharmaceutical Sciences, 1961. **50**(10): p. 874-875.
145. Noyes, A.A. and W.R. Whitney, *THE RATE OF SOLUTION OF SOLID SUBSTANCES IN THEIR OWN SOLUTIONS.* Journal of the American Chemical Society, 1897. **19**(12): p. 930-934.
146. Ulf, M., K.-L. Povl, and L. Tommy, *Textbook of drug design and discovery*2002, Washington DC: Taylor & Francis.
147. *Figure 55-1. Normal therapeutic range*. Available from: www.medicinescomplete.com.
148. Grzesiak, A.L., et al., *Comparison of the four anhydrous polymorphs of carbamazepine and the crystal structure of form I.* Journal of Pharmaceutical Sciences, 2003. **92**(11): p. 2260-2271.
149. Ping, H., *Bridging in vitro dissolution tests to in vivo dissolution for poorly soluble acidic drugs*, in *Pharmaceutical Sciences*2010, University of Michigan.
150. Boetker, J.P., et al., *Insights into the Early Dissolution Events of Amlodipine Using UV Imaging and Raman Spectroscopy.* Mol. Pharm., 2011. **8**(4): p. 1372-1380.
151. Qiao, N., et al., *In situ monitoring of carbamazepine–nicotinamide cocrystal intrinsic dissolution behaviour.* Eur. J. Pharm. Biopharm., 2013. **83**(3): p. 415-426.
152. Østergaard, J., et al., *Monitoring lidocaine single-crystal dissolution by ultraviolet imaging.* J. Pharm. Sci., 2011. **100**(8): p. 3405-3410.
153. Østergaard, J., et al., *Real-Time UV Imaging of Nicotine Release from Transdermal Patch.* Pharm. Res., 2010. **27**(12): p. 2614-2623.
154. Ye, F., et al., *Real-time UV imaging of drug diffusion and release from Pluronic F127 hydrogels.* Eur. J. Pharm. Sci. , 2011. **43**(4): p. 236-243.
155. Wren, S. and J. Lenke *Pharmaceutical Dissolution and UV Imaging*. Feb 2011.
156. Gardiner, D.J., *Practical Raman spectroscopy*, 1989, Springer-Verlag ISBN 978-0-387-50254-0.
157. Wikipedia. *Raman spectroscopy*. Available from: http://en.wikipedia.org/wiki/Raman_spectroscopy.
158. Wikipedia. *IR spectroscopy*. Available from: http://en.wikipedia.org/wiki/IR_spectroscopy.
159. Wikipedia. *Differential scanning calorimetery*. Available from: http://en.wikipedia.org/wiki/Differential_scanning_calorimetry.
160. Wikipedia. *Thermogravimetric analysis*. Available from: http://en.wikipedia.org/wiki/Thermogravimetric_analysis.
161. Wikipedia, *Scanning electron microscope.*
162. KRÜSS. *Advancing your surface science*. [cited 2014 January 06]; Available from: http://www.kruss.de/services/education-theory/glossary/cmc/.
163. *British Pharmacopeia. Volume V.Appendix I D. Buffer solutions*, 2010.
164. *British Pharmacopeia. Volume V.Appendix XII B. Dissoluiton*, 2013.
165. Lefebvre, C., et al., *Polymorphic Transitions of Carbamazepine During Grinding and Compression.* Drug Dev. Ind. Pharm., 1986. **12**(11-13): p. 1913-1927.
166. McMahon, L.E., et al., *Characterization of dihydrates prepared from carbamazepine polymorphs.* J. Pharm. Sci. , 1996. **85**(10): p. 1064-1069.

167. O'Brien, L.E., et al., *Use of in situ FT-Raman spectroscopy to study the kinetics of the transformation of carbamazepine polymorphs.* J. Pharm. Biomed. Anal., 2004. **36**(2): p. 335-340.
168. Bayarı, S., A. Ataç, and Ş. Yurdakul, *Coordination behaviour of nicotinamide: an infrared spectroscopic study.* J. Mol. Struct. , 2003. **655**(1): p. 163-170.
169. Strachan, C.J., et al., *A theoretical and spectroscopic study of carbamazepine polymorphs.* J. Raman Spectrosc., 2004. **35**(5): p. 401-408.
170. Anquetil, P.A., et al., *Laser Raman spectroscopic analysis of polymorphic forms in microliter fluid volumes.* J. Pharm. Sci. , 2003. **92**(1): p. 149-160.
171. Levich, V.G., *Physicochemical Hydrodynamics*1962: Prentice-Hall: Englewood Cliffs, NJ.
172. Higuchi, W.I., N.A. Mir, and S.J. Desai, *Dissolution rates of polyphase mixtures.* J. Pharm. Sci., 1965. **54**(10): p. 1405-1410.
173. Sanghvi, R., D. Evans, and S.H. Yalkowsky, *Stacking complexation by nicotinamide: A useful way of enhancing drug solubility.* Int. J. Pharm., 2007. **336**(1): p. 35-41.
174. Chen, L., et al., *Dissolution Behavior of a Poorly Water Soluble Compound in the Presence of Tween 80.* Pharm. Res., 2003. **20**(5): p. 797-801.
175. Mullin, J.W., *Crystallization.* Butter Worth-Heinemann, Oxford, 1993.
176. Dokoumetzidis, A. and P. Macheras, *A century of dissolution research: From Noyes and Whitney to the Biopharmaceutics Classification System.* Int. J. Pharm., 2006. **321**(1–2): p. 1-11.
177. Dressman, J.B., et al., *Estimating drug solubility in the gastrointestinal tract.* Adv. Drug Deliv. Rev., 2007. **59**(7): p. 591-602.
178. Bhise, S.B. and M. Rajkumar, *Influence of Simulated Gastrointestinal Fluids on Polymorphic Behavior of Anhydrous Carbamazepine Form III and Biopharmaceutical Relevance.* PDA J. Pharmaceut. Sci. Tech., 2010. **64**(1): p. 28-36.
179. Tomaszewska, I., et al., *Pharmaceutical characterisation and evaluation of cocrystals: Importance of in vitro dissolution conditions and type of coformer.* Int. J. Pharm., 2013. **453**(2): p. 380-388.
180. Augustijns, P., et al., *A review of drug solubility in human intestinal fluids: Implications for the prediction of oral absorption.* Eur. J. Pharm. Sci., (0).
181. Heikkilä, T., et al., *Equilibrium drug solubility measurements in 96-well plates reveal similar drug solubilities in phosphate buffer pH 6.8 and human intestinal fluid.* Int. J. Pharm., 2011. **405**(1–2): p. 132-136.
182. Annaert, P., et al., *Ex vivo permeability experiments in excised rat intestinal tissue and in vitro solubility measurements in aspirated human intestinal fluids support age-dependent oral drug absorption.* Eur. J. Pharm. Sci., 2010. **39**(1–3): p. 15-22.
183. Clarysse, S., et al., *Intestinal drug solubility estimation based on simulated intestinal fluids: Comparison with solubility in human intestinal fluids.* Eur. J. Pharm. Sci., 2011. **43**(4): p. 260-269.

APPENDIXES

A1 Figures for Chapter 6

A 1.1 Figures for equilibrium solubility tests in chapter 6

A 1.1.1 IR spectra of solid residue from equilibrium solubility tests

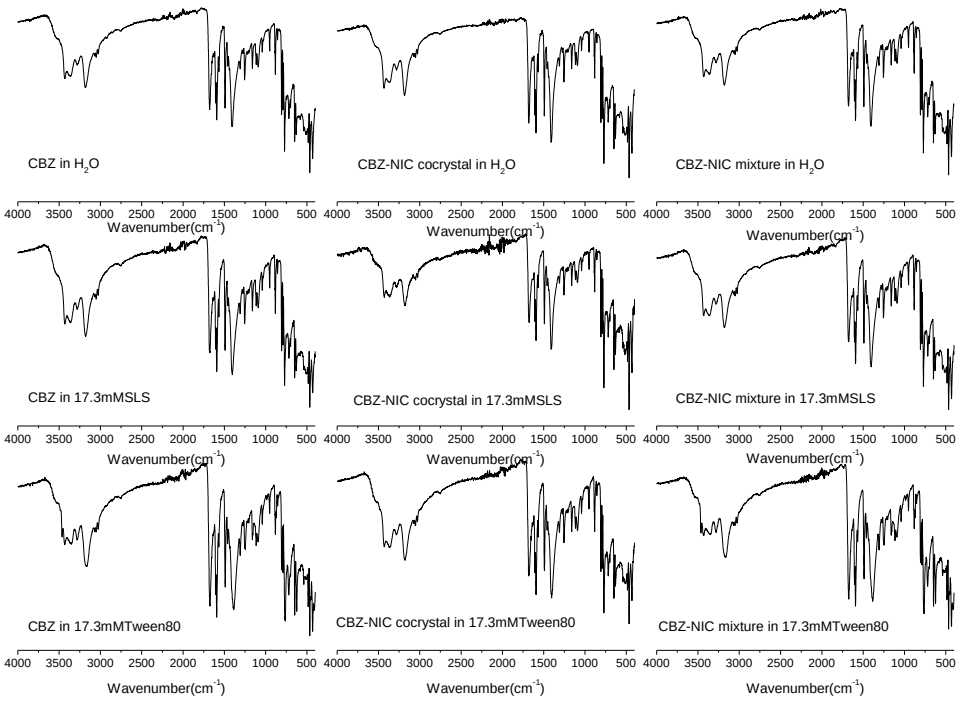

A 1.1.2 Raman spectra of solid residue from equilibrium solubility tests

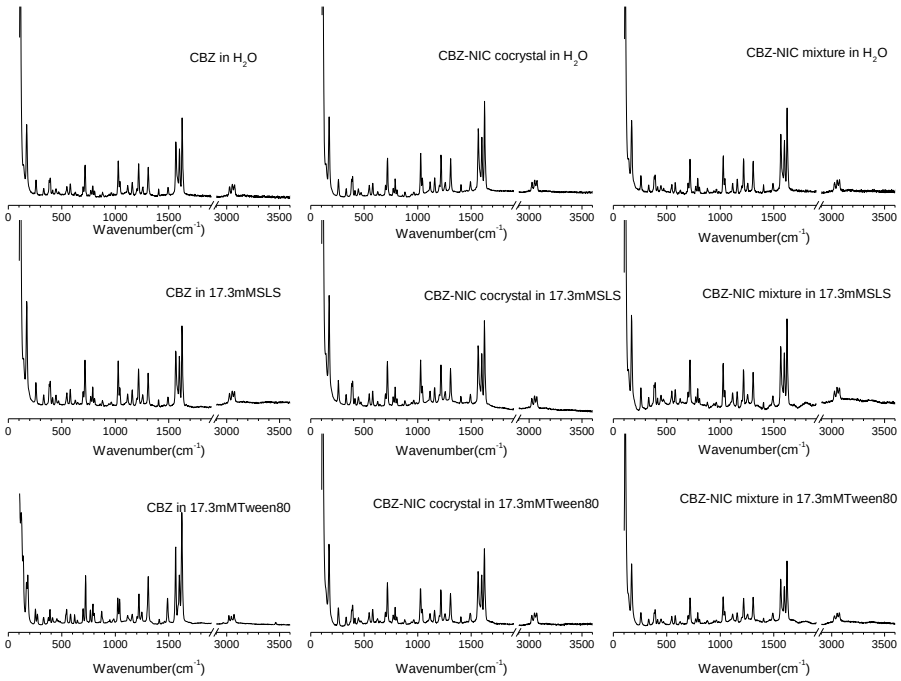

A 1.2 Figures for CBZ solubility as function of NIC tests in chapter 6

A1.2.1 DSC thermal graphs of solid residue from solubility test of CBZ as function of NIC

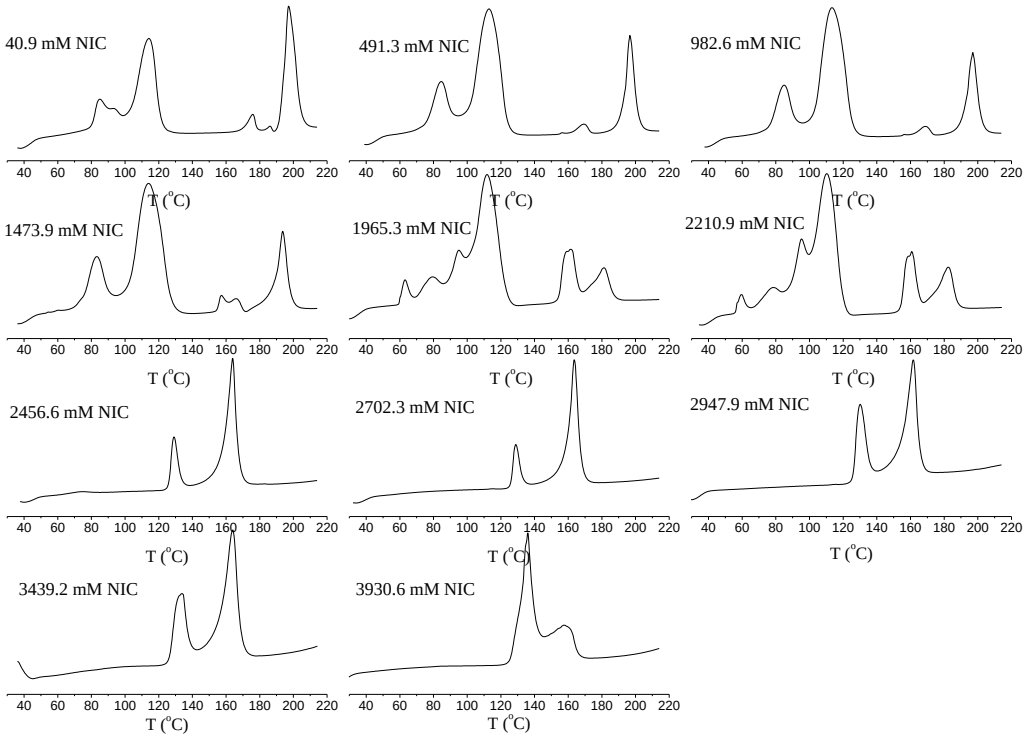

A1.2.2 IR spectra of solid residue from solubility test of CBZ as function of NIC

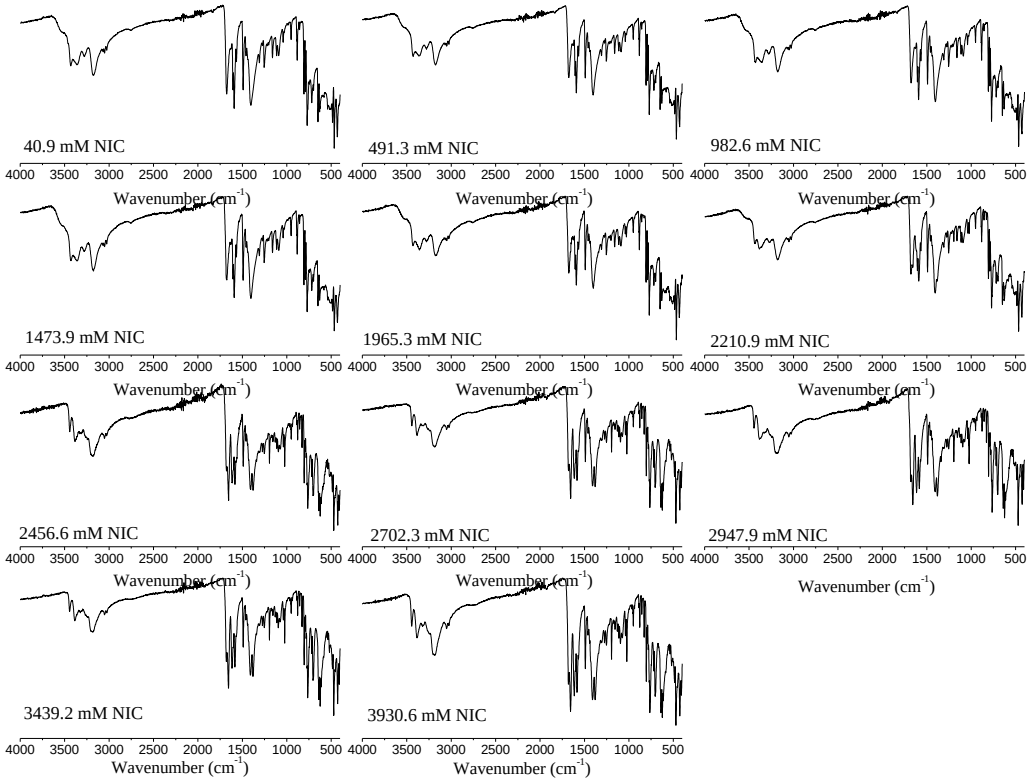

A1.2.3 Raman spectra of solid residue from solubility test of CBZ as function of NIC

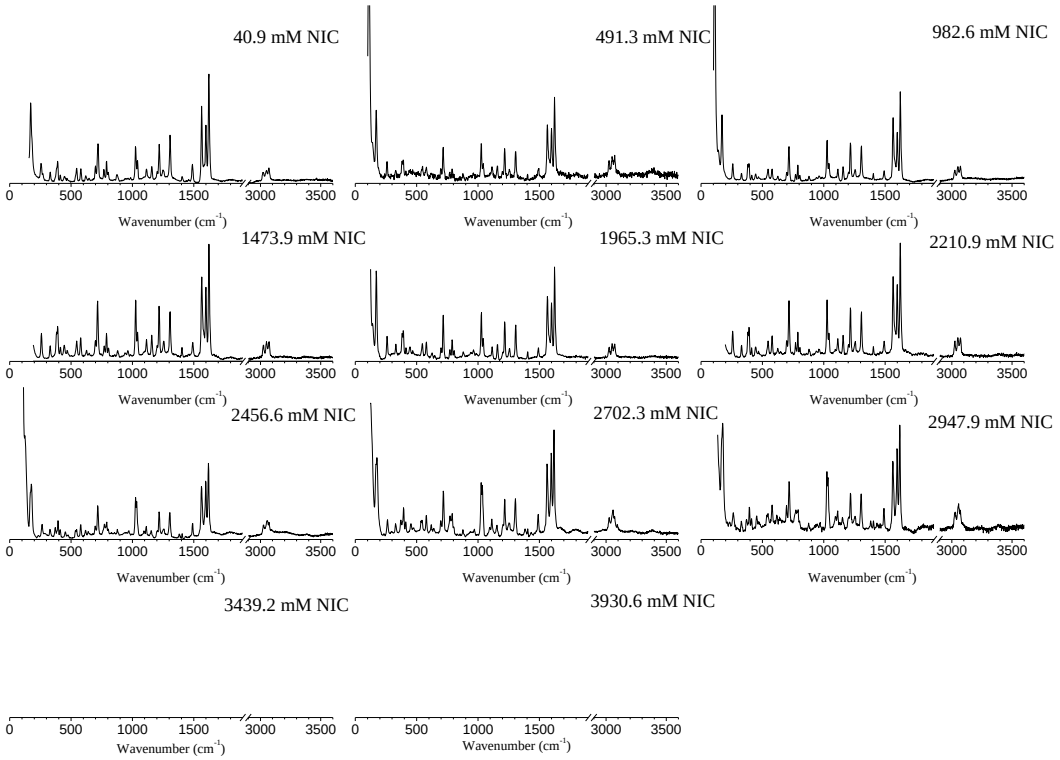

A2 Figures for Chapter 7

A 2.1 Figures for equilibrium solubility tests in chapter 7

A2.1.1 DSC thermal graphs of solid residue from the experiment of equilibrium solubility test in four buffers: (a) CBZ DH; (b) CBZ-NIC cocrystal; (c) CBZ-NIC mixture; (d) CBZ-SUC cocrystal; (e) CBZ-SUC mixture.

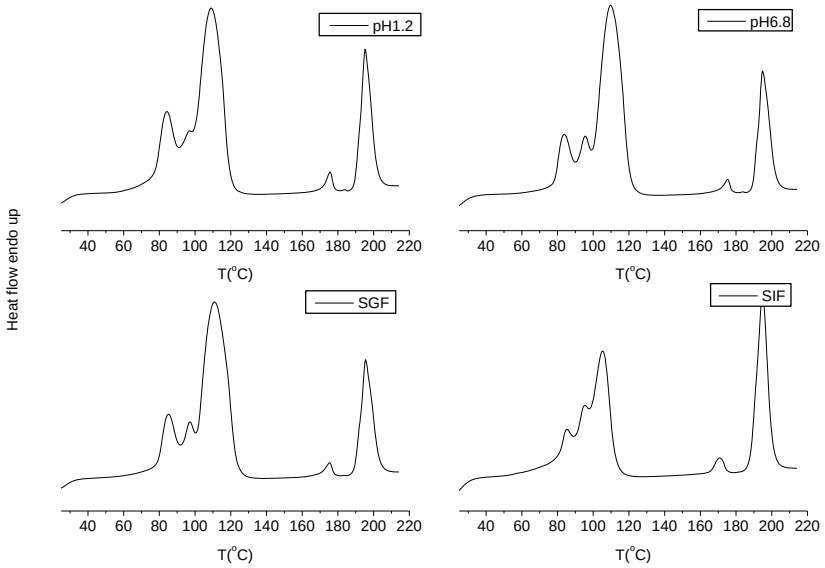

(a) CBZ DH

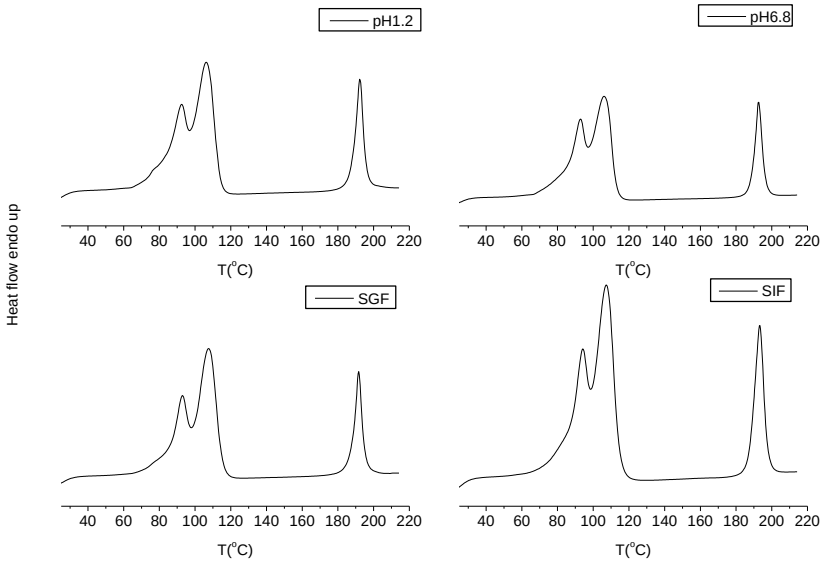

(b) CBZ-NIC cocrystal

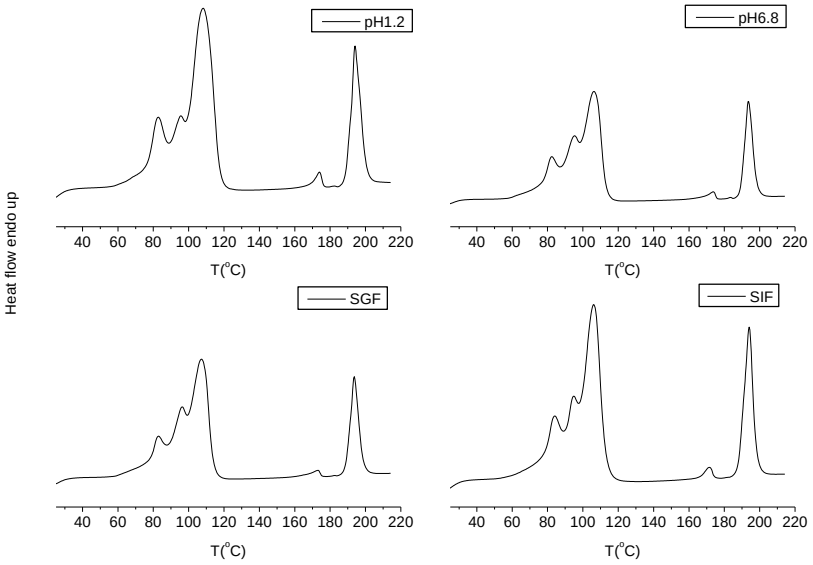

(c) CBZ-NIC mixture

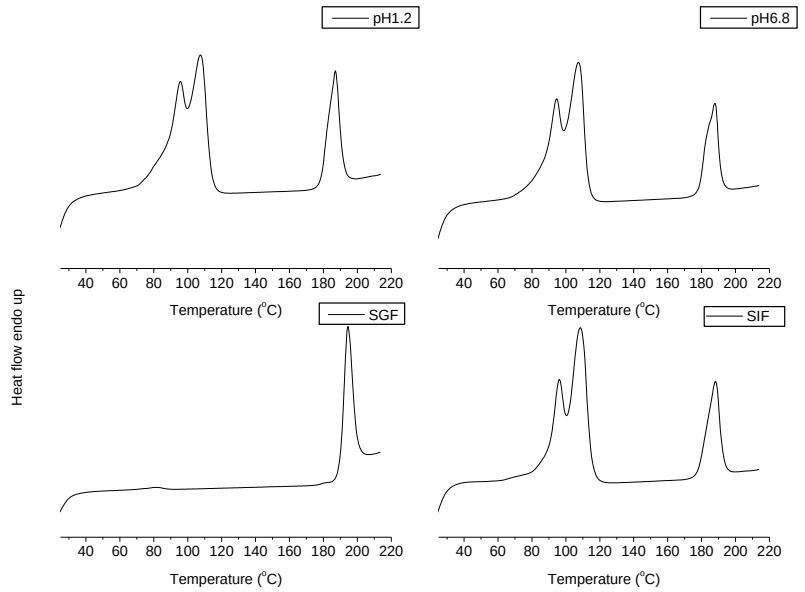

(d) CBZ-SUC cocrystal

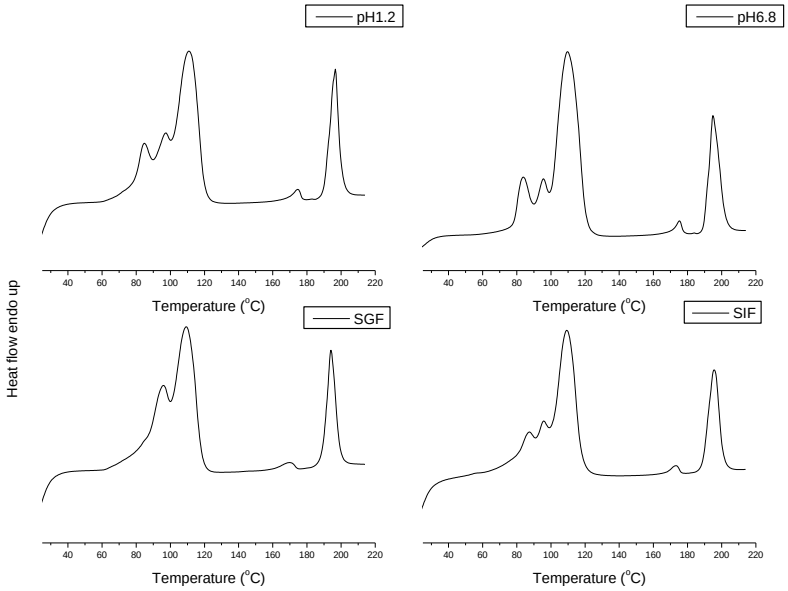

(e) CBZ-SUC mixture

A2.1.2 IR spectra of solid residue from the experiment of equilibrium solubility test in four buffers: (a) CBZ DH; (b) CBZ-NIC cocrystal; (c) CBZ-NIC mixture; (d) CBZ-SUC cocrystal; (e) CBZ-SUC mixture.

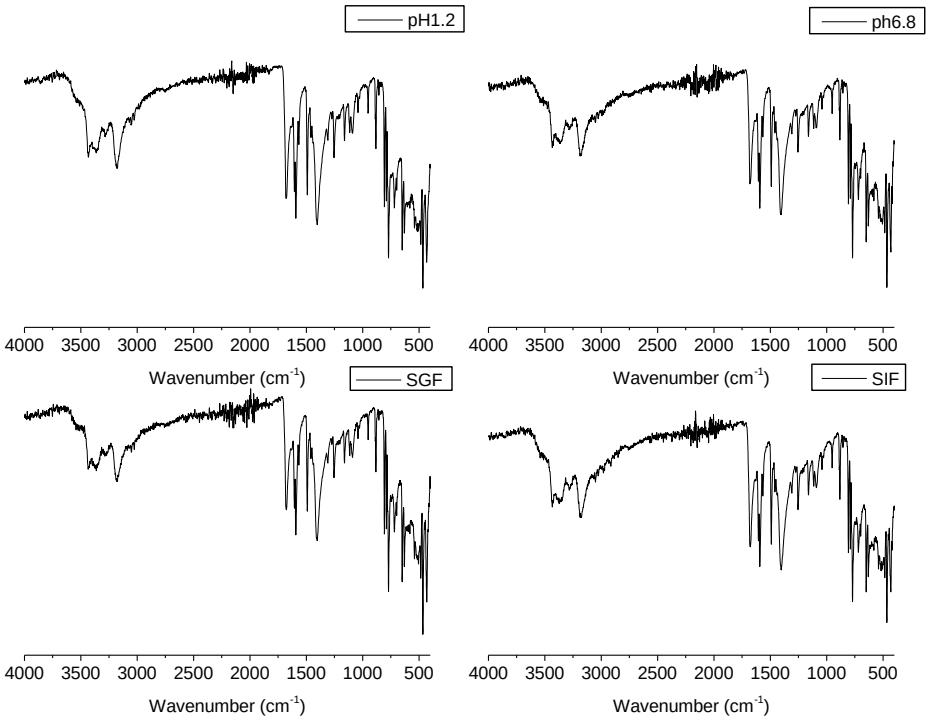

(a) CBZ DH

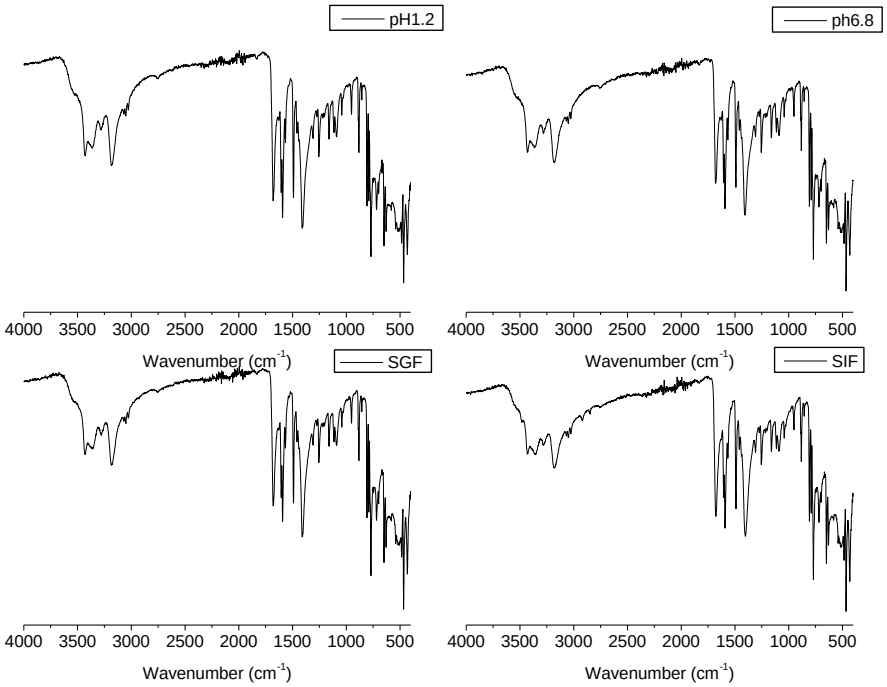

(b) CBZ-NIC cocrystal

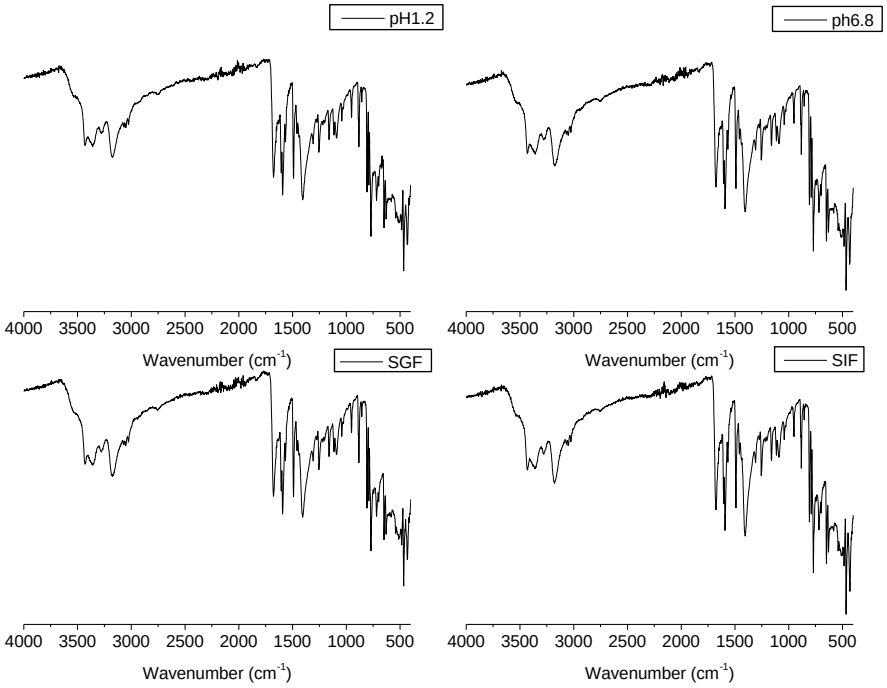

(c) CBZ-NIC mixture

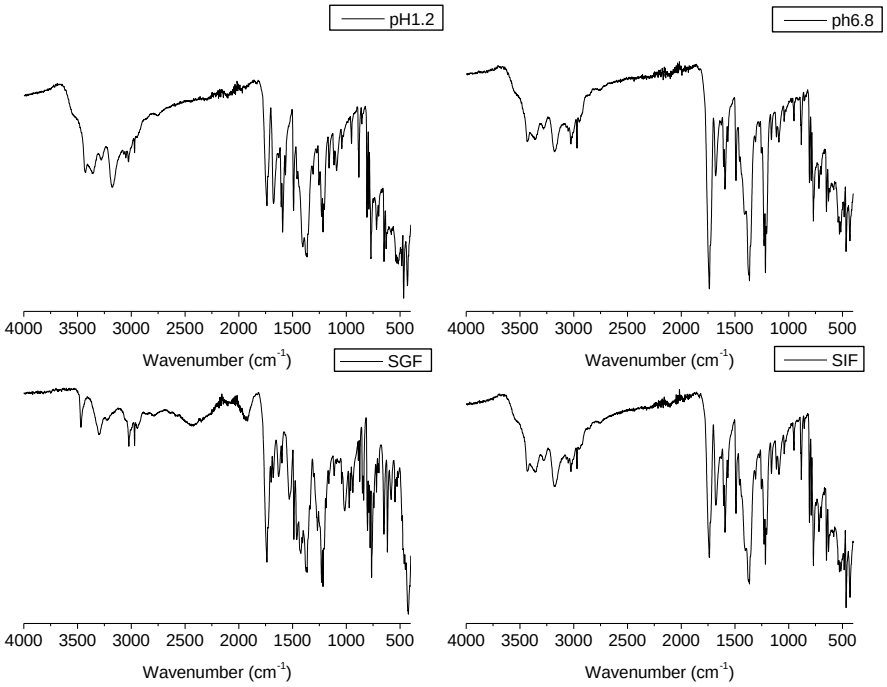

(d) CBZ-SUC cocrystal

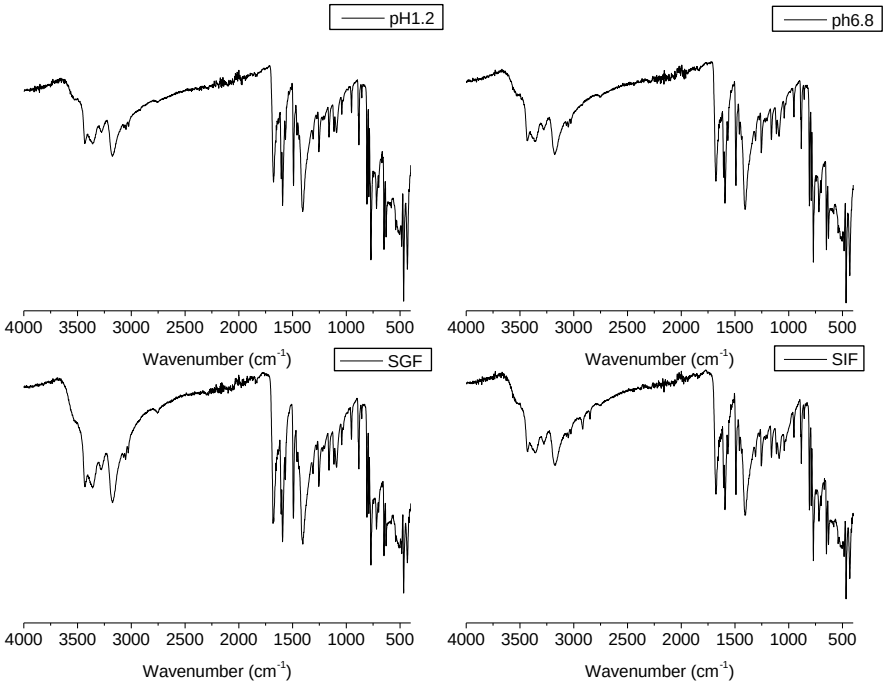

(e) CBZ-SUC mixture

A2.1.3 Raman spectra of solid residue from the experiment of equilibrium solubility test in four buffers: (a) CBZ DH; (b) CBZ-NIC cocrystal; (c) CBZ-NIC mixture; (d) CBZ-SUC cocrystal; (e) CBZ-SUC mixture.

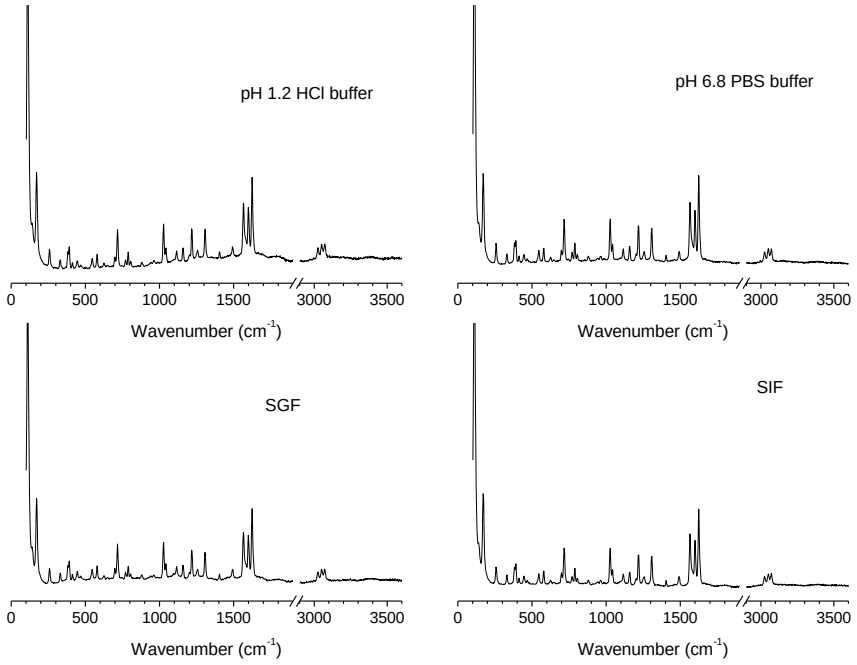

(a) CBZ DH

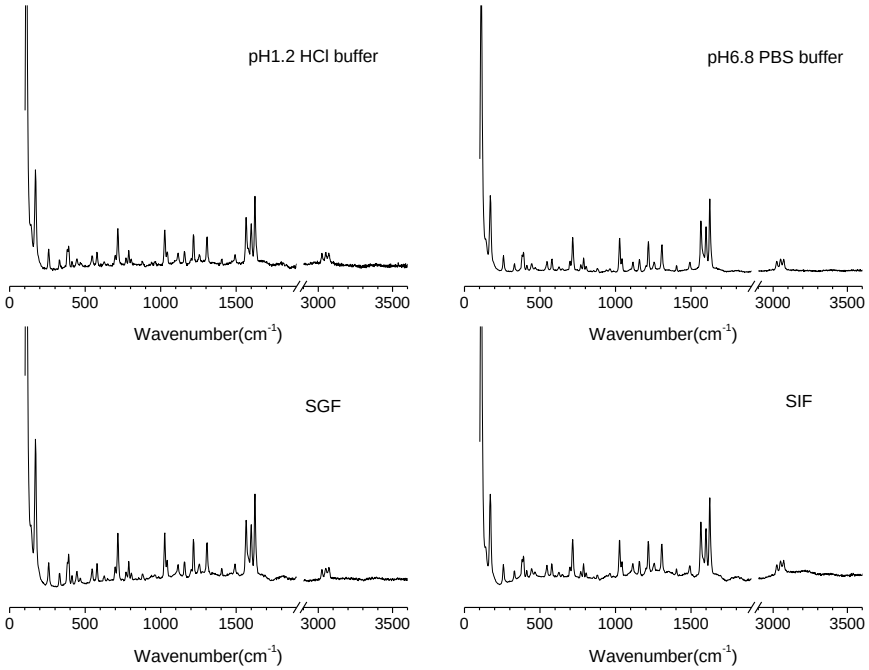

(b) CBZ-NIC cocrystal

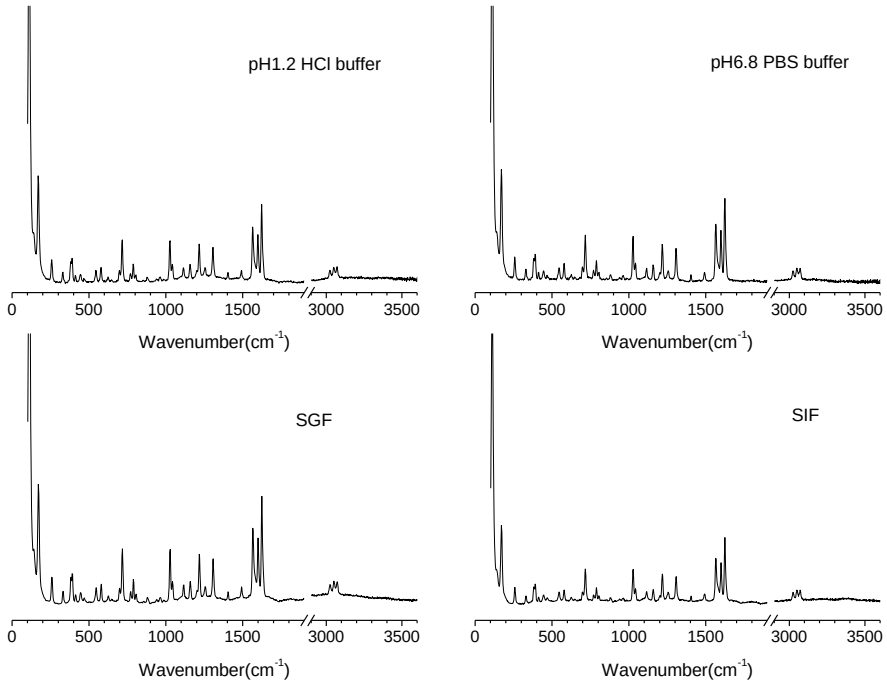

(b) CBZ-NIC mixture

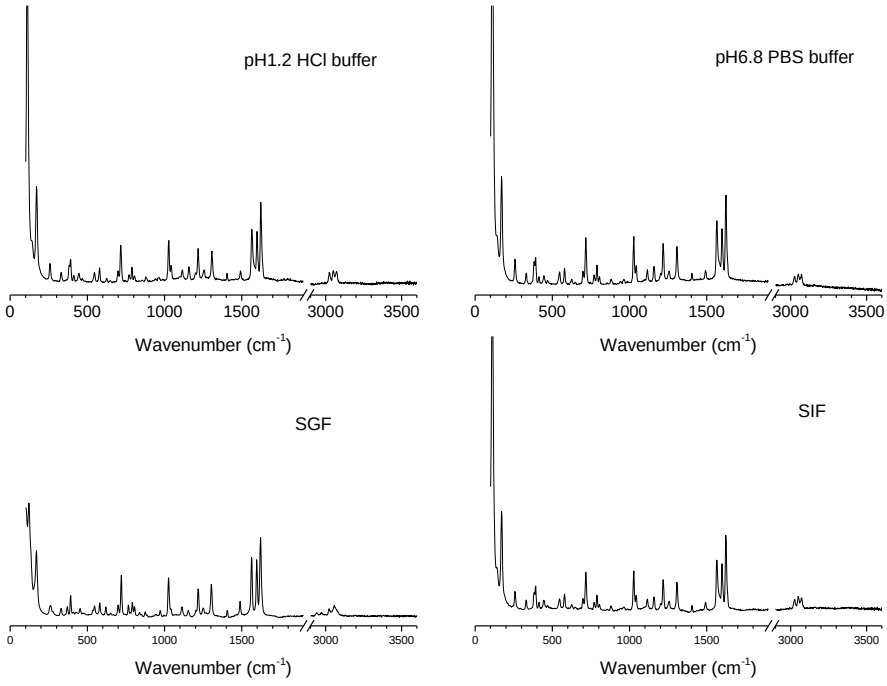

(c) CBZ-SUC cocrystal

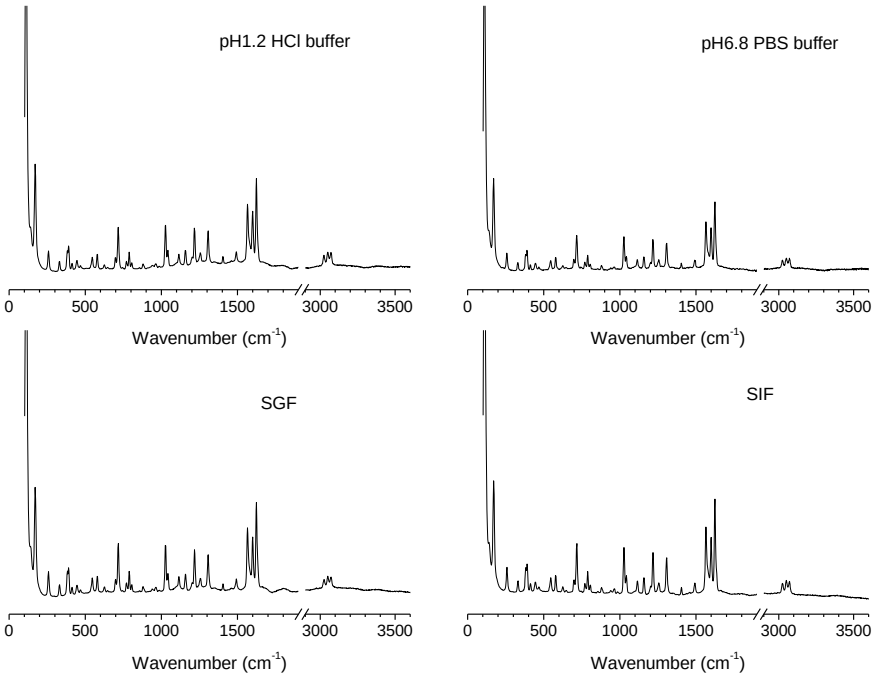

(d) CBZ-SUC mixture

A 2.2 Figures for CBZ solubility tests as function of coformers in chapter 7

A2.2.1 DSC thermal graphs of solid residue from the experiment of CBZ solubility tests as function of coformer in biomedia:

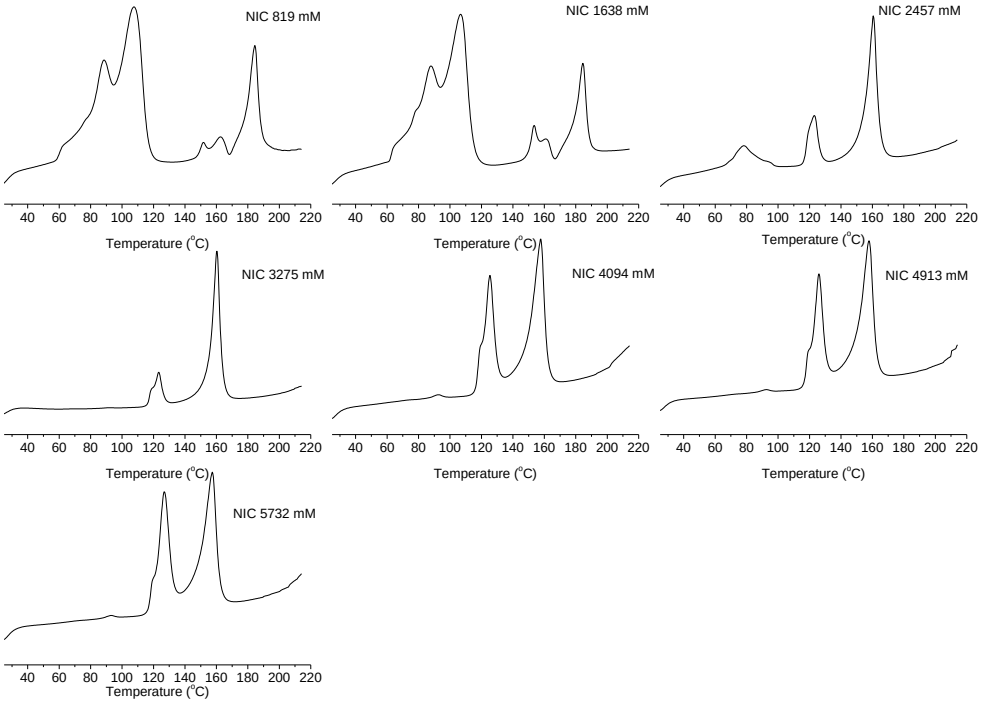

(a) CBZ solubility as function of NIC in pH1.2 buffer

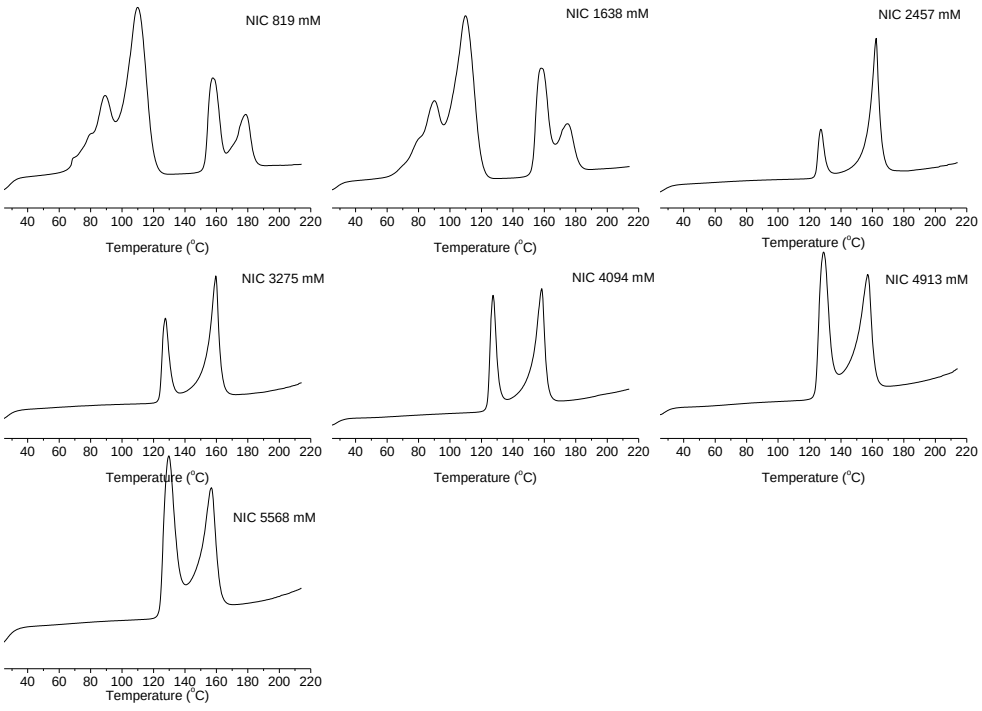

(b) CBZ solubility as function of NIC in pH6.8 buffer

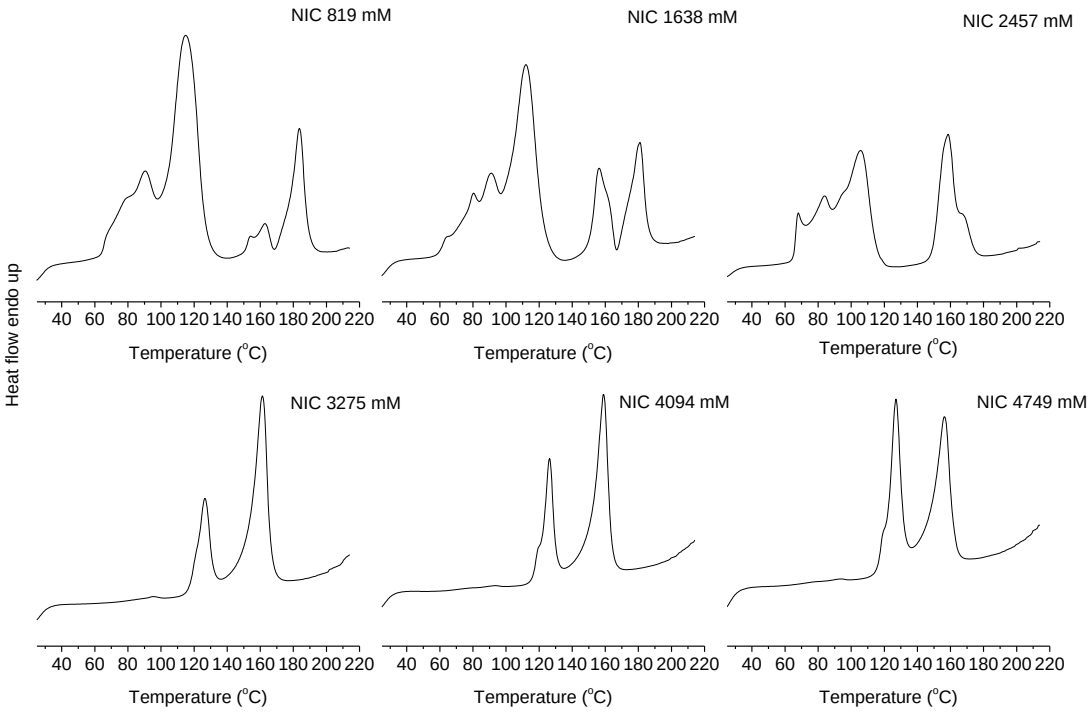

(c) CBZ solubility as function of NIC in SGF

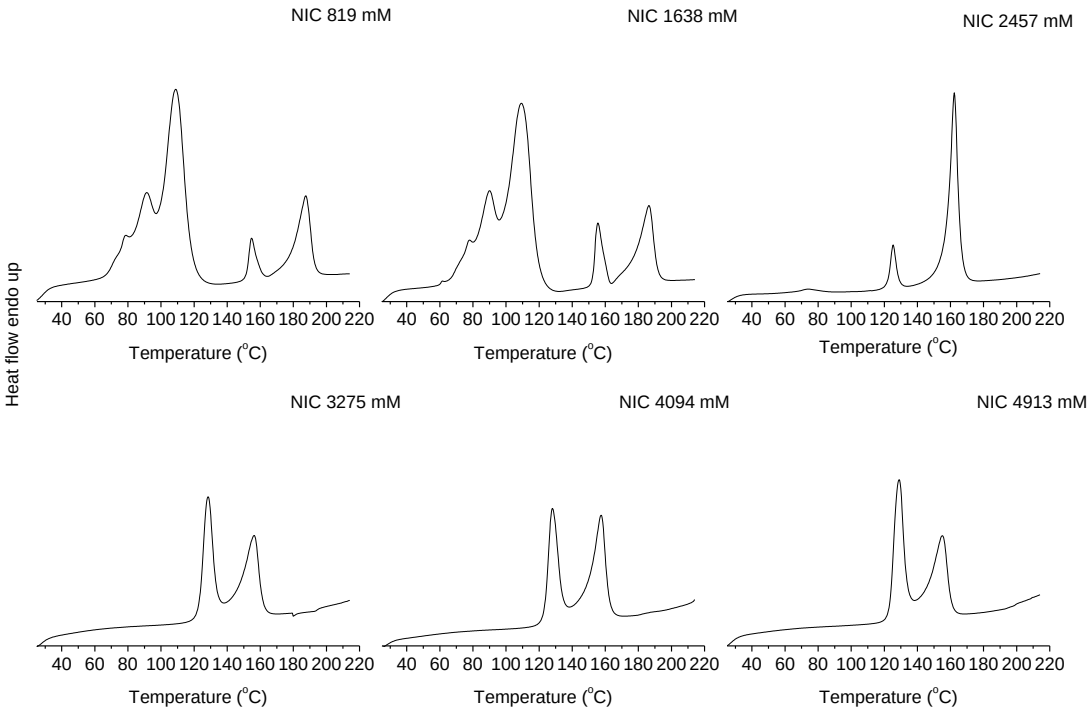

(d) CBZ solubility as function of NIC in SIF

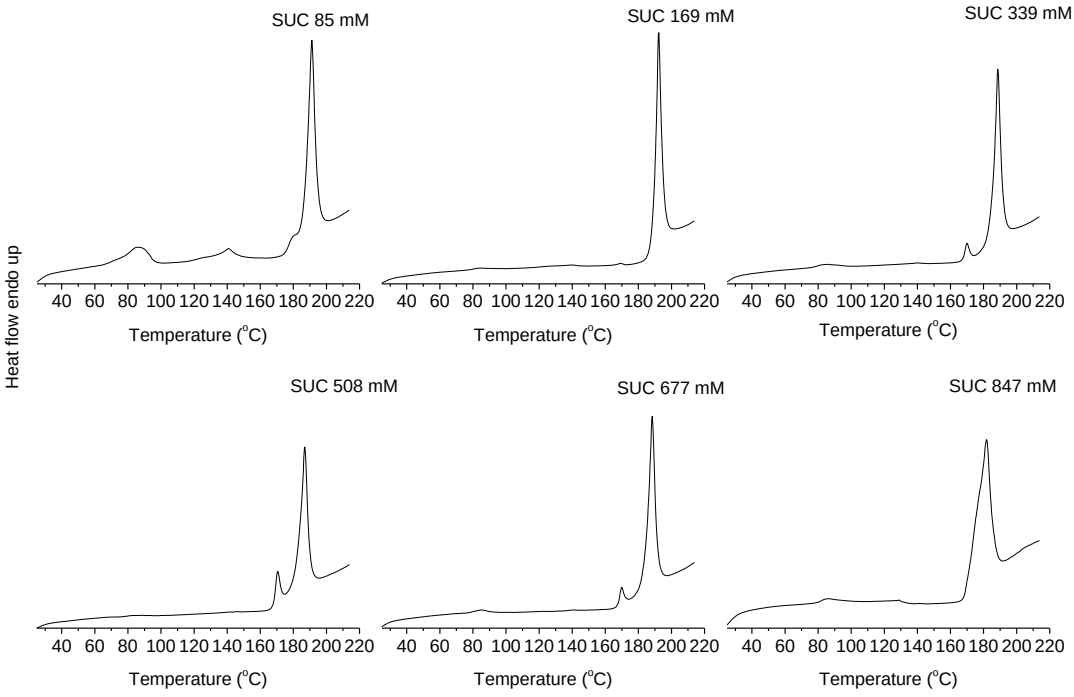

(e) CBZ solubility as function of SUC in pH1.2

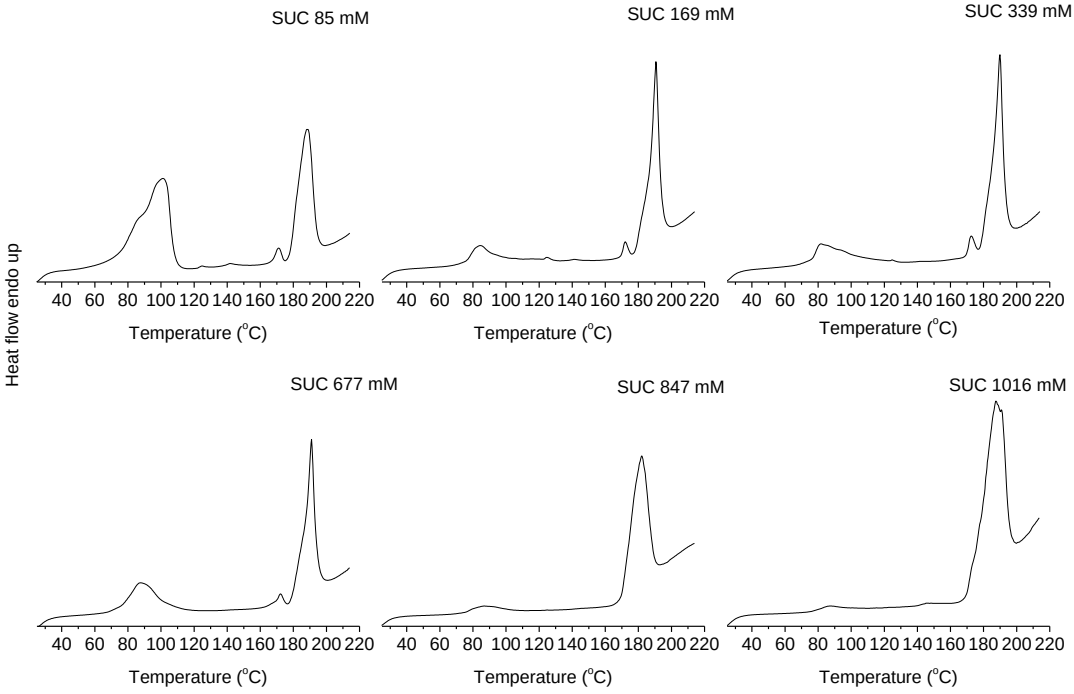

(f) CBZ solubility as function of SUC in pH6.8

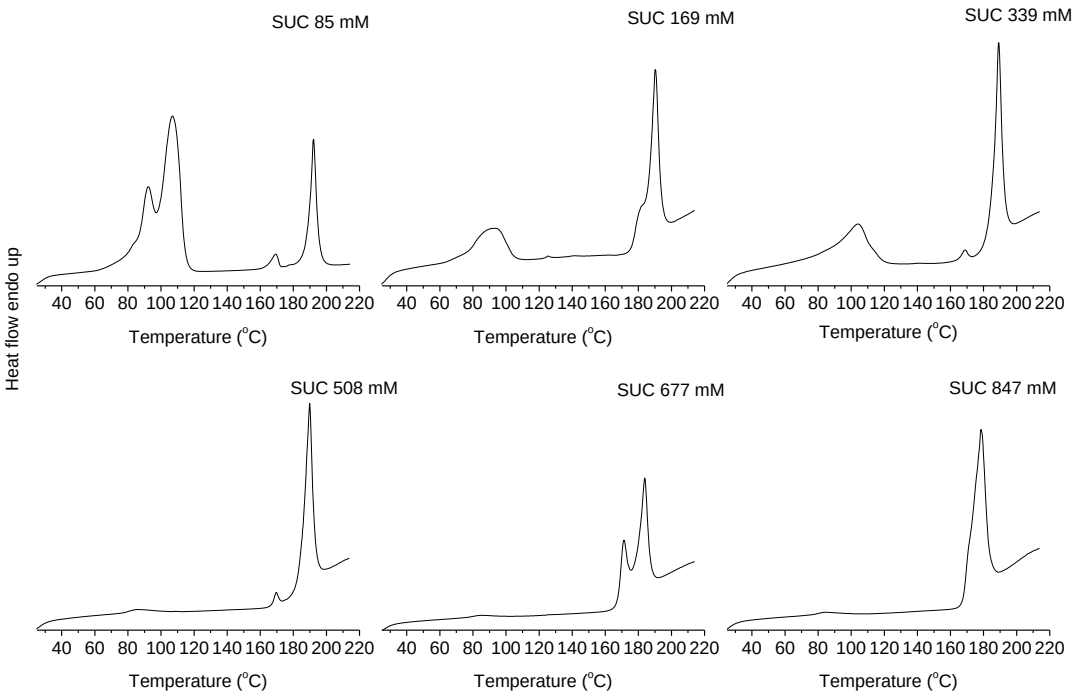

(g) CBZ solubility as function of SUC in SGF

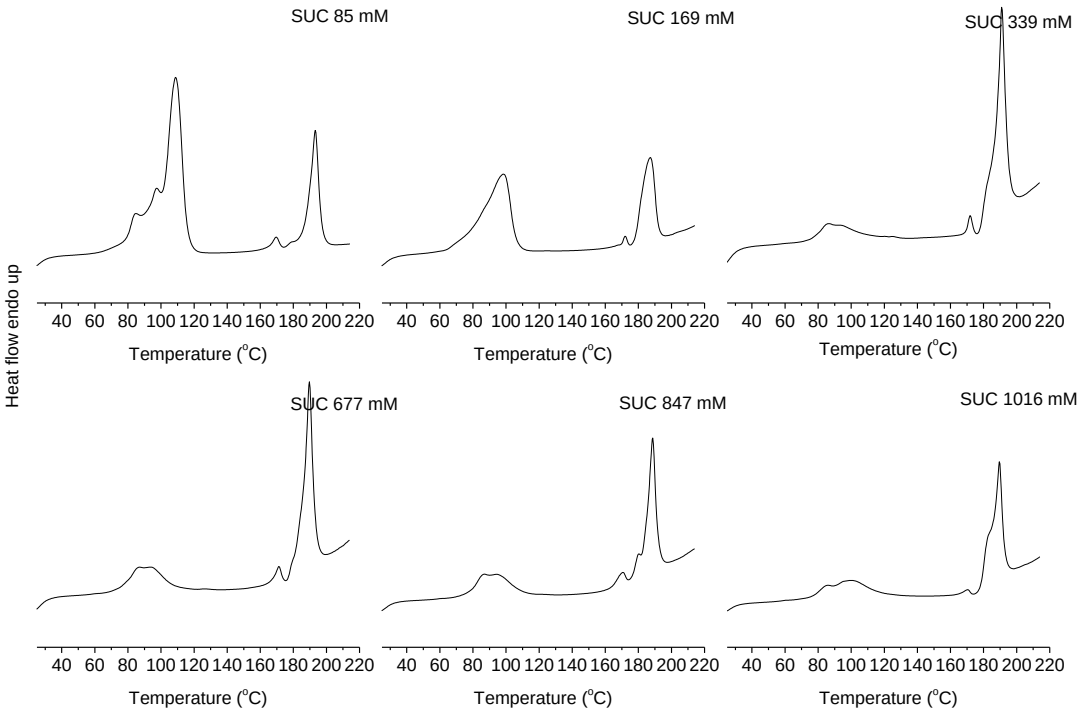

(h) CBZ solubility as function of SUC in SIF

A2.2.2 IR spectra of solid residue from the experiment of CBZ solubility tests as function of coformer in biomedia:

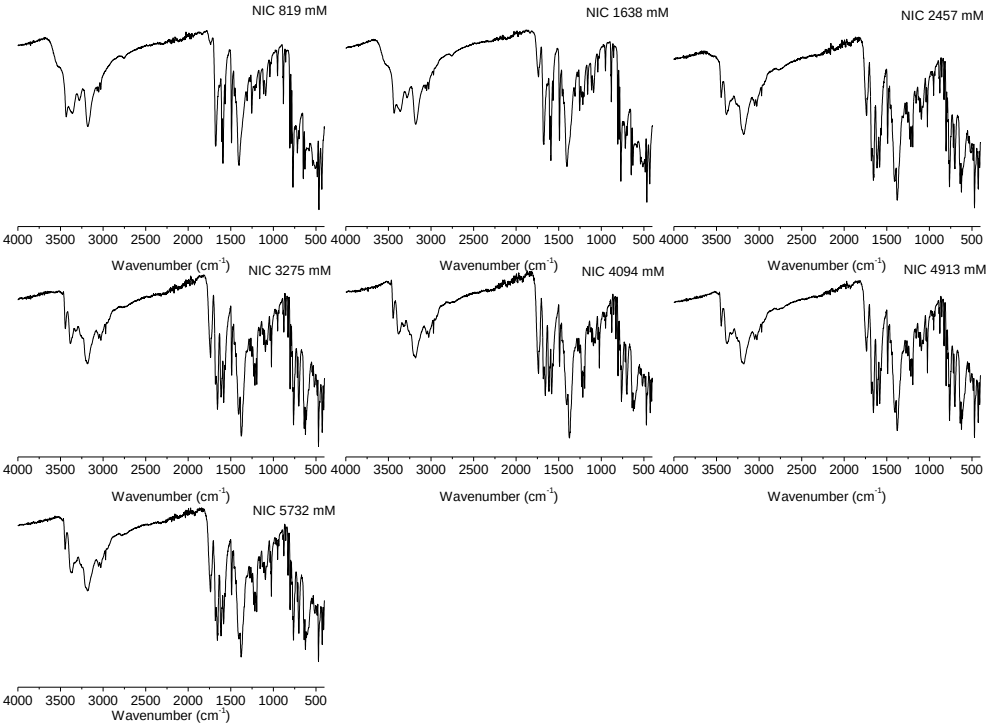

(a) CBZ solubility as function of NIC in pH1.2 buffer

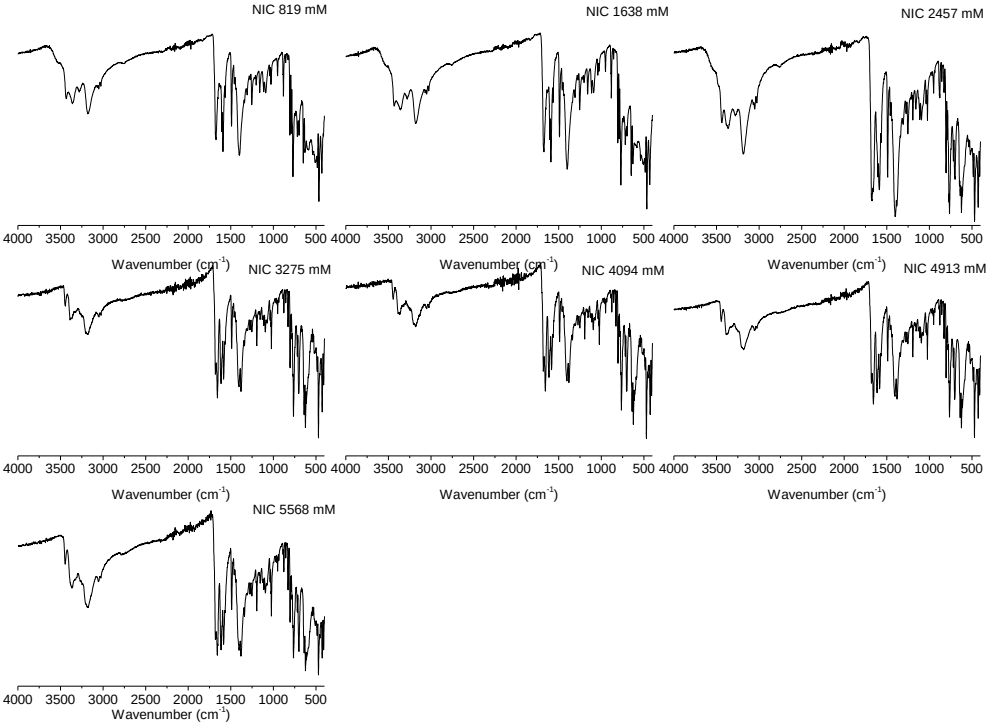

(b) CBZ solubility as function of NIC in pH6.8 buffer

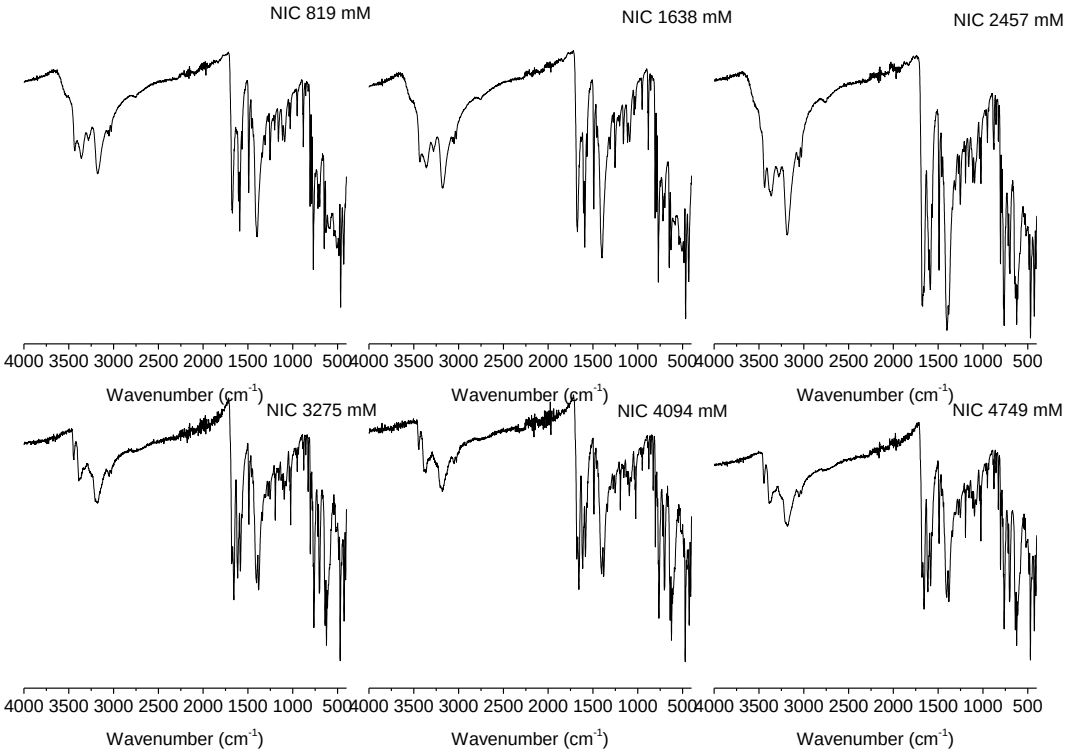

(c) CBZ solubility as function of NIC in SGF

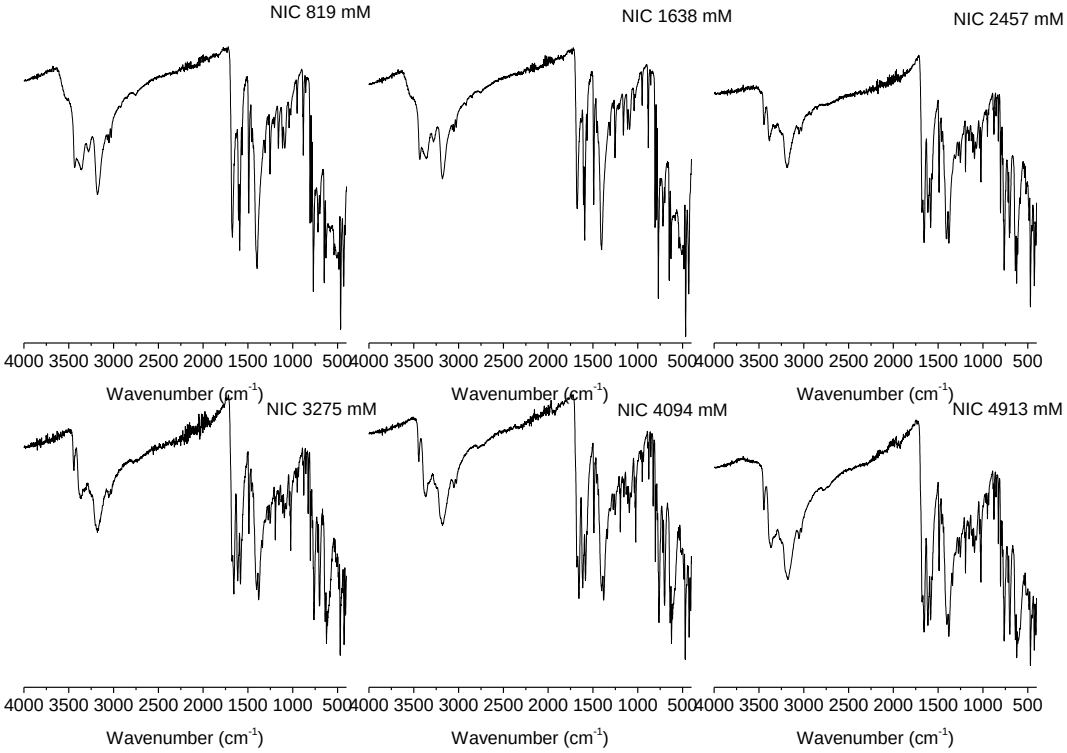

(d) CBZ solubility as function of NIC in SIF

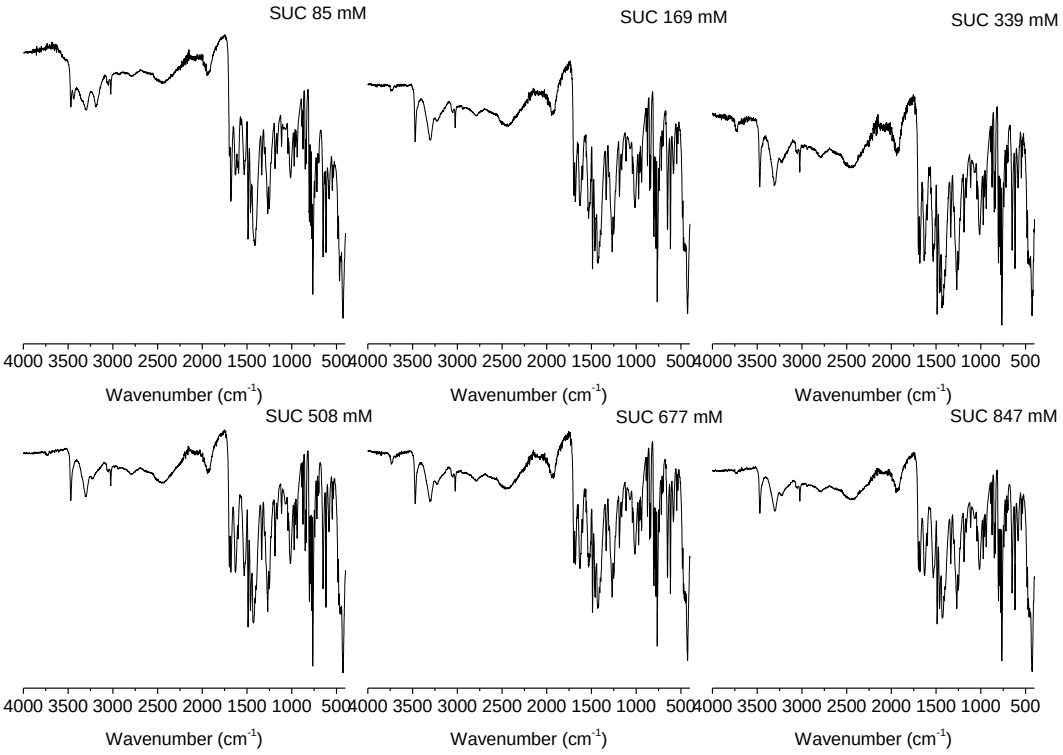

(e) CBZ solubility as function of SUC in pH1.2

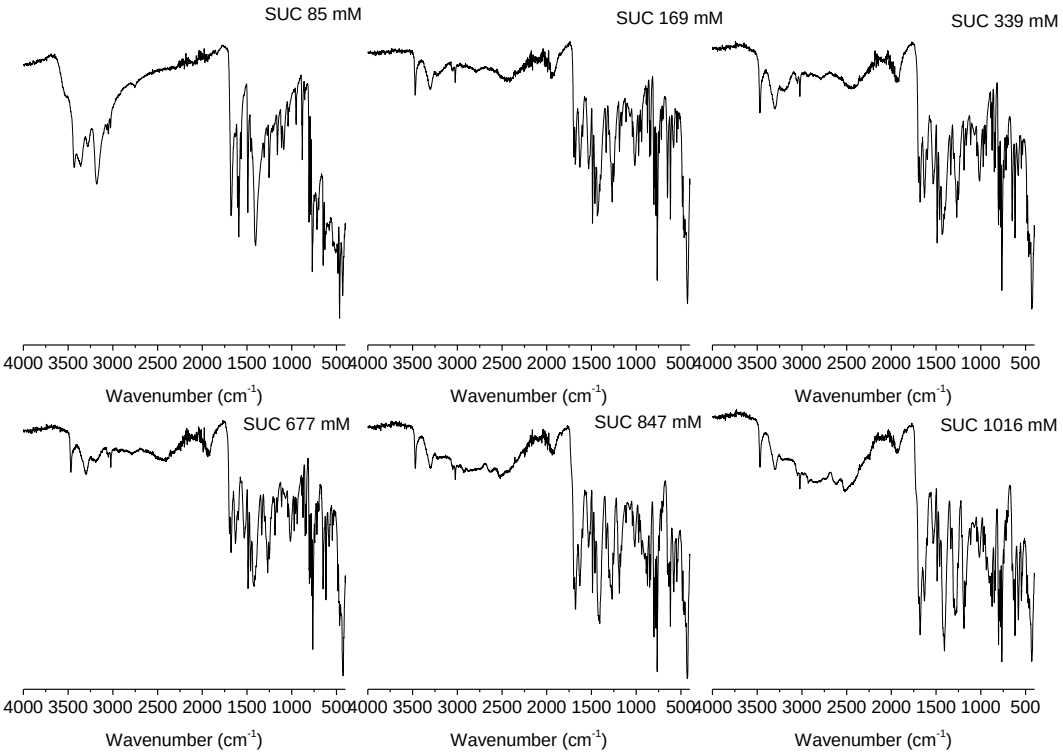

(f) CBZ solubility as function of SUC in pH6.8

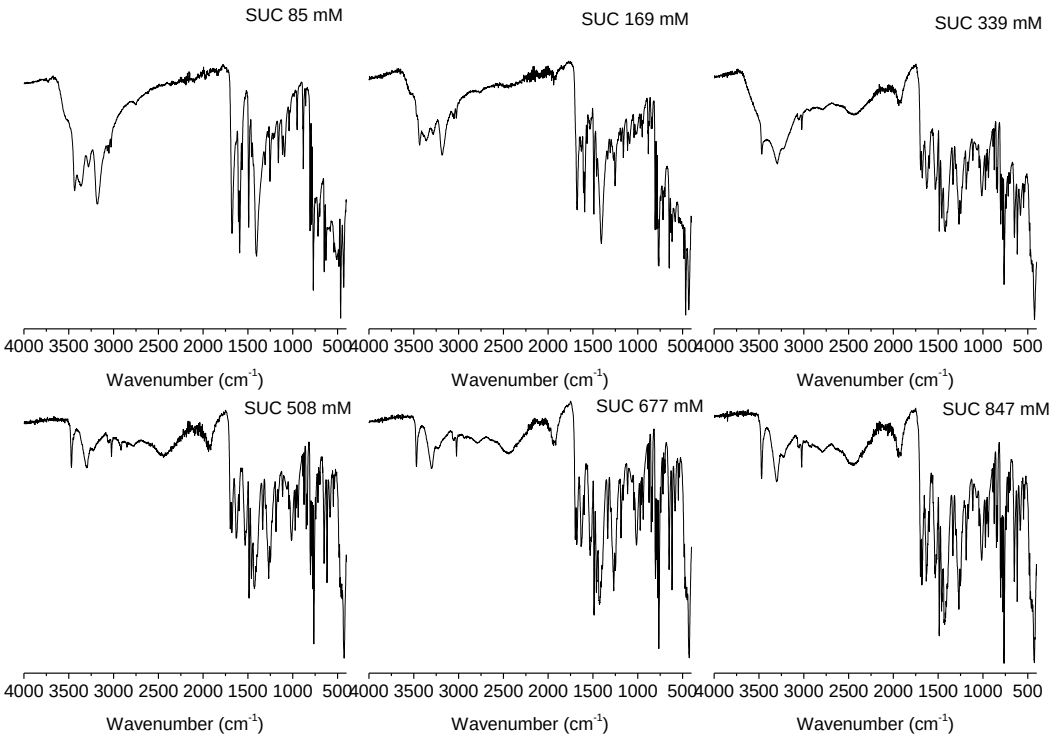

(g) CBZ solubility as function of SUC in SGF

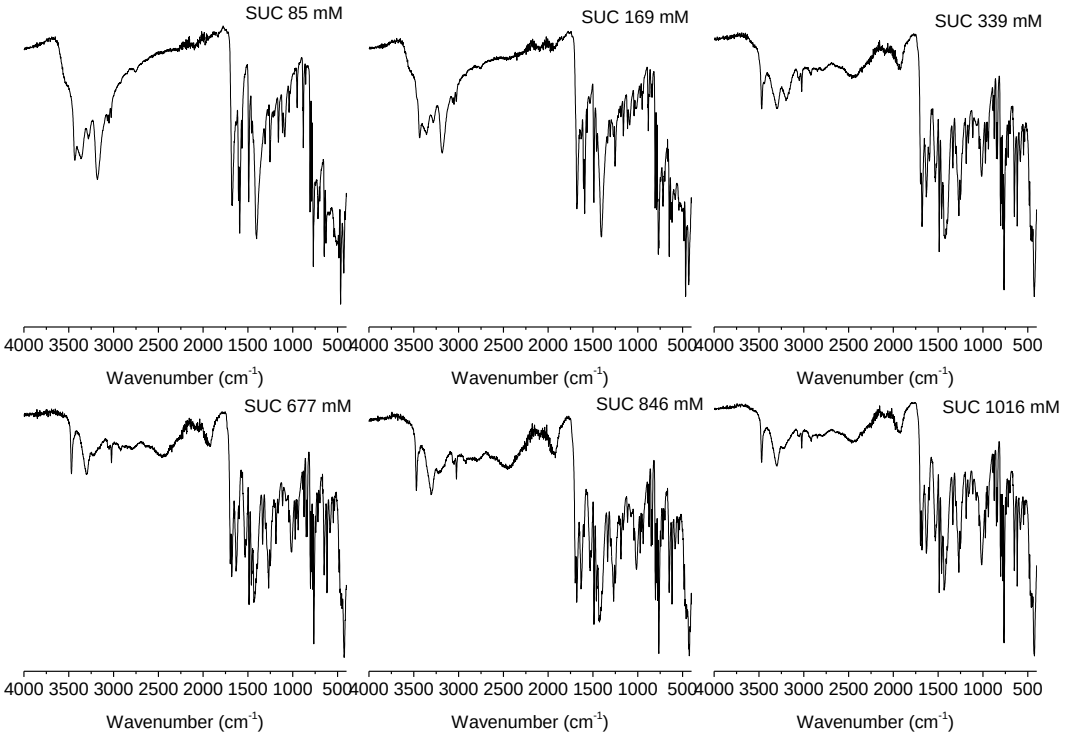

(h) CBZ solubility as function of SUC in SIF

A2.2.3 Raman spectra of solid residue from the experiment of CBZ solubility tests as function of coformer in biomedia:

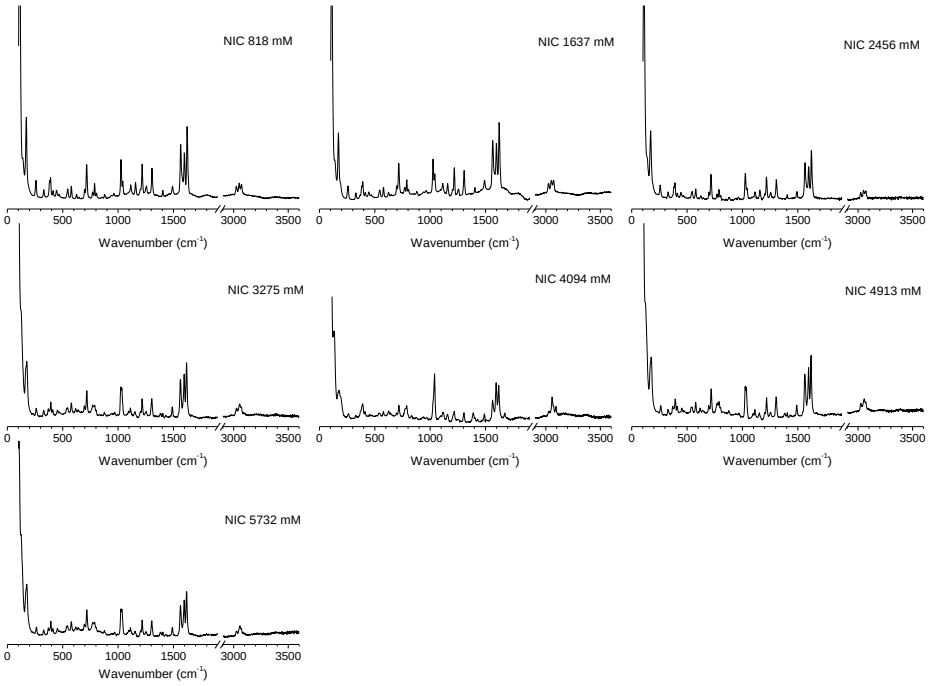

(a) CBZ solubility as function of NIC in pH1.2 buffer

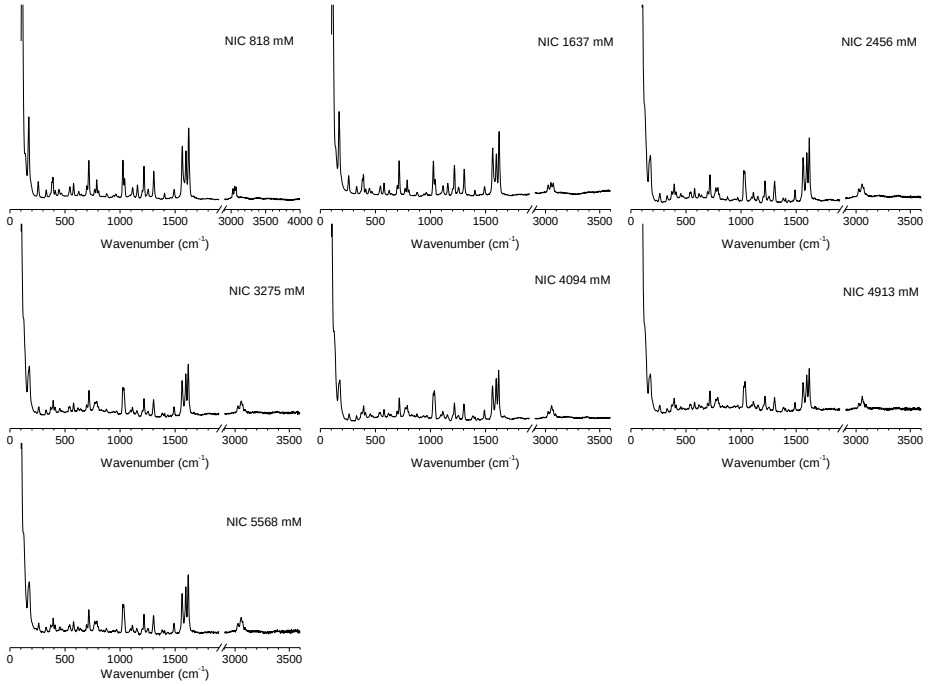

(b) CBZ solubility as function of NIC in pH6.8 buffer

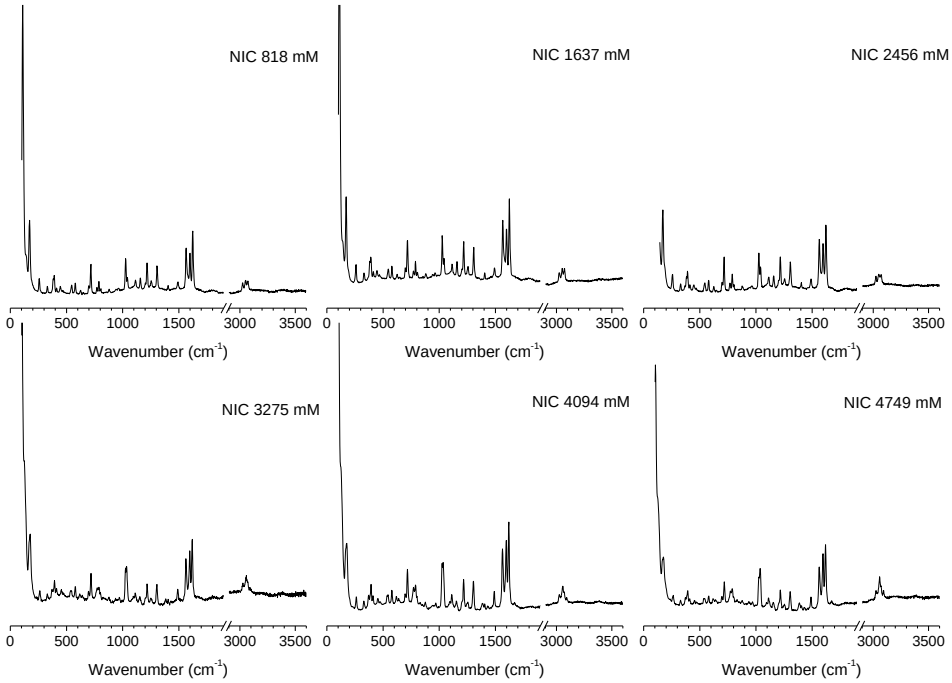

(c) CBZ solubility as function of NIC in SGF

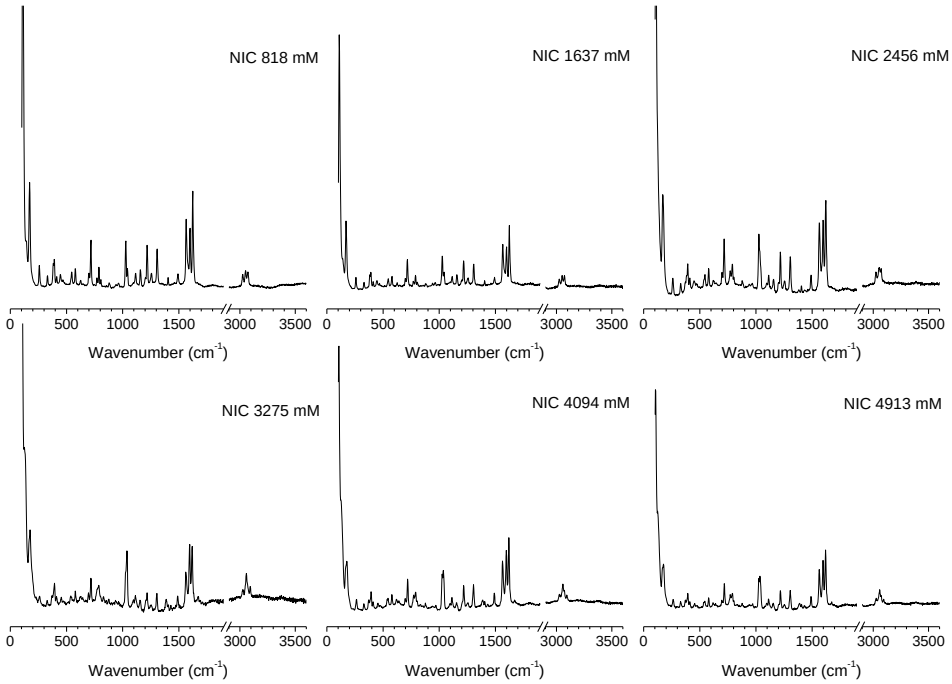

(d) CBZ solubility as function of NIC in SIF

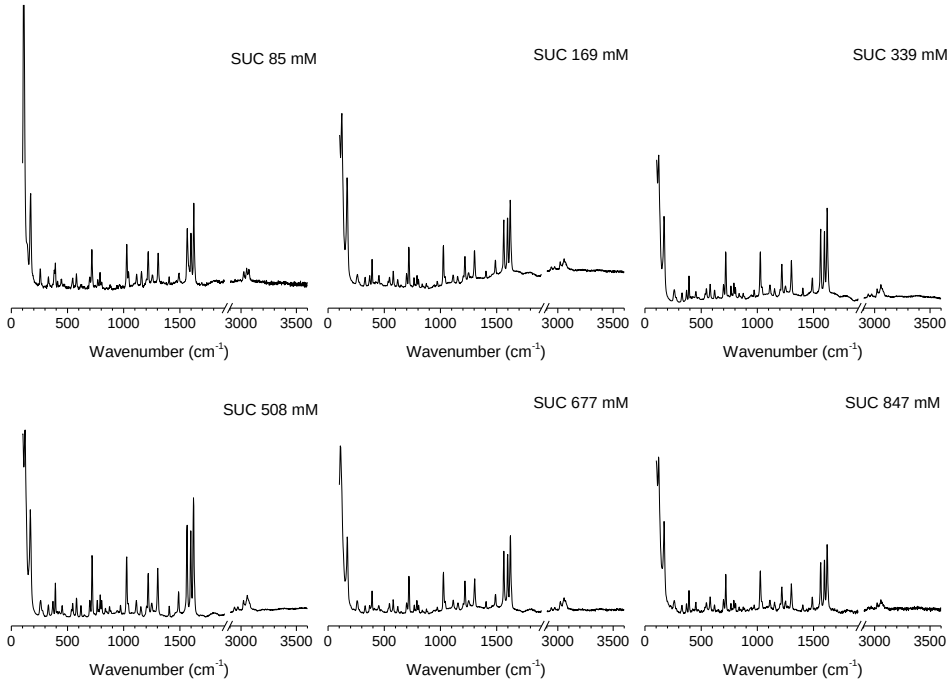

(e) CBZ solubility as function of SUC in pH1.2

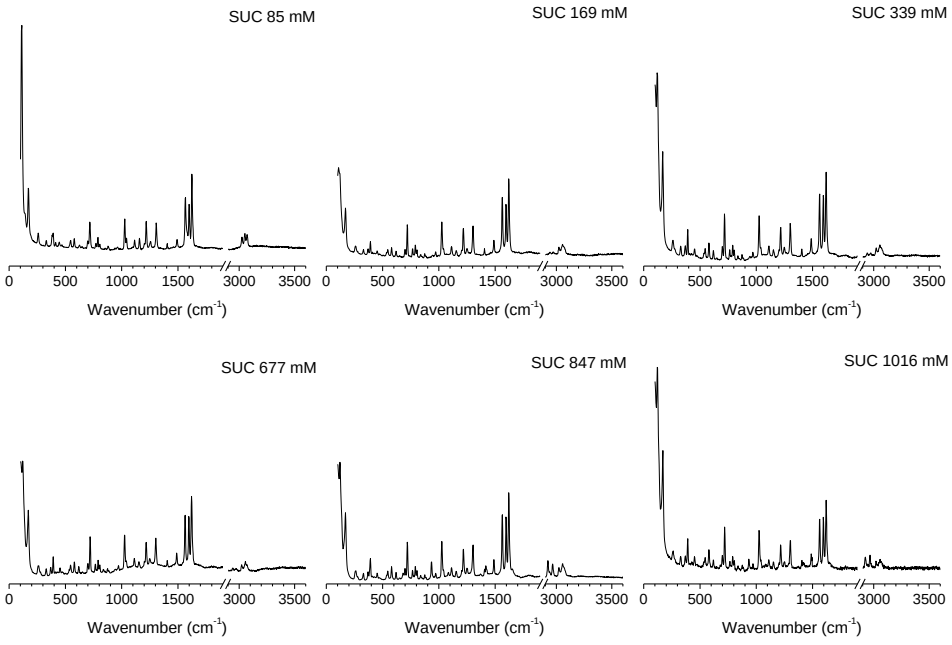

(f) CBZ solubility as function of SUC in pH6.8

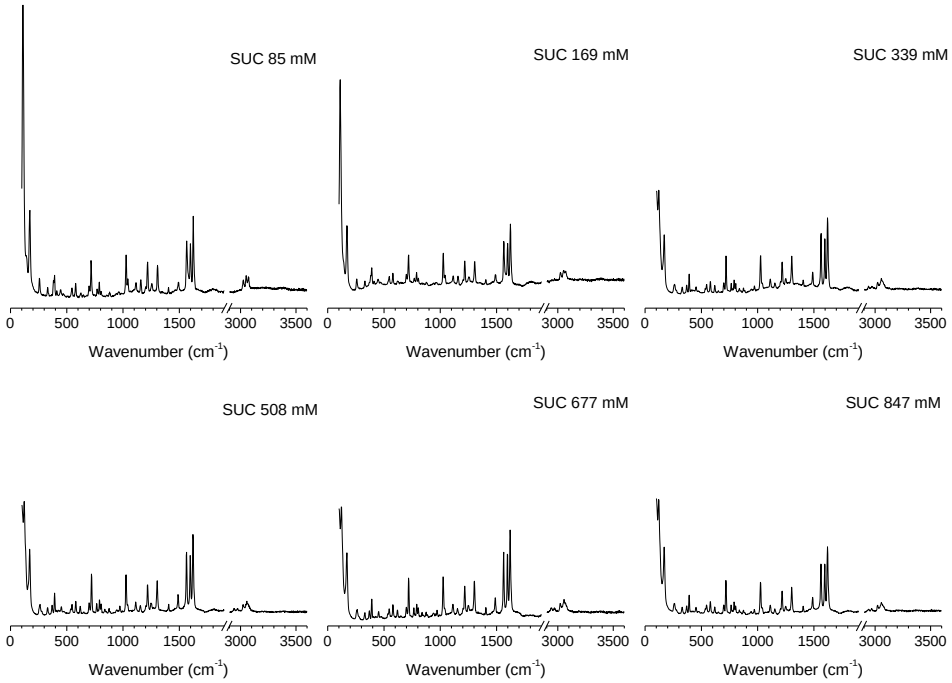

(g) CBZ solubility as function of SUC in SGF

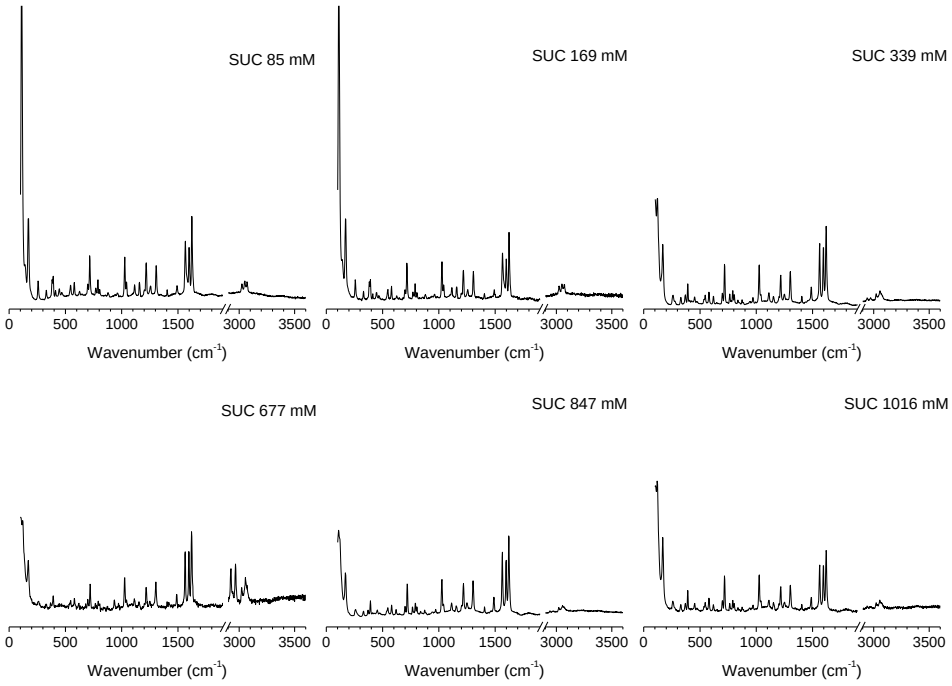

(h) CBZ solubility as function of SUC in SIF